University of Yaounde I

Faculty of Science

Department of Physics

QUANTUM BREATHER-LIKE EXCITATIONS IN 1D FERROMAGNETIC MATERIAL

Dissertation

Submitted for the award
of a Doctorat/PhD in Physics
Specialty: Materials Science

By

Djoufack Zacharie Isidore
Registration Number: 01R472
DEA in Physics

Under the Supervisor of:

Samuel Domngang
Emeritus Professor
University of Yaounde I

Jean-Pierre Nguenang
Associate Professor
University of Douala

Year 2015

List of the Permanent Teaching Staff of the Faculty of Science, University of Yaounde I

UNIVERSITE DE YAOUNDE I

UNIVERSITY OF YAOUNDE I

FACULTE DES SCIENCES

FACULTY OF SCIENCE

Dean	:	BILONG Paul (Professor)
Vice-Dean (Academic affairs)	:	NJOPWOUO Daniel (Professor)
Vice-Dean (DARR)	:	DONGO Etienne (Professor)
Vice-Dean (Research and Cooperation)	:	ESSIMBI ZOBO Bernard (Professor)
Head Administrative and Financial Division	:	NDOYE FOE Marie C. F. (Senior Lecturer)
Head Academic Affairs, Research Division	:	ABOSSOLO Monique (Senior Lecturer)

1 - DEPARTMENT OF BIOCHEMISTRY(B.C.) (41)			
01	MOUNDIPA FEWOU PAUL	Professor	Head of Dept
02	OBEN Julius ENYONG	Professor	on duty
03	BENG born NINTCHOM PENLAP V.	Associate Professor	on duty
04	FEKAM BOYOM Fabrice	Associate Professor	on duty
05	FOKOU Elie	Associate Professor	on duty
06	KANSCI Germain	Associate Professor	on duty
07	MBATCHAM Wilfried	Associate Professor	on duty
08	MINKA Samuel	Associate Professor	on duty
09	NGUEFACK Julienne	Associate Professor	on duty
10	ACHU Merci BIH	Senior Lecturer	on duty
11	ATOGHO Barbara Mama	Senior Lecturer	on duty
12	BELINGA born NDOYE FOE F.	Senior Lecturer	Head DAF / FS
13	BIGOGA JUDE	Senior Lecturer	on duty
14	BODA Maurice	Senior Lecturer	on duty
15	BOUDJEKO THADEE	Senior Lecturer	on duty
16	DEMMANO Gustave	Senior Lecturer	on duty
17	DJOKAM TAMO Rosine R.	Senior Lecturer	on duty
18	EFFA ONOMO Pierre	Senior Lecturer	on duty
19	EVEHE BEBANDOUE M.-S.	Senior Lecturer	on duty
20	EWANE CECILE Anne	Senior Lecturer	on duty
21	MOFOR born TEUGWA C.	Senior Lecturer	CE SEP MINESUP
22	NGONDI Judith Laure	Senior Lecturer	on duty
23	NJAYOU Frédéric Nico	Senior Lecturer	on duty
24	TCHANA NKOUATCHOUA A.	Senior Lecturer	on duty
25	WAKAM born NANA Louise	Senior Lecturer	on duty
26	AKINDEH MBUHNJI	Assistant	on duty
27	BEBBE FADIMATOU	Assistant	on duty
28	BEBOY EDZENGUELE S. N.	Assistant	on duty
29	DAKOLE DABOY Charles	Assistant	on duty
30	DJUIKWO NKONGA Ruth V.	Assistant	on duty
31	DONGMO LEKAGNE J. B.	Assistant	on duty
32	KOTUE KAPTUE Charles	Assistant	on duty
33	FONKOUA Martin	Assistant	on duty
34	LUNGA Paul KEILAH	Assistant	on duty
35	MANANGA Marlyse Josephine	Assistant	on duty
36	MBONG ANGIE MOUGANDE M.	Assistant	on duty
37	MBOUCHE FANMOE Marcelline J.	Assistant	on duty
38	PACHANOU NSANGOU S.	Assistant	on duty
39	Palmer MAUMBE NETTONGO	Assistant	on duty
40	TIENCHEU DJONKAM Leopold	Assistant	on duty

2 - DEPARTMENT OF ANIMAL BIOL. AND PHYSIOL. (B.P.A.) (45)			
01	BILONG BILONG Charle F.	Professor	Head of Dept.
02	DIMO Théophile	Professor	on duty
03	FOMENA Abraham	Professor	on duty
04	KAMTCHOUING Pierre	Professor	on duty
05	MINFOUNDI Remy	Professor	on duty
06	NGASSAM Pierre	Professor	on duty
07	NJIOKOU Flobert	Professor	on duty
08	NOLA Moïse	Associate Professor	on duty
09	DJIETO Lordon Champlain	Associate Professor	on duty
10	ESSOMBA born NTSAMA M.	Associate Professor	MINSANTE
11	FOTO MENBOHAN Samuel	Associate Professor	(CT2 MIN. ENERGY)
12	KAMGANG René	Associate Professor	C.S. MINRESI
13	NJAMEN Dieudonné	Associate Professor	on duty
14	TAN VEMYU Paul	Associate Professor	on duty
15	TCHUEM TCHUENTE L.	Associate Professor	C. P. MINSANTE
16	AJEAGAH Gidéon AGHAINDOUM	Senior Lecturer	on duty
17	ALENE Désirée Chantal	Senior Lecturer	on duty
18	BAPFUBUSA Bénoît Alain	Senior Lecturer	on duty
19	BELLET EDIMO Oscar Roger	Senior Lecturer	on duty
20	DJIOGUE Sefirin	Senior Lecturer	on duty
21	DZEUFIET DJOMENI Paul D.	Senior Lecturer	on duty
22	GOUNOUE K. R. wife FOTSING	Senior Lecturer	on duty
23	ENO Anna Arrey	Senior Lecturer	on duty
24	JATSA MEGAPTCHE Hermine	Senior Lecturer	on duty
25	KEKEUNOU Sévilor	Senior Lecturer	on duty
26	MEGNEKOU Rosette	Senior Lecturer	on duty
27	MONY NTONE Ruth	Senior Lecturer	on duty
28	NGUEGUIM TSOFACK Florence	Senior Lecturer	on duty
29	TOMBI Jeannette	Senior Lecturer	on duty
30	ZEBAZE TOGOUET S. H.	Senior Lecturer	on duty
31	ATSAMO ALBERT Donatien	Assistant	on duty
32	ETEME ENAMA Serge	Assistant	on duty
33	KANDELA KAVAYE Antoine	Assistant	on duty
34	KOGA MANG DOBARA	Assistant	on duty
35	LEKEUFACK FOLEFACK Guy B.	Assistant	on duty
36	MAHOB Raymond Joseph	Assistant	on duty
37	MBENOUN MASSE Paul S.	Assistant	on duty
38	MOUGANG Luciane Marlyse	Assistant	on duty
39	MUH Bernice FIEN	Assistant	on duty
40	MVEYO NDANKEU Yves Patrick	Assistant	on duty
41	NGOUATEU KENFACK Omer B.	Assistant	on duty

42	NJUA Clarisse YAFI	Assistant	on duty
43	OBI OBEN Esther	Assistant	on duty
44	TADU Zephirin	Assistant	on duty
45	YEDE	Assistant	on duty
3 - DEPARTMENT OF PLANT BIOLOGY (B.P.V.) (25)			
01	YOUMBI Emmanuel	Professor	Head of Dept.
02	AMBANG Zachée	Associate Professor	on duty
03	BELL Joseph Martin	Associate Professor	on duty
04	DJOCGOUE Pierre F.	Associate Professor	on duty
05	MOSSEBO Dominique C.	Associate Professor	on duty
06	ZAPFACK Louis	Associate Professor	on duty
07	ANGONI Hyacinthe	Senior Lecturer	on duty
08	BIYE Elvire Hortense	Senior Lecturer	on duty
09	KENGNE NOUMSI Yves M.	Senior Lecturer	on duty
10	MALLA Armand William	Senior Lecturer	on duty
11	MBARGA BINDZI Marie A.	Senior Lecturer	CEA MINESUP
12	MBOLO Marie	Senior Lecturer	on duty
13	NDONGO BEKOLO	Senior Lecturer	on duty
14	NGODO MELINGUI Jean B.	Senior Lecturer	on duty
15	NGONKEU MAGAPTCHE E. L.	Senior Lecturer	on duty
16	NGOUO Lucas Vincent	Senior Lecturer	on duty
17	NSOM ZAMO Annie Claude	Senior Lecturer	National expert./UNESCO
18	TONFACK Libert Brice	Senior Lecturer	on duty
19	TSOATA Esaïe	Senior Lecturer	on duty
20	DJEUNI Astride Carole	Assistant	on duty
21	MAHBOU SOMO TOUKAM	Assistant	on duty
22	MAFFO MAFFO Nicole L.	Assistant	on duty
23	NGALLE Hermine BILLE	Assistant	on duty
24	NNANGA MEBENGA R. L.	Assistant	on duty
25	NOUKEU KOUOKAM Armelle	Assistant	on duty
4 - DEPARTMENT OF INORGANIC CHEMISTRY (C.I.) (33)			
01	NDIFON Peter TEKE	Professor	ISI MINRESI
02	NGAMENI Emmanuel	Professor	Dir. MINSUP
03	NJOPWOUO Daniel	Professor	Vice-Dean / DPSAA
04	AGWARA ONDOH M.	Associate Professor	Head Div. MINPMEA
05	AVOM Jérôme	Associate Professor	Director I.A.I Gabon
06	BABALE born DJAM D.	Associate Professor	In Char. of Mis. P.R
07	DJOUFAC WOUMFO E.	Associate Professor	on duty
08	ELIMBI Antoine	Associate Professor	on duty
09	GHOGOMU Paul MINGO	Associate Professor	Dir. cab. PM
10	KETCHA MBADCAM J.	Associate Professor	Head of Dept.
11	LAMINSI Samuel	Associate Professor	on duty

12	MELO born CHINJE U. F.	Associate Professor	Dir. Mipromalo
13	NANSEU Charles Péguy	Associate Professor	on duty
14	NENWA Justin	Associate Professor	on duty
15	NDIKONTAR Maurice KOR	Associate Professor	VD/UBda
16	NGOMO Horace MANGA	Associate Professor	C.T. of P.M
17	YOUNANG Elie	Associate Professor	on duty
18	BAIZOUMI ZOUA	Senior Lecturer	Head Div. MINTOUR
19	EMADACK Alphonse	Senior Lecturer	on duty
20	GWET Simon-Pierre	Senior Lecturer	on duty
21	KEUMEGNE MBOUGUEM J.C.	Senior Lecturer	on duty
22	KONG SAKEO	Senior Lecturer	C.M of P.M
23	NJIOMOU C. wife DJANGANG	Senior Lecturer	on duty
24	NJOYA Dayirou	Senior Lecturer	on duty
25	SIGNING Pierre	Senior Lecturer	on duty
26	ACAYANKA Elie	Senior Lecturer	on duty
27	CHEUMANI YONA Arnaud M.	Senior Lecturer	on duty
28	KAMGANG YOUBI Georges	Senior Lecturer	on duty
29	NYAMEN Linda Dyorisse	Senior Lecturer	on duty
30	PABOUDAM GBAMBIE Awawou	Senior Lecturer	on duty
31	TCHAKOUTE KOUAMO Hervé	Senior Lecturer	on duty
32	BELIBI BELIBI Placide	Assistant	on duty
33	NDI SAMI Julius	Assistant	on duty
5 - DEPARTMENT OF ORGANIC CHEMISTRY (C.O.) (34)			
01	DONGO Etienne	Professor	Vice Dean
02	GHOGOMU TIH Raphäel	Professor	on duty
03	MBAFOR Joseph	Professor	on duty
04	NGADJUI TCHALEU B.	Professor	Head Of Dept.FMBS
05	NGOUELA Silvère A.	Professor	on duty
06	NKENGFACK Augustin E.	Professor	Head of Dept.
07	NYASSE Barthélemy	Professor	on duty
08	PEGNYEMB Dieudonné E.	Professor	Head Div. MINESUP
09	WANDJI Jean	Professor	on duty
10	Alex de Théodore ATCHADE	Associate Professor	on duty
11	FOLEFOC G. NGOSONG	Associate Professor	Vice-Dean U.B.
12	KAPNANG Henriette	Associate Professor	on duty
13	KOUAM Jacques	Associate Professor	on duty
14	NOUNGOUE TCHAMO D.	Associate Professor	on duty
15	TCHOUANKEU Jean-Claude	Associate Professor	Head Serv. Chanc. UYI
16	YANKEP Emmanuel	Associate Professor	on duty
17	TIH née NGO BILONG A.	Associate Professor	on duty
18	AMBASSA Pantaleon	Senior Lecturer	on duty

19	EYONG Kenneth OBEN	Senior lecturer	on duty
20	KEUMEDJIO Félix	Senior Lecturer	on duty
21	KEUMOGNE Marguerite	Senior Lecturer	on duty
22	MBAZOA born DJAMA C.	Senior Lecturer	on duty
23	MKOUNGA Pierre	Senior Lecturer	on duty
24	NGO MBING Josephine	Senior Lecturer	on duty
25	NGONO BIKOBO Dominique S.	Senior Lecturer	on duty
26	NOTE LOUGBOT Olivier P.	Senior Lecturer	on duty
27	OUAHOUO WACHE Blandine M.	Senior Lecturer	on duty
28	TABOPDA KUATE Turibio	Senior Lecturer	on duty
29	TAGATSING FOTSING M.	Senior Lecturer	on duty
30	ZONDEGOUMBA Ernestine	Senior Lecturer	on duty
31	FOTSO WABO Ghislain	Assistant	on duty
32	KAMTO Eutrophe Le Doux	Assistant	on duty
33	NGNINTEDO Dominique	Assistant	on duty
34	NGOMO Orléans	Assistant	on duty
6 - DEPARTMENT OF COMPUTER SCIENCE (IN) (25)			
01	TCHUENTE Maurice	Professor	PCA UB
02	ATSA ETOUNDI Roger	Associate Professor	Head Div. MINFOPRA
03	FOTSO Pauline Laure	Associate Professor	Vice-Chancellor UDs
04	FOUDA NDJODO Marcel	Associate Professor	IA4 MINESUP/H. D. ENS
05	NDOUNDAM René	Associate Professor	on duty
06	CHEDOM FOTSO D. E.	Senior Lecturer	on duty
07	LOUKA Basile	Senior Lecturer	Head Dpt.
08	MELATAGIA YONTA Paulin	Senior Lecturer	on duty
09	TINDO Gilbert	Senior Lecturer	on duty
10	TSOPZE Norbert	Senior Lecturer	on duty
11	WAKU KOUAMOU Jules	Senior Lecturer	on duty
12	ABESSOLO ALO'O Gislain	Assistant	on duty
13	BAYEM Jacques Narcisse	Assistant	on duty
14	DJOUWE MEFFEJA Merline	Assistant	on duty
15	EBELE Serge	Assistant	on duty
16	HAMZA Adamou	Assistant	on duty
17	KAMDEM KENGNE Christiane	Assistant	on duty
18	KAMGUEU Patrick Olivier	Assistant	on duty
19	KENFACK DONGMO C. V.	Assistant	on duty
20	KOMGUEM Rodrigue	Assistant	on duty
21	KOUOKAM KOUOKAM E. A.	Assistant	on duty
22	MEYEMDOU Nadège Sylvianne	Assistant	on duty
23	MONTHE DJIAEU V. M.	Assistant	on duty
24	JIOMEKONG AZANZI Fidel	Assistant	on duty
25	TAPANMO KENFACK Hyppolite	Assistant	on duty

7 - DEPARTMENT OF MATHEMATICS (MA) (35)			
01	BEKOLLE David	Professor	Vice-Chancellor UN
02	BITJONG NDOMBOL	Professor	DIPD UY II
03	DOSSA COSSY Marcel	Professor	on duty
04	NGUETSENG Gabriel	Professor	Head of CUTI UYI
05	NOUTCHEGUEME Norbert	Professor	on duty
06	EMVUDU WONO Yves S.	Associate Professor	Head Div. MINESUP
07	NKUIMI JUGNIA Célestin	Associate Professor	on duty
08	TCHAPNDA NJABO S. B.	Associate Professor	on duty
09	TONGA Marcel	Associate Professor	on duty
10	WAMON François	Associate Professor	Head of Dpt.
11	AGHOKENG JIOFACK Jean G.	Senior Lecturer	on duty
12	AYISSI Raoult Domingo	Associate Professor	on duty
13	FOMEKONG Christophe	Senior Lecturer	on duty
14	KIANPI Maurice	Senior Lecturer	on duty
15	KIKI Maxime A.	Senior Lecturer	on duty
16	MBAKOP Guy Merlin	Senior Lecturer	on duty
17	MBANG Joseph	Senior Lecturer	on duty
18	MBIANDA Gilbert	Senior Lecturer	on duty
19	MENGUE MENGUE David Joe	Senior Lecturer	on duty
20	NGUIMTSA Charles	Senior Lecturer	on duty
21	NOUNDJEU Pierre	Senior Lecturer	on duty
22	TCHANGANG Roger Duclos	Senior Lecturer	on duty
23	TCHOUNDJA Edgar Landry	Senior Lecturer	on duty
24	TIAYA TSAGUE N. A.-M.	Senior Lecturer	on duty
25	CHENDJOU Gilbert	Assistant	on duty
26	DJIADEU NGAHA Michel	Assistant	on duty
27	MBEHOU Mohamed	Assistant	on duty
28	MBELE BEDIMA Martin	Assistant	on duty
29	MBIAKOP Hilaire George	Assistant	on duty
30	NGUEFACK Bertrand	Assistant	on duty
31	NIMPA PEFOUNKEU Romain	Assistant	on duty
32	POLA DOUNDOU Emmanuel	Assistant	on duty
33	TAKAM SOH Patrice	Assistant	on duty
34	TANG AHANDA Barnabé	Assistant	H. S. MINPLAMAT
35	TETSADJIO TCHILEPECK M. E.	Assistant	on duty
8 - DEPARTMENT OF MICROBIOLOGY (MB) (13)			
01	ETOA François-Xavier	Professor	Head of Dept.
02	ESSIA NGANG Jean Justin	Associate Professor	Head of Research Division
03	NWAGA Dieudonné M.	Associate Professor	on duty
04	BODA Maurice	Senior Lecturer	on duty
05	BOYOMO ONANA	Senior Lecturer	on duty
06	ENO Anna Arey	Senior Lecturer	on duty

07	ESSONO OBOUGOU Germain	Senior Lecturer	on duty
08	NYEGUE Maximilienne	Senior Lecturer	on duty
09	RIWOM Sara Honorine	Senior Lecturer	on duty
10	SADO KAMDEM Sylvain	Senior Lecturer	on duty
11	BOUGNOM Blaise Pascal	Senior Lecturer	on duty
12	NJIKI BIKOI Jacky	Assistant	on duty
13	TCHIKOUA Rouger	Assistant	on duty
9 - DEPARTMENT OF PHYSICS (PH) (40)			
01	ESSIMBI ZOBO Bernard	Professor	Vice-Dean in charge of (RC)
02	KOFANE Timoléon Crépin	Professor	Head of Dept.
03	NJOMO Donatien	Professor	on duty
04	WOAFO Paul	Professor	on duty
05	NDJAKA Jean Marie B.	Professor	on duty
06	BEN-BOLIE Germain H.	Associate Professor	on duty
07	EKOBENA FOUDA H. P.	Associate Professor	on duty
08	NJANDJOCK NOUCK P.	Associate Professor	Head Div. MINRESI
09	NOUAYOU Robert	Associate Professor	on duty
10	OUMAROU BOUBA	Associate Professor	Chancellor UYI
11	PEMHA Elkana	Associate Professor	on duty
12	TABOD Charles TABOD	Associate Professor	on duty
13	TCHAWOUA Clément	Associate Professor	on duty
14	ZEKENG Serge Sylvain	Associate Professor	on duty
15	BIYA MOTTO Frédéric	Senior Lecturer	Head Serv. UYI
16	BODO Bernard	Senior Lecturer	on duty
17	DJUIDJE KENMOE. G. wife ALOYEM	Senior Lecturer	on duty
18	EDONGUE HERVAIS	Senior Lecturer	on duty
19	EYEBE FOUDA Jean Sire	Senior Lecturer	on duty
20	FEWO Serge Ibraïd	Senior Lecturer	on duty
21	FOUEDJIO David	Senior Lecturer	on duty
22	HONA Jacques	Senior Lecturer	on duty
23	MBANE BIOUELE	Senior Lecturer	on duty
24	MBONO SAMBA Yves C.U.	Senior Lecturer	Vice-Dean UDS
25	NANA NBENDJO Blaise	Senior Lecturer	on duty
26	NDOP Joseph	Senior Lecturer	on duty
27	OBOUNOU Marcel	Senior Lecturer	on duty
28	SAIDOU	Senior Lecturer	on duty
29	SIEWE SIEWE Martin	Senior Lecturer	on duty
30	SIMO Elie	Senior Lecturer	on duty
31	TABI Conrad Bertrand	Senior Lecturer	on duty
32	TCHOFFO Fidèle	Senior Lecturer	on duty
33	VONDOU Derbetini Appolinaire	Assistant	on duty
34	WAKATA born BEYA Annie	Senior Lecturer	Head Div. MINESUP
35	WOULACHE Rosalie Laure	Assistant	on duty

36	ABDOURAHIMI	Assistant	on duty
37	CHAMANI Roméo	Assistant	on duty
38	ENYEGUE A NYAM F. wife BELINGA	Assistant	on duty
39	MBINACK Clément	Assistant	on duty
40	MBOUSSI NKOMIDIO Aissatou	Assistant	on duty
10 - DEPARTMENT OF EARTH SCIENCE (S.T.) (43)			
01	BILONG Paul	Professor	Dean and Head of Dept.
02	NZENTI Jean-Paul	Professor	on duty
03	BITOM Dieudonné Lucien	Professor	Dean / UN
04	FOUATEU Rose wife YONGUE	Associate Professor	on duty
05	KAMGANG Pierre	Associate Professor	on duty
06	MEDJO EKO Robert	Associate Professor	D.I.P.D. UYI
07	MVONDO ONDOA Joseph	Associate Professor	on duty
08	NDAM NGOUPAYOU Jules-R.	Associate Professor	on duty
09	NDJIGUI Paul-Désiré	Associate Professor	on duty
10	NGOS III Simon	Associate Professor	D.A.A.C./ UM
11	NJILAH Isaac KONFOR	Associate Professor	on duty
12	NKOUMBOU Charles	Associate Professor	on duty
13	TEMDJIM Robert	Associate Professor	on duty
14	ABOSSOLO born ANGUE M.	Senior Lecturer	H. Dept. VD/DSSE
15	BEKOA Etienne	Senior Lecturer	on duty
16	BISSO Dieudonné	Senior Lecturer	Dir. P. B. Memvelle
17	EKOMANE Emile	Senior Lecturer	on duty
18	ESSONO Jean	Senior Lecturer	C.E.A. MINIMDT
19	GANNO Sylvestre	Senior Lecturer	on duty
20	GHOGOMU Richard TANWI	Senior Lecturer	on duty
21	LAMILEN BILLA D.	Senior Lecturer	on duty
22	LIENOU Gaston	Senior Lecturer	on duty
23	MBIDA AYEM L.	Senior Lecturer	on duty
24	MINYEM Dieudonné	Senior Lecturer	Dir. Projet Hydro-MIN
25	MOUAFO Lucas	Senior Lecturer	on duty
26	MOUNDI Amidou	Senior Lecturer	Inspector 1 MINIMDT
27	NGO BIDJECK Louise M.	Senior Lecturer	on duty
28	NGUETCHOUA Gabriel	Senior Lecturer	on duty
29	NJOM Bernard de Lattre	Senior Lecturer	on duty
30	NYECK Bruno	Senior Lecturer	on duty
31	ONANA Vincent	Senior Lecturer	C.S. MINIMDT
32	TCHAKOUNTE J. wife NUMBEN	Senior Lecturer	on duty
33	TCHOUANKOUE Jean-Pierre	Senior Lecturer	on duty
34	YENE ATANGANA Joseph Q.	Senior Lecturer	on duty
35	ZO'O ZAME Philémon	Senior Lecturer	Secretary General MINTP
36	ANABA ONANA Achille B.	Assistant	on duty
37	FUH Calistus Gentry	Assistant	on duty

38	METANG Victor	Assistant	on duty
39	NGO BELNOUN Rose Noël	Assistant	on duty
40	NOMO NEGUE Emmanuel	Assistant	on duty
41	TCHAPTCHET TCHATO De Pesquidoux I.	Assistant	on duty
42	TEHNA Natanael	Assistant	on duty
43	TEMGA Jean Pierre	Assistant	on duty

SHARING OF LECTURERS IN THE FACULTY OF SCIENCE ACCORDING TO DEPARTMENTS
(10 September 2014)

DEPARTMENT	**NUMBER OF LECTURERS**				
	Prof.	**Ass. Prof.**	**Sen. Lect.**	**Asst.**	**Total**
BC	2 (0)	7 (2)	17 (11)	15 (6)	**41 (19)**
BPA	8 (0)	7 (0)	15 (7)	15 (5)	**45 (12)**
BPV	1 (0)	5 (0)	13 (3)	6 (5)	**25 (8)**
C.I.	3 (0)	14(2)	14 (3)	2 (0)	**33 (5)**
C.O.	9 (0)	9 (2)	12 (6)	4 (0)	**34 (8)**
IN	1 (0)	4 (1)	6 (0)	14 (4)	**25 (5)**
MA	5 (0)	5 (0)	14 (1)	11 (1)	**35 (2)**
MB	1 (0)	2 (0)	7 (3)	3 (0)	**13 (3)**
PH	5 (0)	9 (0)	21 (3)	5 (2)	**40 (5)**
ST	2 (0)	11 (1)	22 (3)	8 (1)	**43 (5)**
Total	**37 (0)**	**73 (8)**	**141 (40)**	**83 (23)**	**334 (72)**

So a total of: 334 (72) with
- Professors 37 (0)
- Associate Professors 73 (8)
- Senior Lecturers 141 (40)
- Assistants 83 (23)
- () = Number of Women.

Dedications

I dedicate this dissertation to my family, especially:

To my late Father **NANGUE Clément** and my Mother **TONFACK Jeanne** for giving birth to me;

To my Children **NANGO Elvy Lucresse, TSAFACK Beryl Fadel and NGOGUI Larry Elisson**, whose future is motivated by this work.

Acknowledgements

The work presented in this thesis is a result of collaboration of many persons that have contributed, each one at his/her level to iimprove the quality of this thesis. Their support and assistance can never be overestimated.

First of all, I thank the Almighty GOD, for giving me all the strength, inspiration and courage to do this work.

My sincere thanks go to one of my Co-supervisors **Pr. Samuel Domngang**, for accepting me into his group. His constant encouragements, motivation, enthusiasm and immense knowledge made this work successful.

I would like to express my sincere gratitude to my other Co-supervisor: **Pr. Jean-Pierre Nguenang** for giving the project title and accepting to co-supervise it, availability, advices, scrutiny, excellent guidance, encouragement and support.

I am indebted to **Pr. Kenfack-Jiotsa Aurelien** for the patience to teach me in numerical methods, for his encouragement and insightful comments and questions. His guidance helped me throughout the research and writing of this thesis.

I would like to thank **Members of Jury** who have accepted to evaluate the present work.
I would like to thank all the teachers who taught me from Primary school to University level, with a particular emphasis on the teaching staff of the Departments of Physics of the Faculty of Science of the University of Yaounde I, the Higher Teachers Training College and the National Advanced School of Engineering; I am particularly grateful to **Pr. Kofané Timoléon Crépin, Pr. Ndjaka Jean-Marie, Pr. Zekeng Serges Sylvain, Pr. Tchawoua Clement, Dr. Tchoffo Fidèle, Pr. Beguide Bonoma, Pr. Owono Owono Luc Calvin, Dr. Gnokam Edmond, Dr. Mbouga Jean Marie, Dr. Ndop Joseh, Pr. Tonyé Emmanuel, Dr. Fotsing Janvier and Dr. Bossou Olivier**.
I would like to thank the **Abdus Salam International Centre for Theoretical Physics** (ICTP) and the **International Atomic Energy Agency** (IAEA) for their International school on Non-linear Dynamics in complex systems organized from 31 october to 11 November 2011 in Yaounde, that helped me to learn many things in classical and quantum breathers in non-linear and complex systems.

I express my gratitude to **Dr. Lekeufack Olivier, Dr. Tala Tebue Eric, Dr. Sitamze, Dr. Kenmogne Fabien, Dr. Lontsi Agostiny Marrios, Dr. Fotué Alain, Dr. Djemmo Pascal and Dr. KOUEMO Magloire** for many fruitful discussions. I can not forget their availability and help.

I would like to thank my family for their ecouragement moral and financial support. I thank my senior brother **Nango Mathias** who has supported me since the beginning of my studies. To my brothers **Fofack Jean Marie, Zago Agoss, Amboudem Fidèle, Tsafack Yves Rémi, Assonfack Fidèle** and to my sister **Awoundji Isabel** for their moral assistance.

I would like to thank my wife, **Beasso Angèle Flore**. She was always there cheering me up and stood by me through out the good and bad times.

I would like to thank all my colleagues teachers in BOT MAKAK and ZAMENGOE Government High School for their multiple encouragements during the development of this work, especially **Dr. Kengap Tankeu Rodrigue, Stague Pierre Alain, Mbimbipé Etiènne, Mbezelé Ernest** for their encouragements. This work is the result of all your efforts.

I owe a particular thanks to all my friends especially **Nango Esaie, Djoumekop Jean Basil, Teudem Hubert, Boning Lambert, Tchouansseu Blanchard, Songoung Pierre, Mboutsui Gutembert, Mboutsui Marie, Temgoua Etienne, Tsagué Yves, Tsafack Bodelin, Tanékeu Paulin,Demessée Rigobert, Mboudem Avi Bertrand** for their encouragement.

I would like to thank my family in-law in particular **Donfack Achille and Mbona Augustin**, for their moral assistance and all their encouragements.

Finally, I would like to thank anyone that has in anything to the successful realization of this thesis.

List of Abbreviations

DMI: **D**zyaloshinsky **M**oriya **I**nteraction
DBs: **D**iscrete **B**reathers
ILM: **I**ntrinsic **L**ocalized **M**odes
FPU: **F**ermi **P**asta **U**lam
DNLS: **D**iscrete **N**onlinear **S**chrodinger
qBs: **q**-**B**reathers
QBs: **Q**uantum **B**reathers
RAM: **R**andom **A**ccess **M**emory
GMR: **G**iant **M**agnetoResistive
TMR: **T**unnel **M**agnetoResistive

Contents

List of the Permanent Teaching Staff i

Dedications xi

Acknowledgements xii

List of Abbreviations xiv

Contents xv

List of Figures xix

Abstract xxiv

Résumé xxv

General Introduction 1

Chapter 1 Literature Review and Problems 6

Literature Review and Problems 6

1.1 Generalities on Magnetism 6

1.1.1 Microscopical Origin of magnetism 6

1.1.2 Types of magnetism 7

1.1.3 Magnetic Domains 9

1.2 General form of the spin chains Hamiltonian 10

1.3 Excitations in Magnetic Systems 12

1.3.1 Excitations of ferromagnets in the Heisenberg model 12

1.3.2 Excitations of antiferromagnets in the Heisenberg model 13

1.3.3 Importance of excitations in magnetic systems 13

1.4 Breather 16

1.4.1 Spatial Discreteness and Nonlinearity 16

1.4.2 Examples of Discrete breather solutions 18

1.5 Basic classical Properties of Discrete Breathers 20

1.6 Fermi-Pasta-Ulam Problem 21

1.7 q-breathers 21

1.8 Quantum breathers 22
1.8.1 The Bose-Hubbard chain and related models 23
1.8.2 Dimer and trimer 23
1.8.3 Large lattices with fluctuating numbers of quanta 24
1.8.4 Applications of discrete and quantum breathers 24
1.9 Conclusion 24

Chapter 2 Methodology **25**

Methodology **25**
2.1 Introduction 25
2.2 Particle-number representation: General formalism 25
2.2.1 Second quantization: General formalism 26
2.3 Perturbation methods 29
2.3.1 Stationary perturbation method 29
2.3.2 Nondegenerate perturbation theory 30
2.3.3 Degenerate perturbation theory 32
2.4 Model Hamiltonian 34
2.5 Semi-fermions 36
2.6 Holstein-Primakoff transformation 37
2.6.1 Number of state method 38
2.6.2 Case of non degenerate perturbation method applied to the ground state 39
2.6.3 Case of non degenerate perturbation method applied to the first excited state 39
2.6.4 Case of non degenerate perturbation theory applied to the second excited state 40
2.6.5 Effect of the anisotropy interaction in the Heisenberg ferromagnetic spin chain Model 42
2.6.6 Application of degenerate theory when four or six bosons are involved in the extended Bose-Hubbard chain 42
2.7 Effect of the DMI in the Heisenberg anisotropic exchange ferromagnetic spin chain Model 45
2.7.1 The ground state when DMI are involved 46
2.7.2 The first excited state when DMI are involved 46
2.8 Effect of the long range interaction in a Heisenberg isotropic exchange ferromagnetic spin chain model 47
2.8.1 Effect of the second nearest neighbor 47
2.8.2 Effect of the third, fourth nearest neighbor and generalization . . . 48
2.8.3 Effect of long range interactions when four or six quanta are involved 49
2.9 Localization in the space of normal mode 50

2.10 Conclusion 52

Chapter 3 Results and Discussion **53**

Results and Discussion **53**

3.1 Introduction 53
3.2 Energy spectra in a finite Heisenberg isotropic exchange spin chain 53
3.2.1 Energy at the ground state 53
3.2.2 Energy spectrum for one boson in the model 53
3.2.3 Energy spectrum for the two-boson in the model 54
3.2.4 Effect of the exchange and anisotropy interactions on the two-bosons state energy spectrum 55
3.2.5 Energy spectrum for the four or six bosons in the extended Bose-Hubbard chain 58
3.3 Energy spectra in a finite Heisenberg anisotropic exchange spin chain with antisymmetric interactions 63
3.3.1 Energy at the ground state when DMI are involved 63
3.3.2 Energy spectrum for one boson in the model when DMI are involved 63
3.3.3 Effect of the DMI on the energy spectrum of a planar ferromagnet for two bosons 64
3.3.4 The Heisenberg exchange interaction's impact on the energy spectrum for two bosons when the DMI are involved 66
3.3.5 Effect of the DMI on the energy spectrum of the spin chain when four or six quanta are involved 69
3.4 Energy spectra in a Heisenberg spin chain with long range interactions . . . 75
3.4.1 Influence of the second nearest interaction on the energy spectrum . 75
3.4.2 Influence of the third and fourth nearest neighbor on the energy spectrum 77
3.4.3 Effect of long range interactions on the energy spectrum when four or six quanta are involved 81
3.5 Localization in real space 92
3.5.1 In a Heisenberg spin chain 92
3.5.2 In a Heisenberg spin chain with antisymmetric interactions 93
3.5.3 In a Heisenberg spin chain with longer range interactions 95
3.6 Localization in the space of normal mode 103
3.7 Conclusion 106

General Conclusion **107**

Bibliography **111**

List of Publications **119**

Appendix **120**

List of Figures

Figure 1.1 Motion of electron. 7
Figure 1.2 Types of magnetism:(a)Ferromagnetism; (b) Antiferromagnetism; (c) Ferrimagnetism and (d)Paramagnetism 8
Figure 1.3 (a) Magnetic structures with one and two domains, and the lines of the induced magnetic field; Rotation of the magnetic moment for domain walls in the (y, z) plane (b) Bloch wall and (c) Néel wall (figure adapted from [79]) 10
Figure 1.4 Excitations of ferromagnets: (a) ground state; (b)-(c) symmetry in the chain; (d) a single defect 12
Figure 1.5 Excitations of antiferromagnets: (a) ground state or Néel state; (b) excited state (magnon ΔS=1); (c) excited state (spinon ΔS=1/2) . . 13
Figure 1.6 Magnetic data storage from Encyclopedia of Nanoscience and Nanotechnology 14
Figure 1.7 Reading (and writing) data from a disk,Typical data speed: 120MB/sec. From Encyclopedia of Nanoscience, Nanotechnology [80] 15
Figure 1.8 The frequency versus wave-number dependence of the linear spectrum for a one dimensional chain of anharmonic oscillators with potentials (1.15). The chosen DBs frequencies are marked with green arrows and they lie outside the linear spectrum, ω_q. Red circles indicate the oscillator displacements for a given DBs solution, with all velocities equal to zero. Lines connecting circles are guides for visualization (Figure adapted from [6]) 19

Figure 2.1 Example: 1D lattice, 4 sites and 7 quanta (bosons) 38

Figure 3.1 Energy spectrum of one boson in the extended Bose-Hubbard chain . 54
Figure 3.2 Energy spectrum of the two boson in the extended Bose-Hubbard chain; Here the value of the interaction strength $\gamma = 1$, $n = 2$ and $f = 37$ 55
Figure 3.3 Energy spectrum of the two bosons in the extended Bose-Hubbard chain for different values of exchange interaction and anisotropy parameter where the value of the interaction strength is $\gamma = 1$, $n = 2$, $J = 23.6$ and $f = 37$: (a) $A = 9$; b) $A = 36$; (c) $A = 48$ and (d) $A = 70$. 56

Figure 3.4 Energy spectrum of the two boson in the extended Bose-Hubbard chain for different values of exchange integral parameter where the value of the interaction strength is $\gamma = 1$, $n = 2$, $A = 9$ and $f = 37$: (a) $J = 9$; (b) $J = 4$; (c) $J = 2$ and (d) $J = 0.5$ 57

Figure 3.5 (color online) a) Detail of the Energy Spectrum for the Bose-Hubbard model derive from the anisotropic Heisenberg model in a periodic lattice where $n = 4$, $f = 37$, $J = 22$ and $\gamma = 0.75$: repulsive for $A = 7$ 59

Figure 3.6 Detail of the Energy Spectrum for the extended Bose-Hubbard model, here $n = 6$, $f = 37$: a) case of repulsive nonlinearity where $A = 8$ and $J = 20$, $\gamma = 0.5$; (b) case of repulsive nonlinearity where $A = 9$ and $J = 16$, $\gamma = 0.25$; (c) case of repulsive nonlinearity where $A = 9$; $J = 26$ and $\gamma = 0.17$ 60

Figure 3.7 Detail of the Energy Spectrum for the Bose-Hubbard model derived from an anisotropic Heisenberg model in a periodic lattice where $n = 6$, $f = 37$, $J = 23.6$ and $A = 9$ corresponding to the $\{2, 4\}$ band: (a) case of repulsive nonlinearity where $\gamma = 1$; (b) case of repulsive nonlinearity where $\gamma = 0.5$ 62

Figure 3.8 (a) Detail of the Energy Spectrum where $A = 9.5$, $n = 6$, $f = 37$, $J = 21$ and $\gamma = 0.17$ 62

Figure 3.9 Energy spectrum of one boson for a Heisenberg spin chain with DMI for different values of J_1 and D_z where $J_2 = 0.0$: (a) $J_1 = 0.5$, $D_z = 1.0$; (b) $J_1 = D_z = 0.5$; (c) $J_1 = 1.0$, $D_z = 0.05$ 64

Figure 3.10 Generation of the energy spectrum of a two domain wall by appearance and shifting of a degenerated point in the energy spectrum of two-quanta for a Heisenberg spin chain with DMI for different values of D_z. Here the value of the interaction strength is $\gamma = 1$, $n = 2$, $J_1 = 1$, $J_2 = 0.0$ and $f = 101$: (a) $D_z = 0.0$; (b) $D_z = 0.25$; (c) $D_z = 1$; (d) $D_z = 17.5$ 65

Figure 3.11 Backward shifting process of the degenerated point in energy spectrum of two-quanta in a Heisenberg spin chain with DMI for different values of J_1 where the value of the interaction strength is $\gamma = 1$, $n = 2$, $J_2 = 0.0$, $D_z = 17.5$ and $f = 101$: (a) $J_1 = 1$; (b) $J_1 = 10$; (c) $J_1 = 25$; (d) $J_1 = 600$ 67

Figure 3.12 Energy spectrum of two-quanta in Heisenberg spin chain with DMI for different values of J_2 where the value of the interaction strength is $\gamma = 1$, $n = 2$, $J_1 = 1$ and $f = 101$: (a) $J_2 = 0.5$ and $D_z = 0.0$; (b) $J_2 = 6$ and $D_z = 0.0$; (c) $J_2 = 8$ and $D_z = 1.5$ 68

Figure 3.13 Band structure of two-quanta in Ising and DMI spin chain for different values of J_2 where the value of the interaction strength is $\gamma = 1$, $n = 2$, $J_1 = 0$ and $f = 101$: (a) $J_2 = 0.0$ and $D_z = 0.1$; (b) $J_2 = 0.1$ and $D_z = 0.1$; (c) $J_2 = 0.9$ and $D_z = 0.1$ 69

Figure 3.14 Detail of the energy spectrum for the extended Bose-Hubbard model derived from the Heisenberg spin chain and DMI in a periodic lattice containing four quanta for different values of the DMI where $A = 7$, $n = 4$, $\gamma = 0.05$, $f = 101$ and $J_1 = 1$: (a) $D_z = 0.0$; (b) $D_z = 0.075$; (c) $D_z = 0.5$, (d) $D_z = 1$; (e) $D_z = 1.5$; (f) $D_z = 75$ 70

Figure 3.15 Detail of the energy spectrum for the extended Bose-Hubbard model derived from the Heisenberg spin chain and DMI in a periodic lattice containing four quanta for different values of the J_1 where $A = 7$, $n = 4$, $\gamma = 0.05$, $f = 101$ and $D_z = 1$: (a) $J_1 = 0.0$; (b) $J_1 = 0.075$; (c) $J_1 = 0.5$; (d) $J_1 = 1$ and $\gamma = 0.05$; (e) $J_1 = 1.5$; (f) $J_1 = 75$ . . . 72

Figure 3.16 Detail of the energy spectrum for the extended Bose-Hubbard model derived from the Heisenberg spin chain including DMI in a periodic lattice containing six quanta for different values of the D_z, where $A = 7$, $n = 4$, $\gamma = 0.05$, $f = 101$ and $J_1 = 1$: (a) $D_z = 0.0$; (b) $D_z = 0.5$; (c) $D_z = 2$; (d) $D_z = 50$ 73

Figure 3.17 Energy spectrum for the extended Bose-Hubbard model derived from the Heisenberg spin chain and the DMI in a one periodic lattice containing six quanta for different values of D_z where, $A = 7$, $\gamma = 0.05$ and $f = 101$: (a) $D_z = 0.$ and $J1 = 1$, (b) $D_z = 0.5$ and $J_1 = 100$ 74

Figure 3.18 Energy spectrum of two bosons interacting with second nearest neighbors in the heisenberg chain where $f = 101$: (a) for $\alpha_1 = 0$ and $\gamma_1 = 0.05$; (b) for $\alpha_1 = 0$, $\gamma_1 = 0.5$; (c) for $\alpha_1 = 0.241$, $\gamma_1 = 0.5$ and $\xi_1 = 0.12$; (d) for $\alpha_1 = 0.6$, $\gamma_1 = 0.5$ and $\xi_1 = 0.3$ 77

Figure 3.19 Energy spectrum of two bosons interacting with third and fourth nearest neighbors in the heisemberg spin chain where $f = 101$ and $\gamma_1 = 0.5$: (a) case of third nearest neighbors for $\alpha_1 = 0.8$ and $\xi_1 = 0.4$, $\alpha_2 = 0.241$ and $\xi_2 = 0.12$; (b) case of fourth nearest neighbors, for $\alpha_1 = 0.8$ and $\xi_1 = 0.4$, $\alpha_2 = 0.241$ and $\xi_2 = 0.12$, $\alpha_3 = 0.1$ and $\xi_3 = 0.05$ 78

Figure 3.20 Excitation spectrum of four bosons in the band $\{2, 2\}$ interacting with second nearest neighbors in the extended Bose-Hubbard spin chain of different values of α_1^2 where $A = 1$, $\gamma_1 = 0.5$ and $f = 101$: (a) first nearest neighbors for $\alpha_1^2 = 0$; (b) second for $\alpha_1^2 = 0.4$; (c) second for $\alpha_1^2 = 0.8$ 83

Figure 3.21 Excitation spectrum of four bosons in the $\{2, 2\}$ band interacting with third nearest neighbors in the extended Bose-Hubbard spin chain for different values of α_1^2 and α_2^2 where $A = 1$, $\gamma_1 = 0.5$ and $f = 101$: (a) for $\alpha_1^2 = 0.8$ and $\alpha_2^2 = 0.34$; (b) for $\alpha_1^2 = 0.8$ and $\alpha_2^2 = 0.6$ 85

Figure 3.22 Excitation spectrum of the extended Bose-Hubbard model derived from the Heisenberg spin chain in a periodic lattice containing six bosons in $\{4,2\}$ band and $\{2,4\}$ band interacting with first, second and third nearest neighbors for different values of α_1^2 and α_2^2 where $A = 0.1$, $\gamma_1 = 0.5$ and $f = 101$: (a) first nearest neighbors for $\alpha_1^2 = 0$; (b) second nearest neighbors for $\alpha_1^2 = 0.8$; (c) third nearest neighbors for $\alpha_1^2 = 0.8$ and $\alpha_2^2 = 0.6$ 86

Figure 3.23 Excitation spectrum of the extended Bose-Hubbard model derived from the Heisenberg spin chain in a periodic lattice containing six bosons in the $\{3,3\}$ band interacting with, first second and third nearest neighbors for different values of α_1^2 and α_2^2 where $A = 0.1$, $\gamma_1 = 0.5$ and $f = 101$: (a) first nearest neighbors for $\alpha_1^2 = 0$; (b) second nearest neighbors for $\alpha_1^2 = 0.8$; (c) for third nearest neighbors $\alpha_1^2 = 0.8$ and $\alpha_2^2 = 0.4$ 91

Figure 3.24 Square of the wave function amplitudes corresponding to the eigenvectors as a function of the position of the band along the chain: (a) case of the band located on the energy spectrum in Fig. 3.2, 3.3, 3.4 and 3.8; (b) case of the band in Fig. 3.5; (c) case of the band in Fig. 3.6 and 3.7 92

Figure 3.25 Square of the normalized Eigenfunctions of the localized states located on the energy spectrum: (a) case of the band at the bottom (red color) located in Fig.3.12 and in Fig.3.13(b)- 3.13(c); (b) case where both bound states (red and cyan color) are chosen in Fig.3.16; (c) case of two symmetric bound states (red and magenta color) located in Fig.3.17; (d) Plot of the eigenfunction in log-scale as function of the site number for the case of $k = \pi/4$. The dashed lines added allows to realize the exponential decay of the eigenfunction. 94

Figure 3.26 Square of the normalized Eigenfunctions of the single band (blue square symbols) located below the continuum band in Fig.3.18(b),(d) and Fig.3.19(a): (a) case of first nearest neighbors; (b) case of second nearest neighbors; (c) case of third nearest neighbors 96

Figure 3.27 Square of the normalized Eigenfunctions of the single band (red circle symbols) located above the continuum band in Fig.3.18(b),(d) and Fig.3.19(a): (a) case of first nearest neighbors; (b) case of second nearest neighbors; (c) case of third nearest neighbors 97

Figure 3.28 Square of the normalized Eigenfunctions of the single band (cyan triangle up symbols) located between the continuum and the upper band in Fig.3.18(d) and Fig.3.19(a): (a) case of second nearest neighbors; (b) case of third nearest neighbors 98

Figure 3.29 Square of the normalized Eigenfunctions of the single band (blue color with square symbols) located below the continuum band in Fig.3.20(b) and Fig.3.21(a): case of second nearest neighbors and third nearest neighbors 98
Figure 3.30 Square of the normalized Eigenfunctions of the single band (red color with circle symbols) located above the continuum band in Fig.3.20(a)-(c) and Fig.3.21(a): (a) case of first nearest neighbors; (b) case of second nearest neighbors; (c) case of third nearest neighbors 99
Figure 3.31 Square of the normalized Eigenfunctions of the single band (cyan color with triangle up symbols) located above the continuum band in Fig.3.20(c) and Fig.3.21(a) : (a) case of second nearest neighbors; (b) case of third nearest neighbors 100
Figure 3.32 Square of the normalized Eigenfunctions of the single band (indigo color with triangle left symbols) located above the continuum band in Fig.3.21(a): case of second and third nearest neighbors 100
Figure 3.33 Square of the normalized Eigenfunctions of the single band (blue color with triangle left symbols) located below the continuum band in Fig.3.22(a)-(c): (a) case of first nearest neighbors; (b) case of second nearest neighbors; (c) case of third nearest neighbors 101
Figure 3.34 Square of the normalized Eigenfunctions of the single band (red color with triangle right symbols) located above the continuum band in Fig.3.22(a)-(c): (a) case of first nearest neighbors; (b) case of second nearest neighbors; (c) case of third nearest neighbors 102
Figure 3.35 Square of the normalized Eigenfunctions of the band localized on the energy spectrum in Fig.3.23(a)-(c): case of bands (blue color with square symbols and cyan color with triangle left) 103
Figure 3.36 (Color online) Weight function: (a) for different values of the interaction γ where $f = 101$, $J_2 = J_1 = 1$, $D_z = 0$, $k = 0$ and $\widetilde{k}_1 = \frac{\pi}{2}$; (b) for different sizes of the system where $\gamma = 0.01$, $J_2 = J_1 = 0.5$, $D_z = 0.5$, $k = 0$ and $\widetilde{k}_1 = -\frac{2}{3}\pi$; (c) for different values of exchange interaction J_2 and J_1 where, $\gamma = 1$, $f = 101$, $D_z = 0.5$, $k = \frac{\pi}{2}$ and $\widetilde{k}_1 = -\frac{\pi}{4}$; (d) for different values of DMI D_z where, $\gamma = 1$, $J_2 = J_1 = 23.6$, $f = 101$, $D_z = 0.5$, $k = \frac{\pi}{2}$ and $\widetilde{k}_1 = -\frac{\pi}{4}$. Dashed lines are results using approximation formula Eq.(2.133), Eq.(2.134) and Eq.(2.135). 104
Figure 3.37 (Color online) Weight function: (a) for different values of DMI D_z in log-log scale, the same as in Fig. 3.36(d) where, $\gamma = 1$, $J_2 = J_1 = 1$, $f = 101$, $D_z = 0.5$, $k = \frac{\pi}{2}$ and $\widetilde{k}_1 = -\frac{\pi}{4}$; (b) for different values of $\widetilde{k}_1$ where $\gamma = 1$, $J_2 = J_1 = 0.5$, $D_z = 3.1$, $f = 101$ and $k = \frac{2}{3}\pi$ 105

Abstract

A study of the likelihood of quantum breathers in a 1D Heisenberg spin chain including a Dzyaloshinsky-Moriya and a longer range interaction is done through an extended Bose-Hubbard model. The energy spectrum of the resulting Bose-Hubbard Hamiltonian, on a periodic one-dimensional lattice containing more than two quanta involving spin switches shows interesting detailed band structures. These fines structures are studied using non degenerate and degenerate perturbation theories in addition to a numerical diagonalization. The attention is focussed on the effects of various interactions that are: the anisotropy, the Heisenberg isotropic exchange interaction, the Dzyaloshinsky-Moriya Interaction (DMI), the Heisenberg in-plane (X,Y) as well as the out of plane exchange interaction, the second, third and fourth nearest-neighbors on the energy spectrum of the system. The outcome displays a possibility of an energy self-compensation in the system and the presence of new localized bound states. The signature of the quantum breather is also set up by the computation of the eigenfunctions of new localized bound states that stand as the precursor for local magnetization reversal process when many nearest neighbors are involved. From a non degenerated perturbation theory it is shown that the interaction between the quanta leads to an algebraic localization of the modified extended states in the normal-mode space of the non-interacting system that are coined quantum q-breathers excitations.

Keywords: Quantum Breathers; Heisenberg spin chain; Bose-Hubbard lattice; Dzyaloshinsky-Moriya Interaction.

Résumé

Une étude des excitations quantiques de type breathers dans des réseaux unidimensionnels de spin, incluant des interactions de Dzyaloshinsky-Moriya d'une part, de grande portée d'autre part, est faite à travers un modèle de Bose-Hubbard, à l'image des chaînes d'Heisenberg. Le spectre d'énergie resultant des Hamiltoniens de Bose-Hubbard correspondant, sur un réseau périodique unidimensionnel contenant plus de deux quanta comportant des commutateurs de spins montre des structures de bandes intéressantes. Ces structures sont étudiées en utilisant la théorie des perturbations non dégénérée et dégénérée associée à la diagonalisation numérique. Notre attention est focalisée sur les effets des diverses interactions qui sont: l'anisotropie, l'interaction d'échange isotrope d'Heisenberg, l'interaction Dzyaloshinsky-Moriya (IDM), l'interaction d'échange d'Heisenberg dans le plan (X,Y) aussi bien que dans le plan Z, les interactions de second, troisième et quatrième proches voisins sur le spectre d'énergie du système. Les résultats suggèrent une possibilité d'autocompensation de l'énergie dans le système et la présence des nouveaux états localisés. La signature du breathers quantique est également mise en place par le calcul des fonctions propres des nouveaux états localisées qui se présentent comme des précurseurs du processus de retournement locale de l'aimantation où de nombreux plus proches voisins sont impliqués. Partant d'une théorie des perturbations non dégénérée, il est démontré que l'interaction entre les quanta conduit à une localisation algébrique des états étendus modifiés dans l'espace de modes normaux du système sans interaction qui sont des excitations quantiques de type breather que l'on dénomme q-breathers.

Mots clés: Breathers Quantiques; chaîne de spins de Heisenberg; réseau quantique de Heisenberg; modèle de Bose-Hubbard; interaction de Dzyaloshinsky-Moriya

General Introduction

Magnetization reversal process is known to be a spin switching property that can be obtained through an understanding of the underlying dynamics in magnetic systems. Magnetization switching process has gained numerous importances thanks to the success and development of random access memories. This process is normally based on a coherent rotation of magnetization and domain walls in the presence of a magnetic field. Another approach when the magnetic field is not necessarily applied that assume its importance is the magnetization switching by stress induced anisotropy and thermal activation [1, 2]. Most often, among the various approaches, magnetization switching occurs locally but tends to propagate along the lattice. In our present study, we propose that based on the electronic properties of the atoms constituting, a magnetic material, bosonic excitations can be a good candidate for activating localized magnetization reversal processes in ferromagnets whenever a magnetic field is not applied. For a nice localized process, first of all the lattice should be discrete and a good candidates for such a process are discrete breathers. Discrete breathers have received considerable attention in recent years, in the phenomenon of localization and transport of energy in discrete lattices, both from the theoretical and experimental investigations points of view [3–6]. These excitations are generic time-periodic and spatially localized solutions of the underlying classical Hamiltonian lattice with translational invariance. They can modify system's properties such as lattice thermodynamics and introduce the possibility of non dispersive energy transport. An attempt to connect them with biological functions could be assisted by the help of a model for bio-molecular system. Ivestigations on discrete breathers or intrinsic localized modes in recent years has revealed a wealth of new properties of classical energy localization in many physical systems. Their spatial profiles localize exponentially for short-range interactions. Recently, the application of these ideas to the normal-mode space has allowed to explain some facets of the Fermi-Pasta-Ulam (FPU) paradox [7–11]. The problem consists of the nonequipartition of energy among normal modes of a weakly anharmonic atomic model. In the harmonic limit, each normal mode corresponds to a periodic orbit in phase space and is characterized by its wavenumber q. Such an investigation of localized excitations in normal modes space from the harmonic limit into the FPU parameter

regime allowed to realize the persistence of periodic orbits, termed q-breathers. In the normal mode space, although the interaction is long ranged, it is selective and purely nonlinear, thus q-breathers localize exponentially for classical investigations.

Quantum breathers consist of superpositions of nearly degenerate many-quanta bound states, with very long times to tunnel from one lattice site to another [5]. These quantum excitations although being extended states in a translationally invariant system are characterized by exponentially localized weight functions, in full analogy to their classical counterparts.
Studies of quantum modes on small lattice are of interest for quantum devices based on quantum dot, for studies of photonic crystals, Josephson junction arrays [12, 13], arrays of weakly coupled waveguides, protein-like crystals [14], and possibly in myoglobin [15], for the studies of Bose-Einstein condensates in periodic optical traps [16], light propagation in interacting optical waveguide, cantilever vibrations in micromechanical arrays. It has also been shown that the intrinsic localized modes can occur in isotropic ferromagnetic chains [17]. In many cases, quantum dynamics is important.
Discrete breathers are nonlinear localized modes that can be created in translationally invariant nonlinear lattice models. They can modify the system's property such as the thermodynamics of lattice and introduce the possibility of non dispersive energy during its transport. Investigations of discrete breathers or intrinsic localized modes in recent years has revealed a wealth of new properties of energy localization [18]. The study of the spectrum and eigenstates of the quantum breathers is less known for the case of system containing more than two bosons. Indeed there are several published papers for the case of two bosons. For instance, Nguenang et *al* [19] investigated the localization properties of the eigenstates in a finite Bose-Hubbard chain and they observe localization of the weight function as a function of the wave number, which they interpret as a signature of quantum q-breather excitations displaying an algebraic decay, at variance to the exponential decay of the q-breathers in the case of a classical nonlinear systems [19]. Two-Vibron Bound States has been investigated in the $\beta-$ Fermi-Pasta-Ulam model [20] as well as in ref. [21–28, 30]. The most extensively studied system is the quantum discrete nonlinear Schrödinger equation with two particles (a dimer). This system is integrable due to the existence of two integral of motion (energy and boson number). The classical version can be completely solved. Bernstein et *al.* [31–35] and Aubry et al. [36] studied the expected splitting of degenerate pairs of eigenvalues in the quantum system. Less is known for systems with many degrees of freedom. Dorignac et al. [11] and J. C. Eilbeck [30] are the first to study the spectrum of the quantum discrete nonlinear Schrödinger

equation, in the case of four and six bosons using degenerate perturbation theory. The output suggested exponentially small band widths for quantum breather bands with large boson number [21, 30, 31].

However, the existence of discrete breathers in ferro and anti-ferromagnetic spin chains with many other interactions like the anti-symmetric interaction proposed by Dzyaloshinsky [37] and Moriya [38–40] that is designed to describe weak ferromagnet has not been investigated so far to probe intrinsic localized modes. Weak ferromagnet plays an important role in describing insulators, spin glasses and low temperature phases of copper oxide super conductor [41], and more recently it opened up some new possibilities in data storage technologies [42]. Indeed the DMI has been the subject of many theoretical and experimental investigation during the recent years. Most of theoretical studies are focussed on the role of this interaction in the magnetic behavior. It was shown that DMI can be significant in the magnetic behavior of Kagome lattice which are allowed by the low symmetry [43]. They can determine the chirality of the magnetic ground state and more over chiral magnetic ordering that are due to DMI, can explain much the dynamics of the systems discussed in Ref. [44, 45], in particular the splitting and dispersion of the triplet modes [46], suppresses quantum fluctuations, driving the system to a more classical ground state [47]. Segienko et al. [48] have shown that the role of the DMI in multiferrioc perovskite is to provide the microscopic mechanism for the coexistence of strong coupling between ferroelectricity and incommensurate magnetism. Other interesting effects in systems with DMI exist such as the field-induced gap phenomena and a peculiar energy level structure [49, 50]. Experimentally, Zorko et *al* could explain why the DMI is the dominant magnetic anisotropy term in the Kagome spin $-\frac{1}{2}$ compound $Z_nCu_3(OH)_6Cl_2$ using analysis of the high - temperature electron spin resonance [51, 52]. Oren ofer explained why geometrically frustrated magnets are ideal to explore perturbation beyond the Heisenberg model and demonstrated that exchange anisotropy is a relevant perturbation in the Kagome lattice that contributes to its ground-state properties [53]. Other authors have argued that DMI is also important especially at low temperature. The above cited work on theoretical and experimental investigations on DMI effects are just a few among others.

It is worth mentioning the fact that one dimensional (1D) quantum magnetism [54] exhibits a variety of interesting phenomena thanks to their signifying quantum spin nature. Various models of spin chain have been proposed with different ranges of interactions such as, spin-Peirels states [55, 56], and many others to investigate various phenomena. For instance, the behavior of quantum entanglement in frustrated spin systems was studied by many authors [57–61], and its importance for

resonance in quantum information processing to describe quantum teleportation was set up [62]. In regarding to our study it is worth mentioning that the necessity of considering next-nearest neighbors has been prove in the studies of the entanglement state between two spins in Heisenberg spin chain [63–67], even in the investigation entanglement in three-qubit Heisenberg model [68].

In another viewpoint, longer range interactions was considered for the study of ground state properties of the 1D isotropic spin -1/2 Heisenberg antiferromagnet [69–71]. These next-nearest neighbor interactions leads, in general, to a competition of interactions which in turn gives rise to the dimer state where neighboring spins end with forming singlet pair [72, 73]. In the same spirit the fidelity for the Heisenberg chain was probed with aim to find its connection with quantum phase transition [74].

However, in the case of Heisenberg spin system few studies where devoted to classical discrete breathers within the modulational instability framework [75]. Recently in 2001, Y. Zolotaryuk et al. [76] studied the dynamics of classical spins interacting via the Heisenberg exchange on spatial d-dimensional lattices (with and without presence of single-ion anisotropy). They have shown that discrete breathers exist for the cases where the continuum theory does not allow for their presence (easy-axis ferromagnets with anisotropic exchange and easy-plane ferromagnets). They have also proved the existence of localized excitations, using the implicit function theorem, and have obtained necessary conditions for this existence. From the foregoing, it is clear that from the above mentioned authors, very few studies were devoted on the existence of quantum discrete breathers in Heisenberg spin chain. Moreover, it is clear that, the local magnetization switching process that can help understanding data storage process, while investigating a 1D Heisenberg spin model including DMI and longer range interactions has not yet been investigated and needs a profound inspection.

The purpose of this thesis is, to investigate the quantum version of the eigenvalue spectrum, in the Bose-Hubbard like lattice derived from a specific map of a 1D Heisenberg spin model without and with including the DMI, to probe local magnetization switching process while investigating the quantum version of the eigenvalue spectrum in a 1D Heisenberg spin model including longer range interactions. The attention is focussed on the effect of the anisotropy interaction, of the DMI, Heisenberg exchange interaction, of second, third, fourth nearest neighbors interaction and the next longer nearest neighbors interactions on the energy spectrum of the system. From such an investigation, important and new features are set up. Using

the number state method, non degenerate, degenerate perturbation theory and numerical diagonalization, we have studied the localization of the energy with more than two quanta, the localization of the eigenfunction in the real space and we have computed the weight function of the eigenstates in the space of normal modes using perturbation theory. The work of this thesis is organized as follows:

The first chapter elaborates on literature review on the magnetism, spin Hamiltonian and exchange interaction that allows to characterize the magnetic systems, different types of magnetic excitations and their importance, with focussing on breather-like excitation in magnetic chains. We also present the basic classical properties of discrete breathers to the normal mode space that explain some facets of the Fermi-Pasta-Ulam (FPU) paradox. Quantum breathers and its applications are also reviewed.

The second chapter is devoted to our methodology where we present different methods used to model our system. These methods are: general formalism of particle number representation, general formalism of second quantization, nondegenerate and degenerate perturbation method, of Holstein-Primakoff transformation for the local spins operators to treat the system from semi-classical as compared to the quantum version in terms of bosonic creation and annihilation operator and there after the number state method is used to derive the basis states.

The third chapter extends to the results and discussion of our work. The study ends with a general conclusion summarising the most important results obtained. The study also presents the outlook opened by this work.

Chapter 1

Literature Review and Problems

In this chapter, we present the literature review on the magnetism, spin Hamiltonian and exchange interaction that allow to characterize the magnetic systems, different types of magnetic excitations and their importance, with focussing on breather-like excitation considered in this work. We also present the basic classical properties of discrete breathers to the normal mode space that explain some facets of the Fermi-Pasta-Ulam (FPU) paradox. The quantum breathers and their applications are also set up.

1.1 Generalities on Magnetism

Magnetism is a property of material that responds to an applied magnetic field. The Origin of magnetism is at microscopic channel.

1.1.1 Microscopical Origin of magnetism

We know from the experiment of Stern and Gerlach in 1922 [77], that an electron is not only characterized by its charge **e**, but also by an intrinsic magnetic moment (by opposition to the orbital magnetic moment, proportional to its angular momentum, then nil to the rest), called moment magnetic of spin. Magnetism finds its origin in the properties of electrons. Their spin quantum state is responsible of one part of magnetism; that can be attributed to the motion of electrons around themselves, and partly attributable to the orbital motion of electrons (orbital magnetism) and also the magnetism of nucleus itself (nuclear magnetism) (see Fig.1.1). The spin of electron can only take two separate discrete states denoted up and down. In an atom, the nucleons (the protons and neutrons), have a mass of about 2000 fold higher than that of electrons. Their magnetic moment is then about 2000 fold lower than that of the electrons, and will be subsequently neglected. The magnetic character of an atom is therefore only linked to electrons of its electrons cloud. The electrons cloud is separated into shells and distinct shells, corresponding to different energy levels. The filling of these layers and lower shells is governed by the Pauli principle (as all fermions, two electrons can not be in the same quantum state) and Hund's rules [78]. If a shell is full, all the magnetic moments are compensated because of the presence of pairs spin up / down. In this case, the shell is not magnetic. The shells

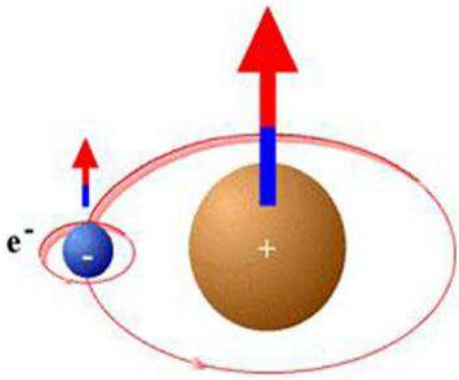

Figure 1.1: Motion of electron.

not totally filled are the only ones that contribute to the magnetism. In condensed matter, only substances with unsaturated inner shells (unpaired spins) can have a permanent magnetic moment. This is typically the case of the elements in 3d group, such as manganese, iron, cobalt, nickel, and rare earth (4f) or lanthanides . In this study, only elements of 3d group have been used.

1.1.2 Types of magnetism

By approaching a sample of material in the presence of a magnet, it addresses various behaviors that reflect the different types of magnetism. These are principally: diamagnets, paramagnets, ferrimagnets, antiferromagnets and ferromagnets.

Diamagnetism

In a diamagnetic substance, electrons are grouped in pairs so as to cancel the respective magnetic moments of the atoms so that the substance has no permanent moment. Such a substance can be magnetized in the presence of a external magnetic field. In this case, it will induce an opposite magnetic moment at the direction of the external field. This explains why diamagnetic substances are repelled by magnets. The magnetization of diamagnetic materials is nil in the absence of an applied field and weak when a field is applied. Diamagnetism is an extremely weak effect, even compared to paramagnetism.

Paramagnetism

In a paramagnet, the magnetic moments are randomly orientated (see Fig.1.2(d)) due to thermal fluctuations when there is no magnetic field. In the presence of an applied magnetic field, these moments start to align parallel to the field, such that the magnetization of the material is proportional to the applied field. This

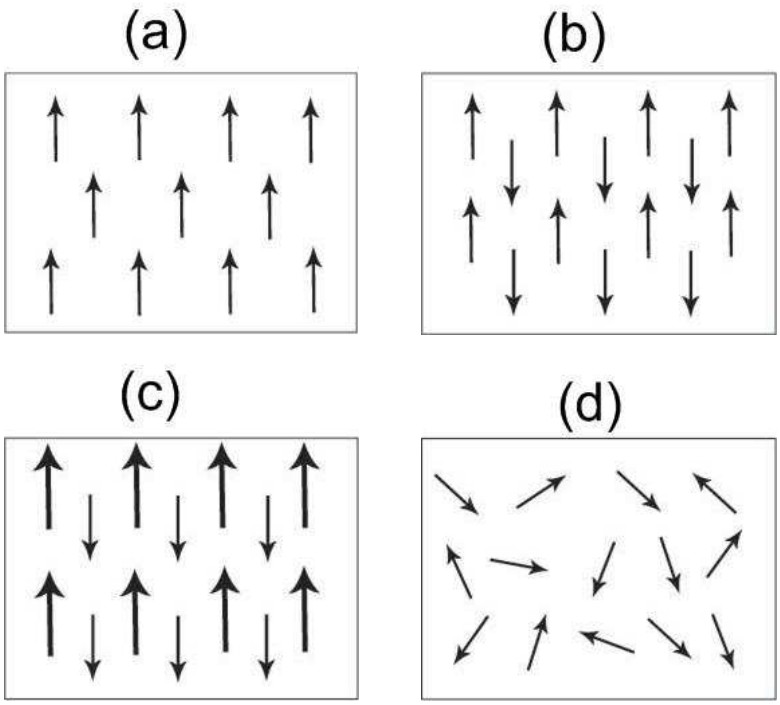

Figure 1.2: Types of magnetism:(a)Ferromagnetism; (b) Antiferromagnetism; (c) Ferrimagnetism and (d)Paramagnetism

magnetization is only temporary because it stops as soon as the external field is no longer applied. Paramagnetic substances are attracted by magnets. Paramagnetic materials include magnesium, molybdenum, lithium and tantalum.

Ferrimagnetism

The magnetic moments of the atoms on different sublattices are opposed in ferrimagnetic material as in antiferromagnetism without an applied field. However, the opposing moments are not of the same size (see Fig.1.2(c) and a spontaneous magnetization remains. An overall magnetization is produced but not all the magnetic moments may give a positive contribution to the overall magnetization. This happens when the sublattices consist of different materials or ions (such as Fe^{2+} and Fe^{3+}). Ferrites and magnetic garnets are ferrimagnetic materials.

Antiferromagnetism

Adjacent magnetic moments from the magnetic ions tend to align anti-parallel to each other without an applied field (see Fig.1.2(b)). In the simplest case, adjacent magnetic moments are equal in magnitude and opposite therefore there is no overall magnetization. The elements manganese (Mn), chrome (Cr) and many of their alloys are typical antiferromagnetic materials.

Ferromagnetism

The magnetic moments in a ferromagnet have the tendency to become aligned parallel to each other under the influence of a magnetic field. However, these moments will then remain parallel when a magnetic field is not applied (see Fig.1.2(a)). From these properties, ferromagnetic materials therefore have a permanent magnetization. The important term in the interaction of the localized moments is called the exchange interaction. The exchange interaction occurs due to the Pauli Exclusion Principle. If two electrons have different spins then they can occupy the same orbital (angular momentum state), hence be closer to each other and they will therefore have a stronger Coulomb repulsion. If the electrons have the same spin then they will occupy different orbitals and therefore have less Coulomb repulsion as they will be further apart. In this way, the exchange energy (the energy due to the repulsion between the two electrons) is minimized. Therefore the Coulomb repulsion force favours the parallel alignment of all the electron spins as the exchange energy is minimized. The elements iron (Fe), nickel (Ni), cobalt (Co) and gadolinium (Gd) and many of their alloys are typical ferromagnetic materials.

1.1.3 Magnetic Domains

Domains are microscopical regions of a ferromagnetic material. These regions are divided into billions of micro domains called Weiss domains. Their interfaces of separation are usually named Bloch walls. In each Weiss domain, magnetic moments are aligned spontaneously in parallel. Ferromagnetic materials are instinctively divided into magnetic domains because the exchange interaction is a short-range force, so over long distances of many atoms the tendency of the magnetic moments to reduce their energy by orienting in opposite directions wins out. When the material is demagnetized, the vector summation of all the moments from all the domains equals zero. When the material is magnetized the vector summation of the moments gives an overall magnetic moment. Inside a domain, the direction of magnetization is determined by anisotropy. The antiparallel orientation of the moments on the two sides of the wall is equally favorable from the view point of anisotropy. However, there is a significant increase in the exchange energy. With a slow rotation over a longer distance, the increase in the exchange energy can be reduced. The competition of the two contributions determine the details of the reversal of the moment across the domain wall. Assuming uniaxial anisotropy, where the upward or downward orientation of the moments is preferred, there are two characteristic types of domain walls. In most cases, the rotation of the magnetic moment is such that it remains in the plane of the wall everywhere. Such a domain wall is called a Bloch wall(see Fig.1.3(b)). When the rotation of the moment is in a plane perpendicular to the wall, we speak of a Néel wall(see Fig.1.3(c)); the wall is perpendicular to the x-axis.

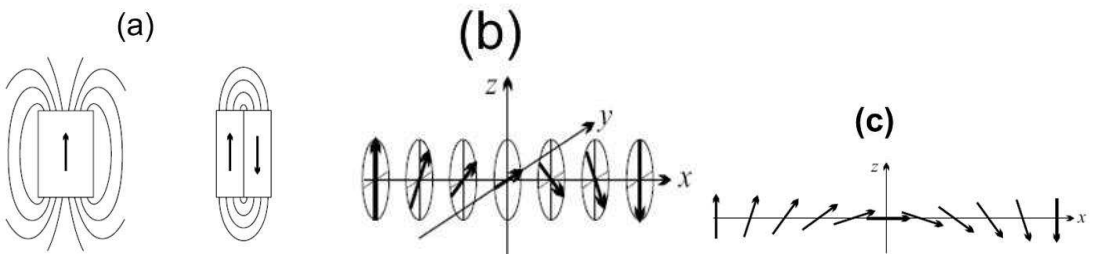

Figure 1.3: (a) Magnetic structures with one and two domains, and the lines of the induced magnetic field; Rotation of the magnetic moment for domain walls in the (y, z) plane (b) Bloch wall and (c) Néel wall (figure adapted from [79])

1.2 General form of the spin chains Hamiltonian

A spin S is a discrete degree of freedom that transforms like an angular momentum under rotations. A spin Hamiltonian consists of a sum of one-spin and two-spin term. This is very analogous to the Hamiltonian of a particle system, where one has one-body terms (an external potential) plus two-body terms (particle-particle interactions). A spin Hamiltonian in its general form, is a sum of several terms, where each term plays an important role in the Hamiltonian of the magnetic system. The general form of the spin Hamiltonian can be written as

$$H_{spin} = H_{Mf} + H_{An} + H_{Ex} + H_M + H_{dip} \tag{1.1}$$

Where H_{Mf} is the magnetic field coupling. An external field H couples as

$$H_{Mf} = -\vec{H} \cdot \sum_i g_i \mu_B \vec{S}_i \tag{1.2}$$

This term looks anisotropic in that H defines a special direction in space. But the material is isotropic in spin space, in the sense that the strength of its field coupling is independent of the field's direction. Here, $\vec{S}_i$ is the spin which resides at the i-th magnetic site called the spin angular momentum vector, μ_B is the Bohr magneton. H_{An} is the single-ion anisotropy. This term has the form

$$H_{An} = \sum_i A(S_i^z)^2 \tag{1.3}$$

The term proportional to A represents the single-ion uniaxial anisotropy due to crystal field effect and A is the anisotropy parameter. If the anisotropy parameter

$A < 0$, the system is associated with an easy axis spin chain while if $A > 0$, the spin system is said to have an easy plane anisotropy for the spin chain.
H_{Ex} is the exchange interaction (sometimes called Heisenberg exchange) is bilinear in spins and isotropic under rotations. The Heisenberg spin chain model was set up in 1928. The most basic form of the Heisenberg Model has the Hamiltonian expressed as the inner product of the spins in the form:

$$H_{Ex} = -\sum_{<ij>} J_{ij}\vec{S}_i \cdot \vec{S}_j \tag{1.4}$$

J_{ij} is the exchange integral.
If $J_{ij} > 0$, the Heisenbgerg model has a ferromagnetic ordering, all spins are parallel, that is to say all aligned in the same direction and otherwise If $J_{ij} < 0$, the model has an antiferromagnet ordering, the environment can be seen as two sub lattices with up and down spins respectively and the same modules. From this equation, the Heisenberg model Hamiltonian can be subdivided in two components as follows

$$H_{Ex} = -\sum_{<ij>} J_{ij}^{\perp}(S_i^x S_j^x + S_i^y S_j^y) - \sum_{<ij>} J_{ij}^{\parallel} S_i^z S_j^z \tag{1.5}$$

The first antiparallel interaction term is a planar ferromagnet model and the second parallel interaction term is reduced to the Ising ferromagnet model while $J_{ij}^{\perp} > 0$ and $J_{ij}^{\parallel} > 0$.
If $J_{ij}^{\perp} = J_{ij}^{\parallel} = J$, the Heisenberg Model is isotropic.
If $\mid J_{ij}^{\perp} \mid > \mid J_{ij}^{\parallel} \mid$, the model is planar XY and the interaction is stronger in the XY plane.
If $J_{ij}^{\perp} < 0$, the interaction is planar antiferromagnetic.
If $\mid J_{ij}^{\perp} \mid < \mid J_{ij}^{\parallel} \mid$, the Heisenberg anisotropic model is reduced to the Ising model and the interaction is stronger along the z axis.
If $J_{ij}^{\parallel} < 0$, the interaction is Ising antiferromagnetic.

H_D is the Dzyaloshinsky-Moriya interaction, or antisymmetric exchange, has the form

$$H_M = -\sum_{<ij>} \vec{D}_{ij} \cdot (\vec{S}_i \wedge \vec{S}_j) \tag{1.6}$$

is an antisymmetric exchange interaction between two magnetic moments $\vec{S}_i$ and $\vec{S}_j$. $\vec{D}_{ij}$ is the Dzyaloshinsky-Moriya vector. It is antisymmetric with regards to site permutation $D_{ij} = -D_{ji}$. This term is used for modelling a weak ferromagnet. It was proposed by Dzyaloshinsky and Moriya [40, 41] and it has a microscopic origin. Can be indispensable to explain the structure of some compounds like $Z_nCu_3(OH)_6Cl_2$.

The last term H_{dip} is the dipolar interaction. It is a special case extending beyond nearest neighbors. However, in this case the interaction does not depend on the crystal axes, and its microscopic origin is not in exchange, so it makes sense to treat it separately:

$$H_{dip} = -\sum_{<ij>} \frac{(g\mu_B)^2}{r_{ij}^3}[3(\hat{r}_{ij}\cdot S_i)(\hat{r}_{ij}\cdot S_j) - \vec{S}_i\cdot\vec{S}_j] \tag{1.7}$$

Dipolar interactions are important when exchange is small, and also in nuclear magnets. In this thesis we are not taking into account the dipolar interaction.

1.3 Excitations in Magnetic Systems

There are two types of elementary excitations in magnetic systems that are: spin waves or magnons and solitons. The soliton is a solitary wave that propagates without deformation in a nonlinear and dispersive medium whereas a magnon is a quantized spin wave.

1.3.1 Excitations of ferromagnets in the Heisenberg model

From equation (1.5), parallel spin orientation is energetically favorable. The ground

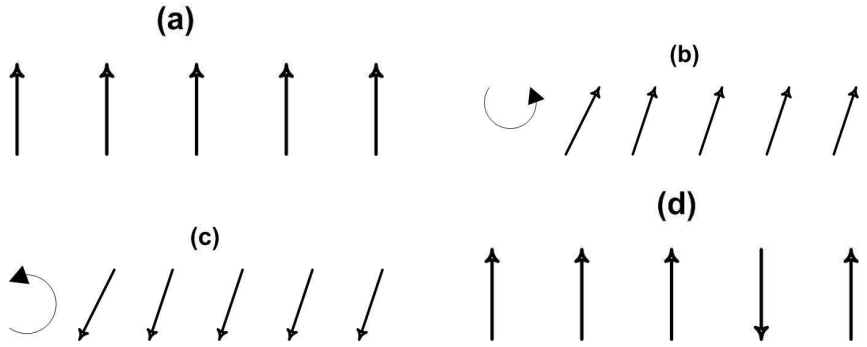

Figure 1.4: Excitations of ferromagnets: (a) ground state; (b)-(c) symmetry in the chain; (d) a single defect

state corresponds to the case where all spins are parallels in any direction (see Fig.1.4(a)). Here, the symmetry of the Hamiltonian is set up (see Fig.1.4(b-c)). The degeneracy of this configuration is (2NS+1)-fold, N is the number of sites. Due to the degeneracy, it is easy to choose the z quantization axis. If $\mid J_{ij}^{\perp} \mid < \mid J_{ij}^{\parallel} \mid$, the Heisenberg anisotropic model is reduced to the Ising model and the interaction is stronger along the z axis and, if $J_{ij}^{\parallel} > 0$, the interaction is ferromagnetic. The ground state is only 2-fold degenerate i.e. all spins in the site can be oriented up or down along the z axis. The mobility of magnons or spin waves is provided by

the first term of the Hamiltonian (1.5) also called spin-flip terms. In this case, the ground state is excited and a single defect is added (see Fig.1.4(d)).

1.3.2 Excitations of antiferromagnets in the Heisenberg model

From equation (1.5), if $\mid J_{ij}^{\perp} \mid < \mid J_{ij}^{\parallel} \mid$, the Heisenberg anisotropic model is reduced to the Ising model and the interaction is stronger along the z axis and if $J_{ij}^{\parallel} < 0$, the interaction is antiferromagnetic. The ground state can be represented as

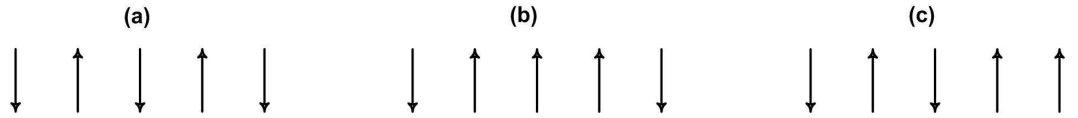

Figure 1.5: Excitations of antiferromagnets: (a) ground state or Néel state; (b) excited state (magnon ΔS=1); (c) excited state (spinon ΔS=1/2)

an alternated spins alignment along the z axis (see Fig.1.5(a)). This arrangement corresponds to the Néel state. This state is doubly degenerated because the same configuration is defined at π close. The soliton is precisely an elementary anisotropic excitation system, that authorizes the passage from one configuration to another. It takes the form of a magnetic wall where the spins undergo a rotation of π. The classical image of a such wall is given by the Fig.1.5(a). Those walls are very localized. In the antiferromagnetic materials, the spin waves or magnons correspond to the magnetic transitions. A reversal of a spin of the chain suffice therefore to create a spin wave. On the other hand, a soliton state requisite to reverse the half spins of the chain. The states corresponding to those excitations are represented in the Fig.1.5(b-c). The mobility of solitons is provided by the first term of the Hamiltonian (1.5).

However, there are others types of excitations in magnetic systems like breather. A breather is a nonlinear wave in which energy concentrates in a localized and oscillatory fashion. A breather is a localized periodic solution of discrete lattice. There are two types of breathers that are: standing and travelling. Standing breather corresponds to localized solutions whose amplitude varies in time whereas travelling breather corresponds to solutions localized in all the lattice where amplitude do not vary in time.

1.3.3 Importance of excitations in magnetic systems

For modern applications, excitations in magnetic systems play important roles in computer materials to develop Random Access Memories (RAM) in magnetic data storage and in the functions of devices. In magnetic systems, excitations can also provide energy thresholds in lattices by discrete Breathers like excitations. The areas

of applications of excitations in magnetic systems are:

Magnetic data storage

The hard disk is formed of small circular plates of aluminum on which a magnetic layer is deposited, divided into billions of micro domains called Weiss domain (see Fig.1.6). Each of these domains has a magnetization. The orientation of the magne-

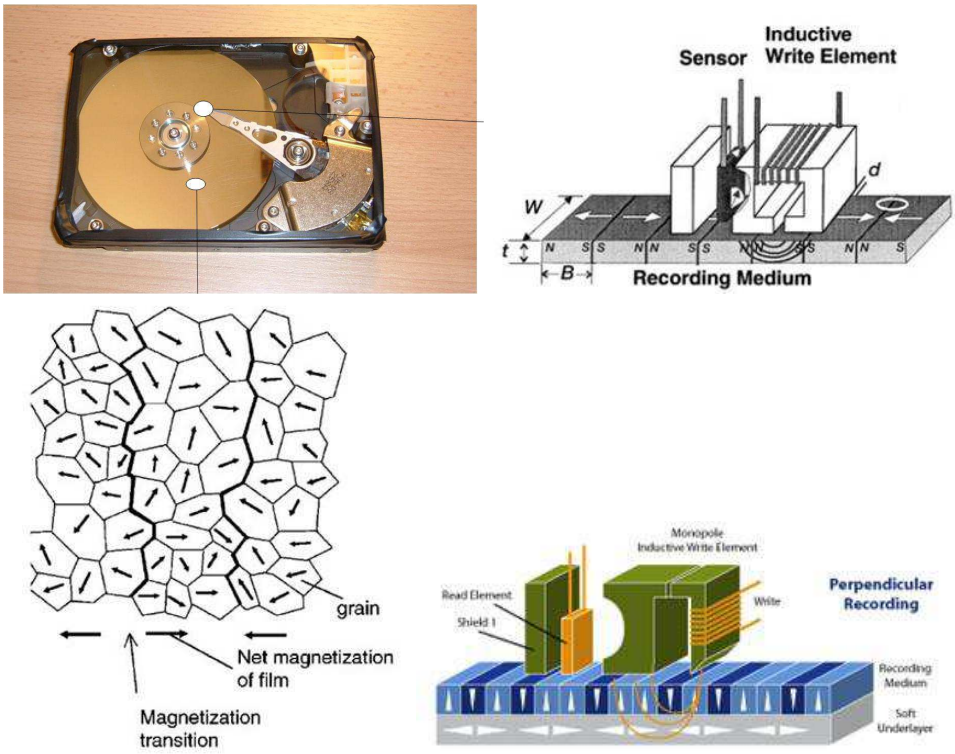

Figure 1.6: Magnetic data storage from Encyclopedia of Nanoscience and Nanotechnology

tization of each domain is random. The magnetizations of these microdomains are moving gradually on the direction of the excitation in the same way. When the excitation is strong, all Weiss domains have their magnetization aligned on the excitator field and the material becomes saturated. When the excitator field is not applied, these domains remain aligned on the direction of the excitation: they undergo a remanent magnetization, which keep in memory the trace of the magnetic excitation. This process is known as magnetic hysteresis. Magnetic data storage depends on this process. Depending in the direction of the current in the bobbin, each of these Weiss domains can be magnetized independently to store the bit "1" or demagnetized to store the bit "0". Initially, the magnetization was performed longitudinally. By changing the geometry of the write head, it has succeeded in bits perpendicular (see Fig.1.6), which helped to improve the storage density today. A reading head runs the hard disk to read or write information magnetically. Magnetism is used in

computer storage because it will store information even when the power is turned off. Other examples of magnetic storage media are floppy disks, magnetic tapes and magnetic strips of credit cards. However, the plates are in constant rotation. That they are composed of mechanical parts that move and rotate, the hard drives are relatively slow mechanisms to read and write data. To improve the speed of the hard drive, it is important to associate in each hard drive a RAM which is a type of memory that allow any computer and mobile to store temporary information. Its major advantage is that its ability of reading is very fast than the hard drive.

Reading (and writing) data from a disk

The write head is an electromagnet. When a current passes in an electromagnet, the electromagnet creates a magnetic field. A magnetic particle located on the plate surface can be oriented in two different ways according that, the current across the electromagnet in one sense or in the other to give the 0 or 1 bit; and we can record the write signal as a function of time (see Fig.1.7). During the writing, the electromagnet passes over a track. It orients the magnetic particles arranged in one way, according the current passes through it. The phenomenon of Giant

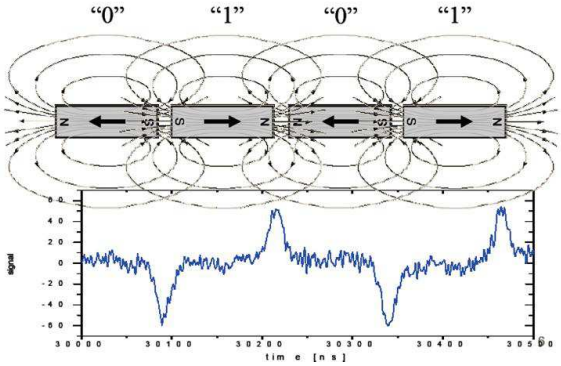

Figure 1.7: Reading (and writing) data from a disk,Typical data speed: 120MB/sec. From Encyclopedia of Nanoscience, Nanotechnology [80]

Magnetoresistance (GMR) is widely used in read heads of modern hard disks. GMR is a quantum effect observed in the structures of thin films consisting of alternating ferromagnetic layers and non-magnetic layers. It manifests itself as a significant decrease in resistance observed under the application of an external magnetic field, at zero field, the two adjacent ferromagnetic layers are antiparallel magnetization, as they undergo a weak ferromagnetic coupling. An external magnetic field induces a magnetization reversal, the respective magnetization of the two layers are aligned and the resistance of the multilayer decreases abruptly. The effect occurs because the electron spin of the non-magnetic metal is equally distributed in parallel and antiparallel, and undergoes diffusion magnetic less important when the ferromagnetic

layers are magnetized in parallel.
Another read heads have a magnetic tunnel junction (TMR) technology since 2005 [80] that detects the magnetic field radiated by the bit read.
The above cited domains applications of excitations in magnetic systems are just a few among others.

However, in the absence of magnetic field in ferromagnets, breathers like excitation can play important role for activating localized magnetization reversal processes. This process has gain numerous importance thanks to the success and development of random access memories.
Before continuing, let us remind of the breathers origin in past decades.

1.4 Breather

The term breather originates from the characteristic that most breathers are localized in space and oscillate (breathe) in time [81] or oscillated in space and localized in time.

1.4.1 Spatial Discreteness and Nonlinearity

Before defining the term discrete breather (DBs), it is important for us to review the results already known about the study of the combined effect of nonlinearity and discreteness on the spatial localization that leads to the emergence of a new class of nonlinear excitations like discrete breathers [6]. For that D. K. Campbell et al. have considered a one-dimensional chain of interacting (scalar) oscillators with the Hamiltonian

$$H = \sum_n [\frac{1}{2} p_n^2 + V(x_n) + W(x_n - x_{n-1})] \tag{1.8}$$

The integer n marks the lattice site number of a possibly infinite chain, and x_n and p_n are the canonically conjugated coordinate and momentum of a degree of freedom associated with site number n. The on-site potential V and the interaction potential W satisfy $V'(0) = W'(0) = 0$, $V''(0), W''(0) \geq 0$. This choice ensures that the classical ground state $x_n = p_n = 0$ is a minimum of the energy H. The equations of motion read

$$\dot{x_n} = p_n, \dot{p_n} = -V'(x_n) - W'(x_n - x_{n-1}) + W'(x_{n+1} - x_n) \tag{1.9}$$

They have linearized the equations of motion around the classical ground state and obtained a set of linear coupled differential equations with solutions being small

amplitude plane waves:

$$x_n(t) \sim \exp i(\omega_q t - q_n), \omega_q^2 = V''(0) + 4W''(0) sin^2(\frac{q}{2}) \tag{1.10}$$

These waves are characterized by a wave number q and a corresponding frequency ω_q. All allowed plane wave frequencies fill a part of the real axis which is coined linear spectrum. Due to the underlying lattice, the frequency ω_q depends periodically on q and its absolute value has always a finite upper bound. The maximum (Debye) frequency of small amplitude waves $\omega_\pi = \sqrt{V''(0) + 4W''(0)}$. Depending on the choice of the potential V(x), ω_q can be either acoustic or optic-like, $V(0) = 0$ and $V(0) \neq 0$, respectively. In the first case, the linear spectrum covers the interval $-\omega_\pi \leq \omega_q \leq \omega_\pi$ which includes $\omega_{q=0} = 0$. In the latter case, there exists an additional (finite) gap opens for $\mid \omega_q \mid$ below the value $\omega_0 = \sqrt{V''(0)}$. For large amplitude excitations the linearization of the equations of motion is not correct anymore. Similar to the case of a single anharmonic oscillator, the frequency of possible time-periodic excitations will depend on the amplitude of the excitation, and thus may be located outside the linear spectrum. They assumed that a time-periodic and spatially localized state, i.e. a discrete breather, $\hat{x}_n(t + T_b) = \hat{x}_n(t)$ exists as an exact solution of Eqs.(1.9) with the period $T_b = 2\pi/\Omega_b$. Due to its time periodicity, they expanded $\hat{x}_n(t)$ into a Fourier series

$$\hat{x}_n(t) = \sum_k A_{kn} \exp ik\Omega_b t \tag{1.11}$$

The Fourier coefficients are by assumption also localized in space

$$A_{k,|n|\to\infty} \to 0 \tag{1.12}$$

Inserting this ansatz into the equations of motion (1.9) and linearizing the resulting algebraic equations for Fourier coefficients in the spatial breather tails (where the amplitudes are by assumption small) they arrive at the following linear algebraic equations:

$$k^2\Omega_b^2 A_{kn} = V''(0)A_{kn} + W''(0)(2A_{kn} - A_{k,n-1} - A_{k,n+1}) \tag{1.13}$$

If $k\Omega_b = \omega_q$, the solution to (1.13) is $A_{k,n} = c_1 e^{iqn} + c_2 e^{-iqn}$. Any nonzero (whatever small) amplitude $A_{k,n}$ will thus oscillate without further spatial decay, contradicting the initial assumption. If however

$$k\Omega_b \neq \omega_q \tag{1.14}$$

for any integer k and any q, then the general solution to (1.13) is given by $A_{k,n} = c_1 k^n + c_2 k^{-n}$ where k is a real number depending on ω_q, ω_b and k. It always admits

an (actually exponential) spatial decay by choosing either c_1 or c_2 to be nonzero. In order to fulfill (1.14) for at least one real value of ω_b and any integer k, they have to request $\mid \omega_q \mid$ to be bounded from above. That is precisely the reason why the spatial lattice is needed. In contrast most spatially continuous field equations will have linear spectra which are unbounded. That makes resonances of higher order harmonics of a localized excitation with the linear spectrum unavoidable. The nonresonance condition (1.14) is thus an (almost) necessary condition for obtaining a time-periodic localized state on a Hamiltonian lattice. The performed analysis can be extended to more general classes of discrete lattices, including e.g. long-range interactions between sites, more degrees of freedom per site, higher-dimensional lattices. But the resulting non-resonance condition (1.14) keeps its generality, illustrating the key role of discreteness and nonlinearity for the existence of discrete breathers. Discreteness provides gap and bounds to the linear oscillation spectrum and nonlinearity makes the amplitude of oscillation frequency dependent.

1.4.2 Examples of Discrete breather solutions

The term breather was first applied to a particular solution of the famous Sine - Gordon Equation [81]. There exist others discrete breather solutions for various lattices. In a chain (1.8) with the functions

$$V(x) = x^2 + x^3 + 14x^4, \quad W(x) = 0.1x^2 \tag{1.15}$$

The spectrum ω_q is optic-like and shown in Fig.(1.8) Discrete breather solutions can have Ω_b which are located both below and above the linear spectrum. The time-reversal symmetry of (1.9) allows to search for DBs displacements $x_n(t = 0)$ when all velocities $\dot{x_n}(t = 0) = 0$. These initial displacements are computed with high accuracy and plotted in the insets in Fig.(1.8) where solutions to two DBs frequencies located above and below ω_q are located. Their actual values are marked with the green arrows. To each DBs frequency correspond two different spatial DBs patterns among an infinite number of other possibilities. The high-frequency DBs $\Omega_b \approx 1.66$ occur for large-amplitude, high-energy motion with adjacent particles moving out of phase. Low-frequency DBs $\Omega_b \approx 1.26$ occur for small-amplitude motion with adjacent particles moving in phase.

From the spatial discreteness and nonlinearity, a new paradigm of nonlinear science has recently emerged the concept of discrete breathers, equally labelled Intrinsic Localized Modes (ILM) in solid state physics and discrete solitons in nonlinear optics. Discrete breathers are localized non linear excitation, generic time periodic and spatially localized solutions of the underlying classical Hamiltonian lattice with translational invariance. Their spatial profiles localize exponentially for short-range interaction, independent of the actual (assumed to be large) size of the lattice, in-

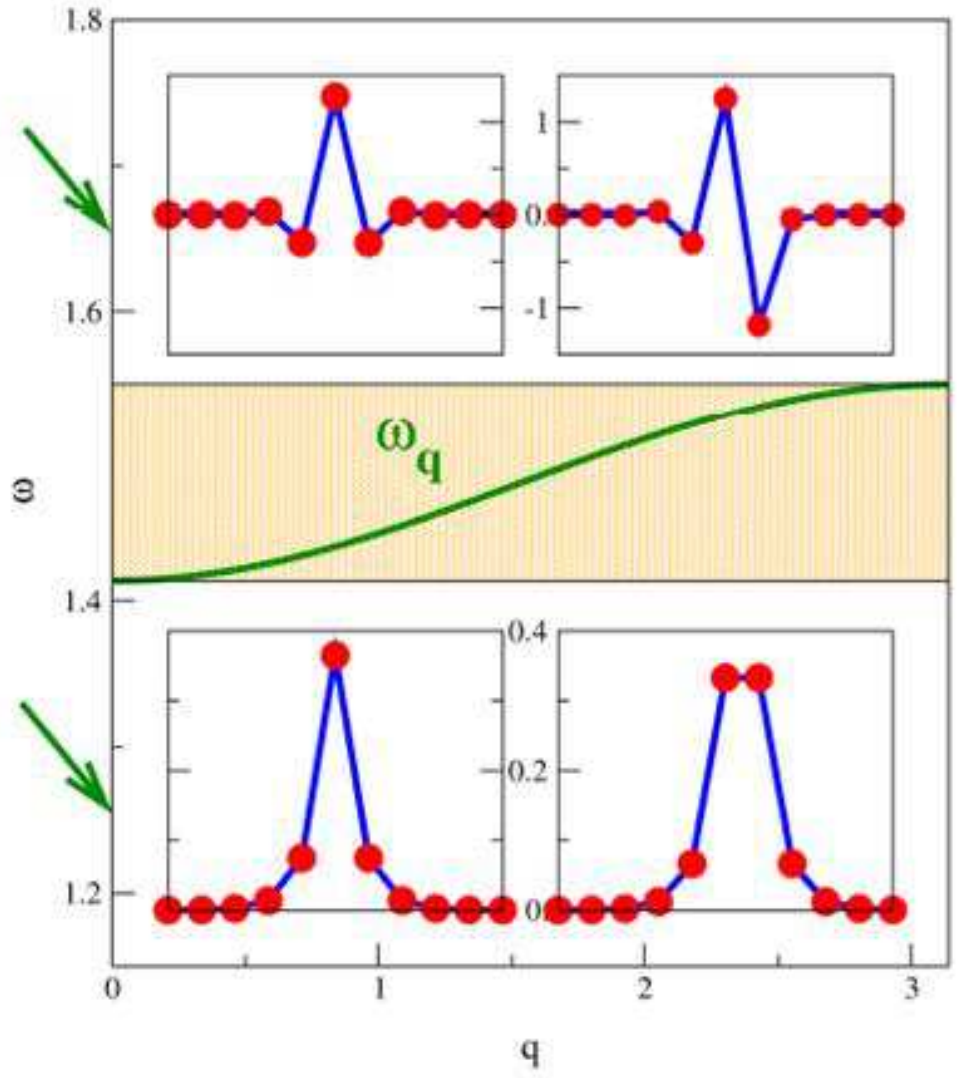

Figure 1.8: The frequency versus wave-number dependence of the linear spectrum for a one dimensional chain of anharmonic oscillators with potentials (1.15). The chosen DBs frequencies are marked with green arrows and they lie outside the linear spectrum, ω_q. Red circles indicate the oscillator displacements for a given DBs solution, with all velocities equal to zero. Lines connecting circles are guides for visualization (Figure adapted from [6])

dependent of the spatial dimension of the lattice, mostly independent of the actual choice of nonlinear forces acting on the lattice, and so on. They can modify the system's properties such as the thermodynamics of the lattice and introduce the possibility of non dispersive energy during its transport.

The existence of two distinct names for the same phenomenon is an indication that separate historical paths led to their discovery and provides key insights into the reasons for their existence [4]. A breather is a localized, oscillatory excitation that is stabilized against decay by the discrete nature of the periodic lattice. An ILM is

an excitation that is localized in space by the intrinsic nonlinearity of the medium, rather than by a defect or impurity. By the early 1990s, researchers following these two paths had converged on the insight that stable localized periodic modes, whether called ILM or DBs, were generic excitations in discrete nonlinear systems.
Investigation of discrete breathers in recent years has revealed a wealth of new properties of energy localization.

1.5 Basic classical Properties of Discrete Breathers

The properties of discrete breathers that can be found in the literature [5, 6] are:
Spatial localization in space: The spatial decay of the breather is thus characterized by the convergence properties of the corresponding Fourier series defined through the analytical properties of the generating periodic function.
The spatial decay of a discrete breather is typically exponential : A Fourier series representation of the time periodic discrete breather leads to Fourier number dependant exponents of the spatial decay.
Short-range interactions: Two DBs profiles spatial localize the exponentially for short-range interaction for a one-dimensional Fermi-Pasta-Ulam (FPU) and Discrete Nonlinear Schrödinger (DNLS) chain with nearest neighbour interaction.
Existence and stability: In 1994 MacKay and Aubry proved a theorem that demonstrates the precise existence of DBs in a wide class of nonlinear lattice models [82]. It is now known that DBs not only exist rigorously in a large class of Hamiltonian systems but are also linearly stable [83].
Nonexponential relaxation: The DBs are then generally very robust and long-lived, although interaction among breathers is possible resulting in some cases in breather accumulation. If the system is placed in contact with a reservoir that absorbs energy, the lattice loses energy yet in a nonexponential fashion. This feature of slow relaxation is directly attributed to the presence of DBs [18, 84].
Mobility: Even though DBs are spatially quite discrete and may occupy very few sites, in many cases they move across the lattice with essentially ballistic, particle-like motion. This DBs motion preserves their shape and frequency although in an approximate fashion. The speed of DBs propagation is slower than the sound speed, i.e., the speed of the linearized phonon modes of the system [18].
Generic and structurally stable solutions : Discrete breathers are generic and structurally stable solutions because the necessary nonresonance condition is easily fulfilled for a lattice. This condition requires the discrete breather frequency as well as all of its multiples to not resonate with the linear spectrum of the system. Nonresonance is easy to achieve because the linear spectrum of a Hamiltonian lattice is bounded. The nonresonance condition explains why breather solutions are nongeneric and structurally unstable in the opposing case of Hamiltonian fields.

Periodic orbits: Discrete breathers are periodic orbits. For generic Hamiltonian systems periodic orbits occur in one parameter families, and so do discrete breathers. The parameter describing the family can be the amplitude of a breather, or its frequency, or any other meaningful observation [85].
Recently, the application of these properties to the normal mode space in a weakly anharmonic atomic chain has helped to explain essential features of the FPU paradox.

1.6 Fermi-Pasta-Ulam Problem

In 1955, FPU published their well-known paper on the absence of thermalization in arrays of particles connected by weakly nonlinear strings [86]. In particular they observed that energy, initially placed in a low-frequency normal mode of the linear problem with a frequency ω_q and a corresponding wave number q, stayed almost completely locked within a few neighbor modes, instead of being distributed among all modes of the system. Moreover, recurrence of energy to the originally excited mode was observed. These later expectation was due to the fact, that nonlinearity does induce a long-range network of interactions among the normal modes. To understand and explain the FPU results. Ten years after, two major approaches were developed. The first one, taken by Zabusky and Kruskal, was to analyze dynamics of the nonlinear string in the continuum limit, which led to a pioneering observation of solitary waves [87]. The second approach, followed by Izrailev and Chirikov, pointed to the existence of a stochasticity threshold in the original FPU system. For strong nonlinearity (or simply large energies) the overlap of nonlinear resonances leads to strong dynamical chaos, destroying the FPU recurrence and ensuring fast convergence to thermal equilibrium. Later studies showed that the local dynamics of four consecutive low-frequency modes may become substantially chaotic, while almost all initial energy stays localized in these modes during the time of computation. The redistributed mode energies fall exponentially with increasing mode numbers in this regime (coined weak chaos) and the energy flow to higher frequency modes was argued to be exponentially slow.

1.7 q-breathers

Recently, S. Flach et al demonstrated the existence of q-breathers (qBs) as exact time-periodic low-frequency for solutions in the nonlinear FPU system continued from the normal modes of the corresponding linearized system [83, 88]. These solutions are exponentially localized in the q-space of the normal modes and preserve stability for small enough nonlinearity.

They continue from their trivial counterparts for zero nonlinearity at finite en-

ergy. The stability threshold of qBs solutions coincides with the weak chaos threshold. Persistence of exact stable qBs modes is shown to be related to the FPU paradox. The FPU trajectories computed in 1955 are perturbations of the exact qBs orbits. M.V. Ivanchenko et al. [89] find the existence of qBs and obtain that the localization and stability of qBs are enhanced with increasing system size in higher lattice dimensions opposite to their one-dimensional analogues.

Recent simulation results on q-breathers, show that the localization properties of a q-breather are characterized by intensive parameters, that is, energy densities and wave numbers. By using scaling arguments, q-breather solutions are constructed in systems of arbitrarily large size. Frequency resonances in certain regions of wave number space lead to the complete delocalization of q-breathers. The relation of these features to the Fermi Pasta Ulam problem have been discussed by S. Flach et al [85]. Moreover Mishagin et al. [90] have studied q-breathers in one, two and tree dimensional discrete nonlinear Schrödinger lattices. They have proved the existence of these solutions for weak nonlinearity and have found that the localization of q-breathers is controlled by a single parameter which depends on the norm density, nonlinearity strength and seed wave vector.

From basic classical properties of discrete breathers and q-breather results which explain some aspects of the FPU paradox on nonequipartion energy described above, it is clear that at present, because the occurrence of classical breathers and q-breather are a relatively well understood phenomena, a great attention is done to characterized their quantum equivalent for which less are known and needs a detailed inspection.

1.8 Quantum breathers

Two decades of intensive research have polished theoretical understanding of DBs in classical nonlinear lattices. Less is known about their quantum counterparts quantum breathers (QBs). Before using quantum breather, it is important to specify the correct correspondence relation between a classical model and its quantum mechanical counterpart. This will be the conventional first or second quantization procedures. Quantum breather consist of superpositions of nearly degenerate many quanta bound states, with very long times to tunnel from one lattice site to another. Because of the bosonic commutation relations one can define quantum breathers as bound boson states. A quantum breather state belongs to a band of N states. Each bound state of such a quantum breather band is characterized by a quantum number or a wave number. The particle property of such a bound state can be probed with the help of correlation functions. These correlation functions should show (exponential) decay in the distance between parts of split bound bosons.
From a computational point of view, it is impossible to study quantum properties

of a lattice problem in the high energy domain and for large lattices, since solving the quantum problem leads to diagonalizing the Hamiltonian matrix with rank b^N where b is the number of states per site, which should be large to make contact with classical dynamics. Thus, typically, quantum breather states have been so far obtained numerically for small one-dimensional systems [91–93].

1.8.1 The Bose-Hubbard chain and related models

The quantum discrete nonlinear Schrödinger equation also called Bose-Hubbard model Hamiltonian is given by

$$H = -\sum_{l=1}^{N} (\frac{1}{2} a_n^\dagger a_n^\dagger a_n a_n + C(a_n^\dagger a_{n+1} + h.c)) \tag{1.16}$$

The second term stand for the hopping of the particle. This Hamiltonian conserves the total number of particles. For b particles and N sites the number of basis state is $\frac{(b+N-1)!}{b!(N-1)!}$. For $b = 0$, there is just one trivial state of an empty lattice. For $b = 1$, there are N states which correspond to one-boson excitations. These states behave pretty much as classical extended wave states. For $b = 2$, the problem is still exactly solvable, because it corresponds to a two body problem on a lattice. A numerical solution displays in addition of continuum, a single band located below the continuum. This single band corresponds to quasiparticle states characterized by one single quantum number. These states are two-particle bound states. Any eigenstate from this two-particle bound state is characterized by exponential localization of correlations.
While increasing the number of particles to b = 3, Eilbeck [94] could set up updated codes in Maple in order to deal with systems with up to b = 4 and N = 14. From another point Dorignac et al. [11] did studied the spectrum of the quantum DNLS equation, in the case of four and six bosons using degenerate perturbation theory.

1.8.2 Dimer and trimer

The dimer describes the dynamics of bosons fluctuating between two sites. The number of bosons is conserved, and together with the conservation of energy the system appears to be integrable. Such a system is integrable due to the existence of two integrals of motion (energy and boson number). The classical version can be completely solved. Bernstein et al. [32] and Aubry et al. [36] studied the expected splitting of degenerate pairs of eigenvalues in the quantum system.
The trimer describes the dynamics of bosons fluctuating between three sites. A trimer adds a third degree of freedom without adding a new integral of motion. Consequently the trimer is nonintegrable. A still comparatively simple numerical quantization of the trimer allows to study the behavior of many tunneling states in

the large energy domain of the eigenvalue spectrum [95].

1.8.3 Large lattices with fluctuating numbers of quanta

A number of papers are so far devoted to the properties of quantum breathers in chains and two-dimensional lattices of coupled anharmonic oscillators [6]. Calculations will typically be restricted to four-six quanta in one and two-dimensional lattices [26]. With these parameters one can calculate properties of quantum breather states. For large enough anharmonic constant a complete gap opens up between the two-quanta free state and quantum breather states [26, 96]. However when decreasing the anharmonic constant, Proville found, that the gap closes for certain wave numbers, but persists for others and turns out to be rather a pseudogap [97].

1.8.4 Applications of discrete and quantum breathers

In past decades, discrete breathers or intrinsic localized modes, which are expected to play fundamental roles in both energy storage and transport in various low dimensional materials, have been the subject of intense research. Experimental and related theoretical work on applying the discrete breather concept to many different branches in physics ranging from electronic and magnetic solid to micro-engineered structures including like superconducting materials, Bose-Einstein condensates loaded on optical lattices, antiferromagnetic structures, crystals and molecules, micromechanical systems, bond excitations in molecules, lattice vibrations, Ultracold atoms in optical lattices, electron-phonon interactions in crystals, spin excitations in solids and others [12, 21, 98–101]. In quantum point of view, studies of quantum modes on small lattice are of interest for quantum devices based on quantum dots, for studies of photonic crystals, protein-like crystals and possibly in myoglobin.

1.9 Conclusion

In this Chapter, we have set out the generalities on Magnetism and the general form of the spin chains Hamiltonian. We have presented different types of magnetic excitations, their areas of applications with insistence on breathers like magnetic spin excitation. We have exposed the basic classical properties of Discrete Breathers which can explain some facets of FPU paradox. Quantum breathers have been defined and some indications on theirs applications have been given.
The following chapter will be devoted to different methods used to tackle the problems of this thesis.

Chapter 2

Methodology

2.1 Introduction

In this chapter, we present different methods used to model our physical system. These methods are: the general formalism of particle number representation, the second quantization formalism, nondegenerate and degenerate perturbation method, the Holstein-Primakoff transformation for the local spins operators to treat the system from semi-classical as compared to the quantum version in terms of bosonic creation and annihilation operator and the number state method.

2.2 Particle-number representation: General formalism

The simplest starting point for a many-body state is a system of noninteracting particles [102–105], i.e. the Hamiltonian of the total system H is simply the sum of the single-particle Hamiltonian h(i) for each individual particle; there are no interaction terms depending on the coordinates of more than one particle:

$$\hat{H} = \sum_{i=1}^{f} \hat{h}(r_i, \hat{p}_i) \tag{2.1}$$

A solution of the Schrödinger equation can be found in terms of a product of single-particle states: i.e. a set of single-particle wave functions $\psi_i(r)$ it fulfills the condition

$$\hat{h}(r_i, \hat{p}_i)\psi_i(r) = \varepsilon_i \psi_i(r) \tag{2.2}$$

A product state like

$$\Psi(r_1, \cdots, r_f) = \psi_{i_1}(r_1) \cdots \psi_{i_f}(r_f) \tag{2.3}$$

will be an eigenstate of H with $\hat{H}\Psi = E\Psi$, $E = \sum_{i=1}^{f} \varepsilon_i$. Additionally the wave function must still be symmetrized for bosons and antisymmetrized for fermions in order to fulfill the requirement that the wave function takes the same value (bosons) or changes its sign (fermions) under the exchange of two particles. We call bosons the particles for which the wave function must be symmetrical, while fermions are particles for which the wave function must be anti-symmetric. For fermions, suitable

basis states are given by Slater-determinants:

$$\Psi(r_1, r_2, \cdots, r_f) = \frac{1}{\sqrt{f!}} \sum_{\pi} (-1)^{\pi} \prod_{i=1}^{f} \psi_i(r_{i\pi}) \tag{2.4}$$

where π is a permutation of the indices i = 1,..., f and $(-1)^{\pi}$ is its sign, i.e., +1 for even and -1 for odd permutations. The permutation changes the index i into i_{π}. For bosons this sign is left out.

2.2.1 Second quantization: General formalism

The second quantization is a good representation of quantum mechanic operators and wave functions through the creation and destruction operators. Strictly speaking, there is not really another quantization. It is a quantum formalism very useful for treating many identical interacting particles systems. The main advantage of this formalism is the guarantee of the indistinguishability principle, which is implicitly in the anticommutation relations of the operators creation and annihilation. Thus, one avoids the cumbersome work of using antisymmetrized products of single-particle wave functions. In Quantum mechanics, the information specifying that a particle occupies a particular level state is meaningless because the particles are indistinguishable. The only meaningful information is how many particles populate each state level $\psi_i(r)$=the occupation numbers n_i. Any state in the Fock space is noted by $\mid n_1, n_2, \cdots, n_i \big\rangle$ designate a product tensor state where there is n_1 particles in the state $\mid 1\big\rangle$, n_2 particles in the state $\mid 2\big\rangle$ and n_i particles in the state $\mid i\big\rangle$. Given the occupation number operator it is natural to introduce the creation operator $a_i^{\dagger}$ that raises the occupation number in the state $\mid i\big\rangle$ by 1,

$$a_i^{\dagger} \mid \cdots, n_{i-1}, n_i, n_{i+1}, \cdots \big\rangle = B_{ni} + 1 \mid \cdots, n_{i-1}, n_i + 1, n_{i+1}, \cdots \big\rangle \tag{2.5}$$

$$a_i \mid \cdots, n_{i-1}, n_i, n_{i+1}, \cdots \big\rangle = B_{ni}^{*} \mid \cdots, n_{i-1}, n_i - 1, n_{i+1}, \cdots \big\rangle \tag{2.6}$$

where B_{ni} and B_{ni}^{*} are the normalization constants to be determined. The creation and annihilation operators $a_i^{\dagger}$ and a_i are the fundamental operators in the occupation number formalism. These operators allow to pass from a sector to another in the Fock space. From equations (2.5) and (2.6), we can deduce that

$$a_i^{\dagger} a_i \mid \cdots, n_i, \cdots \big\rangle = B_{ni}^{*} a_i^{\dagger} \mid \cdots, n_{i-1}, \cdots \big\rangle = \mid B_{ni} \mid^2 \mid \cdots, n_i, \cdots \big\rangle \tag{2.7}$$

It is possible to distinguish in particular:

The vacuum state

$$\mid vac\rangle =\mid n_1 = 0, n_2 = 0, \cdots, n_i = 0, \cdots \rangle \tag{2.8}$$

The action of a_i on this state gives

$$a_i \mid vac\rangle = 0 \tag{2.9}$$

This relation explains the fact that it is impossible to destroy a particle that does not exist.

The state for a single particle

$$\mid \psi_i\rangle =\mid n_1 = 0, n_2 = 0, \cdots, n_{i-1} = 0, n_i = 1, n_{i+1}, \cdots \rangle \tag{2.10}$$

We can construct this state by making the operator $a_i^\dagger$ to act on the vacuum as $vac \mid \psi_i\rangle = a_i^\dagger \mid vac\rangle$. For the sake of simplicity this state will be noted by $\mid 1\rangle$ and we write $\mid 1\rangle = a_i^\dagger \mid vac\rangle$. We can also destroy it by making it to act on the operator a_i

$$a_i \mid 1\rangle = 0 \tag{2.11}$$

The state for two particles

$$\mid \psi_i\rangle =\mid n_1 = 0, n_2 = 0, \cdots, n_{i-1} = 0, n_i = 2, n_{i+1}, \cdots \rangle \tag{2.12}$$

The states for two particles are generated from the vacuum by

$$\mid 2\rangle = a_i^\dagger a_i^\dagger \mid vac\rangle \tag{2.13}$$

or from the state for a particle as

$$\mid 2\rangle = a_i^\dagger \mid 1\rangle \tag{2.14}$$

If the particles are bosons, the state must be symmetrical. In this case for any i, j the following equality must be true.

$$a_i^\dagger a_j^\dagger \mid vac\rangle = a_j^\dagger a_i^\dagger \mid vac\rangle \tag{2.15}$$

We deduce from equation (2.15) for the bosons that:

$$a_i^\dagger a_j^\dagger = a_j^\dagger a_i^\dagger \Longleftrightarrow [a_i^\dagger, a_j^\dagger] = 0 \tag{2.16}$$

In the same way, we can also have

$$a_i a_j = a_j a_i \Longleftrightarrow [a_i, a_j] = 0 \tag{2.17}$$

On contrary, for the fermions, the state will be antisymmetrical and the equality from the equation (2.15) becomes

$$a_i^\dagger a_j^\dagger \mid vac\rangle = -a_j^\dagger a_i^\dagger \mid vac\rangle \tag{2.18}$$

we deduce that

$$a_i^\dagger a_j^\dagger = -a_j^\dagger a_i^\dagger \Longleftrightarrow \{a_i^\dagger, a_j^\dagger\} = 0 \tag{2.19}$$

and from equation (2.19), we have

$$a_i a_j = -a_j a_i \Longleftrightarrow \{a_i, a_j\} = 0 \tag{2.20}$$

In the Fock space, $N_i \equiv a_i^\dagger a_i$ is where the number for farther ith state. It is hermitian and its eigenvalues which are $n_i = \mid B_{ni} \mid^2$ give effectively the number of particles placed on the site i. For the bosons, the constants of proportionality B_{ni} and B_{ni}^* are such that a state that can accept any number of particles. From the conventional fashion, we take the constant B_{ni} positive.

$$B_{ni} = \sqrt{n_i} \tag{2.21}$$

From equation (2.21), it is clear that

$$a_i^\dagger \mid \cdots, n_i, \cdots\rangle = \sqrt{1+n_i} \mid \cdots, n_i + 1, \cdots\rangle \tag{2.22}$$

$$a_i \mid \cdots, n_i, \cdots\rangle = \sqrt{n_i} \mid \cdots, n_i - 1, \cdots\rangle \tag{2.23}$$

$$a_i^\dagger a_i \mid \cdots, n_i, \cdots\rangle = \sqrt{n_i}\sqrt{1+(n_i-1)} \mid \cdots, (n_i-1)+1, \cdots\rangle \tag{2.24}$$

For the fermions, $n_i = 0, 1$ according to Pauli exclusion principle, we have

$$a_i^\dagger \mid \cdots, n_i, \cdots\rangle = \sqrt{1-n_i} \mid \cdots, n_i + 1, \cdots\rangle \tag{2.25}$$

$$a_i \mid \cdots, n_i, \cdots\rangle = \sqrt{n_i} \mid \cdots, n_i - 1, \cdots\rangle \tag{2.26}$$

These relations allow us to obtain the commutation or anti commutation relations

between $a_i^\dagger$ and a_i that are: for bosons

$$[a_i, a_j^\dagger] = \delta_{ij}, \qquad [a_i^\dagger, a_j^\dagger] = [a_i, a_j] = 0 \tag{2.27}$$

for fermions

$$\{a_i, a_j^\dagger\} = \delta_{ij}, \qquad \{a_i^\dagger, a_j^\dagger\} = \{a_i, a_j\} = 0 \tag{2.28}$$

2.3 Perturbation methods

Quantum study of a physical system is based on the resolution of the Schrödinger equation associated with that system. That resolution can be done exactly only in very special cases where the Hamiltonian is simple to be easily diagonalized, to derive analytically energies and wave functions. In the general case, the Schrödinger equation is very difficult to solve. For this, we use the numerical formulation to approximate analytical solutions by approximation methods. The approximations methods are numerous in quantum physics. These methods are: the derivation method, the Hartree-Fock method, the variational method, the time-dependent perturbation method and the stationary perturbation method. We describe in this section only the stationary perturbation one [104–106].

2.3.1 Stationary perturbation method

This method is applied if a real system is stationary and can be described by small changes in an ideal system where the solutions of Schrödinger equation can be obtained easily. The Hamiltonian of the system is written as

$$H = H_0 + H_1 \tag{2.29}$$

where H_0 is the unperturbed Hamiltonian and H_1 is the perturbing Hamiltonian. $\mid \psi_k^0 \rangle$ is defined as unperturbed eigenvector, and E_k^0 is the unperturbed eigenenergy. Also, $\mid \psi_k \rangle$ is perturbed eigenvectors and E_k is the perturbed eigenenergy. E_k^n is the n-th order energy correction. $\mid \psi_k^n \rangle$ is the n-th order correction of the wave function. We shall consider the orthogonality constraint for the basis i.e. $\langle \psi_k^0 \mid \psi_l^0 \rangle = \delta_{k,l}$; it also requires an intermediate normalization $\langle \psi_k^0 \mid \psi_k \rangle = 1$. The resulting orthogonal constraint is $\langle \psi_k^i \mid \psi_k^j \rangle = \delta_{i,j}$. To understand better the modifications brought by the perturbation method, we introduce a real parameter γ which can be continuously varied between 0 and 1, this can allow us to install gradually the perturbation. The general Hamiltonian takes the form

$$H(\gamma) = H_0 + \gamma H_1 \tag{2.30}$$

The eigenvalue equation of $H(\gamma)$ is written

$$H(\gamma) \mid \psi_k\rangle = (H_0 + \gamma H_1) \mid \psi_k\rangle = E(\gamma) \mid \psi_k\rangle \tag{2.31}$$

2.3.2 Nondegenerate perturbation theory

As $0 < \gamma < 1$, we develop $E(\gamma)$ and $\mid \psi_k\rangle$ in the following form

$$E(\gamma) = E_k^0 + \gamma^1 E_k^1 + \gamma^2 E_k^2 + \gamma^3 E_k^3 + \cdots\cdots\cdots = \sum_{n=0}^{\infty} \gamma^n E_k^n \tag{2.32}$$

$$\mid \psi_k\rangle = \mid \psi_k^0\rangle + \gamma^1 \mid \psi_k^1\rangle + \gamma^2 \mid \psi_k^2\rangle + \gamma^3 \mid \psi_k^3\rangle + \cdots\cdots\cdots = \sum_{n=0}^{\infty} \gamma^n \mid \psi_k^n\rangle \tag{2.33}$$

we substitute (2.32)and (2.33) in (2.31) and we get

$$(H_0 + \gamma H_1)(\sum_{n=0}^{\infty} \gamma^n \mid \psi_k^n\rangle) = (\sum_{n=0}^{\infty} \gamma^n E_k^n)(\sum_{n=0}^{\infty} \gamma^n \mid \psi_k^n\rangle) \tag{2.34}$$

regrouping the terms in power of γ, in each member of (2.34) we obtain the series of equations known as perturbation equations

$$(H_0 - E_k^0) \mid \psi_k^0\rangle = 0 \tag{2.35}$$

$$(H_0 - E_k^0) \mid \psi_k^1\rangle = (E_k^1 - H_1) \mid \psi_k^0\rangle \tag{2.36}$$

$$(H_0 - E_k^0) \mid \psi_k^2\rangle = (E_k^1 - H_1) \mid \psi_k^1\rangle + E_k^2 \mid \psi_k^0\rangle \tag{2.37}$$

$$(H_0 - E_k^0) \mid \psi_k^3\rangle = (E_k^1 - H_1) \mid \psi_k^2\rangle + E_k^2 \mid \psi_k^1\rangle + E_k^3 \mid \psi_k^0\rangle \tag{2.38}$$

$$\vdots \qquad \vdots \qquad \vdots \qquad \vdots$$

$$(H_0 - E_k^0) \mid \psi_k^n\rangle = (E_k^1 - H_1) \mid \psi_k^{n-1}\rangle + E_k^2 \mid \psi_k^{n-2}\rangle + \cdots + E_k^n \mid \psi_k^0\rangle \tag{2.39}$$

Correction of the energy: general case

The correction of the energy at γ^0 order is $H_0 \mid \psi_k^0\rangle = E_k^0 \mid \psi_k^0\rangle$, this is only the eigenvalue equation. The projection of the perturbation equations (2.35-2.39) on a

state $\langle\psi_k^0 \mid$ taking into account the orthogonality constraint for the basis, becomes

$$\begin{aligned} E_k^0 &= \langle\psi_k^0 \mid H_0 \mid \psi_k^0\rangle \\ E_k^1 &= \langle\psi_k^0 \mid H_1 \mid \psi_k^0\rangle \\ E_k^2 &= \langle\psi_k^0 \mid H_1 \mid \psi_k^1\rangle \\ &\vdots \\ E_k^n &= \langle\psi_k^0 \mid H_1 \mid \psi_k^{n-1}\rangle \end{aligned} \tag{2.40}$$

correction of eigenvector: general case

The projection of (2.39) on a state $\langle\psi_{k'}^0 \mid$ gives for $k \neq k'$

$$\langle\psi_{k'}^0 \mid \psi_k^n\rangle = \frac{\langle\psi_{k'}^0 \mid H_1 - E_k^1 \mid \psi_k^{n-1}\rangle - E_k^2\langle\psi_{k'}^0 \mid \psi_k^{n-2}\rangle + \cdots - E_k^n\langle\psi_{k'}^0 \mid \psi_k^0\rangle}{E_k^0 - E_{k'}^0} \tag{2.41}$$

for $k' = k$, we have $\langle\psi_{k'}^0 \mid \psi_k^n\rangle = 0$. As the basis of eigenvectors associated to H_0 is completed, it comes that

$$\mid \psi_k^0\rangle\langle\psi_k^0 \mid = \sum_{k'} \mid \psi_{k'}^0\rangle\langle\psi_{k'}^0 \mid = 1 \tag{2.42}$$

Multiplying (2.42) by $\mid \psi_k^n\rangle$ we get the correction for the perturbing state at the n order:

$$\mid \psi_k^n\rangle = \sum_{k' \neq k} \langle\psi_{k'}^0 \mid \psi_k^n\rangle \mid \psi_{k'}^0\rangle \tag{2.43}$$

using (2.41)

$$\mid \psi_k^n\rangle = \sum_{k' \neq k} \frac{\langle\psi_{k'}^0 \mid \left[H_1 \mid \psi_k^{n-1}\rangle - E_k^1 \mid \psi_k^{n-1}\rangle - E_k^2 \mid \psi_k^{n-2}\rangle - \cdots - E_k^n \mid \psi_k^0\rangle\right]\rangle}{E_k^0 - E_{k'}^0} \mid \psi_{k'}^0\rangle \tag{2.44}$$

First order correction

The first order correction of the energy is non-degenerated and equal to the average value of the perturbation H_1 in the unperturbed state $E_k^1 = \langle\psi_k^0 \mid H_1 \mid \psi_k^0\rangle$. The energy at that order is:

$$E(\gamma) = E_k^0 + \gamma\langle\psi_k^0 \mid H_1 \mid \psi_k^0\rangle \tag{2.45}$$

The correction of the eigenvector at the first order is based on (2.41) and equal to:

$$\mid \psi_k^1 \rangle = \sum_{k' \neq k} \frac{\langle \psi_{k'}^0 \mid H_1 \mid \psi_k^0 \rangle}{E_k^0 - E_{k'}^0} \mid \psi_{k'}^0 \rangle \tag{2.46}$$

and the eigenvector at this order is:

$$\mid \psi_k \rangle = \mid \psi_k^0 \rangle + \gamma \sum_{k' \neq k} \frac{\langle \psi_{k'}^0 \mid H_1 \mid \psi_k^0 \rangle}{E_k^0 - E_{k'}^0} \mid \psi_{k'}^0 \rangle \tag{2.47}$$

Second order correction

According to (2.40), it comes that the second order correction is equal to:

$$E_k^2 = \langle \psi_k^0 \mid H_1 \mid \psi_k^1 \rangle \tag{2.48}$$

i.e. using equation (2.46) we get:

$$E_k^2 = \sum_{k' \neq k} \frac{\mid \langle \psi_k^0 \mid H_1 \mid \psi_{k'}^0 \rangle \mid^2}{E_k^0 - E_{k'}^0} \tag{2.49}$$

The energy at this order is:

$$E(\gamma) = E_k^0 + \gamma \langle \psi_k^0 \mid H_1 \mid \psi_k^0 \rangle + \gamma^2 \sum_{k' \neq k} \frac{\mid \langle \psi_k^0 \mid H_1 \mid \psi_{k'}^0 \rangle \mid^2}{E_k^0 - E_{k'}^0} \tag{2.50}$$

2.3.3 Degenerate perturbation theory

This method is applied in the case where different states have the same energy. The treatment is similar to nondegerate case. By taking into account the degeneracy, we introduce a supplementary index $i = 1, 2, \cdots g_l$, where g_l is the degeneracy order. The energies and eigenvectors of H will be noted respectively by:

$$E(\gamma) = E_{ki}^0 + \gamma^1 E_{ki}^1 + \gamma^2 E_{ki}^2 + \gamma^3 E_{ki}^3 + \cdots\cdots\cdots = \sum_{n=0}^{\infty} \gamma^n E_{ki}^n \tag{2.51}$$

$$\mid \psi_{ki} \rangle = \mid \psi_{ki}^0 \rangle + \gamma^1 \mid \psi_{ki}^1 \rangle + \gamma^2 \mid \psi_{ki}^2 \rangle + \gamma^3 \mid \psi_{ki}^3 \rangle + \cdots\cdots\cdots = \sum_{n=0}^{\infty} \gamma^n \mid \psi_{ki}^n \rangle \tag{2.52}$$

The eigenvalue equation is written as:

$$H(\gamma) \mid \psi_{ki} \rangle = E(\gamma) \mid \psi_{ki} \rangle \tag{2.53}$$

Using the same technique as in nondegenerate case, we obtain:

$$(H_0 - E^0_{ki}) \mid \psi^0_{ki}\rangle = 0 \tag{2.54}$$

$$(H_0 - E^0_{ki}) \mid \psi^1_{ki}\rangle = (E^1_{ki} - H_1) \mid \psi^0_{ki}\rangle \tag{2.55}$$

$$(H_0 - E^0_{ki}) \mid \psi^2_{ki}\rangle = (E^1_{ki} - H_1) \mid \psi^1_{ki}\rangle + E^2_{ki} \mid \psi^0_{ki}\rangle \tag{2.56}$$

$$(H_0 - E^0_{ki}) \mid \psi^3_{ki}\rangle = (E^1_{ki} - H_1) \mid \psi^2_{ki}\rangle + E^2_{ki} \mid \psi^1_{ki}\rangle + E^3_{ki} \mid \psi^0_{ki}\rangle \tag{2.57}$$

$$\vdots \qquad \vdots \qquad \vdots \qquad \vdots$$

$$(H_0 - E^0_{ki}) \mid \psi^n_{ki}\rangle = (E^1_{ki} - H_1) \mid \psi^{n-1}_{ki}\rangle + E^2_{ki} \mid \psi^{n-2}_{ki}\rangle + \cdots + E^n_{ki} \mid \psi^0_{ki}\rangle \tag{2.58}$$

In the case of degenerate perturbation theory, the relation of orthonormalization is written as: $\langle \psi^0_{ki'} \mid \psi^n_{ki}\rangle = 0$, $\langle \psi^0_{ki''} \mid \psi^0_{ki}\rangle = \delta_{ii''}$. Multiplying equation (2.55) by the bra $\langle \psi^0_{k'i''} \mid$ we get

$$\langle \psi^0_{k'i''} \mid H_0 - E^0_{ki} \mid \psi^1_{ki}\rangle = E^1_{ki}\delta_{kk'}\delta_{ii''} - \langle \psi^0_{k'i''} \mid H_1 \mid \psi^0_{ki}\rangle \tag{2.59}$$

For k=k' we get the first order perturbation as:

$$E^1_{ki}\delta_{ii''} = \langle \psi^0_{ki''} \mid H_1 \mid \psi^0_{ki}\rangle \tag{2.60}$$

For $k \neq k'$

$$\langle \psi^0_{k'i''} \mid \psi^1_{ki}\rangle = \frac{\langle \psi^0_{k'i''} \mid H_1 \mid \psi^0_{ki}\rangle}{E^0_{ki} - E^0_{k'i''}} \tag{2.61}$$

Multiplying (2.56) by the bra $\langle \psi^0_{ki'} \mid$ and taking into account the relation of orthonormalization, it comes that

$$E^2_{ki}\delta_{ii'} = \langle \psi^0_{ki'} \mid H_1 \mid \psi^1_{ki}\rangle \tag{2.62}$$

Introducing the relation

$$\sum_{k\neq k',i''} \mid \psi^0_{k'i''}\rangle\langle \psi^0_{k'i''} \mid + \sum_{k,i''} \mid \psi^0_{ki''}\rangle\langle \psi^0_{ki''} \mid = 1$$

into equation (2.62) we get

$$E^2_{ki}\delta_{ii'} = \sum_{k\neq k',i''} \langle \psi^0_{k'i} \mid H_1 \mid \psi^0_{k'i''} \rangle \langle \psi^0_{k'i''} \mid \psi^1_{ki} \rangle + \sum_{k,i''} \langle \psi^0_{ki'} \mid H_1 \mid \psi^0_{ki''} \rangle \langle \psi^0_{ki''} \mid \psi^1_{ki} \rangle \tag{2.63}$$

For $i' \neq i''$, it comes that

$$E^2_{ki}\delta_{ii'} = \sum_{k\neq k',i''} \langle \psi^0_{k'i} \mid H_1 \mid \psi^0_{k'i''} \rangle \langle \psi^0_{k'i''} \mid \psi^1_{ki} \rangle \tag{2.64}$$

Replacing equation (2.61) into (2.64), the correction of energy at the second order becomes for $i = i' \neq i''$:

$$E^2_{ki} = \sum_{k\neq k',i''} \frac{\langle \psi^0_{k'i} \mid H_1 \mid \psi^0_{k'i''} \rangle \langle \psi^0_{k'i''} \mid H_1 \mid \psi^0_{ki} \rangle}{E^0_{ki} - E^0_{k'i''}} \tag{2.65}$$

2.4 Model Hamiltonian

We use a model for the classical Heisenberg ferromagnetic spin chain.

$$H = H_{Ex} = -\sum_{<ij>} J_{ij}\vec{S}_i \cdot \vec{S}_j = -\sum_{<ij>} J_{ij}[S^x_i S^x_j + S^y_i S^y_j + S^z_i S^z_j] \tag{2.66}$$

Here, $\vec{S}_i = (S^x_i, S^y_i, S^z_i)$ is the spin angular momentum vector, J_{ij} is the exchange interaction parameter. We consider in this first section, the isotropic ferromagnetic spin chain case where $J_{ij} = J^x_{ij} = J^y_{ij} = J^z_{ij} = J$. We introduce the classical quantity $S_c = \hbar S$ and a condition which allows the transformation of equation (2.66) into a quantum spin system. We also introduce a dimensionless form $\widehat{S}_i = \frac{\vec{S}_i}{\hbar}$ and define $\widehat{S}^{\pm}_i = \widehat{S}^x_i \pm i\widehat{S}^y_i$ and $\widehat{S}^{\pm}_j = \widehat{S}^x_j \pm i\widehat{S}^y_j$. We recast the Hamiltonian into the following dimensionless form.

$$\widehat{H} = -\sum_{<ij>} \frac{J}{2}[\widehat{S}^{\dagger}_i \widehat{S}^{-}_j + \widehat{S}^{-}_i \widehat{S}^{\dagger}_j - 2\widehat{S}^z_i \widehat{S}^z_j] \tag{2.67}$$

It is impossible to diagonalize the Hamiltonian(2.67) by a canonical transformation, but it is possible to transform to the new dimensionless one, using either pure Bose or pure Fermi operators [109,111]. $\widehat{S}_i$ satisfies the commutation relations $[\widehat{S}^{\dagger}_i, \widehat{S}^{-}_j] = 2\widehat{S}^z_i\delta_{ij}$, $[\widehat{S}^{\pm}_i, \widehat{S}^z_j] = \pm\widehat{S}^{\pm}_i\delta_{ij}$, with $\widehat{S}_i \cdot \widehat{S}_i = S(S+1)$. In this respect, the Hamiltonian maintains a relatively simple form.

If $J_{ij}^{\perp} \neq J_{ij}^{\parallel}$, the Hamiltonian (2.67) becomes

$$\widehat{H} = -\frac{1}{2}\sum_{<ij>} J_{ij}^{\perp}(\widehat{S}_i^{-}\widehat{S}_j^{+} + \widehat{S}_j^{-}\widehat{S}_i^{+}) + \sum_{<ij>} J_{ij}^{\parallel}\widehat{S}_i^{z}\widehat{S}_j^{z} \tag{2.68}$$

It is also possible to use the Fourier transformation defined as follow

$$\widehat{S}_i^{\pm} = \frac{1}{\sqrt{f}}\sum_{\overrightarrow{q}} \widehat{S}_{\overrightarrow{q}}^{\pm} \exp^{\pm} i(\overrightarrow{q}.\overrightarrow{i}), \quad \widehat{S}_{\overrightarrow{q}}^{\pm} = \frac{1}{\sqrt{f}}\sum_{i} \widehat{S}_i^{\pm} \exp^{\pm} i(\overrightarrow{q}.\overrightarrow{i}) \tag{2.69}$$

The Hamiltonian(2.68) can be subdivided in two terms, where the first one is the perpendicular component.

$$\widehat{H}_{\perp} = -\frac{1}{\sqrt{f}}\sum_{<ij>} J_{ij} \sum_{<q_1 q_2>} \widehat{S}_{q_1}^{-}\widehat{S}_{q_2}^{+} \exp -i(\overrightarrow{q_1}.\overrightarrow{i} + \overrightarrow{q_2}.\overrightarrow{j})$$

$$= \sum_j \frac{1}{f}\exp -i(\overrightarrow{q_1} - \overrightarrow{q_2}).\overrightarrow{j} \sum_l J \mid \overrightarrow{l} \mid \sum_{<q_1 q_2>} \widehat{S}_{q_1}^{-}\widehat{S}_{q_2}^{+} \exp -i(\overrightarrow{q}.\overrightarrow{l}) \tag{2.70}$$

with $\overrightarrow{l} = \overrightarrow{i} - \overrightarrow{j}$ then $\overrightarrow{i} = \overrightarrow{j} + \overrightarrow{l}$ and $\sum_j \exp -i(\overrightarrow{q_1} - \overrightarrow{q_2}).\overrightarrow{j} = N\delta\overrightarrow{q_1}\overrightarrow{q_2}$

$$\widehat{H}_{\perp} = \sum_q \widehat{S}_q^{-}\widehat{S}_q^{+} \sum_l J(l) \exp -i(\overrightarrow{q}.\overrightarrow{l}) \tag{2.71}$$

Spins operators must satisfy this anti- commutation relation $[\widehat{S}_j^{+}, \widehat{S}_i^{-}] = 2\widehat{S}_i^{z}\delta ij$
$\widehat{S}_{q_1}^{+}\widehat{S}_{q_2}^{-} - \widehat{S}_{q_1}^{-}\widehat{S}_{q_2}^{+} = \frac{1}{f}\sum_{<ij>}[\widehat{S}_j^{+}\widehat{S}_i^{-} - \widehat{S}_j^{-}\widehat{S}_i^{+}] = \frac{2}{f}\sum_j \widehat{S}_j^{z} \exp -i(\overrightarrow{q_1} - \overrightarrow{q_2}).\overrightarrow{j}$
If T= 0, then all spins are lined up $\Longrightarrow 2S\delta\overrightarrow{q_1}\overrightarrow{q_2}$.
If $T \neq 0$, then all spins are randomly aligned $\Longrightarrow 2 < S^z > \delta\overrightarrow{q_1}\overrightarrow{q_2}$.
$[\widehat{S}_{q_1}^{+}, \widehat{S}_{q_2}^{-}] = Const\delta\overrightarrow{q_1}\overrightarrow{q_2} \Longrightarrow$ bosons.
If does make sense to introduce bosons, we use $\widehat{S}_q^{-} = \sqrt{2S}a_q^{+}$ and $\widehat{S}_q^{+} = \sqrt{2S}a_q$ where $S \gg 1$ and $[a_q, a_q^{+}] = 1$
$\overrightarrow{S_j^2} = (S_j^x)^2 + (S_j^y)^2 + (S_j^z)^2 = S(S+1)$
$\widehat{S}_j^{-}\widehat{S}_j^{+} + \widehat{S}_j^{+}\widehat{S}_j^{-} = (S_j^x)^2 + (S_j^y)^2$
$= \frac{1}{2f}\sum_{<q_1 q_2>}(S_{q_1}^{+}S_{q_2}^{-} - S_{q_2}^{-}S_{q_1}^{+}) \exp -i(\overrightarrow{q_1} - \overrightarrow{q_2}).\overrightarrow{j}$
$= \frac{2S}{2f}\sum_{<q_1 q_2>}(a_{q_1}a_{q_2}^{+} - a_{q_2}^{+}a_{q_1} + \delta q_1 q_2) \exp -i(\overrightarrow{q_1} - \overrightarrow{q_2}).\overrightarrow{j}$
$= \frac{S}{f}\sum_{<q_1 q_2>}\delta q_1 q_2 \exp -i(\overrightarrow{q_1} - \overrightarrow{q_2}).\overrightarrow{j} + \frac{2S}{f}\sum_{<q_1 q_2>} a_{q_2}^{+}a_{q_1} \exp -i(\overrightarrow{q_1} - \overrightarrow{q_2}).\overrightarrow{j}$
$(\widehat{S}_j^{z})^2 = S(S+1) - S - \frac{2S}{f}\sum_{<q_1 q_2>} a_{q_2}^{+}a_{q_1} \exp -i(\overrightarrow{q_1} - \overrightarrow{q_2}).\overrightarrow{j}$ therefore
$\widehat{S}_j^{z} = S\sqrt{1 - \frac{2}{Sf}\sum_{<q_1 q_2>} a_{q_2}^{+}a_{q_1} \exp -i(\overrightarrow{q_1} - \overrightarrow{q_2}).\overrightarrow{j}}$. After approximation, we get
$\widehat{S}_j^{z} = S - \frac{1}{f}\sum_{<q_1 q_2>} a_{q_2}^{+}a_{q_1} \exp -i(\overrightarrow{q_1} - \overrightarrow{q_2}).\overrightarrow{j}$

$$\widehat{H}_{\perp} = -\frac{1}{2}\sum_{<ij>} J_{ij}^{\perp}(\widehat{S}_i^{-}\widehat{S}_j^{+} + \widehat{S}_j^{-}\widehat{S}_i^{+})$$

$$= -\frac{1}{2}\sum_{<ij>}\sum_{<q_1 q_2>} J_{ij}^{\perp}(\widehat{S}_{q_1}^{-}\widehat{S}_{q_2}^{+} + \widehat{S}_{q_2}^{+}\widehat{S}_{q_1}^{-})\exp -i(\overrightarrow{q_1}.\overrightarrow{i} + \overrightarrow{q_2}.\overrightarrow{j})$$

$$= -\frac{S}{f}\sum_{j}\sum_{l} J^{\perp}(l)(a_{q_1}^{+}a_{q_2} + a_{q_2}a_{q_1}^{+})\exp[i(\overrightarrow{q_1} - \overrightarrow{q_2}).\overrightarrow{j} - i\overrightarrow{q}.\overrightarrow{l}]$$

$$= -2S\sum_{q} a_q^{+}a_q \sum_{<ql>} J^{\perp}(l)\exp -i\overrightarrow{q}.\overrightarrow{l} + Sf\sum_{<ql>} J^{\perp}(l)\exp -i\overrightarrow{q}.\overrightarrow{l} \qquad (2.72)$$

The second component of the Hamiltonian (2.68) is called parallel component and is defined as

$$\widehat{H}_{\parallel} = -\sum_{<ij>} J_{ij}^{\parallel}\widehat{S}_i^{z}\widehat{S}_j^{z}$$

$$= -\sum_{<ij>} J_{ij}^{\parallel}(S - \frac{1}{f}\sum_{<q_1 q_2>} a_{q_2}^{+}a_{q_1}\exp -i(\overrightarrow{q_1} - \overrightarrow{q_2}).\overrightarrow{j})(S - \frac{1}{f}\sum_{<q_1 q_2>} a_{q_2}^{+}a_{q_1}\exp -i(\overrightarrow{q_1} - \overrightarrow{q_2}).\overrightarrow{j})$$

$$= -\sum_{<ij>} J_{ij}^{\parallel}(S^2 - \frac{2S}{f}\sum_{<q_1 q_2>} a_{q_2}^{+}a_{q_1}\exp -i(\overrightarrow{q_1} - \overrightarrow{q_2}).\overrightarrow{j})$$

$$= -S^2 fZJ^{\parallel} + 2SZJ^{\parallel}\sum_{q} a_q^{+}a_q \qquad (2.73)$$

f is the number of sites and Z is the number of next neighbors. If $J_{ij}^{\parallel} = J_{ij}^{\parallel} = J$, the Hamiltonian is written as

$$\widehat{H} = \widehat{H}_{\perp} + \widehat{H}_{\parallel} = E_0 + \sum_{q}\epsilon_q a_q^{+}a_q \qquad (2.74)$$

where, $\epsilon_q = 2SJZ(1-\gamma_q)$, $\gamma_q = \frac{1}{Z}\sum_q \exp -i\overrightarrow{q}.\overrightarrow{l} = \frac{1}{3}(\cos(q_x a)+\cos(q_y a)+\cos(q_z a))$ and $E_0 = -S^2 fZJ$

2.5 Semi-fermions

In **Spin algebra**, the general commutation and anti-commutation relation is given by: $[S_i^{\alpha}, S_j^{\beta}] = i\varepsilon_{\alpha\beta\gamma}S_i^{\gamma}\delta_{ij}$. Spins commute on different sites and anti-commute on the same site. This implies that, for different site, the commutation relation is $[S_i^{\alpha}, S_j^{\beta}] = 0$ and in the same site,the anti-commutation relation is $[S_i^{\alpha}, S_i^{\beta}] = i\varepsilon_{\alpha\beta\gamma}S_i^{\gamma}$. To this end, we use the Holstein-Primakoff transformation for the local spin operators to

treat the system from semi-classical as compared to the quantum version in terms of bosonic creation and annihilation operator.

2.6 Holstein-Primakoff transformation

The original [107] Holstein-Primakoff transformation in quantum mechanic is a mapping from the angular momentum operators to boson creation and annihilation operators as:

$$\begin{aligned} \widehat{S}_i^+ &= \sqrt{2}[1-\epsilon^2\tfrac{a_i^\dagger a_i}{2}]^{1/2}\epsilon a_i \\ \widehat{S}_i^- &= \sqrt{2}\epsilon a_i^\dagger[1-\epsilon^2\tfrac{a_i^\dagger a_i}{2}]^{1/2} \\ \widehat{S}_i^z &= [1-\epsilon^2 a_i^\dagger a_i] \end{aligned} \tag{2.75}$$

where $\epsilon = \frac{1}{\sqrt{S}}$, the creation and annihilation bosonic operators $a_i^\dagger$ and a_i satisfy the anti-commutation relation $[a_i, a_i^\dagger] = 1$. The square root of equation (2.75) can be expanded as Taylor series in power of ϵ if $S \to \infty$ and $a_i^\dagger a_i \leqslant 2S$ i.e. $n \leq 2S$ as:

$$[1-\epsilon^2\tfrac{a_i^\dagger a_i}{2}]^{1/2} = 1 - \tfrac{\epsilon^2}{4}a_i^\dagger a_i - \tfrac{\epsilon^4}{32}a_i^\dagger a_i a_i^\dagger a_i - \tfrac{\epsilon^6}{126}a_i^\dagger a_i a_i^\dagger a_i a_i^\dagger a_i - o(\epsilon^8) \tag{2.76}$$

Any states with more that 2S bosons is a perfect bosonic state.

Replacing equation (2.75) and (2.76) in (2.67), a quantum Hamiltonian can be obtained in a power series of ϵ, which is rescaled by J as a sum of

$$\widehat{H}_0 = -S^2 f - \sum_i^f [a_i^\dagger a_{i+1} + a_i a_{i+1}^\dagger - (a_i^\dagger a_i + a_{i+1}^\dagger a_{i+1})] \tag{2.77}$$

that is the unperturbed Hamiltonian and

$$\begin{aligned} \widehat{H}_1 = \frac{1}{4}\sum_i^f \Big[& a_i^\dagger a_i^\dagger a_i a_{i+1} + a_i^\dagger a_{i+1}^\dagger a_{i+1} a_{i+1} + a_i^\dagger a_i a_i a_{i+1}^\dagger \\ & + a_i a_{i+1}^\dagger a_{i+1}^\dagger a_{i+1} - 4 a_i^\dagger a_i a_{i+1}^\dagger a_{i+1} \Big] \end{aligned} \tag{2.78}$$

that is the perturbing Hamiltonian; f is the number of sites in a one-dimensional periodic lattice. In this way, the total Hamiltonian of the system can be written as the sum of two terms as in (2.30), where $\gamma = \epsilon^2$ is the parameter controlling the strength of the interaction.
The Hamiltonian (2.30) conserves the number of bosons $N = \sum_i^f a_i^\dagger a_i$ whose eigenvalue is $n = \sum_i^f n_i$, and it is possible to apply the number state method to calculate the eigenvalues and eigenvectors of the Hamiltonian operator.

2.6.1 Number of state method

To describe the components of the quantum states, we use a position state representation $\mid \psi_i \rangle = \mid n_1, n_2, \cdots, n_f \rangle$, where n_i represents the number of bosons at site i ($n = \sum_i n_i$).

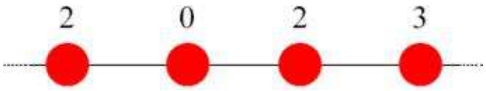

Figure 2.1: Example: 1D lattice, 4 sites and 7 quanta (bosons)

For example, the state $\mid 2023 \rangle$ represents a state with two bosons at the site 1, nothing at site 2, two bosons at site 3 and three bosons at site 4 as seen in Fig. 2.1. Considering the fact that the chain of length f is subject to periodic boundary conditions, we can apply the translation operator to these states. The chain is tanslationally invariant and the Hamiltonian of this quantum system commutes with the number operator $\widehat{N} = \sum_{i=1}^{f} a_i^\dagger a_i$, whose eigenvalue is n. For a given number of bosons, each eigenstate is a linear combination of the number state with fixed n. In addition to the number of quanta n, there are $n-1$ further quantum numbers which define the relative distance between the bosons. The number of states for n particles and f sites is given by $(n+f-1)!/(n!(f-1)!)$, a quantity which expands rapidly with n and f.
For the sake of simplicity, we consider an odd number of sites $f = 2\sigma - 1$, where σ can take $\frac{f+1}{2}$ different values. A general eigenfunction of these states for the Hamiltonian (2.30) is a Bloch wave that can be written as (see the notation in [3, 11, 19, 21, 22])

$$\mid \Psi \rangle = \sum_{i=1}^{\sigma} C_i \mid \psi_i \rangle \tag{2.79}$$

We can construct from the number states technique that a Bloch states as

$$\mid \psi_i \rangle = \frac{1}{\sqrt{f}} \sum_{s=1}^{f} \left(\frac{\widehat{T}}{\tau} \right)^{s-1} \mid 1 \underbrace{0 \cdots 0}_{i-1} 1 \rangle \tag{2.80}$$

Here $\widehat{T}$ is the translation operator and $k = 2\pi\nu/f$, with $\nu \in \{-\frac{f+1}{2}, \frac{f-1}{2}\}$ and $\tau = e^{ik}$ being the eigenvalue of the translational operator $\widehat{T}$. The lattice under consideration is an homogeneous quantum lattice with periodic boundary conditions. Therefore it is possible to block-diagonalize the Hamiltonian operator using eigenfunctions of the translation operator $\widehat{T}$ defined as $\widehat{T} a_i^\dagger = a_{i+1}^\dagger \widehat{T}$, so that $\widehat{T}[n_1, n_2, \cdots, n_f] = [n_f, n_1, \cdots, n_{f-1}]$. In each block, the eigenfunctions have a fixed value of the momentum k [20].

2.6.2 Case of non degenerate perturbation method applied to the ground state

The ground state of the operator $\widehat{H}$ is then obtained when all the spins of f sites are oriented in parallel and there are no spin excited. In this case, the number states constructed is

$$\mid \psi_i\rangle = \frac{1}{\sqrt{f}} \sum_{s=1}^{f} \left(\frac{\widehat{T}}{\tau}\right)^{s-1} \mid 0\underbrace{0\cdots 0}_{i-1}0\rangle \tag{2.81}$$

From periodic boundary conditions, the operators Hamiltonian and $\hat{N}$ commute with the translational operator $\hat{T}$, and τ is the egienvalue of the translational operator $\hat{T}$. For more precision, we define an eigenstate with the following eigenvector

$$\begin{array}{l} \mid \psi_0\rangle = \frac{1}{\sqrt{f}}\{\mid 0,0,0,0,\cdots,0\rangle + \frac{1}{\tau} \mid 0,0,0,0,0,\cdots,0\rangle \\ +\frac{1}{\tau^2} \mid 0,0,0,0,0,\cdots,0\rangle + \cdots + \frac{1}{\tau^{(f-1)}} \mid 0,0,0,0,0,\cdots,0\rangle\} \end{array} \tag{2.82}$$

We apply the eigenvector (2.82) in each term of the operator Hamiltonian

$$\begin{array}{l} \widehat{H} \mid \Psi\rangle = (\widehat{H}_0 + \gamma \widehat{H}_1) \mid \psi_0\rangle \\ = -S^2 f J \mid \psi_0\rangle = E_0 \mid \psi_0\rangle \end{array} \tag{2.83}$$

2.6.3 Case of non degenerate perturbation method applied to the first excited state

This state corresponds to the case where a single local spin-flip excitation occurs in a ferromagnetic spin chain with f sites. The number states proceeded here lead to a Bloch states given through.

$$\mid \psi_i\rangle = \frac{1}{\sqrt{f}} \sum_{s=1}^{f} \left(\frac{\widehat{T}}{\tau}\right)^{s-1} \mid 1\underbrace{0\cdots 0}_{i-1}0\rangle \tag{2.84}$$

For a given eigenstate chosen as $\mid \phi\rangle$, we get $\widehat{T} \mid \phi\rangle = \tau \mid \phi\rangle$. The periodic condition also requires that $\widehat{T}^f \mid \phi\rangle = \tau^f \mid \phi\rangle = \mid \phi\rangle$. Thus it comes that $\tau^f = 1$. For more precision, we define an eigenstate with the following eigenvector

$$\begin{array}{l} \mid \psi_1\rangle = \frac{1}{\sqrt{f}}\{\mid 1,0,0,0,\cdots,0\rangle + \frac{1}{\tau} \mid 0,1,0,0,0,\cdots,0\rangle \\ +\frac{1}{\tau^2} \mid 0,0,1,0,0,\cdots,0\rangle + \cdots + \frac{1}{\tau^{(f-1)}} \mid 0,0,0,0,0,\cdots,1\rangle\} \end{array} \tag{2.85}$$

We apply the eigenvector (2.85) in each term of the operator Hamiltonian

$$\begin{aligned} &a_i^\dagger a_{i+1} \mid \psi_1\big\rangle = \tfrac{1}{\sqrt{f}}\{\mid 0,1,0,0,\cdots,0\big\rangle + \tfrac{1}{\tau} \mid 0,0,1,0,0,\cdots,0\big\rangle \\ &+\tfrac{1}{\tau^2} \mid 0,0,0,1,0,\cdots,0\big\rangle + \cdots + \tfrac{1}{\tau^{(f-1)}} \mid 1,0,0,0,0,\cdots,0\big\rangle\} \\ &= \tau \mid \psi_1\big\rangle \end{aligned} \tag{2.86}$$

$$\begin{aligned} &a_i a_{i+1}^\dagger \mid \psi_1\big\rangle = \tfrac{1}{\sqrt{f}}\{\mid 0,0,0,0,\cdots,1\big\rangle + \tfrac{1}{\tau} \mid 0,1,0,0,0,\cdots,0\big\rangle \\ &+\tfrac{1}{\tau^2} \mid 0,0,1,0,0,\cdots,0\big\rangle + \cdots + \tfrac{1}{\tau^{(f-1)}} \mid 0,0,0,0,0,\cdots,1\big\rangle\} \\ &= \tau^{-1} \mid \psi_1\big\rangle \end{aligned} \tag{2.87}$$

$$\begin{aligned} &(a_i^\dagger a_i + a_{i+1}^\dagger a_{i+1}) \mid \psi_1\big\rangle = \tfrac{1}{\sqrt{f}}\{\mid 1,0,0,0,\cdots,0\big\rangle + \tfrac{1}{\tau} \mid 0,1,0,0,0,\cdots,0\big\rangle \\ &+\tfrac{1}{\tau^2} \mid 0,0,1,0,0,\cdots,0\big\rangle + \cdots + \tfrac{1}{\tau^{(f-1)}} \mid 0,0,0,0,0,\cdots,1\big\rangle\} \\ &= 2 \mid \psi_1\big\rangle \end{aligned} \tag{2.88}$$

Applying the eigenvector (2.85) in equation (2.30) and using respectively (2.86), (2.87) and (2.88), we found that eigenenergy at the first excited state is

$$\widehat{H} \mid \Psi\big\rangle = (\widehat{H}_0 + \gamma \widehat{H}_1) \mid \psi_1\big\rangle = (-S^2 f J - (\tau + \tau^{-1} - 2)) \mid \psi_1\big\rangle = (E_0 + E_1) \mid \psi_1\big\rangle \tag{2.89}$$

It is important to mention here that the response of the eigenfunction by the application of $\widehat{H}_1$ is nil i.e. $\widehat{H}_1 \mid \psi_1\big\rangle = 0$. This eigenenergy E_1 will be plotted and commented in the next chapter.

2.6.4 Case of non degenerate perturbation theory applied to the second excited state

We consider the two local spin-flip excitations in the model. The general eigenfunction is given by

$$\begin{aligned} &\mid \Psi\big\rangle = \tfrac{1}{\sqrt{f}}\{C_1 \textstyle\sum_{s=1}^{f} (\frac{\hat{T}}{\tau})^{s-1} \mid 2,0,\cdots,0\big\rangle + C_2 \sum_{s=1}^{f} (\frac{\hat{T}}{\tau})^{s-1} \mid 1,1,0,\cdots,0\big\rangle \\ &+C_3 \textstyle\sum_{s=1}^{f} (\frac{\hat{T}}{\tau})^{s-1} \mid 1,0,1,0,0,\cdots,0\big\rangle + \cdots \\ &+C_{(f+1)/2} \textstyle\sum_{s=1}^{f} (\frac{\hat{T}}{\tau})^{s-1} \mid 1,0,\cdots,0,1,\cdots,0\big\rangle \end{aligned} \tag{2.90}$$

To ensure that $\big\langle \Psi \mid \Psi \big\rangle = 1$, it is necessary that $C_1, C_2, ...$ are normalized as $\sum_{i=1}^{(f+1)/2} \Big|C_i\Big|^2 = 1$. The general eigenfunction is the linear combination basic state where we note here that $\mid \psi_1\big\rangle = \frac{1}{\sqrt{f}}\{C_1 \sum_{s=1}^{f} (\frac{\hat{T}}{\tau})^{s-1} \mid 2,0,\cdots,0\big\rangle$, $\mid \psi_2\big\rangle = \frac{1}{\sqrt{f}}\{C_2 \sum_{s=1}^{f} (\frac{\hat{T}}{\tau})^{s-1} \mid 1,1,0,\cdots,0\big\rangle$, $\cdots$,
$\mid \psi_{(f+1)/2}\big\rangle = \frac{1}{\sqrt{f}}\{C_{(f+1)/2} \sum_{s=1}^{f} (\frac{\hat{T}}{\tau})^{s-1} \mid 1,0,\cdots,0,1\cdots 0,0\big\rangle$ are the eigenvectors. The action of the Hamiltonian operator given in equation (2.30) applied to each eigenfunction gives for the case of a value $f = 7$ (number of sites in the lattice) with

4 basis states. The number of basis n depends on the number of site in the lattice and it is given as follows $1 \leq n \leq \frac{f+1}{2}$ if f is odd and $1 \leq n \leq \frac{f}{2}$ for even values of f.

$$\begin{aligned}
\widehat{H} \mid \psi_1\big\rangle &= -\big[\sqrt{2}(\tfrac{\gamma}{4}-1)(1+\tau^{-1}) \mid \psi_2\big\rangle - 4 \mid \psi_1\big\rangle\big] \\
\widehat{H} \mid \psi_2\big\rangle &= -\big[\sqrt{2}(\tfrac{\gamma}{4}-1)(1+\tau) \mid \psi_1\big\rangle + (\tfrac{\gamma}{2}-4) \mid \psi_2\big\rangle + (1+\tau^{-1}) \mid \psi_3\big\rangle\big] \\
\widehat{H} \mid \psi_3\big\rangle &= -\big[(1+\tau) \mid \psi_2\big\rangle - 4 \mid \psi_3\big\rangle + (1+\tau^{-1}) \mid \psi_4\big\rangle\big] \\
\widehat{H} \mid \psi_4\big\rangle &= -\big[(1+\tau) \mid \psi_3\big\rangle - 4 \mid \psi_4\big\rangle + (\tau^3+\tau^{-3}) \mid \psi_4\big\rangle\big]
\end{aligned} \tag{2.91}$$

For successive calculation with increasing of f, it comes that

$$\begin{aligned}
\widehat{H} \mid \psi_{(n-1)}\big\rangle &= -\big[(1+\tau) \mid \psi_{(n-2)}\big\rangle - 4 \mid \psi_{n-1}\big\rangle + (1+\tau^{-1}) \mid \psi_n\big\rangle\big] \\
\widehat{H} \mid \psi_n\big\rangle &= -\big[(1+\tau) \mid \psi_{(n-1)}\big\rangle - 4 \mid \psi_n\big\rangle + (\tau^{\frac{f+1}{2}} + \tau^{-\frac{(f+1)}{2}}) \mid \psi_n\big\rangle\big]
\end{aligned} \tag{2.92}$$

With the basis introduced in equations (2.91) and (2.92), we can derive the matrix elements of the Hamiltonian by the formula

$$H_{ij} = \big\langle \Psi_j \mid \hat{H} \mid \Psi_i \big\rangle = \big\langle \psi_j \mid \hat{H} \mid \psi_i \big\rangle \tag{2.93}$$

From equation (2.93) it is clear that

$$\begin{aligned}
\hat{H}_{11} &= \big\langle \Psi_1 \mid \hat{H} \mid \Psi_1 \big\rangle = \big\langle \psi_1 \mid \hat{H} \mid \psi_1 \big\rangle = -u \\
\hat{H}_{12} &= \big\langle \Psi_2 \mid \hat{H} \mid \Psi_1 \big\rangle = \big\langle \psi_2 \mid \hat{H} \mid \psi_1 \big\rangle = -\sqrt{2}q* \\
\hat{H}_{21} &= \big\langle \Psi_1 \mid \hat{H} \mid \Psi_2 \big\rangle = \big\langle \psi_1 \mid \hat{H} \mid \psi_2 \big\rangle = -\sqrt{2}q \\
\hat{H}_{22} &= \big\langle \Psi_2 \mid \hat{H} \mid \Psi_2 \big\rangle = \big\langle \psi_2 \mid \hat{H} \mid \psi_2 \big\rangle = -y \\
\hat{H}_{23} &= \big\langle \Psi_3 \mid \hat{H} \mid \Psi_2 \big\rangle = \big\langle \psi_3 \mid \hat{H} \mid \psi_2 \big\rangle = -g* \\
\hat{H}_{32} &= \big\langle \Psi_2 \mid \hat{H} \mid \Psi_3 \big\rangle = \big\langle \psi_2 \mid \hat{H} \mid \psi_3 \big\rangle = -g \\
\hat{H}_{33} &= \big\langle \Psi_3 \mid \hat{H} \mid \Psi_3 \big\rangle = \big\langle \psi_3 \mid \hat{H} \mid \psi_3 \big\rangle = -u \\
\hat{H}_{34} &= \big\langle \Psi_4 \mid \hat{H} \mid \Psi_3 \big\rangle = \big\langle \psi_4 \mid \hat{H} \mid \psi_3 \big\rangle = -g* \\
\hat{H}_{43} &= \big\langle \Psi_3 \mid \hat{H} \mid \Psi_4 \big\rangle = \big\langle \psi_3 \mid \hat{H} \mid \psi_4 \big\rangle = -g \\
\hat{H}_{44} &= \big\langle \Psi_4 \mid \hat{H} \mid \Psi_4 \big\rangle = \big\langle \psi_4 \mid \hat{H} \mid \psi_4 \big\rangle = -(u+\tau^3+\tau^{-3})
\end{aligned} \tag{2.94}$$

For successive calculation with increasing of f, it comes that

$$\begin{aligned}
\hat{H}_{\frac{f-1}{2}\frac{f+1}{2}} &= \big\langle \Psi_{\frac{f+1}{2}} \mid \hat{H} \mid \Psi_{\frac{f-1}{2}} \big\rangle = \big\langle \psi_{\frac{f+1}{2}} \mid \hat{H} \mid \psi_{\frac{f-1}{2}} \big\rangle = -g* \\
\hat{H}_{\frac{f+1}{2}\frac{f-1}{2}} &= \big\langle \Psi_{\frac{f-1}{2}} \mid \hat{H} \mid \Psi_{\frac{f+1}{2}} \big\rangle = \big\langle \psi_{\frac{f-1}{2}} \mid \hat{H} \mid \psi_{\frac{f+1}{2}} \big\rangle = -g \\
\hat{H}_{\frac{f+1}{2}\frac{f+1}{2}} &= \big\langle \Psi_{\frac{f+1}{2}} \mid \hat{H} \mid \Psi_{\frac{f+1}{2}} \big\rangle = \big\langle \psi_{\frac{f+1}{2}} \mid \hat{H} \mid \psi_{\frac{f+1}{2}} \big\rangle = -(u+\tau^{-\frac{f+1}{2}}+\tau^{-\frac{f-1}{2}})
\end{aligned} \tag{2.95}$$

2.6.5 Effect of the anisotropy interaction in the Heisenberg ferromagnetic spin chain Model

We describe the novel Hamiltonian for an anisotropic ferromagnetic chain. The corresponding Heisenberg Hamiltonian can be written as

$$H_{An} = H + \sum_i A(S_i^z)^2 \tag{2.96}$$

The term proportional to A represents the single-ion uniaxial anisotropy due to crystal field effect and A is the anisotropy parameter. We can derive the discrete quantum Hamiltonian using Holstein-Primakoff bosonic representation then equation (2.96) can be written after introducing dimensionless Hamiltonian

$$\widehat{H}_{An} = \widehat{H}_{A_0} + \gamma \widehat{H}_{A_1} + O(\gamma^2) \tag{2.97}$$

Hence we set

$$\widehat{H}_{A_0} = \widehat{H}_0 + 2\frac{A}{J}\sum_i^f a_i^\dagger a_i \tag{2.98}$$

and

$$\widehat{H}_{A_1} = \widehat{H}_1 - 4\frac{A}{J}\sum_i^f a_i^\dagger a_i a_i^\dagger a_i \tag{2.99}$$

We also use the basis introduced in equation (2.80) to calculate the matrix elements for a dimensionless Hamiltonian. In this way the Hamiltonian matrix is presented in the next chapter.

2.6.6 Application of degenerate theory when four or six bosons are involved in the extended Bose-Hubbard chain

We consider here the same Hamiltonian given in equation (2.96) with resealing at ϵ^2. Before using degenerated perturbation theory, it is important to know that all bosons on the same band might have the same energy. The Hamiltonian of equation (2.96) shows that all bosons on the same band have different energy at zero anisotropy coupling ($A = 0$). In order to discourage many bosons to occupy the same site, we can derived a Bose-Hubbard like lattice from a specific anisotropic term by using the usual commutation relations of the bosonic operators . For this we start by defining the perturbed Hamiltonian as $\widehat{H} = \widehat{H}_0 + \widehat{V}$, where $\widehat{H}_0$ is the nonlinear

on-site interaction Hamiltonian given by

$$\widehat{H}_0 = -\sum_{i}^{f} A\gamma a_i^\dagger a_i^\dagger a_i a_i \tag{2.100}$$

If $A < 0$, the model is also known to describe an attractive interaction or a repulsive one if $A > 0$. All the other term of the Hamiltonian describe the non-linear interaction within the particles located in adjacent sites, including the hopping term and linear on-site interaction terms. It is denoted by $\widehat{V}$.

$$\begin{aligned}\widehat{V} = &-\textstyle\sum_i^f \Big(J[a_i^\dagger a_{i+1} + a_i a_{i+1}^\dagger - (a_i^\dagger a_i + a_{i+1}^\dagger a_{i+1})] + A(a_i^\dagger a_i) \\ &+\tfrac{\gamma}{4} J[(a_i^\dagger a_i^\dagger a_i a_{i+1} + a_i^\dagger a_{i+1}^\dagger a_{i+1} a_{i+1}) + (a_i^\dagger a_i a_i a_{i+1}^\dagger + a_i a_{i+1}^\dagger a_{i+1}^\dagger a_{i+1}) - 4a_i^\dagger a_i a_{i+1}^\dagger a_{i+1}]\Big)\end{aligned} \tag{2.101}$$

To describe the components of the quantum states, we use a position state basis representation as in the third section. For sake of memory, the state $\mid \psi_i >= \mid 2000110 >$ represents a state with two bosons at site 1, one boson at site 5, one boson at site 6 and no boson elsewhere. In view of the periodic structure of the lattice, the chain is translationally invariant and the Hamiltonian of this quantum system commutes with the number operator $\widehat{N} = \sum_{i=1}^{f} a_i^\dagger a_i$, whose eigenvalue is denoted by n. We can generate an equivalence class of states by applying the translation operator with a periodic boundary conditions to one of these states. We can manage to order these classes. For example, the set of all classes containing $\mid 22 >$, $\mid 202 >$, $\mid 2002 >$, and so on, is referred to as the $\{2, 2\}$ band. All classes containing $\mid 42 >$, $\mid 402 >$, $\mid 4002 >$, ..., is referred to the $\{4, 2\}$ band. All the classes containing $\mid 24 >$, $\mid 204 >$, $\mid 2004 >$, ..., is referred to as the $\{2, 4\}$ band and all the classes containing $\mid 33 >$, $\mid 303 >$, $\mid 3003 >$, ... is referred to $\{3, 3\}$ bands.

Bands involving the interaction of single bosons with composite states, such as $\{2, 1, 1\}$, $\{3, 1\}$, $\{4, 1, 1\}$, $\{3, 1, 1, 1\}$, $\{5, 1\}$, $\{1, 1, 2\}$, $\{1, 3\}$, $\{1, 1, 4\}$, $\{1, 1, 1, 3\}$, $\{1, 5\}$, $\cdots$, are more difficult to analyze and do not reveal interesting structures. Hence, we do not consider these bands in the present study provided that the main information is not loosed. This section is devoted to the fine structure of the $\{2, 2\}$, $\{4, 2\}$, $\{2, 4\}$ and $\{3, 3\}$ band.

If the anisotropy is considered without the Hamiltonian term denoted by $\widehat{V}$, the states $\mid 22 >$, $\mid 202 >$, $\mid 2002 >$, ..., of all previously mentioned bands are degenerated. Therefore, we use degenerated perturbation theory to obtain both eigenvalues and eigenvectors for the case of the perturbed Hamiltonian. For a given number of bosons, each eigenstate is a linear combination of the number of states with fixed n. In addition to the number of quanta n, there are $n-1$ further relative distance $i-1$ between the four and six quanta. We consider an odd number of sites $f = 2\sigma - 1$, which can take $(f+1)/2$ different values for the sake of simplicity. We do proceed

in the same way as in the third section, then the Bloch waves of $\{2,2\}$, $\{4,2\}$, $\{2,4\}$ and $\{3,3\}$ states can be written in the notation of Ref. [19,22,107] as:

$$\mid \psi >= \sum_{i=1}^{\sigma} C_i \mid \psi_i > \tag{2.102}$$

We can construct number states with Bloch waves as

$$\begin{aligned}
\mid \psi_i >&= \frac{1}{\sqrt{f}} \sum_{s=1}^{f} \left(\frac{\widehat{T}}{\tau}\right)^{s-1} \mid 2\underbrace{0\cdots 0}_{i-1}2 > \\
\mid \psi_i >&= \frac{1}{\sqrt{f}} \sum_{s=1}^{f} \left(\frac{\widehat{T}}{\tau}\right)^{s-1} \mid 4\underbrace{0\cdots 0}_{i-1}2 > \\
\mid \psi_i >&= \frac{1}{\sqrt{f}} \sum_{s=1}^{f} \left(\frac{\widehat{T}}{\tau}\right)^{s-1} \mid 2\underbrace{0\cdots 0}_{i-1}4 > \\
\mid \psi_i >&= \frac{1}{\sqrt{f}} \sum_{s=1}^{f} \left(\frac{\widehat{T}}{\tau}\right)^{s-1} \mid 3\underbrace{0\cdots 0}_{i-1}3 >
\end{aligned} \tag{2.103}$$

Here $\widehat{T}$ is the translation operator and $\tau = e^{ik}$, with $k = 2\pi\nu/f$ and $\nu \in \{-\sigma, \cdots, \sigma\}$. Using standard degenerated perturbation to the second order approximation given by equation(2.65), we define the Hamiltonian matrix element in its simplest notation after changing in equation (2.65), $< \psi^0_{k'i} \mid$ by $< \psi_i \mid$, $\mid \psi^0_{k'i''}\big\rangle\big\langle\psi^0_{k'i''} \mid$ by $\mid \widetilde{\psi} >< \widetilde{\psi} \mid$, $\mid \psi^0_{ki}\big\rangle$ by $\mid \psi_{i'} >$, H_1 by V and $E^0_{k'i''}$ by $\widetilde{E}^{(0)}$ as

$$H^{(m,l)}_{i,i'} = \sum_{\widetilde{\psi}} \frac{< \psi_i \mid V \mid \widetilde{\psi} >< \widetilde{\psi} \mid V \mid \psi_{i'} >}{E^{(0)} - \widetilde{E}^{(0)}} \tag{2.104}$$

where $\mid \widetilde{\psi} >$ is any state not in the $\{2,2\}$, $\{4,2\}$, $\{2,4\}$ and $\{3,3\}$ subspace; $\widetilde{E}^{(0)}$ is the corresponding energy of $\mid \widetilde{\psi} >$ while $E^{(0)}$ is the energy of (m,l) bosons on the same site at zero coupling. The expression of this energy is given as

$$E^{(0)}_l = -A\gamma l(l-1) \tag{2.105}$$

We can use equation(2.105) to evaluate the energy of l bosons on the same site. For instance, in the case of $n = 4$, the $\{4\}$ band has energy $E^{(0)}_4 = -12A\gamma$, the $\{3,1\}$ band has energy $E^{(0)}_3 = -6A\gamma$, the $\{2,1,1\}$ band has energy $E^{(0)}_2 = -2A\gamma$, the $\{2,2\}$ band has energy $2E^{(0)}_2 = -4A\gamma$ and so on.
Considering the lattice with four bosons ($n = 4$). We can subdivide this case in several bands. The lowest band is a linear combination of states with four bosons on site i and no bosons somewhere else. The next lowest band is composed of states

with three bosons on site and another boson elsewhere. The third band consists of states with two bosons on one site and two bosons on a separate site. Bands involving the interactions of single bosons with composite states, such as $\{3,1\}$, $\{1,3\}$, $\{1,1,2\}$ and $\{1,1,2\}$ are not consider here because they are more difficult to analyze. We consider here only the $\{2,2\}$ band because it presents great interest since it represents the simplest case of a band describing two particles interacting with each other. The calculations detailed of its elements of Hamiltonian matrix are shown in Appendix.

Next, we consider the case of $n = 6$ bosons. This case displays three bands: namely the bands $\{4,2\}$, $\{2,4\}$ and $\{3,3\}$.
In this case, the first band under consideration is the $\{4,2\}$ band. Then if we proceed as in the case of $\{2,2\}$ band, it turns out that we obtained a Hamiltonian matrix describing this $\{4,2\}$. The second band is the $\{2,4\}$ band and the last band is the $\{3,3\}$.

2.7 Effect of the DMI in the Heisenberg anisotropic exchange ferromagnetic spin chain Model

To describe a weak ferromagnetic system, we consider a one dimensional Heisenberg ferromagnetic spin chain defined by a coupling between the Heisenberg anisotropic exchange H_{Ex} from equation (1.4) and the Dzyaloshinskii-Moriya interaction H_D from equation (1.6) given by the following Hamiltonian :

$$H_M = -\sum_{<ij>}\Big[J_{ij}\vec{S}_i\cdot\vec{S}_j + \vec{D}_{ij}\cdot(\vec{S}_i\wedge\vec{S}_j)\Big] \tag{2.106}$$

The first term is the Heisenberg anisotropic exchange energy between nearest-neighbor spins $< ij >$ where J_{ij} is the exchange interaction parameter, the second term represents the DM interaction, which is an antisymmetric exchange interaction between two magnetic moments $\vec{S}_i$ and $\vec{S}_j$. This term is used for modeling a weak ferromagnet. Here $\vec{D}_{ij}$ is the DM vector. It is antisymmetric with regards to site permutation $D_{ij} = -D_{ji}$. In contrast with D_{ij}, J_{ij} is symmetric and $D_{ij} < J_{ij}$, $\vec{S}_i = (S_i^x, S_i^y, S_i^z)$ is the spin angular momentum operator.
For the sake of simplicity, we will denote $D_{ij} = D$ with $\vec{D} = (D^x, D^y, D^z)$, $\vec{S}_j$ by $\vec{S}_{i+1}$ and J_{ij} will be replaced by J_1 and J_2.
Introducing the dimensionless spin variables $\widehat{S}_i = \frac{S_i}{\hbar}$ and defining $\widehat{S}_i^{\pm} = \widehat{S}_i^x \pm i\widehat{S}_i^y$ and $\widehat{D}_i^{\pm} = \widehat{D}_i^x \pm i\widehat{D}_i^y$, the Hamiltonian(2.106), considering f sites becomes

$$\begin{aligned}\widehat{H}_M = -\frac{1}{2}\sum_i\Big[J_1(\widehat{S}_i^{\dagger}\widehat{S}_{i+1}^{-} + \widehat{S}_i^{-}\widehat{S}_{i+1}^{\dagger}) + 2J_2\widehat{S}_i^z\widehat{S}_{i+1}^z\Big] - i\sum_i\Big[\widehat{D}_i^{\dagger}(\widehat{S}_i^z\widehat{S}_{i+1}^{-} \\ -\widehat{S}_i^{-}\widehat{S}_{i+1}^z) + \widehat{D}_i^{-}(\widehat{S}_i^{\dagger}\widehat{S}_{i+1}^z - \widehat{S}_i^z\widehat{S}_{i+1}^{\dagger}) + \widehat{D}_z(\widehat{S}_i^{-}\widehat{S}_{i+1}^{\dagger} - \widehat{S}_i^{\dagger}\widehat{S}_{i+1}^{-})\Big]\end{aligned} \tag{2.107}$$

Using the Holstein-Primakoff transformation, the quantum Hamiltonian giving by equation (2.107) can be rewritten as a power series in ϵ by two terms after being rescaled with ϵ^2 as a sum of

$$\widehat{H}_M = \widehat{H}_{M_0} + \gamma \widehat{H}_{M_1} \tag{2.108}$$

where $\gamma = \epsilon^2$ is the parameter controlling the strength of the interaction, $\alpha = J_1 + iD_z$, $\alpha^* = J_1 - iD_z$, f is the total number of sites. D_z is DM vector along the z-axis, can be considered by an anisotropy.

$$\widehat{H}_{M_0} = -S^2 f J_2 - \sum_i^f \left[\alpha^* a_i^\dagger a_{i+1} + \alpha a_i a_{i+1}^\dagger - J_2(a_i^\dagger a_i + a_{i+1}^\dagger a_{i+1})\right] \tag{2.109}$$

and

$$\begin{aligned} \widehat{H}_{M_1} = \sum_i^f \tfrac{1}{4}\Big[&\alpha^*(a_i^\dagger a_i^\dagger a_i a_{i+1} + a_i^\dagger a_{i+1}^\dagger a_{i+1} a_{i+1}) \\ &+\alpha(a_i^\dagger a_i a_i a_{i+1}^\dagger + a_i a_{i+1}^\dagger a_{i+1}^\dagger a_{i+1}) - 4J_2(a_i^\dagger a_i a_{i+1}^\dagger a_{i+1})\Big] \end{aligned} \tag{2.110}$$

2.7.1 The ground state when DMI are involved

Using the same non degenerated method, we realize that the energy of the ground state is

$$\widehat{H}_M \mid \Psi\big\rangle = (\widehat{H}_{M_0} + \gamma \widehat{H}_{M_1}) \mid \psi_0\big\rangle = -S^2 f J_2 \mid \psi_0\big\rangle = E_{M_0} \mid \psi_0\big\rangle \tag{2.111}$$

2.7.2 The first excited state when DMI are involved

The energy of the first excited state is

$$\begin{aligned} &\widehat{H}_M \mid \Psi\big\rangle = (\widehat{H}_{M_0} + \gamma \widehat{H}_{M_1}) \mid \psi_1\big\rangle \\ &= (-S^2 f J_2 - (\alpha^* \tau + \alpha \tau^{-1} - 4J_2)) \mid \psi_1\big\rangle = (E_{M_0} + E_{M_1}) \mid \psi_1\big\rangle \end{aligned}$$

For the cases where DMI are taking into account in the model, when two, four and six spins are excited, Let us start by defining the new perturbed Hamiltonian as $\widetilde{H}_M = \widehat{H}_{M_0} + \widehat{V}_M$, where $\widehat{H}_{M_0}$ is the on site interaction part of the Bose-Hubbard Hamiltonian.
All the remaining term of the Hamiltonian describe the nonlinear interactions between the spin located in adjacent sites as well as the linear on site interactions in addition to the hopping terms represented by $\widehat{V}$.

$$\widehat{H}_{M_0} = -\sum_i^f A\gamma a_i^\dagger a_i^\dagger a_i a_i \tag{2.112}$$

and

$$\begin{aligned}\widehat{V}_M = &-\sum_i^f \Big[\alpha^* a_i^\dagger a_{i+1} + \alpha a_i a_{i+1}^\dagger - J_2(a_i^\dagger a_i + a_{i+1}^\dagger a_{i+1}) + A(2a_i^\dagger a_i) \\ &-\tfrac{\gamma}{4}[\alpha^*(a_i^\dagger a_i^\dagger a_i a_{i+1} + a_i^\dagger a_{i+1}^\dagger a_{i+1} a_{i+1}) + \alpha(a_i^\dagger a_i a_i a_{i+1}^\dagger + a_i a_{i+1}^\dagger a_{i+1}^\dagger a_{i+1}) \\ &-4J_2 a_i^\dagger a_i a_{i+1}^\dagger a_{i+1} - A a_i^\dagger a_i]\Big]\end{aligned} \tag{2.113}$$

Using equations (2.104) and (2.126), we obtain the $\{2,2\}$, $\{4,2\}$, $\{2,4\}$ and $\{3,3\}$ band Hamiltonian matrix presented in the next chapter. To avoid overloading the thesis, detailed calculations in this section are presented in the Appendix (A, B, C, D).

2.8 Effect of the long range interaction in a Heisenberg isotropic exchange ferromagnetic spin chain model

In this section, we present different types of Heisenberg Hamiltonians while the effects of longer range interaction are taken into account.

2.8.1 Effect of the second nearest neighbor

We consider a model for a one dimensional Heisenberg ferromagnetic spin chain, which includes in addition to the first nearest neighbors interaction with strength J_1 the second nearest neighbors ferromagnetic interaction with strength J_2.

$$H_{L_1} = -\sum_i \left(\vec{S}_i \cdot \vec{S}_{i+1} + \alpha_1 \vec{S}_i \cdot \vec{S}_{i+2}\right) \tag{2.114}$$

Here, $\alpha_1 = J_2/J_1$ is the ratio controlling the coupling interaction between the first and second nearest-neighbor. We recast the Hamiltonian into the following dimensionless form as an isotropic Heisenberg model where interactions between spin components along each axis are equals $J_x = J_y = J_z = J$

$$\begin{aligned}\widehat{H}_{L_1} = -\sum_i \frac{1}{2}[&\widehat{S}_i^+ \widehat{S}_{i+1}^- + \widehat{S}_i^- \widehat{S}_{i+1}^+ + 2\widehat{S}_i^z \widehat{S}_{i+1}^z \\ &+\alpha_1(\widehat{S}_i^+ \widehat{S}_{i+2}^- + \widehat{S}_i^- \widehat{S}_{i+2}^+ + 2\widehat{S}_i^z \widehat{S}_{i+2}^z)]\end{aligned} \tag{2.115}$$

Using equation (2.75), we transform the Hamiltonian (2.115)in to a quantum Hamiltonian as

$$\begin{aligned}\widehat{H}_{L_1} = &-\sum_i^f \Big[a_i^\dagger a_{i+1} + a_i a_{i+1}^\dagger - (a_i^\dagger a_i + a_{i+1}^\dagger a_{i+1}) + \tfrac{\gamma_1}{4}(a_i^\dagger a_i^\dagger a_i a_{i+1} \\ &+a_i^\dagger a_{i+1}^\dagger a_{i+1} a_{i+1} + a_i^\dagger a_i a_i a_{i+1}^\dagger + a_i a_{i+1}^\dagger a_{i+1}^\dagger a_{i+1} + 2a_i^\dagger a_i a_{i+1}^\dagger a_{i+1}) \\ &+\alpha_1(a_i^\dagger a_{i+2} + a_i a_{i+2}^\dagger - (a_i^\dagger a_i + a_{i+2}^\dagger a_{i+2})) + \tfrac{\xi_1}{4}(a_i^\dagger a_i^\dagger a_i a_{i+2} \\ &+a_i^\dagger a_{i+2}^\dagger a_{i+2} a_{i+2} + a_i^\dagger a_i a_i a_{i+2}^\dagger + a_i a_{i+2}^\dagger a_{i+2}^\dagger a_{i+2} - 4a_i^\dagger a_i a_{i+2}^\dagger a_{i+2}))\Big]\end{aligned} \tag{2.116}$$

where f is the lattice size, $\xi_1 = \alpha_1\gamma_1$ is the parameter controlling the strength of the interaction with $\gamma_1 = \epsilon^2$

2.8.2 Effect of the third, fourth nearest neighbor and generalization

The Hamiltonian of 1D Heisenberg ferromagnetic spin chain, which in addition to a second nearest neighbor interaction includes the third nearest neighbors is written as follows

$$H_{L_2} = -\sum_i \left(\vec{S}_i \cdot \vec{S}_{i+1} + \alpha_1 \vec{S}_i \cdot \vec{S}_{i+2} + \alpha_2 \vec{S}_i \cdot \vec{S}_{i+3}\right) \tag{2.117}$$

Here, $\alpha_2 = J_3/J_1$ is the ratio controlling the coupling between first and third nearest neighbor. We transform also equation (2.117) into a quantum spin system by using the same technique as in the previous section into the following dimensionless form

$$\widehat{H}_{L_2} = \widehat{H}_{L_1} - \sum_i \frac{1}{2}\alpha_2(\widehat{S}_i^+ \widehat{S}_{i+3}^- + \widehat{S}_i^- \widehat{S}_{i+3}^+ + 2\widehat{S}_i^z \widehat{S}_{i+3}^z) \tag{2.118}$$

Using Holstein-Primakoff's transformation scheme, we bosonise this later Hamiltonian through the following :

$$\begin{aligned}\widehat{H}_{L_2} = \widehat{H}_{L_1} - \textstyle\sum_i^f \alpha_2 \Big[& a_i^\dagger a_{i+3} + a_i a_{i+3}^\dagger - (a_i^\dagger a_i + a_{i+3}^\dagger a_{i+3}) + \tfrac{\xi_2}{4}(a_i^\dagger a_i^\dagger a_i a_{i+3} \\ & + a_i^\dagger a_{i+3}^\dagger a_{i+3} a_{i+3} + a_i^\dagger a_i a_i a_{i+3}^\dagger + a_i a_{i+3}^\dagger a_{i+3}^\dagger a_{i+3} - 4 a_i^\dagger a_i a_{i+3}^\dagger a_{i+3})\Big]\end{aligned} \tag{2.119}$$

where $\xi_2 = \alpha_2\gamma_1$. Another puzzling point is how will be the new Hamiltonian of a 1D Heisenberg ferromagnetic spin chain if it includes the fourth nearest neighbors? The new Hamiltonian is written as follow:

$$H_{L_3} = H_{L_2} - \sum_i \alpha_3 \vec{S}_i \cdot \vec{S}_{i+4} \tag{2.120}$$

where, $\alpha_3 = J_4/J_1$ is the ratio. We can once more bosonise equation (2.120) using Holstein-Primakoff technique of transformation into the following dimensionless form.

$$\begin{aligned}\widehat{H}_{L_3} = \widehat{H}_{L_2} - \textstyle\sum_i^f \alpha_3 \Big[& a_i^\dagger a_{i+4} + a_i a_{i+4}^\dagger - (a_i^\dagger a_i + a_{i+4}^\dagger a_{i+4}) + \tfrac{\xi_3}{4}(a_i^\dagger a_i^\dagger a_i a_{i+4} \\ & + a_i^\dagger a_{i+4}^\dagger a_{i+4} a_{i+4} + a_i^\dagger a_i a_i a_{i+4}^\dagger + a_i a_{i+4}^\dagger a_{i+4}^\dagger a_{i+4} - 4 a_i^\dagger a_i a_{i+4}^\dagger a_{i+4})\Big]\end{aligned} \tag{2.121}$$

Where the parameter ξ_3 is $\xi_3 = \alpha_3\gamma_1$. To generalize the effects of a given nearest neighbors in one dimensional ferromagnetic Heisenberg spin chain, we consider a

general Hamiltonian as

$$H_{L_{(m-1)}} = -\sum_{m=1}^{f}\sum_{i=1}^{f}\left(\vec{S}_i\cdot\vec{S}_{i+1} + \alpha_{(m-1)}\vec{S}_i\cdot\vec{S}_{i+m}\right) \tag{2.122}$$

Where $\alpha_{(m-1)}$ is the ratio the of the exchange interaction of a given nearest neighbors m. For $m = 1$, we get α_0, which is a parameter that will always be nil and corresponds to the case in 1D Heisenberg spin chain where only the first nearest neighbors are taken into account. We can once more quantize the Eq.(2.122) by the Holstein-Primakoff bosonic transformation and it reads:

$$\begin{aligned}\widehat{H}_{L_{(m-1)}} = &-\textstyle\sum_{m=1}^{f}\sum_{i}^{f}\Big[a_i^\dagger a_{i+1} + a_i a_{i+1}^\dagger - (a_i^\dagger a_i + a_{i+1}^\dagger a_{i+1}) + \frac{\gamma_1}{4}(a_i^\dagger a_i^\dagger a_i a_{i+1}\\ &+a_i^\dagger a_{i+1}^\dagger a_{i+1}a_{i+1} + a_i^\dagger a_i a_i a_{i+1}^\dagger + a_i a_{i+1}^\dagger a_{i+1}^\dagger a_{i+1} - 4a_i^\dagger a_i a_{i+1}^\dagger a_{i+1})\\ &+\alpha_{(m-1)}[a_i^\dagger a_{i+m} + a_i a_{i+m}^\dagger - (a_i^\dagger a_i + a_{i+m}^\dagger a_{i+m}) + \tfrac{\xi_{(m-1)}}{4}(a_i^\dagger a_i^\dagger a_i a_{i+m}\\ &+a_i^\dagger a_{i+m}^\dagger a_{i+m}a_{i+m} + a_i^\dagger a_i a_i a_{i+}^\dagger + a_i a_{i+m}^\dagger a_{i+m}^\dagger a_{i+m} - 4a_i^\dagger a_i a_{i+m}^\dagger a_{i+m})]\Big]\end{aligned} \tag{2.123}$$

Here m is a given number of nearest neighbors and $\xi_{(m-1)} = \alpha_{(m-1)}\gamma_1$.

2.8.3 Effect of long range interactions when four or six quanta are involved

Let us start by defining a perturbed Hamiltonian as $\widetilde{H}_{L_{(m-1)}} = \widehat{H}_{L_0} + \widehat{V}_{L_{(m-1)}}$, where $\widehat{H}_{L_0}$ is the on site Hamiltonian of the usual Bose-Hubbard term.

$$\widehat{H}_{L_0} = -\sum_{m=1}^{f}\sum_{i=1}^{f} A\gamma_m a_i^\dagger a_i^\dagger a_i a_i \tag{2.124}$$

and

$$\begin{aligned}\widehat{V}_{L_{(m-1)}} = &-\textstyle\sum_{m=1}^{f}\sum_{i=1}^{f}\Big[a_i^\dagger a_{i+1} + a_i a_i^\dagger - (a_i^\dagger a_i + a_{i+1}^\dagger a_{i+1}) + 2\frac{A}{J_1}a_i^\dagger a_i - \frac{\gamma_1}{4}(a_i^\dagger a_i^\dagger a_i a_{i+1}\\ &+a_i^\dagger a_{i+1}^\dagger a_{i+1}a_{i+1} + a_i^\dagger a_i a_i a_{i+1}^\dagger + a_i a_{i+1}^\dagger a_{i+1}^\dagger a_{i+1} - 4a_i^\dagger a_i a_{i+1}^\dagger a_{i+1})\\ &+\alpha_{(m-1)}[a_i^\dagger a_{i+m} + a_i a_{i+m}^\dagger - (a_i^\dagger a_i + a_{i+m}^\dagger a_{i+m}) + 2\tfrac{A}{J_m}a_i^\dagger a_i - \tfrac{\xi_{(m-1)}}{4}(a_i^\dagger a_i^\dagger a_i a_{i+m}\\ &+a_i^\dagger a_{i+m}^\dagger a_{i+m}a_{i+m} + a_i^\dagger a_i a_i a_{i+m}^\dagger + a_i a_{i+m}^\dagger a_{i+m}^\dagger a_{i+m} - 4a_i^\dagger a_i a_{i+m}^\dagger a_{i+m})]\Big]\end{aligned} \tag{2.125}$$

Where $\alpha_{(m-1)} = \frac{J_m}{J_1}$ is the ratio of Heisenberg exchange interaction between the first and the second nearest-neighbor.

2.9 Localization in the space of normal mode

In the case of classical nonlinear system, quantum breathers are characterized by exponential localized weight functions [5]. Before continuing let us remind that recently, Nguenang et al. [19] studied the properties of quantum q-breathers in a one-dimensional optical lattice containing two quanta modeled by the Bose-Hubbard Hamiltonian. They explored the localization phenomenon in the system by computing appropriate weight functions of the eigenstates in the normal-mode space using perturbation theory. Unlike the classical case where the localization is exponential, they found algebraic localization. Although the model derived from the spin Hamiltonian here which is also a Bose Hubbard-like Hamiltonian, it is important to probe the localization properties since this model involve also various other linear and nonlinear intersite coupling. In this respect, we start by the energy of our system when γ is so small that it can be assimilated to the case of $\gamma = 0$, corresponding to the case for which the sum of two single particles energies with the constraint that the sum of their momenta equals the Bloch momentum k. Considering the equation (2.109) and (2.110) while two spins are excited, we get

$$E^0_{k,k_1} = -2[J_1(\cos(k_1 + k) + \cos k_1) - D_z(\sin(k_1 + k) - \sin k_1)] + 4J_2 \quad (2.126)$$

where $k_1 = 2\pi\nu/(f+1) - k/2$ is the conjugated momentum of the relative distance of both quanta and $\nu = 1, \cdots, \frac{f+1}{2}$. E_{k,k^0_1} has a finite spread at fixed k. However, for $k = \pm\pi$, the spectrum of the continuum band becomes degenerate. Thus, for $\mid k \pm \pi \mid \ll 1$, the eigenenergies are very close.

We use a non degenerated perturbation theory to find the weight function in the normal-mode space in order to probe the signature of quantum q-breathers. Here H_1 is the perturbing Hamiltonian, $\mid \psi^0_{k_1} >$ is an eigenstate of the unperturbed case ($\gamma = 0$). In the first-order approximation, the eigenfunction of the perturbed system is given by

$$\mid \psi_{\widetilde{k}_1} > = \mid \psi^{(0)}_{\widetilde{k}_1} > + \gamma \sum_{k'_1 \neq \widetilde{k}_1} \frac{< \psi^0_{k'_1} \mid \widehat{H}_1 \mid \psi^0_{\widetilde{k}_1} >}{E^0_{\widetilde{k}_1} - E^0_{k'_1}} \mid \psi^0_{k'_1} > \quad (2.127)$$

where γ is the strength of the perturbation which is local in the Hamiltonian matrix (3.12) and the perturbation parameters are γ/f, γ/D_z and γ/J_1. For Bloch wave numbers far from $\pm\pi$, the spacing is of order $1/f$, so the approximation should work for $\gamma < 1$. For Bloch wave numbers close to $\pm\pi$, the appraximation breaks down if $\gamma \geq \pi - \mid k \mid$. For $\gamma = 0$, $\mid \psi_{\widetilde{k}_1} > = \mid \psi^0_{\widetilde{k}_1} >$ the weight function is compact. The off-diagonal ($k_1 \neq \widetilde{k}_1$) weight function at the first-order approximation is also given

by

$$C(k_1,\widetilde{k}_1) =|< \psi^0_{k_1} \mid \psi_{\widetilde{k}_1} >|^2 = \frac{|<\psi^{(0)}_{k_1}|\widehat{H}_1|\psi^{(0)}_{\widetilde{k}_1}>|^2}{|E^0_{\widetilde{k}_1}-E^0_{k_1}|^2}, \qquad k_1 \neq \widetilde{k}_1 \tag{2.128}$$

$E^0_{k_1}$ and $E^0_{\widetilde{k}_1}$ are the eigenenergies of the unperturbed system. Setting $\Delta = k_1 - \widetilde{k}_1$, the weight function of the system can be written as follows. For $\mid \Delta \mid \ll 1$,

$$C(k_1,\widetilde{k}_1) \approx \frac{\gamma^2[J_2^2+16[D_z^2+J_1^2+(J_1^2-D_z^2)\cos(k)-D_zJ_1\sin(k)]]}{256(f+1)^2\Delta^2[J_1\cos(\frac{k}{2})+D_z\sin(\frac{k}{2})]^2[\sin(\frac{2\widetilde{k}_1+k}{2})+\frac{\Delta}{2}\cos(\frac{2\widetilde{k}_1+k}{2})]^2} \tag{2.129}$$

We can derive several results using the general form of the equation (2.129). The decay of the weight function with increasing Δ means that we have localization in the normal-mode space. For $2\widetilde{k}_1 + k \equiv 0 \pmod{2\pi}$ and $k = 0$ we have the weight function with Heisenberg interaction parameter.

$$C(k_1,\widetilde{k}_1) \approx \frac{\gamma^2(J_2^2+32J_1^2)}{16(f+1)^2J_1^2\Delta^4} \tag{2.130}$$

Equation (2.130) shows the algebraic decay $\sim \frac{1}{\Delta^4}$ of the weight function. For $2\widetilde{k}_1 + k \equiv 0 \pmod{2\pi}$ and $k = \pm\pi$ we have the weight function with DMI interaction parameter.

$$C(k_1,\widetilde{k}_1) \approx \frac{\gamma^2(J_2^2+32D_z^2)}{16(f+1)^2D_z^2\Delta^4} \tag{2.131}$$

Here we find an algebraic decay $\sim \frac{1}{\Delta^4}$ of the weight function. For $2\widetilde{k}_1 + k \equiv 0 \pmod{2\pi}$ and $k = \pm\frac{\pi}{2}$ we have the weight function with Heisenberg and DMI interaction parameters.

$$C(k_1,\widetilde{k}_1) \approx \frac{\gamma^2[J_2^2+16(D_z^2+J_1^2\pm D_zJ_1)]}{8(f+1)^2(D_z+J_1)^2\Delta^4} \tag{2.132}$$

For $2\widetilde{k}_1 + k \neq 0 \pmod{2\pi}$, $k = 0$ and $\widetilde{k}_1 = \pm\frac{\pi}{2}$ the weight function is reduced to

$$C(k_1,\widetilde{k}_1) \approx \frac{\gamma^2(J_2^2+32J_1^2)}{64(f+1)^2J_1^2\Delta^2} \tag{2.133}$$

we find an algebraic decay $\sim \frac{1}{\Delta^2}$ of the weight function. For $2\widetilde{k}_1 + k \neq 0 \pmod{2\pi}$, $k = \pi$ and $\widetilde{k}_1 = \pm\pi$ the weight function is

$$C(k_1,\widetilde{k}_1) \approx \frac{\gamma^2(J_2^2+32D_z^2)}{16(f+1)^2D_z^2\Delta^2} \tag{2.134}$$

we find algebraic decay $\sim \frac{1}{\Delta^2}$ of the weight function. For $2\widetilde{k}_1 + k \neq 0 \pmod{2\pi}$,

$k = \frac{\pi}{2}$ and $\widetilde{k}_1 = \pm 2\frac{\pi}{3}$ the weight function is

$$C(k_1, \widetilde{k}_1) \approx \frac{\gamma^2[J_2^2 + 16(D_z^2 + J_1^2 \pm D_z J_1)]}{16(f+1)^2(J_1 + D_z)^2(1 + \frac{\Delta}{2})^2\Delta^2} \tag{2.135}$$

We find also the algebraic decay of the weight function is $\sim \frac{1}{(1+\Delta)^2\Delta^2}$

2.10 Conclusion

In this chapter, we have developed a mathematical model which allows us to transform the Heisenberg classical spin chain Hamiltonian into its quantum version. Using general formalism of particle number representation, number state method, perturbation method, we have derive the matrix elements to obtain analytically the Hamiltonian matrices and weight function that can be solved numerically.
The following Chapter will be devoted to the presentation of different results and discussion.

Chapter 3

Results and Discussion

3.1 Introduction

This chapter is devoted to resume the analytical and numerical results obtained in this thesis. In this respect we will discuss the result on the phenomenon of localization and transport of energy in 1D ferromagnetic materials. With aim at probing the magnetization reversal process that is a process that undergoes an energy cost, we therefore start by elaborating the energy spectrum in 1D Heisenberg ferromagnetic spin chain with varying the exchange energy parameter and also that of the anisotropy. In the same time we also show the effect of the DMI on the energy spectrum. Then after the effect of longer range interaction on the energy spectrum is probed. Finally, we present the localization in real space and in the space of normal mode.

3.2 Energy spectra in a finite Heisenberg isotropic exchange spin chain

In this section, we present the analytical and numerical results in the model by using the numerical diagonalization.

3.2.1 Energy at the ground state

For the ground state, all spins are oriented in parallel and there is no spin-flip excitation in a Heisenberg spin chain. The energy of the ground state is

$$E_0 = -S^2 f J \tag{3.1}$$

There are (2Sf+1) states that have the same energy E_0.

3.2.2 Energy spectrum for one boson in the model

In the model (2.89), when one spin is excited, its energy is

$$E_1 = -2(\cos(ka) - 1) \tag{3.2}$$

Where $a = 1$ is the lattice step. The energy spectrum displays only a bound state.

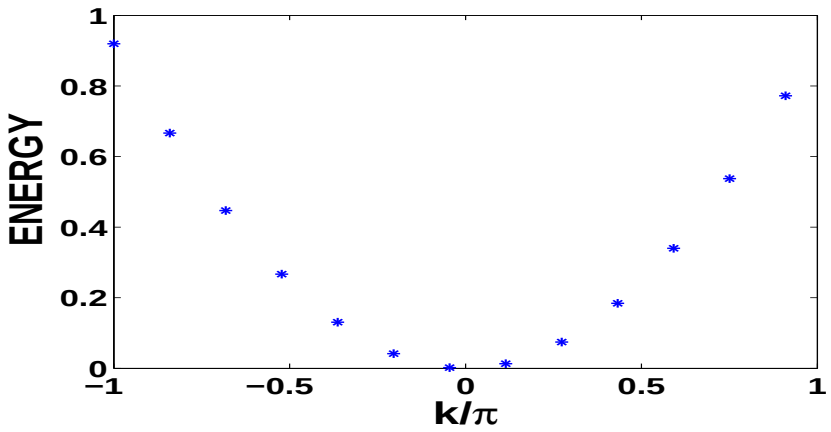

Figure 3.1: Energy spectrum of one boson in the extended Bose-Hubbard chain

The bound state occurring in Fig.3.1 is the result of a localized state, constituted by one spin engaged in a switching process.

3.2.3 Energy spectrum for the two-boson in the model

From the equations (2.94) and (2.95) obtained in chapter 2, the Hamiltonian matrix for the two-boson in the model is

$$H_1 = \frac{\widehat{H}_1}{J} = -\begin{pmatrix} u & \sqrt{2}q & \cdots & & & \\ \sqrt{2}q^* & y & g & & & \\ & g^* & u & g & & \\ \vdots & & \ddots & \ddots & \ddots & \\ & & & g^* & u & g \\ & & & & g^* & P \end{pmatrix} \tag{3.3}$$

where $P = \tau^{-\frac{f+1}{2}} + \tau^{-\frac{f-1}{2}} + u$, $u = -4$, $y = u + \frac{\gamma}{2}$, $q = (\frac{\gamma}{4} - 1)g$ and $g = 1 + \tau$.
The structure of the Hamiltonian matrix obtained in equation (3.3) is similar to the two-bosons case described in refs. [5, 13, 18–20, 22, 23] and four bosons described in ref. [11]. We can derive the eigenenergies for each given Bloch wave number k from the Schrödinger equation given by $\widehat{H} \mid \psi_k >= E \mid \psi_k >$.
Using numerical diagonalization as in [22, 109, 111], we can derive the eigenvalue spectrum of the corresponding Heisenberg spin chain. We have plotted numerically the energy spectrum as a function of wave number k for the interaction strength $\gamma = 1$. This is shown in Fig.3.2, where the result is obtained from the numerical diagonalization of the Hamiltonian matrix (3.3). Here, it is clear that, an isolated ground-state eigenvalue appears for each k that corresponds to a bound state [19,

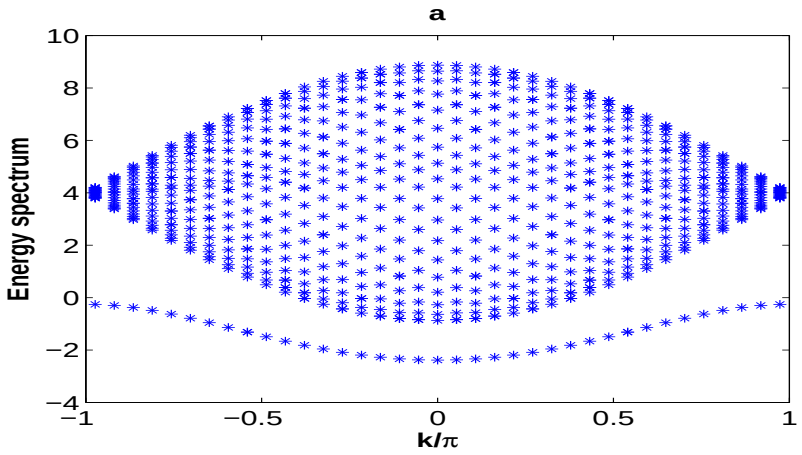

Figure 3.2: Energy spectrum of the two boson in the extended Bose-Hubbard chain; Here the value of the interaction strength $\gamma = 1$, $n = 2$ and $f = 37$

22, 24]. The same similar phenomena have been obtained in other nonlinear models in Ref. [11] for the case of four particles and in Ref. [19, 20, 22, 24, 26–28] for two particles'case. Figure3.2 clearly shows the energy spectrum composed essentially by a localized band below the delocalized band.

3.2.4 Effect of the exchange and anisotropy interactions on the two-bosons state energy spectrum

In presence of the exchange and anisotropy interactions, the Hamiltonian matrix becomes:

$$H = \frac{H}{J} = -\begin{pmatrix} t & \sqrt{2}q & & \cdots & & \\ \sqrt{2}q^* & t+\gamma/2 & g & & & \\ & g^* & t & g & & \\ \vdots & & \ddots & \ddots & \ddots & \\ & & & g^* & t & g \\ & & & & g^* & P \end{pmatrix} \tag{3.4}$$

where $P = \tau^{-\frac{f+1}{2}} + \tau^{-\frac{f-1}{2}} + t$, $q = (\frac{\gamma}{4} - 1)g$, $t = -4[1 + \frac{A}{J}(1-\gamma)]$, $g = 1 + \tau$
Now let us use a numerical diagonalization to derived the eigenvalue spectrum for the anisotropic ferromagnetic chain and probe the influence of the exchange interaction on the energy spectrum.

In this respect we introduce as an example the following set of parameters of the $CsNiF_3$ material which is a best example of 1D spin system namely $J = 23.6$ and $A = 9$. For this case, the energy spectrum is composed also by the continuum band above the single band as illustrated in Fig.3.3(a) and (b).
Modifying the parameters of the $CsNiF_3$ material is also supported by the idea

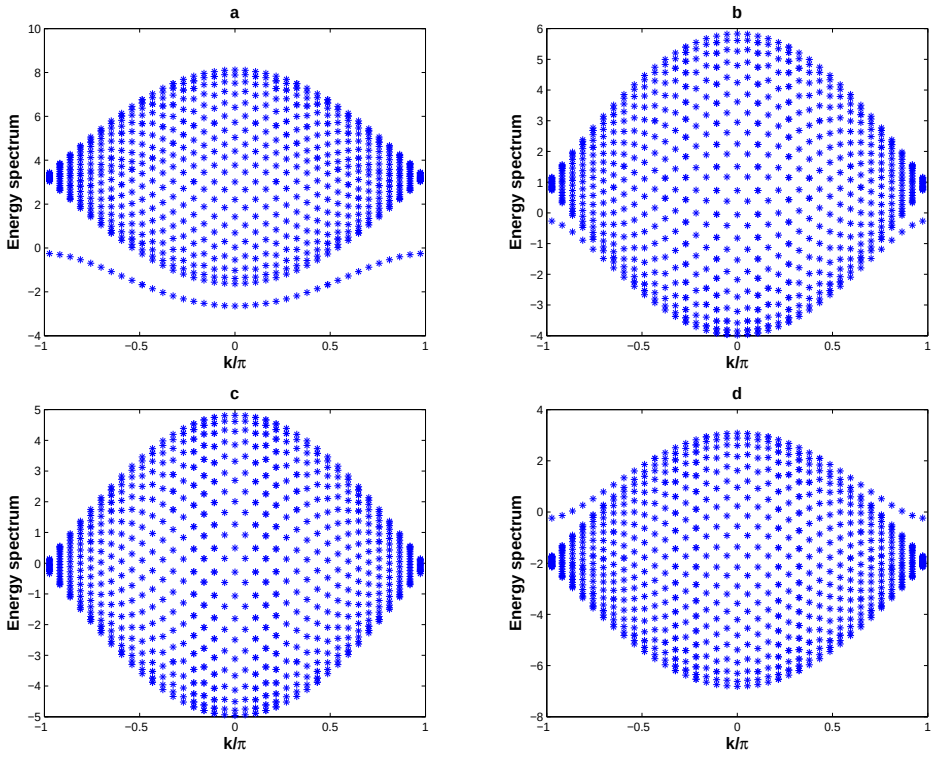

Figure 3.3: Energy spectrum of the two bosons in the extended Bose-Hubbard chain for different values of exchange interaction and anisotropy parameter where the value of the interaction strength is $\gamma = 1$, $n = 2$, $J = 23.6$ and $f = 37$: (a) $A = 9$; b) $A = 36$; (c) $A = 48$ and (d) $A = 70$.

that such a material may also face some physical constraints such as heating or magnetostriction effects that can led to the modification of its physical parameters. For the ferromagnetic materials case characterized by $J = 23.6$ and $A > 9$, the energy spectrum for these materials is always composed by the continuum band above the single band. Here we notice that, with increasing the anisotropy parameter of the material the single band progressively merge into the continuum band and the complete merging of the single band into the continuum occurs for the anisotropy parameter $A = 48$. This is clearly shown in Fig. 3.3(c). It is also realized that keeping this value of the the exchange integral parameter in the range $J = 23.6$ and then increasing the anisotropy parameter to $A = 70$, the single band can appear above the continuum as seen in Fig.3.3(d).

From these later figures, we notice that when the exchange interaction is constant, increasing the anisotropy parameter contributes to modify the localized states.

In the case of ferromagnetic materials with $J = 23.6$ and $A < 9.$, the continuum band does not merge with the single band, the width of the gap progressively increase when the anisotropy parameter's value decreases. However, for $A \leq 0.01$ the width of the gap turns out to remain unchanged.

We also noticed that for ferromagnetic materials where $J > 23.6$ and $A > 9.$, their energy spectrum is comparable to the case of ferromagnet with $J = 23.6$ and $A < 9$, displaying a gap with constant width.
Needless to mention here is the fact that, for the ferromagnetic materials with $J < 23.6$ and $A = 9$, it is realized that as the exchange integral parameter is decreasing, the gap between the continuum and the single band reduces so that a complete merging of the single band into the continuum band occurs for $J = 4$ and $A = 9$ such as the case seen in Fig.3.3(c). When the exchange integral $J < 4$, it is realized that the single band changes its concavity initially below and takes a reverse concavity above the continuum. The continuum band leaves the single band and the width of the gap becomes more larger when J decreases. This phenomenon is depicted in Fig.3.4(a-d).

Here we also noticed that, the width of the gap progressively increases as the

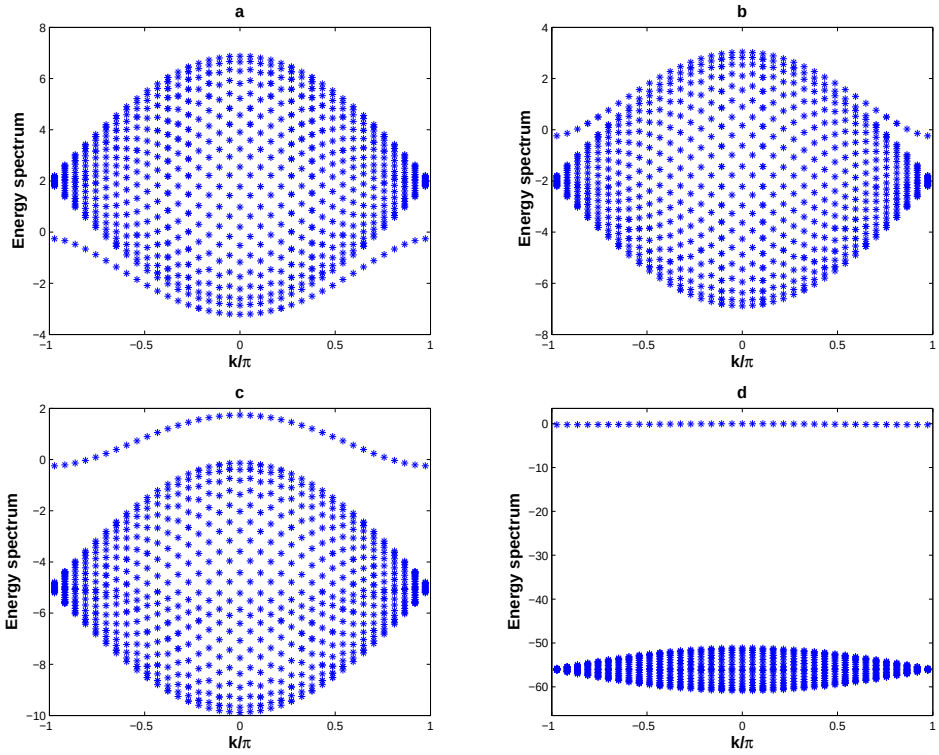

Figure 3.4: Energy spectrum of the two boson in the extended Bose-Hubbard chain for different values of exchange integral parameter where the value of the interaction strength is $\gamma = 1$, $n = 2$, $A = 9$ and $f = 37$: (a) $J = 9$; (b) $J = 4$; (c) $J = 2$ and (d) $J = 0.5$

exchange integral J decreases. On varying the values of the exchange interaction parameter some little difference in the spectrum occurs just as a matter of ordering the position of the bands in the energy spectrum.
From a physical picture applied to a magnetic material in the framework of a spin system it is important to mention the fact that there is a limitation i.e. $n \leq 2S$. In

the case of $CsNiF_3$ material $S = 1$ and since the localized states occur for $n = 2$ the states occurring in Fig. 3.2 and 3.3 are the results of a localized state constituted of two adjacent spins engaged in a switching process. This process reveals an intrinsic local magnetization reversal process that occurs in such a ferromagnet.

3.2.5 Energy spectrum for the four or six bosons in the extended Bose-Hubbard chain

Using the previous formulation given by equations (2.104) and (2.126), we obtain the $\{2, 2\}$ band Hamiltonian matrix as:

$$\widehat{H}^{(2,2)} = -\frac{4J^2B}{A\gamma}I_\sigma - \frac{J^2B}{A\gamma}\begin{pmatrix} \Gamma & W & & & \\ W^* & 0 & W & & \\ & \ddots & \ddots & \ddots & \\ & & W^* & 0 & W \\ & & & W^* & P \end{pmatrix} \tag{3.5}$$

where $B = (\frac{\gamma}{4} - 1)^2$, I_σ is the $\sigma \times \sigma$ unity matrix, $W = 1 + \tau = 2e^{ik/2}\cos(k/2)$, $P = 2\cos(\sigma k)$, $\Gamma = 6(\frac{C}{B} - 1)$, $C = (\frac{3\gamma}{4} - 1)^2$ and A is always the anisotropy parameter.
The structure of the matrix in equation (3.5) is very similar to the four bosons case described in Ref. [11]. and two-boson case described in Ref. [3, 19, 22]. Exact result can be obtained in the limit case for which the number of sites tends to infinity. Hence, for $f \to \infty$,

$$E(k) = -\frac{3}{2}\frac{J^2B}{A\gamma} - \frac{J^2B}{A\gamma}\left(4 + \Gamma + \frac{4\cos^2(k/2)}{\Gamma}\right) \tag{3.6}$$
$$if \left|\Gamma\right| > 2\cos(k/2)$$

Using the same technique, we have plotted the energy spectrum of the $CsNiF_3$ structure with few bosons but with a different value of γ according to the limitation given by $n \leq 2S$. The energy spectrum of the Hamiltonian matrix (3.5) is obtained by numerical diagonalization method. The sign of the anisotropy parameter here determine whether the underlying Bose-Hubbard model is repulsive ($A > 0$) as shown by Fig.3.5(a) or not. The fine structure of the ferromagnetic materials in the $\{2, 2\}$ band is constituted by a continuum band in addition to an isolated band and represents the ground state of a system with four bosons. The isolated band that appears either above or below the continuum is composed of states constituted with adjacent sites that are each occupied by two quanta. In the continuum, band most of the sites are separated by one or more vacant sites. The localized band clearly

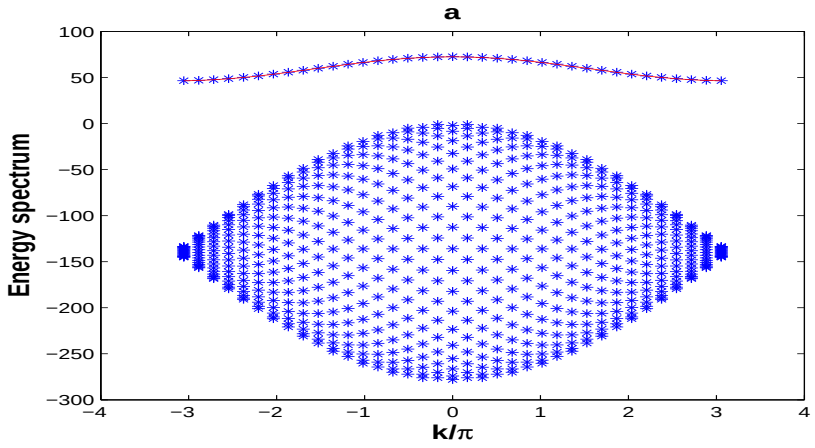

Figure 3.5: (color online) a) Detail of the Energy Spectrum for the Bose-Hubbard model derive from the anisotropic Heisenberg model in a periodic lattice where $n = 4$, $f = 37$, $J = 22$ and $\gamma = 0.75$: repulsive for $A = 7$

describes the localization of energy that corresponds to the breather solution of the classical nonlinear system. This is the so-called the soliton band [108]. The stars correspond to the energy spectrum obtained from an exact numerical diagonalization of the matrix (3.5). For the case of the breather band, the lines represent its plot from the analytical equation (3.6) obtained in the limit when the number of sites tends to infinity. From a physical picture referred to the spin system, we shall keep in mind that the limitation given by $n \leq 2S$ allows only material with sufficiently high spin in order to display such a localization phenomenon that would lead a localized magnetization reversal process involving two groups of two spins each.
Next, we consider the case of $n = 6$ bosons. This case displays three bands: namely the bands $\{4, 2\}$, $\{2, 4\}$ and $\{3, 3\}$.
In this case, the first band under consideration is the $\{4, 2\}$ band. Then if we proceed as in the case of $\{2, 2\}$ band, it turns out that we obtained a Hamiltonian matrix describing this $\{4, 2\}$ band as

$$H^{(4,2)} = -\frac{2J^2}{3A\gamma}(3B + 2C)I_\sigma - \frac{BJ^2}{A}\begin{pmatrix} \Gamma & 1 & & & P^* \\ 1 & 0 & 1 & & \\ & \ddots & \ddots & \ddots & \\ & & 1 & 0 & 1 \\ P & & & 1 & \Gamma \end{pmatrix} \tag{3.7}$$

where $P = 6e^{ik\frac{D}{B}}$, $B = (\frac{\gamma}{4} - 1)^2$, $C = (\frac{3\gamma}{4} - 1)^2$, $D = (\frac{5\gamma}{4} - 1)^2$ and $\Gamma = -\frac{1}{3B}(3B + 2C - 13D)$.
The structure of the matrix in equation (3.7) is also a three diagonal matrix, which is different from previous matrix for the position of their elements and very similar

to the case of the six bosons described in Ref. [11]. The energies of this band do not depend on the crystal momentum k.
To characterize energy spectrum of this band, we have also used the parameters greater and smaller than those of the $CsNiF_3$ structure. The structure of the energy

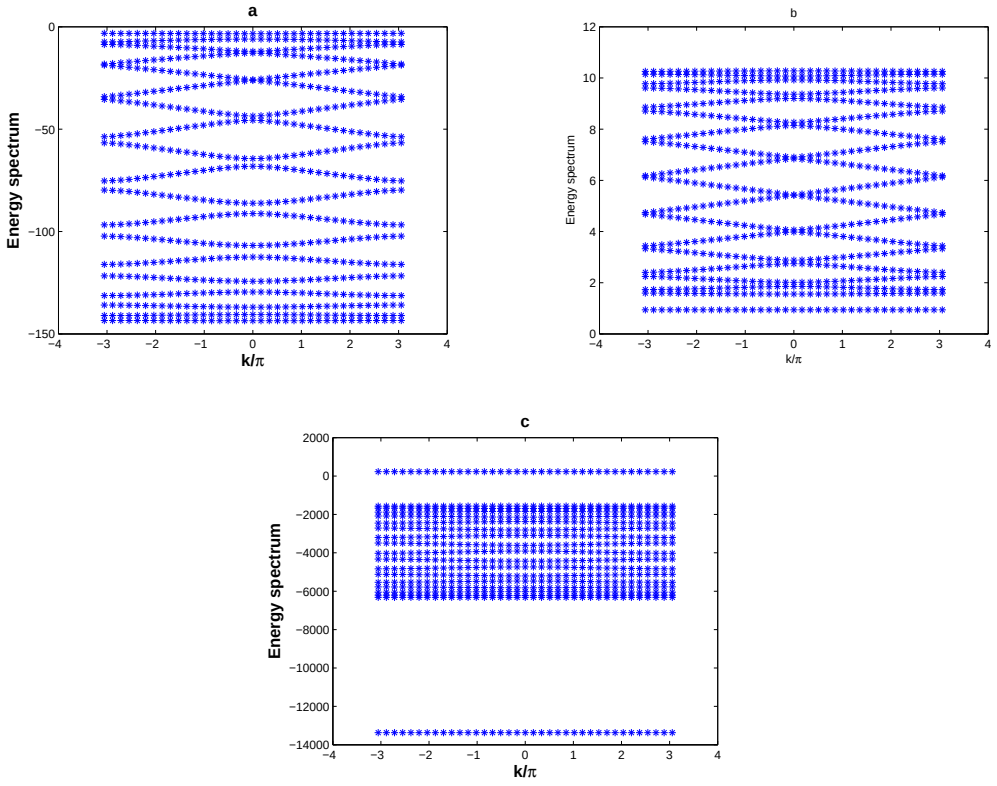

Figure 3.6: Detail of the Energy Spectrum for the extended Bose-Hubbard model, here $n = 6$, $f = 37$: a) case of repulsive nonlinearity where $A = 8$ and $J = 20$, $\gamma = 0.5$; (b) case of repulsive nonlinearity where $A = 9$ and $J = 16$, $\gamma = 0.25$; (c) case of repulsive nonlinearity where $A = 9$; $J = 26$ and $\gamma = 0.17$

spectrum of these ferromagnetic materials is different from the $\{2, 2\}$ band by the rectangular form of the continuum band and always composed by two bands where the single band can appear above for repulsive nonlinearity presented in Fig.3.6(b) while in Fig.3.6(a) the system display only the continuum band. We also notice that in the spectrum of Fig.3.6(a) and Fig.3.6(b), the continuum band appears to be very degenerated at their lower and upper edge. Unlike the case studied by Dorignac and Eilbeck [11] where they observed a continuum band in addition to two-breather bands, we do not get the two-breather bands with the initial parameter used here. However, on varying the parameter A, J and γ we can obtain two-breather bands in addition to a continuum band. This may happen in the singular case of the $CsNiF_3$ material when it faces some physical constraints such as heating or magnetostriction that may lead to change its parameters as seen in Fig.3.6(c).

Henceforth, all ferromagnetic materials displaying a spin value high enough to fulfil the restriction $n \leq 2S$ would present an energy spectrum characterized by a single and continuum bands with a reduced gap.
The second band is $\{2,4\}$ band, we also obtained the Hamiltonian matrix using the same technique as in the case of $\{2,2\}$ or $\{4,2\}$ bands.

$$H^{(2,4)} = -\frac{2J^2}{3A\gamma}(3B+2C)I_\sigma - \frac{BJ^2}{A\gamma}\begin{pmatrix} \Gamma & \tau & & & P^* \\ \tau^* & 0 & \tau & & \\ & \ddots & \ddots & \ddots & \\ & & \tau^* & 0 & \tau \\ P & & & \tau^* & \Gamma \end{pmatrix} \tag{3.8}$$

Where $P = 6e^{ik\frac{D}{B}}$, $B = (\frac{\gamma}{4}-1)^2$, $C = (\frac{3\gamma}{4}-1)^2$, $D = (\frac{5\gamma}{4}-1)^2$ and $\Gamma = -\frac{1}{3B}(3B + 2C - 13D)$, I_σ is the $\sigma \times \sigma$ unity matrix. The structure of the matrix in equation (3.8) appears to be the same as $\{4,2\}$ band, the difference with the previous matrix is very low since it is similar to the two quanta case described in Ref. [11].
The bands presented in the energy spectrum of these ferromagnetic materials appear at a first glance to be composed with flat lines where the single band can appears above the continuum for a repulsive nonlinearity as depicted in Fig.3.7 (b) while only the continuum band appears in Fig.3.7 (a). On varying the values of A, J and γ we can obtain also the $\{4,2\}$-like band with two breathers bands in addition to a continuum band. However they are rather more likely as the $\{2,4\}$ band but with a difference that this energy spectrum is rather degenerate than the $\{4,2\}$ case.
From a physical picture applied to the spin system, it is important to mention that there is a limitation, i.e $n \leq 2S$, while the number of bosons in a pure bosonic system has no such constraint. However there exist some materials for which the spin S is high enough so that from the spin picture the case of $n = 6$ can be seen as two adjacent spins with one being able to proceed to two switches and the other four switches. In the case of the $CsNiF_3$ material, the process may turn out to be more complex since a spin can any be turned down, no more. In this framework the physical picture can be described as that of two groups of four spins and two spins adjacently situated that can be involved in one switch per group. In any case, this can be understood as the result of a local magnetization reversal process that occurs in such a ferromagnet involving only few spins.

Using the same method as in the $\{4,2\}$ case, the Hamiltonian matrix of the $\{3,3\}$ band is

$$H^{(3,3)} = -\frac{3J^2B'}{A\gamma}(I_\sigma + M) \tag{3.9}$$

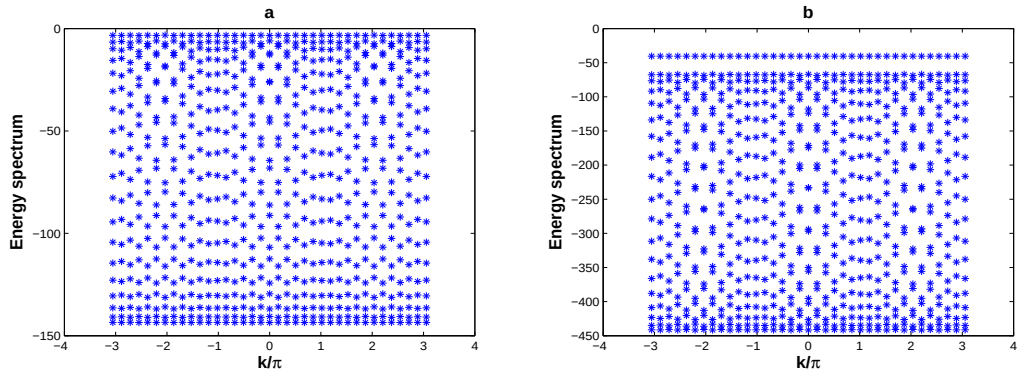

Figure 3.7: Detail of the Energy Spectrum for the Bose-Hubbard model derived from an anisotropic Heisenberg model in a periodic lattice where $n = 6$, $f = 37$, $J = 23.6$ and $A = 9$ corresponding to the $\{2, 4\}$ band: (a) case of repulsive nonlinearity where $\gamma = 1$; (b) case of repulsive nonlinearity where $\gamma = 0.5$

where $B' = (\frac{\gamma}{2} - 1)^2$, $M_{1,1} = \frac{1}{2} - 4\frac{D}{B'}$, $D = (\frac{5\gamma}{4} - 1)^2$ and $M_{i,j} = 0$ for any $i \neq 1$ and $j \neq 1$.

The diagonal form of the matrix in equation (3.9) is similar to the case of six bosons described in Ref. [11]. It is important to stress that the matrix elements in equation (3.9) are independent of the wave vector k. For the sake of simplicity, we have plotted the energy spectrum of this state as function of the wave vector only a ferromagnetic material characterized by the parameter close to the $CsNiF_3$ structure but with a different value of γ, as shown in Fig.3.8(a); the eigenvalue of the corresponding $\{3, 3\}$ band appears only with two symmetric single bands.

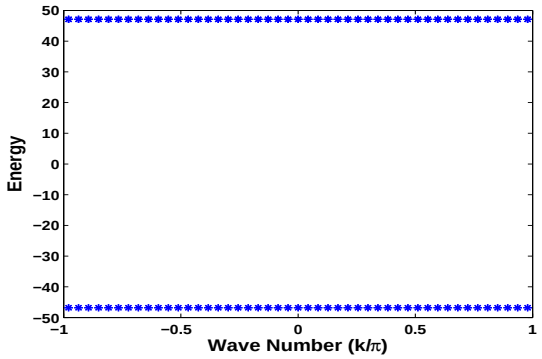

Figure 3.8: (a) Detail of the Energy Spectrum where $A = 9.5$, $n = 6$, $f = 37$, $J = 21$ and $\gamma = 0.17$

The lower single band is in fact a result of the transformation of the continuum band into a single band. From a physical picture applied to the spin system it is also important to mention that there is a limitation, i.e $n \leq 2S$, while the number of bosons in a pure bosonic system has no such constraint. However, there exists

some materials for which the spin S is high enough so that from the spin picture the case of $n = 6$ can be seen as two adjacent spins with each involving three switches. From our results, it is clear that in the framework of six bosons for the case of other ferromagnets with spin not enough the process should be more complex. In such a context, two groups of (three spins) a triplet can be engaged in a single switch each per group or triplet in the same time. Such a process needs experimental investigation. In any case, this can be understood as the result of a local magnetization reversal process. All ferromagnetic materials that display parameters different to those of the $CsNiF_3$ structure, i.e. spin value fulfilling the condition $n \leq 2S$ and the possibility of forming two triplet spins, have the same energy spectrum characterized by two symmetric single bands with a larger width of the gap between those single bands.

3.3 Energy spectra in a finite Heisenberg anisotropic exchange spin chain with antisymmetric interactions

In this section, we present the analytical and numerical results in the novel model by using nondegenerated, degenerate method and numerical diagonalization from the ground state to six spins excited when DMI are involved.

3.3.1 Energy at the ground state when DMI are involved

At the ground state, all spins are oriented in parallel and there is no spin-flip excitation in a finite Heisenberg spin chain. The energy at this ground state is

$$E_{M_0} = -J_2 f S^2 \tag{3.10}$$

We mention here that, the energy of the ground state is without the DMI. This means that, DMI have no effect in the ground state. All spins are oriented in parallel along the z axis.

3.3.2 Energy spectrum for one boson in the model when DMI are involved

In the model, when one spin is excited, replacing in equation (2.112) α and α^* by their values, we obtain the energy as

$$\begin{aligned} E_{M_1} = -J_2 f S^2 - (\alpha^* \tau + \alpha \tau^{-1} - 4J_2) &= -J_1(\tau + \tau^{-1})) - iD_z(\tau - \tau^{-1}) + 4J_2 \\ &= -2[J_1(\cos(k) - D_z \sin(k)] + 4J_2 \end{aligned} \tag{3.11}$$

Figure3.9 shows that in the absence of anisotropic exchange interaction ($J_2 = 0.0$) for $k = 0$, the energy spectrum is not nil. There is a nonzero minimum energy cost to

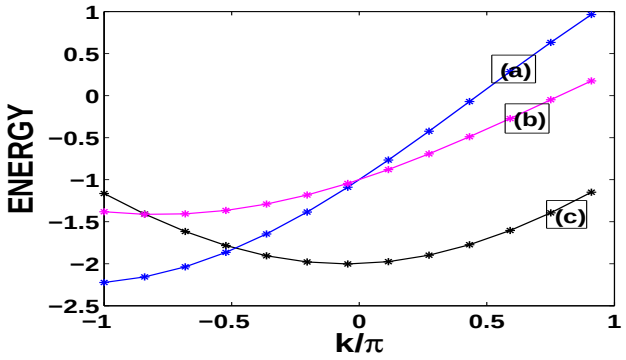

Figure 3.9: Energy spectrum of one boson for a Heisenberg spin chain with DMI for different values of J_1 and D_z where $J_2 = 0.0$: (a) $J_1 = 0.5$, $D_z = 1.0$; (b) $J_1 = D_z = 0.5$; (c) $J_1 = 1.0$, $D_z = 0.05$

create an excitation. According to the Goldstone theory, gapless bosonic excitations will exist in the energy spectrum. This theorem implies that the ground state has broken a continuous symmetry of the Hamiltonian.

3.3.3 Effect of the DMI on the energy spectrum of a planar ferromagnet for two bosons

When the DMI are involved, the new form of the Hamiltonian matrix is written as follow

$$H_M = -\begin{pmatrix} \Gamma & \sqrt{2}q^* & & & & \\ \sqrt{2}q & y & h^* & & & \\ & h & \Gamma & h^* & & \\ & & \ddots & \ddots & \ddots & \\ & & & h & \Gamma & h^* \\ & & & & h & p \end{pmatrix} \tag{3.12}$$

where $\Gamma = -4J_2$, $P = J_1[\tau^{-\frac{f+1}{2}} + \tau^{-\frac{f-1}{2}}] + \Gamma$, $y = \Gamma + \gamma\frac{J_2}{2}$, $q = gh$, $g = (\frac{\gamma}{4} - 1)$, $h = \alpha\tau + \alpha^*$ and $\alpha = J_1 + iD_z$.

We use numerical diagonalization method to derive the energy spectrum of the spin chain including antisymmetric interaction. To be more explicit, we have fixed the in-plane intersite exchange interaction constant to $(J_1 = 1)$ and we suppose that the out-of-plane coupling J_2 is nil. By increasing the DMI parameter, we have plotted

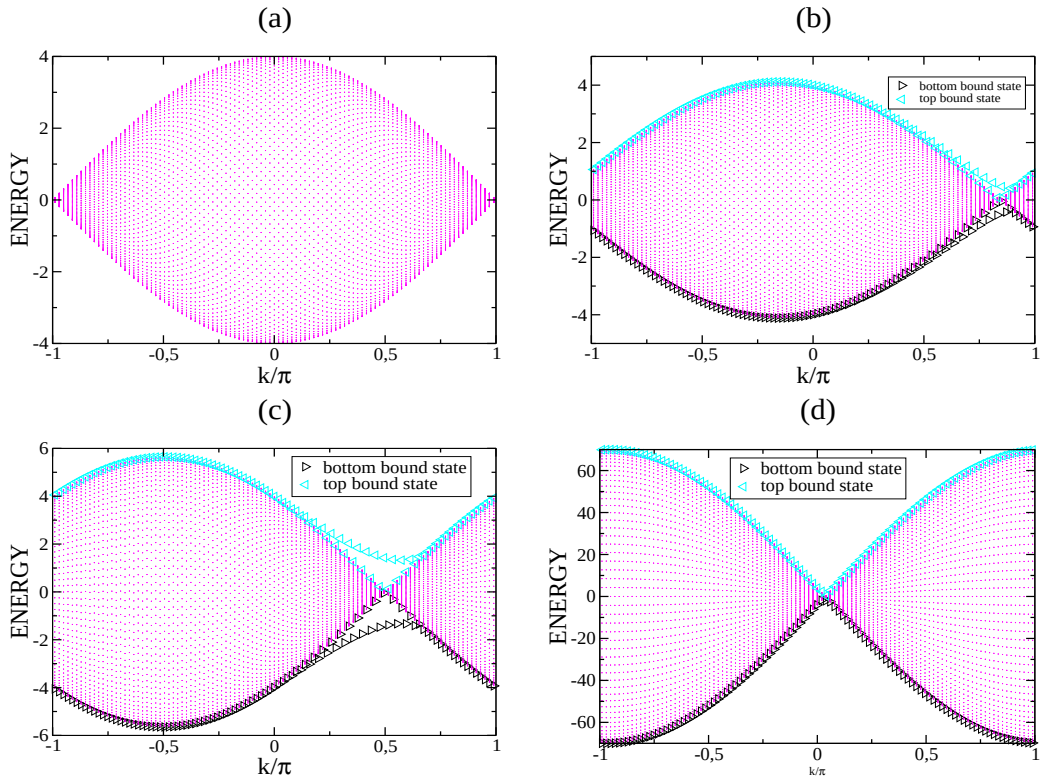

Figure 3.10: Generation of the energy spectrum of a two domain wall by appearance and shifting of a degenerated point in the energy spectrum of two-quanta for a Heisenberg spin chain with DMI for different values of D_z. Here the value of the interaction strength is $\gamma = 1$, $n = 2$, $J_1 = 1$, $J_2 = 0.0$ and $f = 101$: (a) $D_z = 0.0$; (b) $D_z = 0.25$; (c) $D_z = 1$; (d) $D_z = 17.5$

the corresponding energy spectrum as a function of Bloch wave. From a physical picture applied to magnetic material in the framework of a spin system, it is important to mention the fact that there is a limitation i.e. $n \leq 2S$, while the number of bosons in a pure bosonic system has no such constraint. In the first case of Fig.3.10(a), the energy spectrum of the system is plotted in absence of antisymmetric interaction D_z, and without exchange interaction along the z axis ($J_2 = 0.0$). The energies spectrum of these ferromagnetic materials represented by stars displays a continuum, which is a delocalized band. In the continuum band most of the sites are separated by one or more vacant sites. This result is already known in Fig.3.3. For a ferromagnetic material where $D_z = 0.25$, the energy spectrum is always formed by a continuum but in addition there are two bound states arising, which are merged to the continuum respectively above (cyan color) and another below (black color) over the entire Brillouin zone. However, the main difference when compared with the Fig. 3.10(a) is that, the energy is not degenerated for $k = \pm\pi$ as in Fig.3.10(a) but it becomes degenerate at $k/\pi = 0.8$. At this point, we also mention that both bound states appear as single bands that are symmetric with respect to the degen-

erate point. It's important to mention that, there is cut-off in the left part of the energy spectrum that is automatically pasted to the right extremity of the energy spectrum. This is an energy conservation process in the Brillouin zone through a self compensation effect as seen in Fig. 3.10(b). This shifting of the degenerated point in the energy spectrum continues with an increasing value of DMI interaction D_z. In Fig.3.10(c) this shifting increases rapidly with an increasing value of DMI until the DMI takes the value $D_z = 9$ where around the degenerated point there are two bound states arising on the spectrum. Beyond this value, the degenerated point moves slowly. Then the splitting of the continuum spectrum definitely led to a degenerated point located at $k/\pi = 0$, for $D_z \geq 17.5$ while the bound state are completely merged with the continuum. Beyond this value of DMI ($D_z > 17.5$), the shifting phenomenon of the degenerated point in the energy spectrum do no longer occurs. From a physical picture of Fig.3.10(d), the structure of the energy spectrum appears to display two domains walls, in the well known elementary excitations of the Néel phase of an XXZ model of the antiferromagnet. In the spin picture this corresponds to two spins with the same orientation incrusted twice in different sites in an antiferromagnetic spin chain. Whereas two symmetric bound states appearing nearby the degenerated point of Fig.3.10(b) and Fig.3.10(c) correspond to a spin lattice with two neighboring spins that flip together in the same time. Let us mention the fact that the variation of the DMI parameter to negative values will only swap the shifting of the degenerated point in the energy spectrum from the left to the right.

3.3.4 The Heisenberg exchange interaction's impact on the energy spectrum for two bosons when the DMI are involved

In this section, unlike the previous paragraph, with aim to focus our attention on the effect of the parameter J_1 on the energy spectrum of ferromagnetic materials, we shall keep the value of DMI parameter constant, and vary the Heisenberg inter site in-plane(X,Y) exchange interaction($J_1 > 1$).

We distinguish two cases in this section: firstly, the case of the ferromagnetic materials where $D_z = 17.5$ and $J_1 \leq 1$, which corresponds to the limit of shifting the degenerated point of the energy observed in Fig.3.10(d), where the energy spectrum has a symmetric form and corresponds to the energy spectrum of antiferromagnetic materials in the Néel phase with two domain walls. What happen while $D_z = 17.5$ and $J_1 \geq 1$? Contrarily to Fig.3.10 where the shifting of the energy spectrum was strongly proportional to the DMI and occurred from the right to the left, we notice a backward effect and as far as the parameter J_1 increases the initial profile of Fig.3.10(a) is recovered as they crosses different steps from Fig.3.11(b) and 3.11(c). The size of the energy increases with an increasing value of J_1. Figure 3.11(d) shows the end of this process, which is similar to Fig.3.10(a). However, the main difference

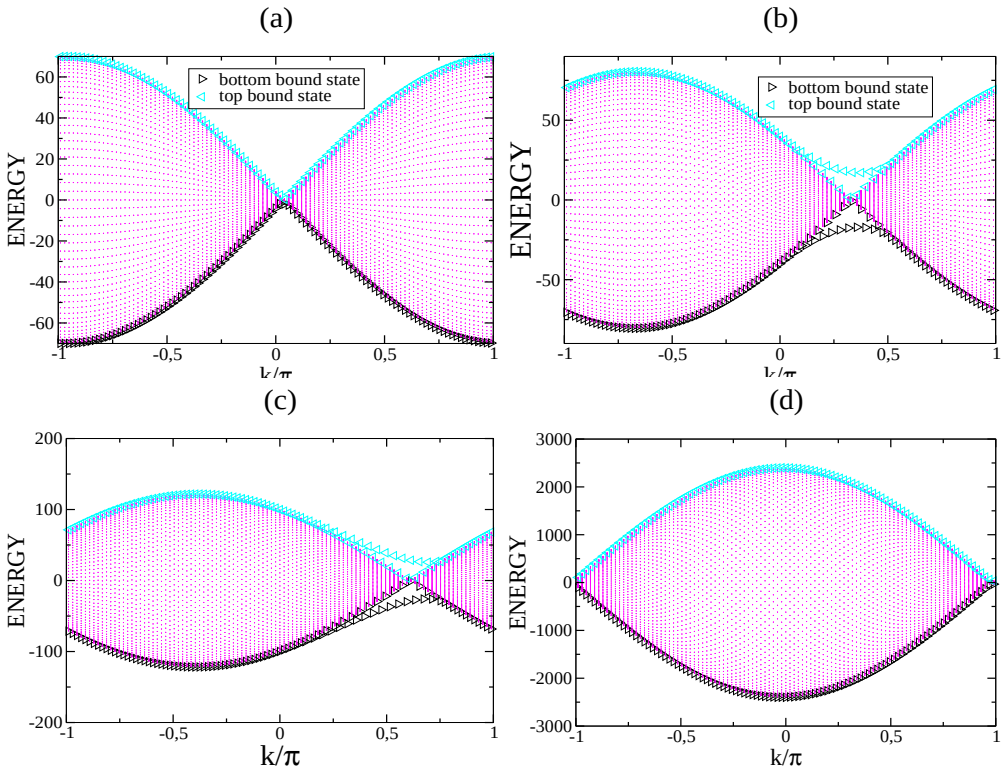

Figure 3.11: Backward shifting process of the degenerated point in energy spectrum of two-quanta in a Heisenberg spin chain with DMI for different values of J_1 where the value of the interaction strength is $\gamma = 1$, $n = 2$, $J_2 = 0.0$, $D_z = 17.5$ and $f = 101$: (a) $J_1 = 1$; (b) $J_1 = 10$; (c) $J_1 = 25$; (d) $J_1 = 600$

when compared with the result in Fig.3.10(a) is that, the size of the energy here which is larger in Fig.3.11(d) is related to the larger values of D_z. We also mention the fact that, for all value of $J_1 \geq 600$ the form of Fig.3.11(d) remains the same. These later figures show that, the exchange interaction J_1 and the DMI have an antagonist effect in a planar ferromagnet.

To probe the influence of J_2 on the energy spectrum, we re-plot the energy spectrum of our system, assuming that the Heisenberg parameter intersite coupling J_2 along the Z axes is not nil. Keeping in mind the previous question, here we keep J_1 constant to the value $J_1 = 1$ and on varying the value of J_2 from 0.1 to 8. While J_2 takes the value from 0.1 to 0.3, the energy spectrum is always identical to the case obtained in Fig.3.10(a). While for $J_2 = 0.5$ the single bound state arise below but merged to the continuum in the Brillouin zone this case is illustrated in Fig.3.12(a). While for $J_2 = 6$, the single bound state in Fig.3.12(b) is clearly separated to the continuum. From those later figures, it is important to mention that, the exchange interaction J_2 along the Z axes is responsible for the gap that is opening between the single bound state and the continuum. For non zero values of D_z, Fig.3.12(c) illustrates the energy spectrum exhibiting clearly the presence

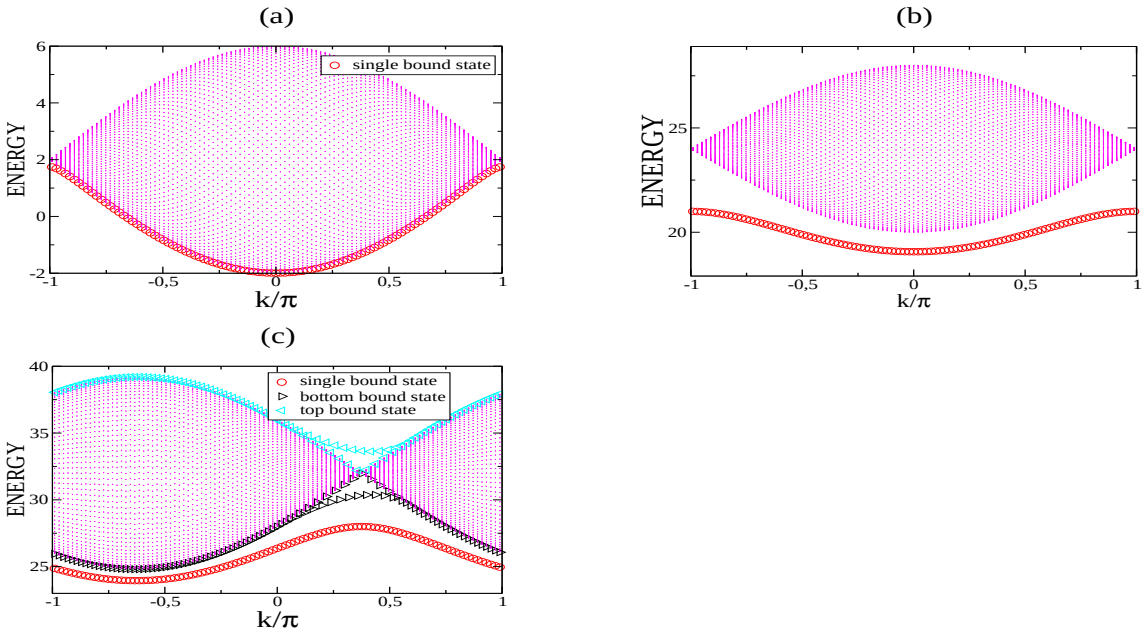

Figure 3.12: Energy spectrum of two-quanta in Heisenberg spin chain with DMI for different values of J_2 where the value of the interaction strength is $\gamma = 1$, $n = 2$, $J_1 = 1$ and $f = 101$: (a) $J_2 = 0.5$ and $D_z = 0.0$; (b) $J_2 = 6$ and $D_z = 0.0$; (c) $J_2 = 8$ and $D_z = 1.5$

of two single band of bound states that appears to be symmetric with respect to the degenerate point whereas they are merged to the continuum in the remaining brillouin zone, respectively. This is a scenario that often appears in antiferromagnet. However, here there is an additional single bound state that appears bellow and completely separated from the continuum. A question arising is what shape should the energy spectrum displays if $(J_1 = 0)$?

While the parameter J_1 is nil, the Heisenberg spin chain is reduced to an Ising ferromagnetic model. We have considered in this section these two following cases: firstly the case where the DMI D_z is non zero and $J_2 = 0$. Here , the energy spectrum is constituted only by the symmetric continuum band degenerated for $k = 0$. This spectrum appears to be similar to the energy spectrum of an antiferromagnetic material. It is important to notice that this energy spectrum presented in Fig.3.13 (a) keeps its shape and remains unchanged for all non zero values of D_z. It is worth mentioning that the value of this energy increases when the parameter D_z is high and that it decreases when it is weak without modifying the symmetric form of the energy spectrum. Secondly, we examine the case where J_2 and D_z are both non zero. Here, the energy spectrum is always similar to those of an antiferromagnetic material, the single bound state appears below and the continuum for $J_2 = 0.1$ and it is separated from the continuum for $J_2 = 0.9$. This case also confirm the role of the parameter J_2 that is to open up a gap between the single bound state and the continuum as seen in Fig.3.13(b) and 3.13(c).

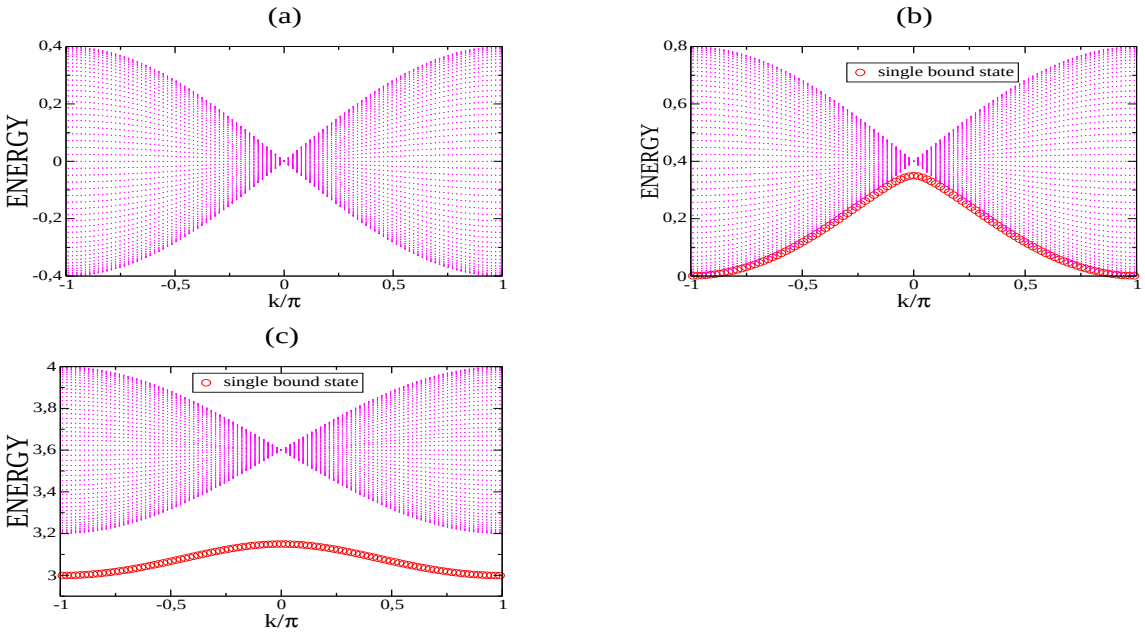

Figure 3.13: Band structure of two-quanta in Ising and DMI spin chain for different values of J_2 where the value of the interaction strength is $\gamma = 1$, $n = 2$, $J_1 = 0$ and $f = 101$: (a) $J_2 = 0.0$ and $D_z = 0.1$; (b) $J_2 = 0.1$ and $D_z = 0.1$; (c) $J_2 = 0.9$ and $D_z = 0.1$

3.3.5 Effect of the DMI on the energy spectrum of the spin chain when four or six quanta are involved

When four quanta are involved in presence of DMI, the Hamiltonian matrix is

$$H_M^{(2,2)} = -\frac{4mB}{A\gamma} I_\sigma - \frac{B}{A\gamma} \begin{pmatrix} \Gamma & W^* & & & \\ W & 0 & W^* & & \\ & \ddots & \ddots & \ddots & \\ & & W & 0 & W^* \\ & & & W & P \end{pmatrix} \tag{3.13}$$

where $B = (\frac{\gamma}{4} - 1)^2$, I_σ is the $\sigma \times \sigma$ unity matrix, $W = m'q' + 2iJ_1D_zq$, $m = J_1^2 + D_z^2$, $q = 2ie^{ik/2}\sin(k/2)$, $q' = 2e^{ik/2}\cos(k/2)$, $P = 2m'\cos(\sigma k) + 4J_1D_z\sin(\sigma k)$, $m' = J_1^2 - D_z^2$, $\Gamma = 6(\frac{C}{B} - 1)$, $C = (\frac{3\gamma}{4} - 1)^2$ and A is the anisotropy parameter. Remarkably, the matrix elements of the matrix (3.31) are independent of the exchange interaction parameter along the S^z direction J_2. This parameter disappears in the degenerate perturbation theory used here to calculate the matrix elements. The energy spectrum of the Hamiltonian matrix (3.31) is derived from a numerical diagonalization method. Where we have plotted the energy spectrum as a function of wave number k of a given ferromagnetic material. In this way, we can distinguish several configurations of the energy spectrum of ferromagnetic materials such as:
For a ferromagnetic material where $J_1 = 1$, $A = 7$ and $D_z \leq 1$, their energy spec-

trum are plotted in Fig.3.14. Let us start by emphasizing that when four quanta are

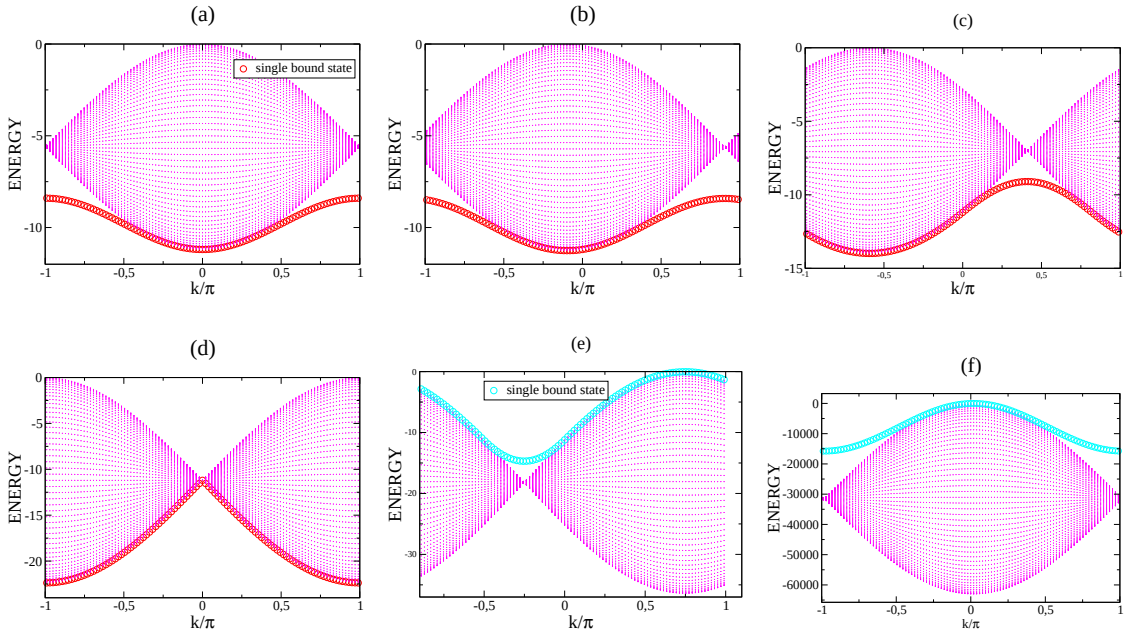

Figure 3.14: Detail of the energy spectrum for the extended Bose-Hubbard model derived from the Heisenberg spin chain and DMI in a periodic lattice containing four quanta for different values of the DMI where $A = 7$, $n = 4$, $\gamma = 0.05$, $f = 101$ and $J_1 = 1$: (a) $D_z = 0.0$; (b) $D_z = 0.075$; (c) $D_z = 0.5$, (d) $D_z = 1$; (e) $D_z = 1.5$; (f) $D_z = 75$

involved the energy spectrum form of the ferromagnetic material without the DMI parameter ($D_z = 0.0$) shows in Fig.3.14(a), a fine band structure constituted by the $\{2, 2\}$ band in addition to the continuum. The isolated band which appears either above or below the continuum spectrum, as the sign of the anisotropy parameter changes, stands for the localized state. This isolated band is composed of the states consisting of adjacent sites that are each occupied by two quanta. Whereas in the continuum band, most of the sites are separated by one or more vacant sites. The localized band is a signature of the localization of energy that corresponds to the quantum counterpart of the breather solution of the classical nonlinear system. From a physical picture referred to the spin system, we shall also mentioned that the limitation given by $n \leq 2S$ allows only materials with sufficiently high spin in order to display such a localization phenomenon that would lead a localized magnetization reversal process involving two groups of two spins each (doubled). Figure3.14(b) shows the case where the DMI is non zero and represents the beginning of appearance of a degenerated point not at the edge that is progressively shifted from the right to the left. This profile is similar to the case of two quanta previously presented in Fig.3.10(b). The degenerated point move further with an increasing value of DMI parameter as seen in Fig.3.14(c) and Fig.3.14(d). Figure 3.14(d), obtained for $D_z = 1$ displays an energy spectrum comparable to an energy spectrum in the

antiferromagnetic materials in the Néel phase for $k = 0$ in the middle of the Brillouin zone. From these later figures, the main difference when compared to the plots of Fig.3.10 for two quanta is that, the continuum band is not surrounded by two bound states that are more visible nearby the degenerated point.
Needless to mention the fact that unlike the case of Fig.3.10 corresponding to the case of two quanta, where the spectrum keep the same profile for larger values of the DMI parameter than $D_z = 17.5$. Here in Fig.3.14, we see that for four quanta it is no longer the same because as soon as the DMI parameter is greater than exchange interaction ($D_z > J_1$ i.e $D_z > 1$) the single bound state that is initially situated below the continuum turns out to appear above the continuum (see Fig.3.14(e)). Further increasing of the DMI parameter led to Fig.3.14(f) that shows the end of this process, which is similar to Fig.3.14(a). However, the main difference with the result in Fig.3.14(a) is that, the size of the energy here which is smaller in Fig.3.14(f) is related to the large values of D_z (the size of the energy decreases with an increasing value of D_z) and the single bound state appears above the continuum. For any value of $D_z \geq 75$, the form of Fig.3.14(f) remains unchanged. Furthermore, increasing progressively the values of the exchange interaction, the energy spectrum can recover the form of Fig.3.14(a).
For a good explanation of the peculiarity of the DMI interaction in the system when more than two quanta are involved, we start by the case where the parameter J_1 is nil, the system is described only with the Dzyaloshinsky-Moriya interaction. By so doing, we realized that for $D_z = 1$ the energy spectrum of the DMI spin chain appears at first glance identical to the one described in Fig.3.14(a) with the difference that the single bound state is located above the continuum (see Fig.3.15(a)). While for a fixed value of $D_z = 1$, on varying the value of the exchange interaction J_1, we get once more all the plots of Fig.3.14. The main difference being that, here the single bound state occurs above the continuum while $J_1 < D_z$ and below for $J_1 > D_z$. This situation is exhibited respectively in Fig.3.15(a-c) and Fig.3.15(d-f). From these later plots of the energy spectrum in a ferromagnetic spin chain, the outcome reveals an antagonist behavior between the Heisenberg in-plane exchange interaction (J_1) and DMI (D_z). Next, we consider the case of $n = 6$ bosons. This case displays three bands: namely $\{4, 2\}$, $\{2, 4\}$ and $\{3, 3\}$, bands.
In this case, the first band under consideration is the $\{4, 2\}$ band. Then if we proceed as in the case of the $\{2, 2\}$ band, it turns out that we obtain a Hamiltonian

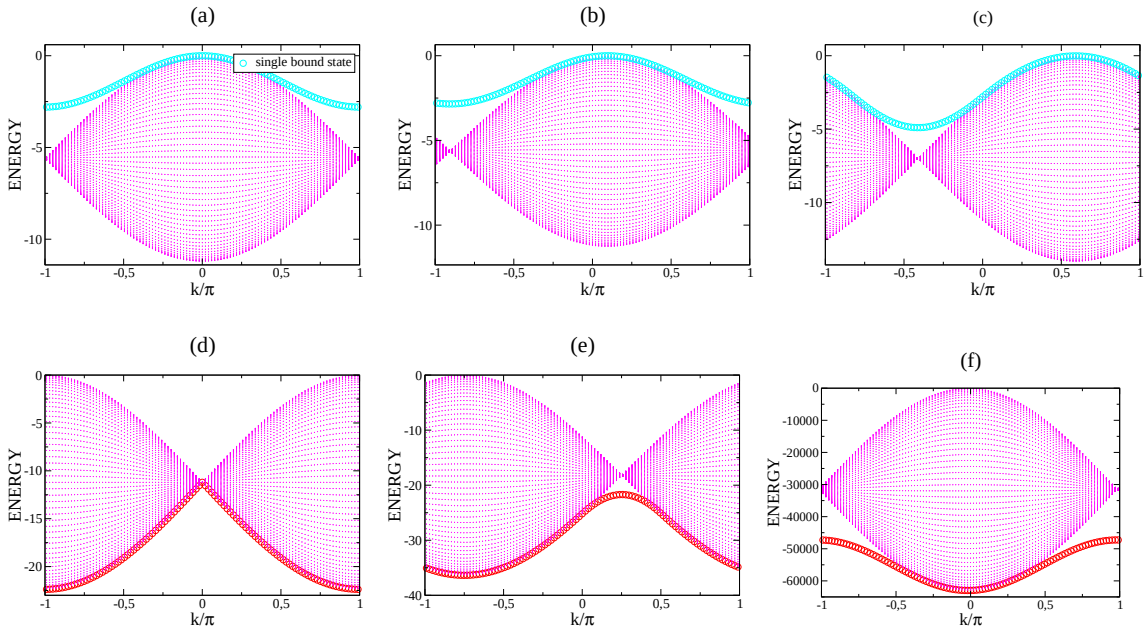

Figure 3.15: Detail of the energy spectrum for the extended Bose-Hubbard model derived from the Heisenberg spin chain and DMI in a periodic lattice containing four quanta for different values of the J_1 where $A = 7$, $n = 4$, $\gamma = 0.05$, $f = 101$ and $D_z = 1$: (a) $J_1 = 0.0$; (b) $J_1 = 0.075$; (c) $J_1 = 0.5$; (d) $J_1 = 1$ and $\gamma = 0.05$; (e) $J_1 = 1.5$; (f) $J_1 = 75$

matrix describing this $\{4, 2\}$ band as

$$H_M^{(4,2)} = -\frac{2m}{3A\gamma}(3B + 2C)I_\sigma$$
$$-\frac{B}{A\gamma}\begin{pmatrix} \Gamma & \alpha^{*2} & & & P \\ \alpha^2 & 0 & \alpha^{*2} & & \\ & \ddots & \ddots & \ddots & \\ & & \alpha^2 & 0 & \alpha^{*2} \\ P^* & & & \alpha^2 & \Gamma \end{pmatrix} \tag{3.14}$$

where $P = 6e^{ik\frac{D}{B}}$, $m = J_1^2 + D_z^2$, $\alpha^2 = (J_1 + iD_z)^2$, $\alpha^{*2} = (J_1 + iD_z)^2$, $B = (\frac{\gamma}{4} - 1)^2$, $C = (\frac{3\gamma}{4} - 1)^2$, $D = (\frac{5\gamma}{4} - 1)^2$ and $\Gamma = -\frac{1}{3B}(3B + 2C - 13D)$.

To answer the question on how will the shape of the energy spectrum in presence of the DMI appears, we start by distinguishing two cases: firstly, the case of the ferromagnetic materials where $J_1 = 1$ and varying the parameter D_z.

When the DMI parameter is zero, the energy spectrum of these ferromagnetic materials appears at first glance composed by three single lines similar to bound states. Whenever increasing the values of J_1 this structure of the energy spectrum remains unchanged. On varying the DMI parameter, we realized that the same scenario as the one observed in Fig. 3.6 occurs. These results reveal that DMI can also influence the position of the localized bound state in the spin chain in which the DMI is the

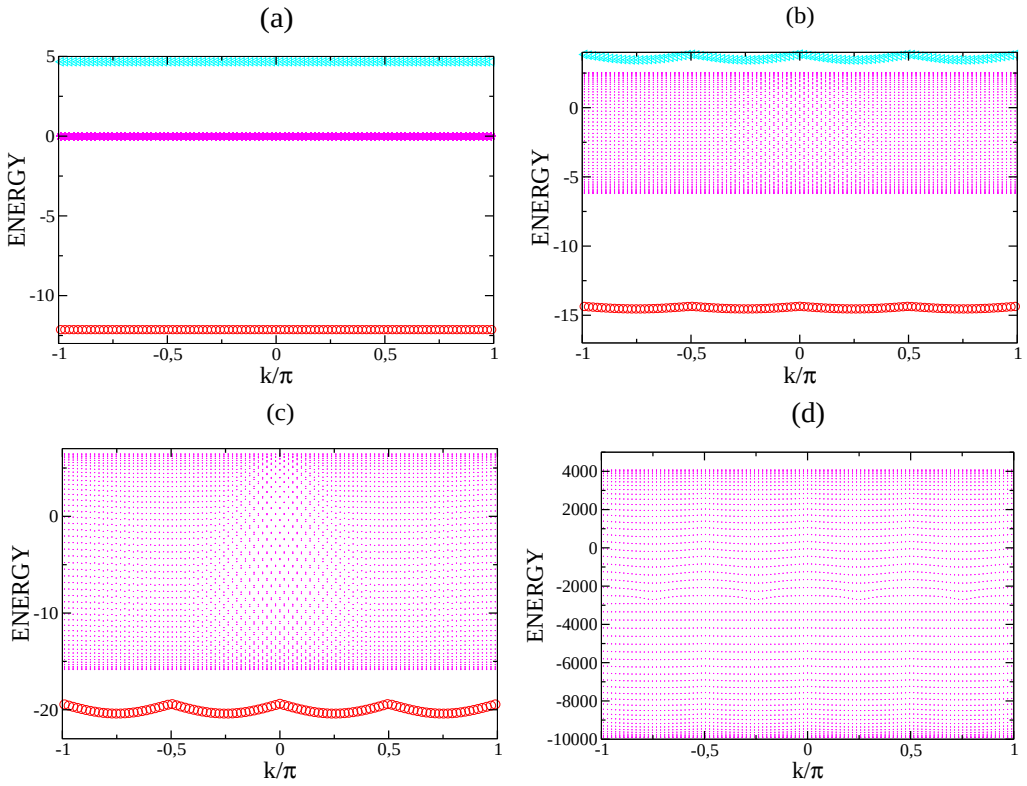

Figure 3.16: Detail of the energy spectrum for the extended Bose-Hubbard model derived from the Heisenberg spin chain including DMI in a periodic lattice containing six quanta for different values of the D_z, where $A = 7$, $n = 4$, $\gamma = 0.05$, $f = 101$ and $J_1 = 1$: (a) $D_z = 0.0$; (b) $D_z = 0.5$; (c) $D_z = 2$; (d) $D_z = 50$

leading interaction.

The second band is the $\{2, 4\}$ band, from which we also obtained the Hamiltonian matrix using the same technique as in the case $\{2, 2\}$ or $\{4, 2\}$ bands.

$$\widetilde{H}_M^{(2,4)} = -\frac{2m}{3A\gamma}(3B + 2C)I_\sigma$$

$$-\frac{B}{A\gamma}\begin{pmatrix} \Gamma & \alpha^{*2}\tau^{-1} & & & P \\ \alpha^2\tau & 0 & \alpha^{*2}\tau^{-1} & & \\ & \ddots & \ddots & \ddots & \\ & & \alpha^2\tau & 0 & \alpha^{*2}\tau^{-1} \\ P^* & & & \alpha^2\tau & \Gamma \end{pmatrix} \tag{3.15}$$

Where $P = 6e^{ik}\frac{D}{B}$, $m = J_1^2 + D_z^2$, $\tau^{-1} = e^{-ik}$, $\alpha^2 = (J_1 + iD_z)^2$, $\alpha^{*2} = (J_1 + iD_z)^2$, $B = (\frac{\gamma}{4} - 1)^2$, $C = (\frac{3\gamma}{4} - 1)^2$, $D = (\frac{5\gamma}{4} - 1)^2$ and $\Gamma = -\frac{1}{3B}(3B + 2C - 13D)$. Here, the energy spectrum appears to be composed by three single bands isolated from each other (see Fig.3.16(a)), but if the value of DMI goes to zero then we get a continuum band; in addition to two breather bands as seen in Fig.3.16(b) or just

the continuum and a breather band (see Fig.3.16(c)). Also we may get only the continuum band as exemplified in Fig.3.16(d). However, they are rather more like the $\{2,4\}$ band but with a difference that this energy spectrum is more degenerated than the $\{4,2\}$ band. Another difference is that while increasing the DMI parameter to ($D_z = 0.5$) both of single band described in Fig.3.16(b) display a sinusoidal form. This form of a lower single band is clearly shown in Fig.3.16(c) for $D_z = 2$. From a physical picture applied to the spin system, it is important to re-mention that there is a limitation i.e. $n \leq 2S$, while the number of bosons in a pure bosonic system has no such constraint. In this framework, the physical picture can be described as that of two groups of four spins (a quadruplet) and two spins (a doublet) adjacently situated in the lattice that can undergo a switching process one group first and then after the next. This can be understood as the result of a local magnetization reversal process that occurs in such ferromagnet involving only few spins.
Using the same technique as in the $\{4,2\}$ case, the Hamiltonian matrix of the $\{3,3\}$ band is

$$\widetilde{H}_M^{(3,3)} = -\frac{3mB'}{A\gamma}(I_\sigma + M) \tag{3.16}$$

where $B' = \left(\frac{\gamma}{2} - 1\right)^2$, $m = J_1^2 + D_z^2$, $M_{1,1} = 1/2 - 4D/B'$, $D = (\frac{5\gamma}{4} - 1)^2$ and $M_{i,j} = 0$ for any $i \neq 1$ and $j \neq 1$.
Comparing the structure of the matrix obtained in equation (3.32), this structure is similar to the six bosons case described in Ref. [41,112]. To derive the eigenvalue of

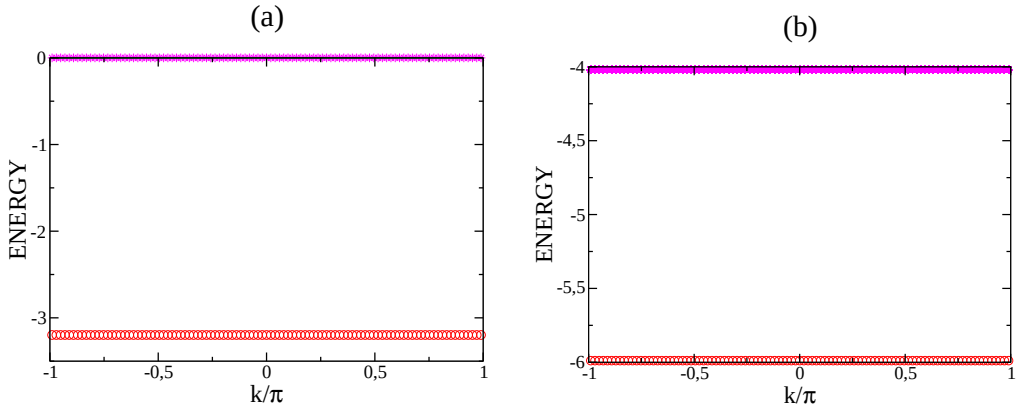

Figure 3.17: Energy spectrum for the extended Bose-Hubbard model derived from the Heisenberg spin chain and the DMI in a one periodic lattice containing six quanta for different values of D_z where, $A = 7$, $\gamma = 0.05$ and $f = 101$: (a) $D_z = 0.$ and $J1 = 1$, (b) $D_z = 0.5$ and $J_1 = 100$

the corresponding $\{3,3\}$ band, we assume these two following cases: In the first case, the exchange interaction is constant ($J_1 = 1$) and we vary the DMI parameter. In absence of the DMI, Fig.3.17(a) shows that the energy of such ferromagnetic materials

is composed only by two lines of bands broadly separated. It is impossible to know, without plotting their eigenfunctions, which of them corresponds to the continuum band. The answer to this issue will be given in the next section of the localization in the real space. For D_z different to zero, the form of the spectrum remains the same like in Fig.3.17(a). The difference is that the levels of energies of those bands decrease with an increasing value of D_z (see Fig.3.17(b)). The outcome shows that in the absence of the DMI, while increasing the value of J_1, the spectrum keeps constant the levels of energies of bands as seen in Fig.3.17(a) and it remains unchanged. Secondly we keep $D_z = 1$ and on varying the exchange interaction, the form of the energy remains unchanged and the levels of energies of the bands also decrease with an increasing of J_1. From our results it is clear that in the framework of six bosons for the other ferromagnets with spin not high enough the process should be more complex. In such a context, two groups of (three spins) a triplet can be engaged in a single switch each per group of triplet in the same time. We also realized that the shape of the energy spectrum of the $\{3,3\}$ band remains unchanged when the values of the parameters J_1 and D_z varies in the same time or while J_1 is absent and vice versa i.e. The parameters J_1 and D_z therefore do only translate the bands from one level to another on the spectrum when the number of quanta is greater than four.

3.4 Energy spectra in a Heisenberg spin chain with long range interactions

In this section, we present the effects of second, third, fourth and long range interactions on the energy system.

3.4.1 Influence of the second nearest interaction on the energy spectrum

When the second nearest neighbor are taken into account, using the equation (2.115), the Hamiltonian matrix is written as follow

$$\widehat{H}_1 = -\begin{pmatrix} u_2 & \sqrt{2}q_1^* & \sqrt{2}q_2^* & 0 & 0 & 0 & 0 & 0 \\ \sqrt{2}q_1 & w_2 + y_{-1,1}^2 & g_1^* & g_2^* & 0 & 0 & 0 & 0 \\ \sqrt{2}q_2 & g_1 & z_2 & g_1^* & g_2^* & 0 & 0 & 0 \\ 0 & g_2 & \ddots & \ddots & \tilde{U}_2 & \ddots & 0 & 0 \\ 0 & 0 & \ddots & \ddots & \ddots & \ddots & \ddots & 0 \\ 0 & 0 & 0 & \ddots & \ddots & \ddots & \ddots & g_2^* \\ 0 & 0 & 0 & 0 & g_2 & g_1 & \tilde{U}_2 & g_1^* + y_{-\sigma,(\sigma-1)}^2 \\ 0 & 0 & 0 & 0 & 0 & g_2 & g_1 + y_{-(\sigma-1),\sigma}^2 & p_2 \end{pmatrix} \quad (3.17)$$

where $u_2 = -4 - 4\alpha_1$, $w_2 = -2 + \gamma_1 - 2\alpha_1$, $\tilde{U}_2 = -2 - 2\alpha_1$, $z_2 = -2 - 2\alpha_1 + \xi_1$, $q_1^* = (\frac{\gamma_1}{4} - 1)g_1^*$, $q_1 = (\frac{\gamma_1}{4} - 1)g_1$, $g_1 = 1 + \tau^1$, $p_2 = \tau^{-\frac{f+1}{2}} + \tau^{\frac{f+1}{2}}) + \tilde{U}_2$, $q_2^* = (\frac{\xi_1}{4} - \alpha_1)g_2^*$, $q_2 = (\frac{\xi_1}{4} - \alpha_1)g_2$, $g_2 = \alpha_1(1 + \tau^2)$, $g_2^* = \alpha_1(1 + \tau^{-2})$, $y_{-1,1}^2 = \alpha_1(\tau^{-1} + \tau^1)$, $y_{-(\sigma-1),\sigma}^2 = \alpha_1(\tau^{-(\sigma-1)} + \tau^\sigma)$ and $y_{-\sigma,(\sigma-1)}^2 = \alpha_1(\tau^{-\sigma} + \tau^{(\sigma-1)})$, $\sigma = \frac{f+1}{2}$.
The structure of this matrix Hamiltonian is constituted by five diagonals. We notice here an appearance of three new terms that are $y_{-1,1}^2$, $y_{-(\sigma-1),\sigma}^2$ and $y_{-\sigma,(\sigma-1)}^2$ in the matrix elements. Using numerical diagonalization, we have derived the energies spectrum of the system as function of Bloch wave number k.

Let us start by emphasizing the results of the case where the ratio is zero (i.e. $\alpha_1 = 0.0$ and $\gamma_1 = 0.05$). The energy spectrum is constituted with a single band (red color with circle symbol see Fig.3.18(a)), which stays above the continuum band. This single band stands for localized bound states and corresponds to the case of a ferromagnetic materials described in Ref [112]. We notice that while increasing the parameter γ_1 up to a value of $\gamma_1 = 0.5$, the energy spectrum displays a new bound state (blue color with square symbol see Fig.3.18(b)), which is merged with the continuum in its major part.
To probe the influence of second nearest neighbors on the energy spectrum, let us choose $\alpha_1 = 0.241$ and $\xi_1 = 0.12$ for which the energy spectrum of such a ferromagnetic materials displays in addition to a continuum band two single bands located respectively above and below the continuum band (see Fig.3.18(c)). However, the main difference when comparing this result with that of Fig.3.18(b) is that, the continuum band is less degenerated at the edge i.e for $k = \pm\pi$. It also appears that the gap between the continuum and the lower single band starts to occur nearby the momentum value of $k = \pm\frac{\pi}{2}$ up to the edge of the Brioullion zone. For $\alpha_1 = 0.6$ and $\xi_1 = 0.3$, the energy spectrum displays in addition to a continuum band and two previous single bands, a new single band (see the cyan color with triangle up symbol) located between the free state's band and the band located on the top of the panel. This is clearly shown in Fig.3.18(d) where, the shape of the continuum band is more affected for $k = 0$ and at the edge of the Brillouin zone. The presence of two isolated bands above and below the free state band is a signature of multi bound states in the system. Here the one with triangle up is induced by the presence of second nearest neighbors interactions. To testify the existence of these localized bound states whose signature seems to appear in the energy spectrum obtained in this section, we need to compute the corresponding eigenfunctions. This will be done in section localization in real space .

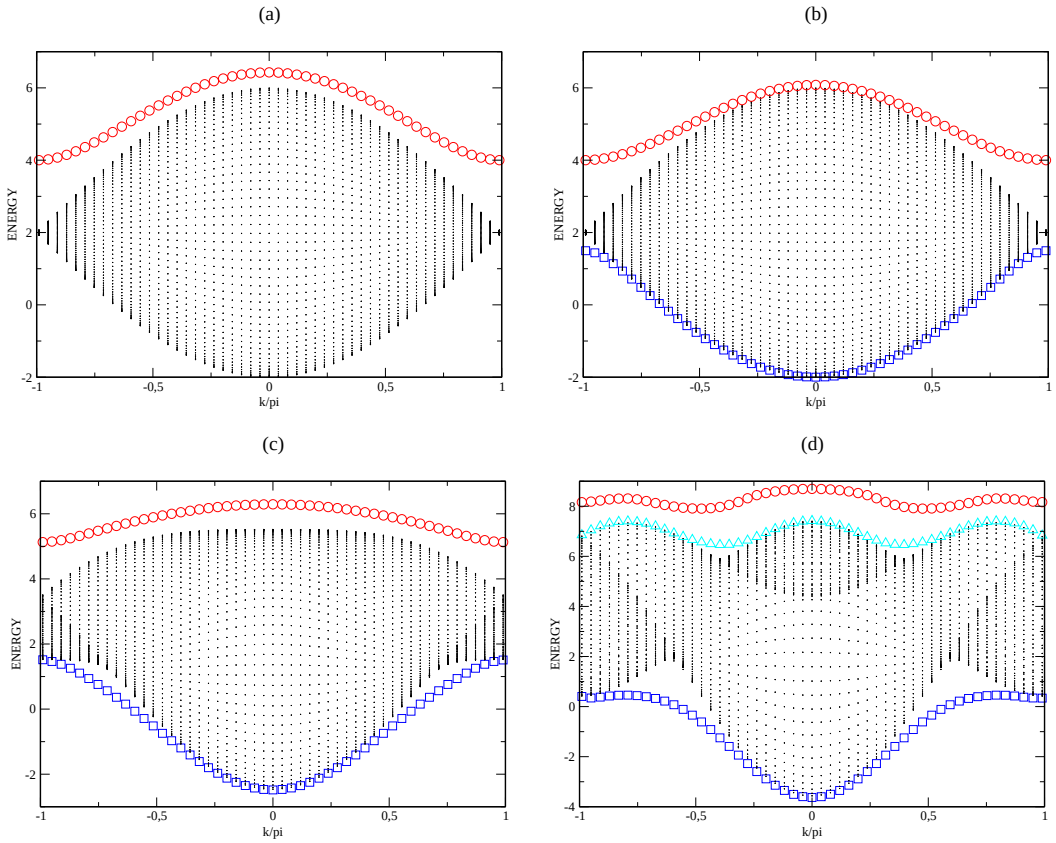

Figure 3.18: Energy spectrum of two bosons interacting with second nearest neighbors in the heisenberg chain where $f = 101$: (a) for $\alpha_1 = 0$ and $\gamma_1 = 0.05$; (b) for $\alpha_1 = 0$, $\gamma_1 = 0.5$; (c) for $\alpha_1 = 0.241$, $\gamma_1 = 0.5$ and $\xi_1 = 0.12$; (d) for $\alpha_1 = 0.6$, $\gamma_1 = 0.5$ and $\xi_1 = 0.3$

3.4.2 Influence of the third and fourth nearest neighbor on the energy spectrum

While using the basis states constructed within number state framework, the matrix Hamiltonian of equation (2.119) reads

$$\widehat{H}_2 = -\begin{pmatrix} u_3 & \sqrt{2}q_1^* & \sqrt{2}q_2^* & \sqrt{2}q_3^* & 0 & 0 & 0 & 0 & 0 & 0 \\ \sqrt{2}q_1 & Q_3 & Q_1^* & g_2^* & g_3^* & 0 & 0 & 0 & 0 & 0 \\ \sqrt{2}q_2 & Q_1 & z_3 & g_1^* & g_2^* & g_3^* & 0 & 0 & 0 & 0 \\ \sqrt{2}q_3 & g_2 & g_1 & \tilde{U}_3 & \ddots & \ddots & \ddots & 0 & 0 & 0 \\ 0 & g_3 & \ddots & \ddots & \ddots & \ddots & \ddots & \ddots & 0 & 0 \\ 0 & 0 & \ddots & \ddots & \ddots & \ddots & \ddots & \ddots & \ddots & 0 \\ 0 & 0 & 0 & \ddots & \ddots & \ddots & \ddots & \ddots & \ddots & g_3^* \\ 0 & 0 & 0 & 0 & \ddots & \ddots & \ddots & \ddots & \ddots & Q_{2,3}^* \\ 0 & 0 & 0 & 0 & 0 & \ddots & \ddots & g_2 & Q_{3,3} & Q_{1,2}^* \\ 0 & 0 & 0 & 0 & 0 & 0 & g_3 & Q_{2,3} & Q_{1,2} & P_3 \end{pmatrix} \tag{3.18}$$

where $P_3 = \tau^{-\frac{f+1}{2}} + \tau^{\frac{f+1}{2}} + \tilde{U}_3$, $q_3^* = (\frac{\xi_2}{4} - \alpha_2)g_3^*$, $q_3 = (\frac{\xi_2}{4} - \alpha_2)g_3$, $g_3 = \alpha_2(1+\tau^3)$, $g_3^* = \alpha_2(1+\tau^{-3})$, $u_3 = u_2 - 4\alpha_2$, $w_3 = w_2 - 2\alpha_2$, $z_3 = z_2 - 2\alpha_2 + \xi_2$, $\tilde{U}_3 = \tilde{U}_2 - 2\alpha_2$, $y^3_{-2,1} = \alpha_2(\tau^{-2} + \tau^1)$, $y^3_{-1,2} = \alpha_2(\tau^{-1} + \tau^2)$, $y^3_{-(\sigma-2),\sigma} = \alpha_2(\tau^{-(\sigma-2)} + \tau^\sigma)$, $Q_3 = w_3 + y^2_{-1,1}$, $Q_1 = g_1 + y^3_{-1,2}$, $Q_1^* = g_1^* + y^3_{-2,1}$, $Q_{3,3} = \tilde{U}_3 + y^3_{-(\sigma-2),(\sigma-2)}$, $Q_{2,3} = g_2 + y^3_{-(\sigma-2),\sigma}$, $Q^*_{2,3} = g_2^* + y^3_{-\sigma,(\sigma-2)}$, $Q_{1,2} = g_1 + y^2_{-(\sigma-1),\sigma}$, $Q^*_{1,2} = g_1^* + y^2_{-\sigma,(\sigma-1)}$ $y^3_{-(\sigma-2),(\sigma-2)} = \alpha_2(\tau^{-(\sigma-2)} + \tau^{(\sigma-2)})$ and $y^3_{-\sigma,(\sigma-2)} = \alpha_2(\tau^{-\sigma} + \tau^{(\sigma-1)})$.

The structure of this Hamiltonian matrix is more complex than the case described in Eq.(3.17). Here, the main difference is that, it involves seven diagonals instead of five. Thus the number of diagonal increases with the number of nearest neighbors and there is also an appearance of new terms such as $y^3_{l,n}$.
In this section, we consider only the case where $\alpha_1 = 0.8$, $\xi_1 = 0.4$, $\alpha_2 = 0.241$ and $\xi_2 = 0.12$. Energies spectrum obtained from a numerical digonalization always displays in addition to a continuum band one single band lying below the continuum and two others isolated bands that at a first glance stand for new bound states. Figure 3.19(a) and Fig.3.19(b) really look alike since, the continuum band is non degenerated at the edge of the Brillouin zone. Another question mark is how the energy spectrum will be affected if we consider the case where the Hamiltonian of a 1D Heisenberg ferromagnetic spin chain also includes the fourth nearest neighbors?

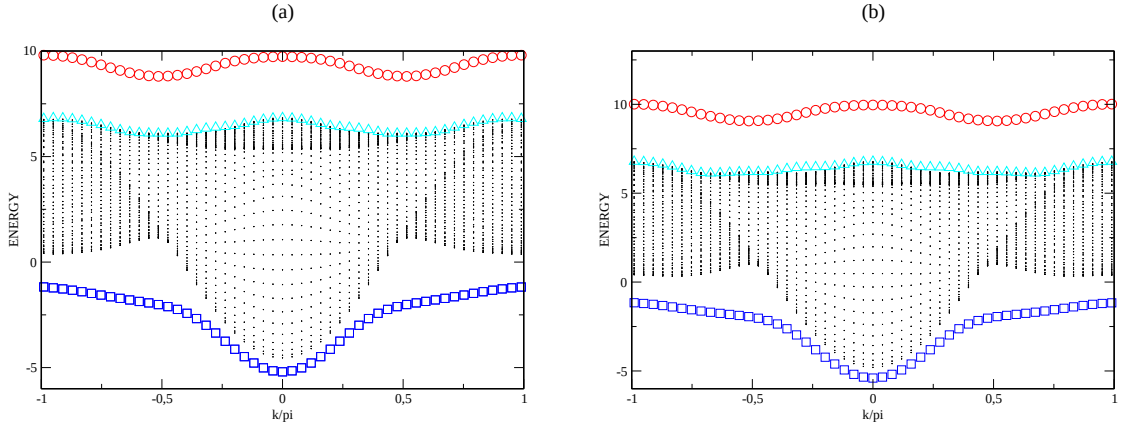

Figure 3.19: Energy spectrum of two bosons interacting with third and fourth nearest neighbors in the heisemberg spin chain where $f = 101$ and $\gamma_1 = 0.5$: (a) case of third nearest neighbors for $\alpha_1 = 0.8$ and $\xi_1 = 0.4$, $\alpha_2 = 0.241$ and $\xi_2 = 0.12$; (b) case of fourth nearest neighbors, for $\alpha_1 = 0.8$ and $\xi_1 = 0.4$, $\alpha_2 = 0.241$ and $\xi_2 = 0.12$, $\alpha_3 = 0.1$ and $\xi_3 = 0.05$

The Hamiltonian matrix is subdivided as the sum of two matrices and the total Hamiltonian matrix is rewritten as $\widetilde{H}_3 = \widehat{H}_3 + \widehat{Y}_3$ where $\widehat{H}_3$ is the first term of the

matrix given by:

$$\widehat{H}_3 = -\begin{pmatrix} u_4 & \sqrt{2}q_1^* & \sqrt{2}q_2^* & \sqrt{2}q_3^* & \sqrt{2}q_4^* & 0 & 0 & 0 & 0 & 0 & 0 & 0 \\ \sqrt{2}q_1 & w_4 & g_1^* & g_2^* & g_3^* & g_4^* & 0 & 0 & 0 & 0 & 0 & 0 \\ \sqrt{2}q_2 & g_1 & z_4 & g_1^* & g_2^* & g_3^* & g_4^* & 0 & 0 & 0 & 0 & 0 \\ \sqrt{2}q_3 & g_2 & g_1 & \tilde{U}_4 & g_1^* & g_2^* & g_3^* & g_4^* & 0 & 0 & 0 & 0 \\ \sqrt{2}q_4 & g_3 & g_2 & g_1 & \tilde{U}_4 & \ddots & \ddots & \ddots & \ddots & 0 & 0 & 0 \\ 0 & g_4 & \ddots & \ddots & \ddots & \ddots & \ddots & \ddots & \ddots & \ddots & 0 & 0 \\ 0 & 0 & \ddots & \ddots & \ddots & \ddots & \ddots & \ddots & \ddots & \ddots & \ddots & 0 \\ 0 & 0 & 0 & \ddots & \ddots & \ddots & \ddots & \ddots & \ddots & \ddots & \ddots & g_4^* \\ 0 & 0 & 0 & 0 & \ddots & \ddots & \ddots & \ddots & \ddots & \ddots & \ddots & g_3* \\ 0 & 0 & 0 & 0 & 0 & \ddots & \ddots & \ddots & \ddots & \ddots & g_1^* & g_2^* \\ 0 & 0 & 0 & 0 & 0 & 0 & \ddots & \ddots & \ddots & g_1 & \tilde{U}_4 & g_1^* \\ 0 & 0 & 0 & 0 & 0 & 0 & 0 & g_4 & g_3 & g_2 & g_1 & p_4 \end{pmatrix} \tag{3.19}$$

where $u_4 = u_3 - 4\alpha_3$, $w_4 = w_3 - 2\alpha_3$, $z_4 = z_3 - 2\alpha_3 + \xi_3$, $\tilde{U}_4 = \tilde{U}_3 - 2\alpha_3$, $P_4 = \alpha_1(\tau^{-\frac{f+1}{2}} + \tau^{\frac{f+1}{2}}) + \tilde{U}_4$; $q_4^* = (\frac{\xi_3}{4} - \alpha_3)g_4^*$, $q_4 = (\frac{\xi_3}{4} - \alpha_3)g_4$, $g_4 = \alpha_3(1+\tau^4)$ and $g_4^* = \alpha_3(1+\tau^{-4})$.

The structure of the first part of the matrix, involve nine diagonals. In addition to five diagonals given by the case of third nearest neighbors interacting spin, there are two news diagonals due to the effect of the fourth nearest neighbors. The last term denoted with $\widehat{Y}_3$ is the matrix that displays the order of appearance of the new elements.

$$\widehat{Y}_3 = -\begin{pmatrix} 0 & 0 & 0 & 0 & 0 & 0 & 0 & 0 & 0 & 0 & 0 & 0 \\ 0 & y_{-1,1}^2 & y_{-2,1}^3 & y_{-3,1}^4 & 0 & 0 & 0 & 0 & 0 & 0 & 0 & 0 \\ 0 & y_{-1,2}^3 & y_{-2,2}^4 & 0 & 0 & 0 & 0 & 0 & 0 & 0 & 0 & 0 \\ 0 & y_{-1,3}^4 & 0 & 0 & 0 & 0 & 0 & 0 & 0 & 0 & 0 & 0 \\ 0 & 0 & 0 & 0 & 0 & 0 & 0 & 0 & 0 & 0 & 0 & 0 \\ 0 & \ddots & \ddots & \ddots & \ddots & \ddots & \ddots & \ddots & \ddots & 0 & 0 & 0 \\ 0 & 0 & \ddots & \ddots & \ddots & \ddots & \ddots & \ddots & \ddots & \ddots & 0 & 0 \\ 0 & 0 & 0 & 0 & 0 & 0 & 0 & 0 & 0 & 0 & 0 & 0 \\ 0 & 0 & 0 & 0 & 0 & 0 & 0 & 0 & 0 & 0 & 0 & A \\ 0 & 0 & 0 & 0 & 0 & 0 & 0 & 0 & 0 & 0 & B & E \\ 0 & 0 & 0 & 0 & 0 & 0 & 0 & 0 & 0 & C & F & H \\ 0 & 0 & 0 & 0 & 0 & 0 & 0 & 0 & D & G & I & 0 \end{pmatrix} \tag{3.20}$$

where, $y^4_{-3,1} = \alpha_3(\tau^{-3} + \tau^1)$, $y^4_{-2,2} = \alpha_3(\tau^{-2} + \tau^2)$, $y^4_{-1,3} = \alpha_3(\tau^{-1} + \tau^3)$, $A = y^4_{-\sigma,(\sigma-3)} = \alpha_3(\tau^{-\sigma}+\tau^{(\sigma-3)})$, $B = y^4_{-(\sigma-1),(\sigma-2)} = \alpha_3(\tau^{-(\sigma-1)}+\tau^{(\sigma-2)})$, $C = y^4_{-(\sigma-2),(\sigma-1)} = \alpha_3(\tau^{-(\sigma-2)}+\tau^{(\sigma-1)})$, $D = y^4_{(\sigma-3),\sigma} = \alpha_3(\tau^{-(\sigma-3)}+\tau^{\sigma})$, $E = y^3_{-\sigma,(\sigma-2)}$, $F = y^3_{-(\sigma-1),(\sigma-1)}$, $G = y^3_{-(\sigma-2),\sigma}$, $H = y^2_{-\sigma,(\sigma-1)}$, $I = y^2_{-(\sigma-1),\sigma}$.

To describe the new shape of the energy spectrum, here, we choose successively $\alpha_1 = 0.8$ and $\xi_1 = 0.4$, $\alpha_2 = 0.241$, $\xi_2 = 0.12$, $\alpha_3 = 0.1$ and $\xi_3 = 0.05$. While looking at Fig.3.19(b) and Fig.3.19(a) where the third nearest neighbors are involved, we realized that the shape of the energy spectrum remains almost identical in both cases. Therefore in this case the energy spectrum is not affected when more than three nearest neighbors are considered. From the generalized form of this Hamiltonian (2.123), we can probe the Fermi-Pasta-Ulam behavior on this generic model. In this respect, we proceed to successive calculations with increasing at each fold the number m of nearest neighbors. It turns out that the general form of the matrix Hamiltonian of our system can be written for the sake of clarification as a sum of two matrices

$$\widehat{H}_{(m-1)} = \begin{pmatrix}
u_1 & \sqrt{2}q_1^* & \sqrt{2}q_2^* & \cdots & & & \cdots & \sqrt{2}q_{m-1}^* & \sqrt{2}q_m^* & 0 & \cdots & 0 \\
\sqrt{2}q_1 & w_2 & g_1^* & g_2^* & \cdots & & \cdots & g_{m-2}^* & g_{m-1}^* & g_m^* & \ddots & \vdots \\
\sqrt{2}q_2 & \ddots & z_3 & \ddots & \ddots & \ddots & \ddots & \ddots & \ddots & \ddots & \ddots & 0 \\
\vdots & g_2 & \ddots & \tilde{U}_4 & & & & & & \ddots & \ddots & g_m^* \\
 & g_3 & \ddots & & & & & & & \ddots & g_{m-2}^* & g_{m-1}^* \\
 & & \ddots & & & & & & & & g_{m-3}^* & \vdots \\
\vdots & & & & & & & & & & & \\
\sqrt{2}q_{m-1} & \ddots & & & & & & & & & \ddots & \\
\sqrt{2}q_m & \ddots & & & & & & & & \ddots & g_2^* & \vdots \\
0 & \ddots & & & & & & & & \ddots & g_1^* & g_2^* \\
\vdots & \ddots & \ddots & \ddots & \ddots & & \ddots & \ddots & \ddots & g_1 & \tilde{U}_{m-1} & g_1^* \\
0 & \cdots & 0 & g_m & g_{m-1} & \cdots & & & \cdots & g_2 & g_1 & p_m
\end{pmatrix} \tag{3.21}$$

and

$$\widehat{Y}_{(m-1)} = \begin{pmatrix}
0 & 0 & \cdots & & & & \cdots & 0 & \cdots & & \cdots & & 0 \\
0 & y^2_{-1,1} & y^3_{-2,1} & y^4_{-3,1} & y^5_{-4,1} & \cdots & \cdots & Y^* & \ddots & & & & \vdots \\
\vdots & y^3_{-1,2} & y^4_{-2,2} & y^5_{-3,2} & y^6_{-3,2} & \ddots & & 0 & & \ddots & & & \vdots \\
 & y^4_{-1,3} & y^5_{-2,3} & \ddots & \ddots & \ddots & 0 & & H & \ddots & & & 0 \\
 & y^5_{-1,4} & y^6_{-2,4} & \ddots & y^m_{-i,i} & 0 & & & \ddots & & 0 & & T \\
 & \vdots & \ddots & \ddots & 0 & \ddots & \ddots & \ddots & & 0 & & & Z^* \\
 & \ddots & \ddots & 0 & & & \ddots & & 0 & & & & \vdots \\
\vdots & Y & 0 & & & \ddots & & 0 & & \ddots & \ddots & & \\
0 & 0 & & & \ddots & & 0 & & W & \ddots & y^5_{-(\sigma-1),(\sigma-3)} & & \vdots \\
\vdots & \ddots & \ddots & \ddots & & 0 & & & \ddots & \ddots & L^* & & K^* \\
\vdots & & \ddots & & 0 & Z & \ddots & \ddots & \ddots & L & X & & y^2_{-\sigma,(\sigma-1)} \\
0 & \cdots & \cdots & 0 & \cdots & & & & \cdots & K & y^2_{-(\sigma-1),\sigma} & & y^1_{-\sigma,\sigma}
\end{pmatrix} \tag{3.22}$$

where $Y = y^m_{-1,(m-1)}$, $Y^* = y^m_{-(m-1),1}$, $H = y^m_{-(m-2),2}$,$Z = y^m_{-(\sigma-m+2),(\sigma-1)}$, $Z^* = y^m_{-(\sigma-1),(\sigma-m+2)}$, $K = y^3_{-(\sigma-2),\sigma}$, $K^* = y^3_{-\sigma,(\sigma-2)}$, $L = y^4_{-(\sigma-2),(\sigma-1)}$, $L^* = y^4_{-(\sigma-1),(\sigma-2)}$, $W = y^m_{-(\sigma-m),(\sigma-m)}$, $X = y^3_{-(\sigma-1),(\sigma-1)}$ and $T = y^m_{-\sigma,(\sigma-m+1)}$.

It is easy to derive from equations (3.21) and (3.22) all others previous results obtained in equations (3.17, 3.18, 3.19 and 3.20). For this, we consider that, an element such as $y^m_{-i,i} = \alpha_{(m-1)}(\tau^{-i} + \tau^i)$ where m is the number of nearest neighbors, $\alpha_{(m-1)}$, denotes the ratio of the Heisenberg exchange interaction, i is the power of parameter τ.

While m is an odd number, all elements written in the same form as $y^m_{-i,i}$ and $y^m_{-(\sigma-m),(\sigma-m)}$ are nil. In particular for $m = 1$, $y^m_{-i,j} = y^m_{-j,i} = 0$. For $m \geq 2$, $y^m_{-i,j}$ and $y^m_{-j,i}$ are non nil. Assuming that n and l are two non zero integers, if $m - l \leq 0$ then $g_{m-l} = y^m_{-(m-l),n} = y^m_{-n,(m-l)} = 0$.

3.4.3 Effect of long range interactions on the energy spectrum when four or six quanta are involved

The $\{2, 2\}$ band Hamiltonian matrix including the second nearest neighbors is.

$$\widehat{H}_1^{(2,2)} = -\frac{4}{A}(\frac{B_1}{\gamma_1} + \frac{\alpha_1^2 B_2}{\gamma_1})I_\sigma - \frac{1}{A}(\frac{B_1}{\gamma_1} + \frac{\alpha_1^2 B_2}{\gamma_1}) \times \tag{3.23}$$
$$\begin{pmatrix} \Gamma_1 & W_1^* & W_2^* & 0 & 0 & 0 & 0 & 0 \\ W_1 & \Gamma_2 & W_1^* & W_2^* & 0 & 0 & 0 & 0 \\ W_2 & W_1 & 0 & W_1^* & W_2^* & 0 & 0 & 0 \\ 0 & W_2 & W_1 & 0 & W_1^* & W_2^* & 0 & 0 \\ 0 & 0 & \ddots & \ddots & \ddots & \ddots & \ddots & 0 \\ 0 & 0 & 0 & W_2 & W_1 & 0 & W_1^* & W_2^* \\ 0 & 0 & 0 & 0 & W_2 & W_1 & \Gamma_2 & W_1^* \\ 0 & 0 & 0 & 0 & 0 & W_2 & W_1 & P_2 \end{pmatrix}$$

where $B_1 = (\frac{\gamma_1}{4} - 1)^2$, $B_2 = (\frac{\gamma_1}{4} - 1)^2$, I_σ is the $\sigma \times \sigma$ unity matrix, $W_1 = 1 + \tau = 2e^{ik/2}\cos(k/2)$, $W_1^* = 2e^{-ik/2}\sin(k/2)$, $W_2 = 1 + \tau = 2e^{ik}\cos k$, $W_2^* = 2e^{-ik}\sin k$, $P_2 = 2\cos(\sigma k)$, $\Gamma_1 = 6(\frac{C_1}{B_1} - 1)$, $C_1 = (\frac{3\gamma_1}{4} - 1)^2$, $\Gamma_2 = 6(\frac{C_2}{B_2} - 1)$, $C_2 = (\frac{3\gamma_1}{4} - 1)^2$ and A is the anisotropy parameter.
We distinguish several configurations of the energy spectrum of ferromagnetic materials depending of ratio α_1.

We distinguish here several configurations of the energy spectrum of ferromagnetic materials depending on the ratio α_1^2.
When four quanta are involved, the shape of energy spectrum of the ferromagnetic materials without the second nearest neighbors i.e. for $\alpha_1^2 = 0.0$ shows in Fig.3.20(a), a single band's structure lying above the continuum. This is the $\{2, 2\}$ band. This isolated band can appear either above or below the continuum spectrum as the sign of the anisotropy parameter changes. The isolated band is a localized band and stands for states consisting of adjacent sites that are each occupied by two quanta, whereas in the continuum band, most of the sites are separated by one or more vacant sites. The localized band describes the localization of energy that is a signature of the presence of the quantum counterpart of the breather solution of the classical nonlinear system. From a physical picture referred to the spin system, we shall also mention that the limitation given by $n \leq 2S$ allows only materials with sufficiently high spin in order to display such a localization phenomenon. That phenomenon is a precursor of a localized magnetization area that would lead to its local reversal process involving two groups of two spins in a single switch. Figure 3.20(b) exhibits the case where the second nearest neighbors are taken into account for $\alpha_1^2 = 0.4$. A dimerized state is a state characterized by two group of two neighboring spins interacting that can thereafter undergo a local magnetization reversal process through a

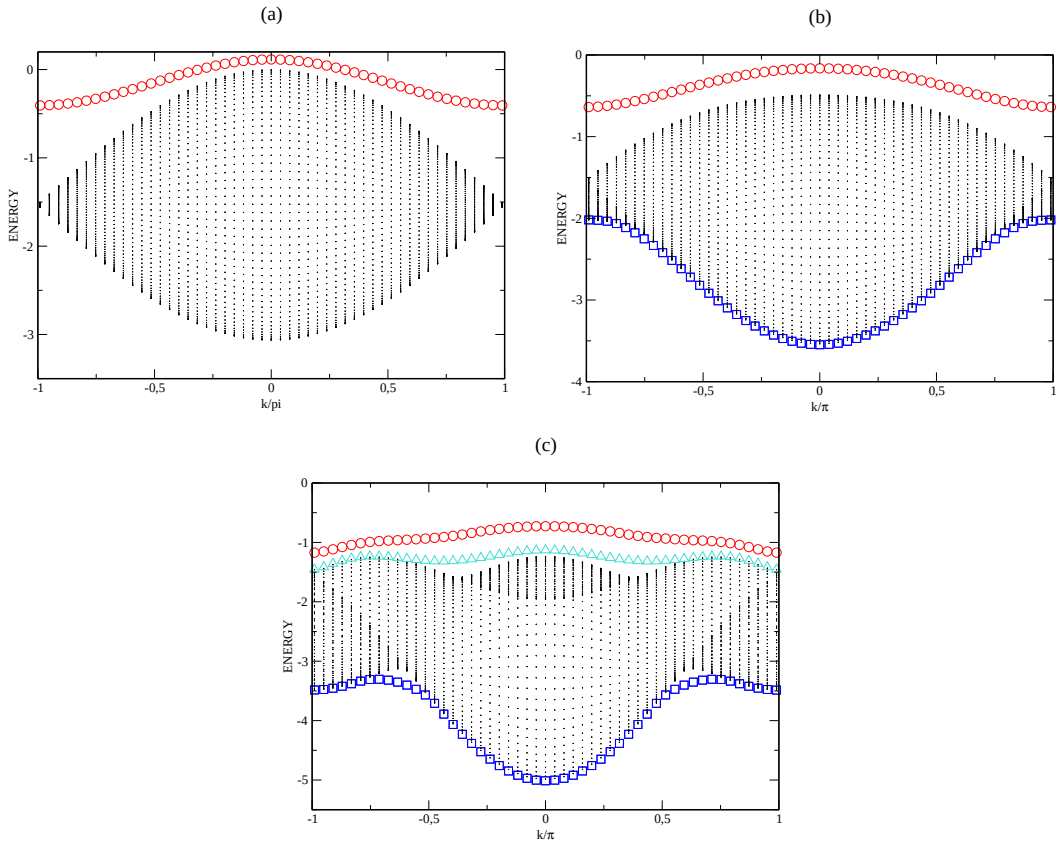

Figure 3.20: Excitation spectrum of four bosons in the band $\{2,2\}$ interacting with second nearest neighbors in the extended Bose-Hubbard spin chain of different values of α_1^2 where $A = 1$, $\gamma_1 = 0.5$ and $f = 101$: (a) first nearest neighbors for $\alpha_1^2 = 0$; (b) second for $\alpha_1^2 = 0.4$; (c) second for $\alpha_1^2 = 0.8$

single switch. Here, the energy spectrum displays in addition to the continuum, a single band (blue color in square symbol) lying below the continuum. It is difficult for us to distinguish if these bands really stand for localized states or not without investigating the amplitudes of the corresponding states. Such an issue will be addressed in section V. The fundamental difference when we compare the energy spectrum in Fig.3.20(b) to the one shown in Fig.3.18(a) or Fig.3.20(a) is that the continuum band begins to be non degenerated at the edge of the Brillouin zone. For $\alpha_1^2 = 0.8$ the new isolated band appears above the continuum but located below the isolated band on the top of the panel (see red color in circle symbol) and the continuum. As the parameter α_1^2 increases, the less degenerated the continuum becomes at the edge of the Brillouin zone (see Fig.3.20(c)).
How will be the shape of the energy spectrum when more than two nearest neighbors will be considered in the system? The Hamiltonian matrix in this case is

$$\widehat{H}_2^{(2,2)} = -\frac{4}{A\gamma_1}(B_1+\alpha_1^2B_2+\alpha_2^2B_3)I_\sigma$$

$$-\frac{1}{A\gamma_1}(B_1+\alpha_1^2B_2+\alpha_2^2B_3)\begin{pmatrix}
\Gamma_1 & W_1^* & W_2^* & W_3^* & 0 & 0 & 0 & 0 & 0 & 0\\
W_1 & \Gamma_2 & W_1^* & W_2^* & W_3^* & 0 & 0 & 0 & 0 & 0\\
W_2 & W_1 & \Gamma_3 & W_1^* & W_2^* & W_3^* & 0 & 0 & 0 & 0\\
W_3 & W_2 & W_1 & 0 & W_1^* & W_2^* & W_3^* & 0 & 0 & 0\\
0 & W_3 & \ddots & \ddots & 0 & \ddots & \ddots & \ddots & 0 & 0\\
0 & 0 & \ddots & \ddots & \ddots & \ddots & \ddots & \ddots & \ddots & 0\\
0 & 0 & 0 & \ddots & \ddots & \ddots & 0 & \ddots & \ddots & W_3^*\\
0 & 0 & 0 & 0 & W_3 & W_2 & W_1 & \Gamma_3 & W_1^* & W_2^*\\
0 & 0 & 0 & 0 & 0 & W_3 & W_2 & W_1 & \Gamma_2 & W_1^*\\
0 & 0 & 0 & 0 & 0 & 0 & W_3 & W_2 & W_1 & p_3
\end{pmatrix} \tag{3.24}$$

where $B_3 = (\frac{\gamma_1}{4}-1)^2$, I_σ is the $\sigma\times\sigma$ unity matrix, $W_2 = 1+\tau = 2e^{3ik/2}\cos(3k/2)$, $W_2^* = 2e^{-3ik/2}\sin(3k/2)$, $P_3 = 2\cos(\sigma k)$, $\Gamma_3 = 6(\frac{C_3}{B_3}-1)$, $C_3 = (\frac{3\gamma_1}{4}-1)^2$ and A is the anisotropy parameter.

To address this issue, two cases are considered. In the presence of the third neighbors where $\alpha_1^2 = 0.8$ and $\alpha_2^2 = 0.34$, the continuum on the spectrum keeps its shape identical to the one of Fig.3.20(c). The new isolated band appears to be partially merged to the continuum (see band with triangle left symbol in Fig.3.21(a)). For $\alpha_1^2 = 0.8$ and $\alpha_2^2 = 0.6$, such a phenomenon appears with the presence of another single band (see magenta color with triangle right in Fig.3.21(b)). It is important to mention that from the outcome, the number of single bands increases as the number of nearest neighbors with increasing α_2^2. The presence of four single bands here is a signature of multi bound states in the system.

The general Hamiltonian matrix of m nearest neighbors in the $\{2,2\}$ band is

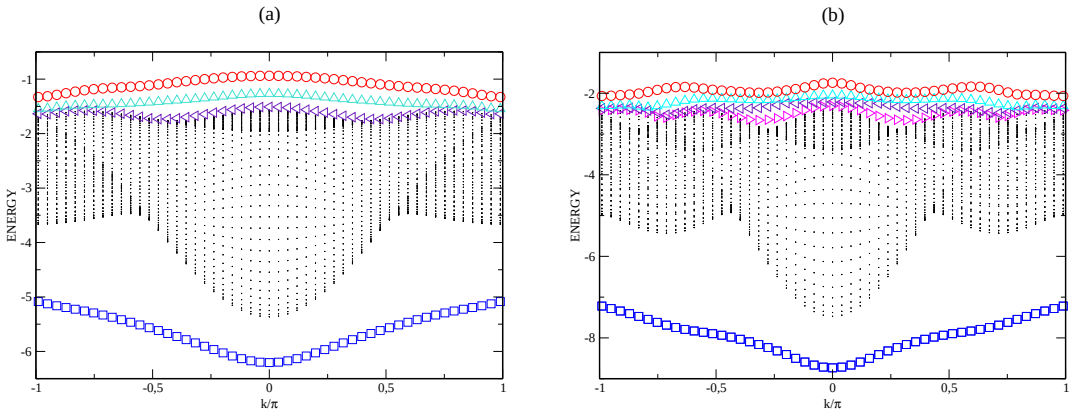

Figure 3.21: Excitation spectrum of four bosons in the $\{2,2\}$ band interacting with third nearest neighbors in the extended Bose-Hubbard spin chain for different values of α_1^2 and α_2^2 where $A=1$, $\gamma_1=0.5$ and $f=101$: (a) for $\alpha_1^2=0.8$ and $\alpha_2^2=0.34$; (b) for $\alpha_1^2=0.8$ and $\alpha_2^2=0.6$

$$\widehat{H}^{(2,2)}_{(m-1)} = -\frac{4}{A\gamma_1}(B_1+\alpha_1^2B_2+\cdots+\alpha^2_{(m-1)}B_m)I_\sigma - \frac{1}{A\gamma_1}(B_1+\alpha_1^2B_2+\cdots+\alpha^2_{(m-1)}B_m)\times$$

$$\begin{pmatrix}
\Gamma_1 & W_1^* & W_2^* & W_3^* & \cdots & & \cdots & W_{m-1}^* & W_m^* & 0 & \cdots & 0\\
W_1 & \Gamma_2 & W_1^* & W_2^* & W_3^* & \cdots & \cdots & W_{m-2}^* & W_{m-1}^* & W_m^* & \ddots & \vdots\\
W_2 & W_1 & \ddots & W_1^* & W_2^* & \ddots & \ddots & \ddots & \ddots & \ddots & \ddots & 0\\
W_3 & \ddots & \ddots & \Gamma_{m-1} & \ddots & \ddots & \ddots & \ddots & \ddots & \ddots & \ddots & W_m^*\\
\vdots & \ddots & \ddots & \ddots & \Gamma_m & \ddots & \ddots & \ddots & \ddots & \ddots & \ddots & W_{m-1}^*\\
\vdots & \ddots & \ddots & \ddots\ddots & \ddots & 0 & \ddots & \ddots & \ddots & \ddots & \ddots & W_{m-2}^*\\
W_{m-2} & \ddots & \ddots & \ddots & \ddots & \ddots & \ddots & \ddots & \ddots & \ddots & \ddots & \vdots\\
W_{m-1} & \ddots & \ddots & \ddots & \ddots & \ddots & \ddots & 0 & \ddots & \ddots & \ddots & \vdots\\
W_m & \ddots & \ddots & \ddots & \ddots & \ddots & \ddots & \ddots & \Gamma_m & \ddots & \ddots & W_3^*\\
0 & \ddots & \ddots & \ddots & \ddots & \ddots & \ddots & W_2 & W_1 & \ddots & W_1^* & W_2^*\\
\vdots & \ddots & W_m & W_{m-1} & W_{m-2} & \cdots & \cdots & W_3 & W_2 & W_1 & \Gamma_2 & W_1^*\\
0 & \cdots & 0 & W_m & W_{m-1} & \cdots & \cdots & \cdots & W_3 & W_2 & W_1 & p_m
\end{pmatrix} \quad (3.25)$$

Next, we consider the case of $n=6$ spins. This case displays three bands: namely $\{4,2\}$, $\{2,4\}$ and $\{3,3\}$, bands.
In this case, the first band under consideration is the $\{4,2\}$ band. Then if we proceed as in the case of the $\{2,2\}$ band, it turns out that we obtain the Hamiltonian matrix describing this $\{4,2\}$ band when second nearest neighbors are taken into account as follows

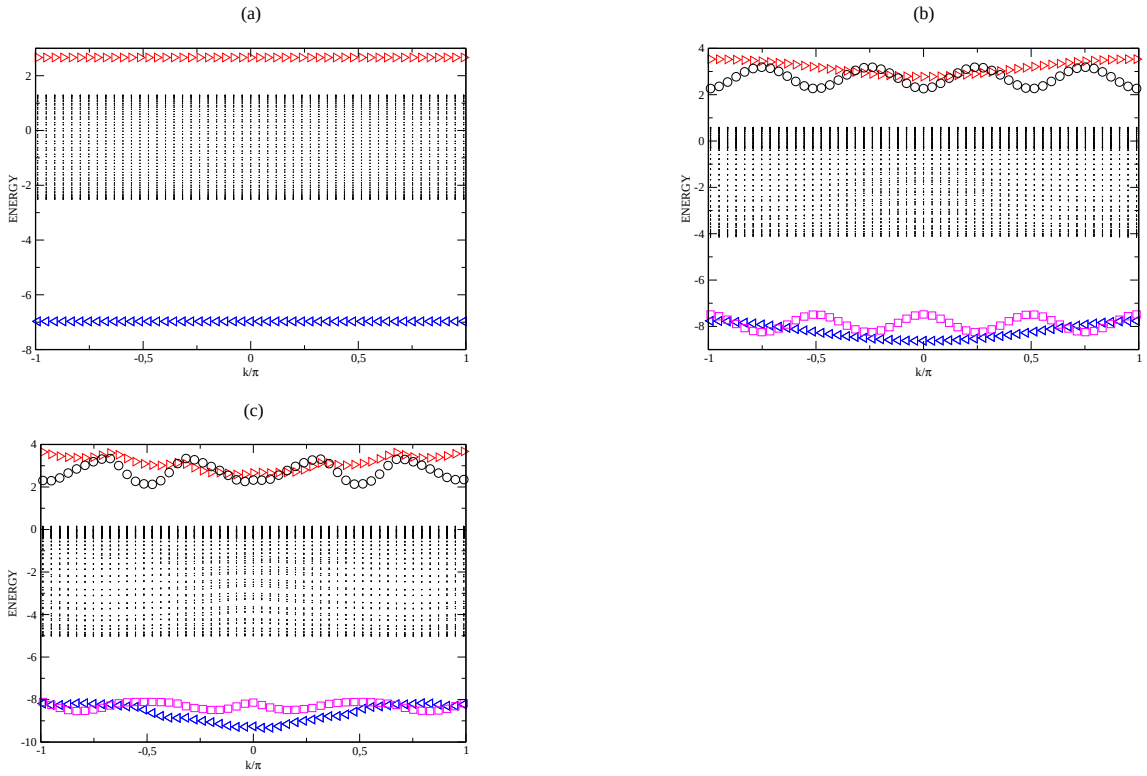

Figure 3.22: Excitation spectrum of the extended Bose-Hubbard model derived from the Heisenberg spin chain in a periodic lattice containing six bosons in $\{4,2\}$ band and $\{2,4\}$ band interacting with first, second and third nearest neighbors for different values of α_1^2 and α_2^2 where $A=0.1$, $\gamma_1=0.5$ and $f=101$: (a) first nearest neighbors for $\alpha_1^2=0$; (b) second nearest neighbors for $\alpha_1^2=0.8$; (c) third nearest neighbors for $\alpha_1^2=0.8$ and $\alpha_2^2=0.6$

$$\widehat{H}_1^{(4,2)} = -\widehat{H}_1^{(4,2)} = -\frac{4}{3A\gamma_1}[(3B_1+2C_1)+\alpha_1^2(3B_2+2C_2)]I_\sigma \tag{3.26}$$

$$-\frac{1}{A\gamma_1}(B_1+\alpha_1^2B_2)\begin{pmatrix} \Gamma_1 & 1 & 1 & 0 & 0 & 0 & P_2^* & P_1^* \\ 1 & \Gamma_2 & 1 & 1 & 0 & 0 & 0 & 0 \\ 1 & 1 & 1 & 1 & 1 & 0 & 0 & 0 \\ 0 & 1 & \ddots & 0 & \ddots & 1 & 0 & 0 \\ 0 & 0 & \ddots & \ddots & \ddots & \ddots & \ddots & 0 \\ 0 & 0 & 0 & 1 & 1 & 0 & 1 & 1 \\ P_2 & 0 & 0 & 0 & 1 & 1 & \Gamma_2 & 1 \\ P_1 & 0 & 0 & 0 & 0 & 1 & 1 & \Gamma_1 \end{pmatrix}$$

where $P_1=6e^{ik}\frac{D_1}{B_1}$, $P_2=6e^{2ik}\frac{D_2}{B_2}$, $B_1=(\frac{\gamma_1}{4}-1)^2$, $B_2=(\frac{\gamma_1}{4}-1)^2$, $C_1=(\frac{\gamma_1}{4}-1)^2$, $C_2=(\frac{3\gamma_1}{4}-1)^2$, $D_1=(\frac{5\gamma_1}{4}-1)^2$ and $\Gamma_1=-\frac{1}{3B_1}(3B_1+2C_1-13D_1)$ $D_2=(\frac{5\gamma_1}{4}-1)^2$ and $\Gamma_2=-\frac{1}{3B_2}(3B_2+2C_2-13D_2)$.

To probe the shape of the energy spectrum when the second nearest neighbors are involved, we consider two cases: firstly, the case of the ferromagnetic materials where $\alpha_1^2 = 0$. In this case, the system is reduced to a case where only the first nearest neighbors are interacting. The energy spectrum of these ferromagnetic materials display in addition to a continuum band that turns out to appear with a flat shape and a size testifying its non degeneracy, two singles bands of a priori bound states above and below this flat band. There is a consistent gap between the continuum band and the lowest band as seen in Fig.3.22(a). Secondly, we realized that for $\alpha_1^2 = 0.8$, the continuum on the spectrum keeps its flat shape identical to the one shown in Fig.3.22(a). Whereas both single bands (see upper band in red with triangle right and lower band in color blue color with triangle left) display an oscillating shape instead of lines. Here, the continuum band in $\{4, 2\}$ band and the $\{2, 4\}$ have the same form. In order to avoid overloading the paper, we have plotted energies spectrum of these bands in the same Fig.3.22(b). As we can see, these bands exhibit the same shape.
While the third neighbors are accounting in the system, the matrix Hamiltonian reads

$$\widehat{H}_2^{(4,2)} = -\frac{4}{3A\gamma_1}[3B_1 + 2C_1 + \alpha_1^2(3B_2 + 2C_2) + \alpha_2^2(3B_3 + 2C_3)]I_\sigma \quad (3.27)$$

$$-\frac{1}{A\gamma_1}(B_1 + \alpha_1^2 B_2 + \alpha_2^2 B_3)\begin{pmatrix} \Gamma_1 & 1 & 1 & 1 & 0 & 0 & 0 & P_3^* & P_2^* & P_1^* \\ 1 & \Gamma_2 & 1 & 1 & 1 & 0 & 0 & 0 & 0 & 0 \\ 1 & 1 & \Gamma_3 & 1 & 1 & 1 & 0 & 0 & 0 & 0 \\ 1 & 1 & 1 & 0 & 1 & 1 & 1 & 0 & 0 & 0 \\ 0 & 1 & \ddots & \ddots & 0 & \ddots & \ddots & \ddots & 0 & 0 \\ 0 & 0 & \ddots & \ddots & \ddots & \ddots & \ddots & \ddots & \ddots & 0 \\ 0 & 0 & 0 & \ddots & \ddots & \ddots & 0 & \ddots & \ddots & 1 \\ P_3 & 0 & 0 & 0 & 1 & 1 & 1 & \Gamma_3 & 1 & 1 \\ P_2 & 0 & 0 & 0 & 0 & 1 & 1 & 1 & \Gamma_2 & 1 \\ P_1 & 0 & 0 & 0 & 0 & 0 & 1 & 1 & 1 & \Gamma_1 \end{pmatrix}$$

where $P_3 = 6e^{3ik\frac{D_3}{B_3}}$, $B_3 = (\frac{\gamma_1}{4} - 1)^2$, $C_3 = (\frac{3\gamma_1}{4} - 1)^2$, $D_3 = (\frac{5\gamma_1}{4} - 1)^2$ and $\Gamma_3 = -\frac{1}{3B_3}(3B_3 + 2C_3 - 13D_3)$.
The shape of the energy spectrum in the presence of the third nearest neighbors exemplified here in Fig.3.22(c) corresponds to the case of $\alpha 1^2 = 0.8$ and $\alpha_2^2 = 0.6$. The shape of the upper and lower band is more sinusoidal when compared to the case of Fig.3.22(b). These results reveal that the next nearest neighbors contribute

to transform the single upper and lower bands into bands with a sinusoidal shape. Henceforth, all ferromagnetic materials displaying a spin value high enough to fulfill the restriction $n \leq 2S$ would exhibit the same energy spectrum described in this section.
For a given number m of nearest neighbor, the general expression of the matrix Hamiltonian is written as follows

$$\widehat{H}^{(4,2)}_{(m-1)} = -\frac{4}{3A\gamma_1}[3B_1 + 2C_1 + \alpha_1^2(3B_2 + 2C_2) + \cdots\cdots + \alpha^2_{(m-1)}(3B_m + 2C_m)]I_\sigma \tag{3.28}$$
$$-\frac{1}{A\gamma_1}(B_1 + \alpha_1^2 B_2 + \cdots\cdots + \alpha^2_{(m-1)}B_m) \times$$
$$\begin{pmatrix}
\Gamma_1 & 1 & 1 & 1 & \cdots & 0 & P^*_m & P^*_{m-1} & P^*_{m-2} & \cdots & P^*_2 & P^*_1 \\
1 & \Gamma_2 & 1 & 1 & 1 & \cdots & \cdots & 0 & \ddots & \ddots & 0 & 0 \\
1 & 1 & \ddots & 1 & 1 & \ddots & \ddots & \ddots & \ddots & 0 & 0 & 0 \\
1 & \ddots & \ddots & \Gamma_{m-1} & \ddots & \ddots & \ddots & \ddots & \ddots & \ddots & 0 & 0 \\
\vdots & \ddots & \ddots & \ddots & \Gamma_m & \ddots & \ddots & \ddots & \ddots & \ddots & \ddots & 0 \\
0 & \ddots & \ddots & \ddots & \ddots & \ddots & 0 & \ddots & \ddots & \ddots & \ddots & 1 \\
P_m & \ddots & \ddots & \ddots & \ddots & \ddots & \ddots & \ddots & \ddots & \ddots & \ddots & \vdots \\
P_{m-1} & 0 & \ddots & \ddots & \ddots & \ddots & \ddots & 0 & \ddots & \ddots & \ddots & \vdots \\
P_{m-2} & 0 & 0 & \ddots & \ddots & \ddots & \ddots & \ddots & \Gamma_m & \ddots & \ddots & 1 \\
\vdots & \ddots & \ddots & \ddots & \ddots & \ddots & \ddots & 1 & 1 & \ddots & 1 & 1 \\
P_2 & \ddots & 0 & 0 & \ddots & \ddots & \ddots & 1 & 1 & 1 & \Gamma_2 & 1 \\
P_1 & \cdots & 0 & 0 & 0 & \cdots & 1 & \cdots & 1 & 1 & 1 & \Gamma_1
\end{pmatrix}$$

The second one is the $\{2, 4\}$ band. Its Hamiltonian matrix is obtained using the same technique as in $\{4, 2\}$

$$\widehat{H}^{(2,4)}_1 = -\frac{4}{3A\gamma_1}[3B_1 + 2C_1 + \alpha_1^2(3B_2 + 2C_2)]I_\sigma$$
$$-\frac{1}{A\gamma_1}(B_1 + \alpha_1^2 B_2)\begin{pmatrix}
\Gamma_1 & \tau^* & \tau^{2*} & 0 & 0 & 0 & P_{2^*} & P_{1^*} \\
\tau & \Gamma_2 & \tau^* & \tau^{2*} & 0 & 0 & 0 & 0 \\
\tau^2 & \tau & 0 & \tau^* & \tau^{2*} & 0 & 0 & 0 \\
0 & \tau^2 & \ddots & 0 & \ddots & \tau^{2*} & 0 & 0 \\
0 & 0 & \ddots & \ddots & \ddots & \ddots & \ddots & 0 \\
0 & 0 & 0 & \tau^2 & \ddots & 0 & \ddots & \tau^{2*} \\
P_2 & 0 & 0 & 0 & \tau^2 & \tau & \Gamma_2 & \tau^* \\
P_1 & 0 & 0 & 0 & 0 & \tau^2 & \tau & \Gamma_1
\end{pmatrix} \tag{3.29}$$

Where $P_1 = 6e^{ik\frac{D_1}{B_1}}$, $P_2 = 6e^{2ik\frac{D_2}{B_2}}$, $B_1 = \frac{9}{16}$, $B_2 = (\frac{\gamma_1}{4} - 1)^2$, $C_1 = (\frac{3\gamma_1}{4} - 1)^2$, $C_2 = (\frac{3\gamma_1}{4} - 1)^2$, $D_1 = (\frac{5\gamma_1}{4} - 1)^2$ and $\Gamma_1 = -\frac{1}{3B_1}(3B_1 + 2C_1 - 13D_1)$ $D_2 = (\frac{5\gamma_1}{4} - 1)^2$ and $\Gamma_2 = -\frac{1}{3B_2}(3B_2 + 2C_2 - 13D_2)$.
The structure of the matrix in equation (3.29) appears to be the same as the $\{4, 2\}$ band, with the difference that, this matrix depends on the element τ. On varying the ratio α_1^2, several cases can be distinguished. Firstly we choose the case where $\alpha_1^2 = 0$. Here the energy spectrum is constituted by two single bands of states respectively located above and below the continuum and very similar to the case of the $\{4, 2\}$ band shown in Fig.3.22(a). Next, we realized in the presence of second neighbors, for $\alpha_1^2 = 0.8$, the difference between the $\{4, 2\}$ band is that the both single bands (upper band in black circle and lower band in magenta square symbols) display a very sinusoidal shape instead of a semi sinusoidal as we can observe in the same shape in Fig.3.22(b). However it is important to notice that these two single bands display sinusoidal shapes.
In order to probe the new shape of the energy spectrum for the $\{2, 4\}$ band when the third nearest neighbors are accounting, the Hamiltonian matrix is given in equation (3.30) and we consider the case where $\alpha_1^2 = 0.8$ and $\alpha_1^2 = 0.4$ (see Fig.3.22(c)). Then the outcome displays an energy spectrum that appears almost identical to the one obtained in Fig.3.22(b). The peculiarity here is that both single bands which are here labeled with square symbols in color magenta below the continuum and with black circle symbols above the continuum occurs with more oscillating shape when comparing to the case of $\{4, 2\}$ band.

$$\widehat{H}_2^{(2,4)} = -\frac{4}{3A\gamma_1}[3B_1 + 2C_1 + \alpha_1^2(3B_2 + 2C_2) + \alpha_2^2(3B_3 + 2C_3)]I_0 \quad (3.30)$$

$$-\frac{1}{A\gamma_1}(B_1 + \alpha_1^2 B_2 + \alpha_2^2 B_3)\begin{pmatrix} \Gamma_1 & \tau^* & \tau^{2*} & \tau^{3*} & 0 & 0 & 0 & P_3^* & P_2^* & P_1^* \\ \tau & \Gamma_2 & \tau^* & \tau^{2*} & \tau^{3*} & 0 & 0 & 0 & 0 & 0 \\ \tau^2 & \tau & \Gamma_3 & \tau^* & \tau^{2*} & \tau^{3*} & 0 & 0 & 0 & 0 \\ \tau^3 & \tau^2 & \tau & 0 & \tau^* & \tau^2* & \tau^3* & 0 & 0 & 0 \\ 0 & \tau^3 & \ddots & \ddots & 0 & \ddots & \ddots & \ddots & 0 & 0 \\ 0 & 0 & \ddots & \ddots & \ddots & \ddots & \ddots & \ddots & \ddots & 0 \\ 0 & 0 & 0 & \ddots & \ddots & \ddots & 0 & \ddots & \ddots & \tau^{3*} \\ P_3 & 0 & 0 & 0 & \tau^3 & \tau^2 & \tau & \Gamma_3 & \tau^* & \tau^{3*} \\ P_2 & 0 & 0 & 0 & 0 & \tau^3 & \tau^2 & \tau & \Gamma_2 & \tau^* \\ P_1 & 0 & 0 & 0 & 0 & 0 & \tau^3 & \tau^2 & \tau & \Gamma_1 \end{pmatrix}$$

Where $P_3 = 6e^{3ik\frac{D_3}{B_3}}$, $B_3 = (\frac{\gamma_1}{4} - 1)^2$, $C_3 = (\frac{3\gamma_1}{4} - 1)^2$, $D_3 = (\frac{5\gamma_1}{4} - 1)^2$ and $\Gamma_3 =$

$-\frac{1}{3B_3}(3B_3+2C_3-13D_3)$.
Using the same technique as when the next nearest neighbors are taken into account, and repeating successfully this technique we get a general expression of the matrix Hamiltonian in the $\{2,4\}$ band as follows

$$\widehat{H}^{(2,4)}_{(m-1)} = -\frac{4}{3A\gamma_1}[3B_1+2C_1+\alpha_1^2(3B_2+2C_2)+\cdots\cdots+\frac{\alpha^2_{(m-1)}}{\gamma_3}(3B_m+2C_m)]I_8 \quad (3.31)$$

$$-\frac{1}{A\gamma_1}[\frac{B_1}{\gamma_1}+\frac{\alpha_1^2B_2}{\gamma_2}+\cdots\cdots+\frac{\alpha^2_{(m-1)}B_m}{\gamma_m}]\times$$

$$\begin{pmatrix}
\Gamma_1 & \tau^* & \tau^{2*} & \cdots & \cdots & \tau^{(m-1)*} & \tau^{m*} & 0 & P_m^* & P_{m-1}^* & \cdots & P_1^* \\
\tau & \Gamma_2 & \tau^* & \tau^{2*} & \cdots & \cdots & \cdots & \ddots & \ddots & \ddots & 0 & 0 \\
\tau^2 & \tau & \ddots & \tau^* & \tau^{2*} & \ddots & \ddots & \ddots & \ddots & 0 & 0 & 0 \\
\tau^3 & \ddots & \ddots & \Gamma_{m-1} & \ddots & \ddots & \ddots & \ddots & \ddots & \ddots & 0 & 0 \\
\vdots & \ddots & \ddots & \ddots & \Gamma_m & \ddots & \ddots & \ddots & \ddots & \ddots & \ddots & 0 \\
\tau^{(m-1)} & \ddots & \ddots & \ddots\ddots & \ddots & 0 & \ddots & \ddots & \ddots & \ddots & \ddots & \tau^{m*} \\
\tau^m & \ddots & \ddots & \ddots & \ddots & \ddots & \ddots & \ddots & \ddots & \ddots & \ddots & \tau^{(m-1)*} \\
0 & 0 & \ddots & \ddots & \ddots & \ddots & \ddots & 0 & \ddots & \ddots & \ddots & \vdots \\
P_m & 0 & 0 & \ddots & \ddots & \ddots & \ddots & \ddots & \Gamma_m & \ddots & \ddots & \tau^{3*} \\
P_{m-1} & \ddots & \ddots & \ddots & \ddots & \ddots & \ddots & \tau^2 & \tau & \ddots & \tau^* & \tau^{2*} \\
\vdots & \ddots & 0 & 0 & \ddots & \ddots & \ddots & \tau^3 & \tau^2 & \tau & \Gamma_2 & \tau^* \\
P_1 & \cdots & 0 & 0 & 0 & \tau^m & \tau^{(m-1)} & \cdots & \cdots & \tau^2 & \tau & \Gamma_1
\end{pmatrix}$$

With the same spirit as in the case of $\{2,4\}$ band, the matrix Hamiltonian of the $\{3,3\}$ band with the next nearest neighbors is given as

$$\widehat{H}^{(3,3)}_{(m-1)} = -\frac{3}{A\gamma_1}(N_1+\alpha_1^2N_2+\cdots\cdots+\alpha^2_{(m-1)}N_m)\times$$

$$\begin{pmatrix}
1+M(1,1) & 0 & 0 & 0 & 0 & 0 & 0 & 0 \\
0 & 1+M(2,2) & 0 & 0 & 0 & 0 & 0 & 0 \\
0 & 0 & \ddots & 0 & 0 & 0 & 0 & 0 \\
0 & 0 & 0 & 1+M(m,m) & 0 & 0 & 0 & 0 \\
0 & 0 & \ddots & \ddots & \ddots & \ddots & \ddots & 0 \\
0 & 0 & 0 & 0 & 0 & \ddots & 0 & 0 \\
0 & 0 & 0 & 0 & 0 & 0 & 1+M(2,2) & 0 \\
0 & 0 & 0 & 0 & 0 & 0 & 0 & 1+M(1,1)
\end{pmatrix} \quad (3.32)$$

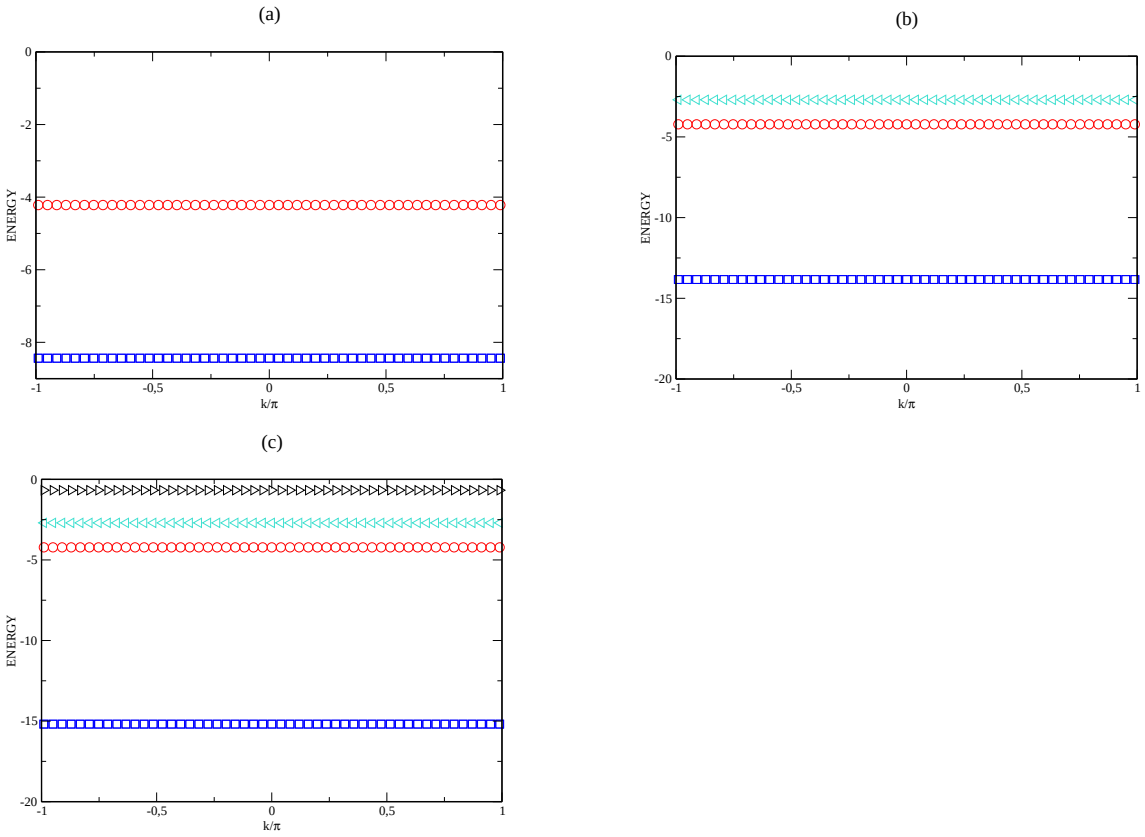

Figure 3.23: Excitation spectrum of the extended Bose-Hubbard model derived from the Heisenberg spin chain in a periodic lattice containing six bosons in the $\{3,3\}$ band interacting with, first second and third nearest neighbors for different values of α_1^2 and α_2^2 where $A = 0.1$, $\gamma_1 = 0.5$ and $f = 101$: (a) first nearest neighbors for $\alpha_1^2 = 0$; (b) second nearest neighbors for $\alpha_1^2 = 0.8$; (c) for third nearest neighbors $\alpha_1^2 = 0.8$ and $\alpha_2^2 = 0.4$

where $N_1 = (\frac{\gamma_1}{2} - 1)^2$, $M_{(1,1)} = 1/2 - 4D_1/N_1$, $D_1 = (\frac{5\gamma_1}{4} - 1)^2$, $M_{(m,m)} = 1/2 - 4D_m/N_m$, and $M_{(i,j)} = 0$ for any $i \neq 1$ and $j \neq 1$.

To depict the energy spectrum of the $\{3,3\}$ band when the second and a third nearest neighbors interactions are accounting , we consider two following cases : the first case does not consider the second nearest neighbors($\alpha_1^2 = 0$). In this respect, Fig.3.23(a) shows that the energy of such ferromagnetic materials is constituted only by two single bands separated by a huge gap. It is impossible without computing their eigenfunctions to know which of them rely to be a localized state. The answer of this issue will be given in the next section. Secondly when the ratio is non zero, it implies that the interactions of the second nearest neighbors are taken into account. For $\alpha_1^2 = 0.8$, which corresponds to a trimerized state where two groups of three spins interact together. Their energy spectrum display

three single bands. When comparing this spectrum to the case of Fig.3.23(a), the main difference is that, the interactions of second nearest neighbor introduce one new single band in the spectrum as seen in Fig.3.23(b) the band with cyan color plotted in triangle left. Finally, for $\alpha_1^2 = 0.8$ and $\alpha_2^2 = 0.4$ we take into account the effect of third neighbors and the resulting energy spectrum displays four single bands (see black color with triangle right symbol in Fig.3.23(c)) instead of three as the case where the third neighbor interactions are absent. Henceforth increasing the number of nearest neighbor influences the energy spectrum by increasing its number of single band.

3.5 Localization in real space

In this section, our aim is to testify the existence of localized bound states whose signature appear in the energy spectrum obtained in sections 3.2, 3.3 and 3.4.

3.5.1 In a Heisenberg spin chain

In section 3.2, Fig.3.2-3.8 show the rise of bound states, which appear sometime above and below the continuum. That seems to be a signature of the existence of the localized states. For this, we plot in real space, the square of eigenfunctions as function of the sites number or sites position in the lattice i, for each bound states. In Figure3.2, which corresponds to

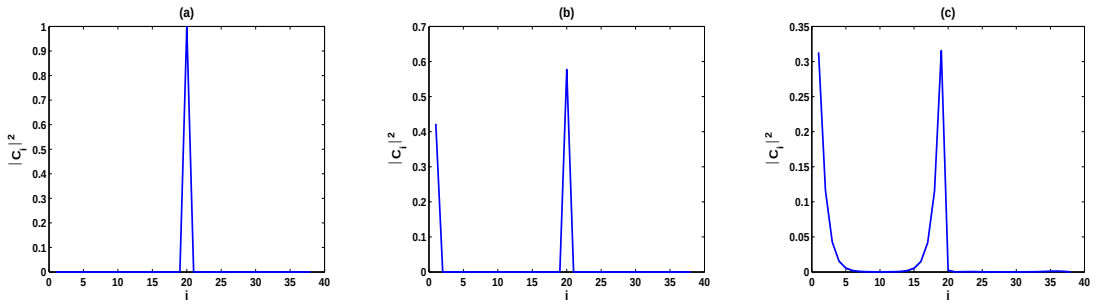

Figure 3.24: Square of the wave function amplitudes corresponding to the eigenvectors as a function of the position of the band along the chain: (a) case of the band located on the energy spectrum in Fig. 3.2, 3.3, 3.4 and 3.8; (b) case of the band in Fig. 3.5; (c) case of the band in Fig. 3.6 and 3.7

the case of isotropic Heisenberg spin chain, the single band that appears below the continuum is a localized bound state. Figure 3.24(a), shows that its wave function is localized

and indicate that there is a high probability of finding two bosons on the same sites. To probe the existence probability of a given localized state given in Fig.3.3 and 3.4 for the corresponding ferromagnetic chain, we also plotted the square of the eigenvectors in the real space for different values of anisotropy and exchange interaction. But it appears to be the same as those plotted in figure 3.24(a).

In the attractive case in Fig.3.5(a), the ground state is a localized state, located on two different positions along the chain illustrated by figure 3.24(b). This also illustrates the fact that there is a high probability to find four bosons in two adjacent sites, each containing two bosons. It also represents the intrinsic localized mode with a complex character that the chain allows us to appreciate while plotting the eigenvector as a function of the position of particles.

In Fig.3.6 and 3.7, their ground state is less localized which means that the probability of finding six particles on two sites, i.e. one site with fours particles and another site with two particles on an adjacent site is weak as shown in Fig. 3.24(c).

Figure 3.8(a) shows two single bands. But only the lower band is a localized state with a probability similar to the one presented in Fig. 3.24(a).

3.5.2 In a Heisenberg spin chain with antisymmetric interactions

In section 3.3, Fig.3.10(b) and 3.10(c) show the rise of bound states, which surround the continuum and are mostly separated from the continuum only nearby the degenerated point. That seems to be a signature of the existence of the localized states that would tend to appear nearby the degenerated point of the energy spectrum. Then it turns out that the eigenfunctions of these bound states display a probability less than five per cent for $k = 0$ and $k = \pi/2$. This is not shown here to avoid overloading the thesis. Such probability indicates that the single band surrounding the continuum and mostly separated from the continuum only nearby the degenerated point is rather a very weak localized state. This result remains whenever the single band appears on top or at the bottom of the continuum.

The energy spectrum in Fig.3.12(a) shows the presence of a single band that is surrounding the continuum tend to appear completely separated from the continuum as exhibited

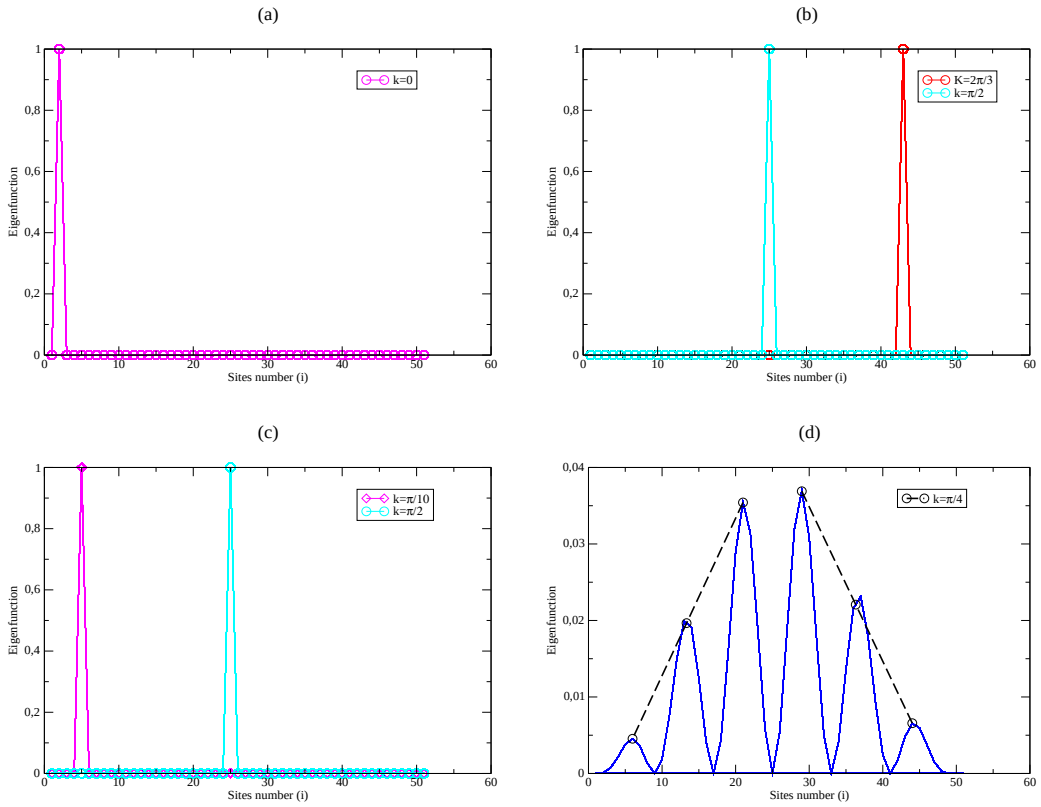

Figure 3.25: Square of the normalized Eigenfunctions of the localized states located on the energy spectrum: (a) case of the band at the bottom (red color) located in Fig.3.12 and in Fig.3.13(b)- 3.13(c); (b) case where both bound states (red and cyan color) are chosen in Fig.3.16; (c) case of two symmetric bound states (red and magenta color) located in Fig.3.17; (d) Plot of the eigenfunction in log-scale as function of the site number for the case of $k = \pi/4$. The dashed lines added allows to realize the exponential decay of the eigenfunction.

in Fig.3.12(b) and 3.12(c). This is a clear signature of a single bound state. This single bound state is really a localized bound state as proved by Fig.3.25(a) where the square of the eigenfunction exhibit a localized profile. This localized bound state's existence is confirmed by its localized profile as for instance when the Bloch wave number is $k = 0$. Such a representation was described in the case of two bosons in Ref. [113]. In Fig.3.13, which corresponds to the case where the Heisenberg spin chain is reduced to the Ising model. The single band that appears below the continuum is also a localized bound state because its probability of localization is the same as the one seen in Fig.3.25(a). The nature of the single band that appears either on top or at the bottom of the continuum of Fig.3.14 and Fig.3.15, is similar to that of a weak localized state because the eigenfunction of this bound state have a weak probability that is around four per cent respectively for $k = 0$

and $k = \pi/2$. This can be understood from the fact that this single band seems to be more merged to the continuum.

For the case of the three bands shown in Fig.3.16 when the value of D_z is very weak or nil, the upper and the lower bands that appear are localized bound states located with a high probability for $k = \pi/2$ and $k = 2\pi/3$ as seen in Fig.3.25(b) whereas the bound state between the upper and the lower bound states is a delocalized band. Figure 3.17 shows two single bands, but the upper band turns out to stand for a delocalized state meanwhile the lower band is a localized band located on the lattice with a high probability as seen in Fig.3.25(c). This profile of the localized eigenfunctions confirms the existence of an intrinsic localized mode in the system that is also coined quantum breather since the quantum effects are considered. Figure 3.25(d), presented here as an example of the eigenfunction plotted in Logarithmic scale allows to confirm the exponential localization of quantum Breathers in real space. This is the proof that the Fermi Pasta-Ulam (FPU) feature of the above mentioned quantum breathers derived in real space from our Heisenberg spin chain including the DMI model, is effective.

3.5.3 In a Heisenberg spin chain with longer range interactions

In this section, we probe the existence of new localized states whose signatures appear on the energy spectrum and we also investigate to the influence of second and third nearest neighbors interactions on their location and shape.
The localization property of these bound states can be seen from the plot of the probability $\mid C_i \mid^2$ of the translational invariant states Eq.(2.80) of the system corresponding to the Bloch wave vector k at the centre ($k/\pi = 0$) and at the edges of the Brillouin zone ($k/\pi = \pm 1$).

In the case of two bosons interacting with second, third and four nearest-neighbors, Fig.3.18(b) and (d) and Fig.3.19(a) show the rise of single bands occurring respectively below and above the continuum. For each of these single bands, while plotting the square of the corresponding eigenfunctions as function of the lattice sites i, and a few selected values of the Bloch wave number, we realized that they look at a first glance as a signature

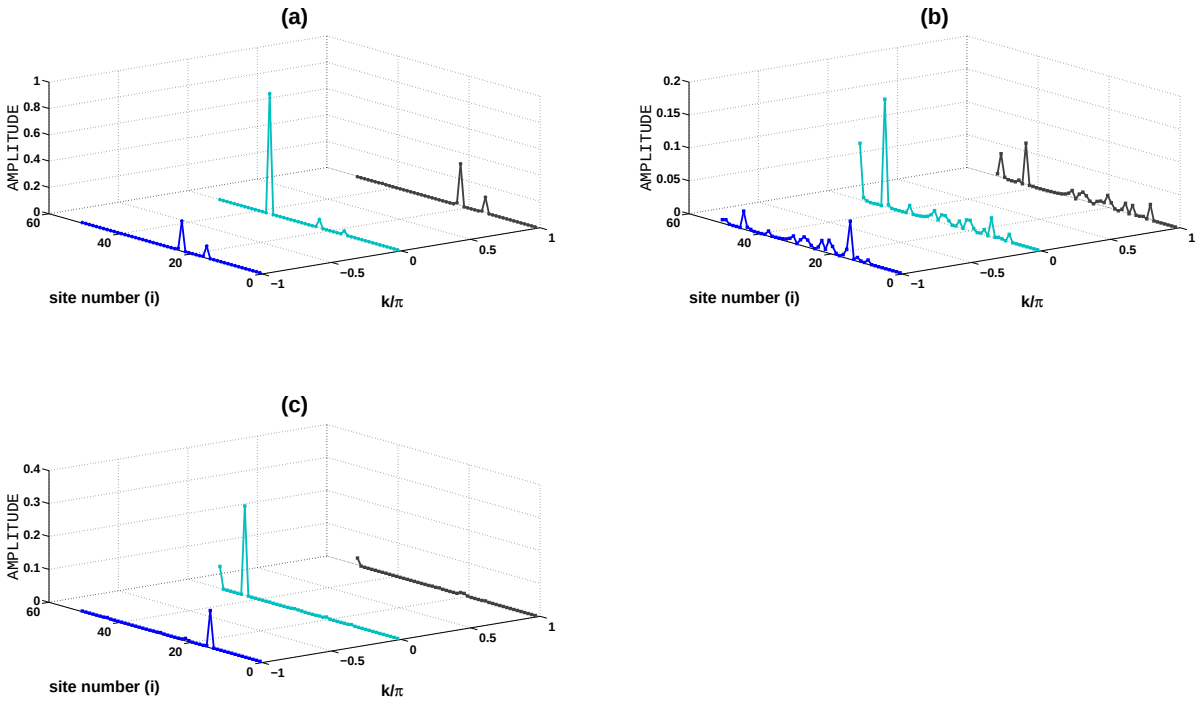

Figure 3.26: Square of the normalized Eigenfunctions of the single band (blue square symbols) located below the continuum band in Fig.3.18(b),(d) and Fig.3.19(a): (a) case of first nearest neighbors; (b) case of second nearest neighbors; (c) case of third nearest neighbors

of new localized states. We start here to analyze the existence and the properties of the lower single band (blue color with square symbols), which lies below the continuum. From Fig.3.26(a), we notice that the value of the square amplitude is high at the centre ($k/\pi = 0$) of the Brillouin zone and displays a probability around 100 per cent. At the edges of Brillouin zone this probability is around 40 per cent for (($k/\pi = -1$) and around 4 per cent for ($k/\pi = 1$). This high probability obtains at the centre shows that, the single lower band stands for a localized state. In such case a local magnetization excitation can occur thanks to the local spin excitations process favored by this localized state. This implies that the ground state of the system prefers to be in the on site bound states and corresponds to the 2-on-site breather band $\mid 20\cdots 0 >$ in addition to its cyclic permutations Eq.(2.80). At the edges of the Brillouin zone hence the system is in the off-site bound state $\mid 110\cdots 0 >$ plus the cyclic permutations of Eq.(2.80) shown recently in Ref. [114]. We also notice in Fig.3.26(b) and Fig.3.26(c) that, when the second and a third nearest neighbors are involved, the probability of localization decreases respectively at the centre and at the edges of the Brillouin zone down to values less than 30 per cent. This implies that the lower

band stands for a delocalized state in the presence of second neighbor and third nearest neighbors.

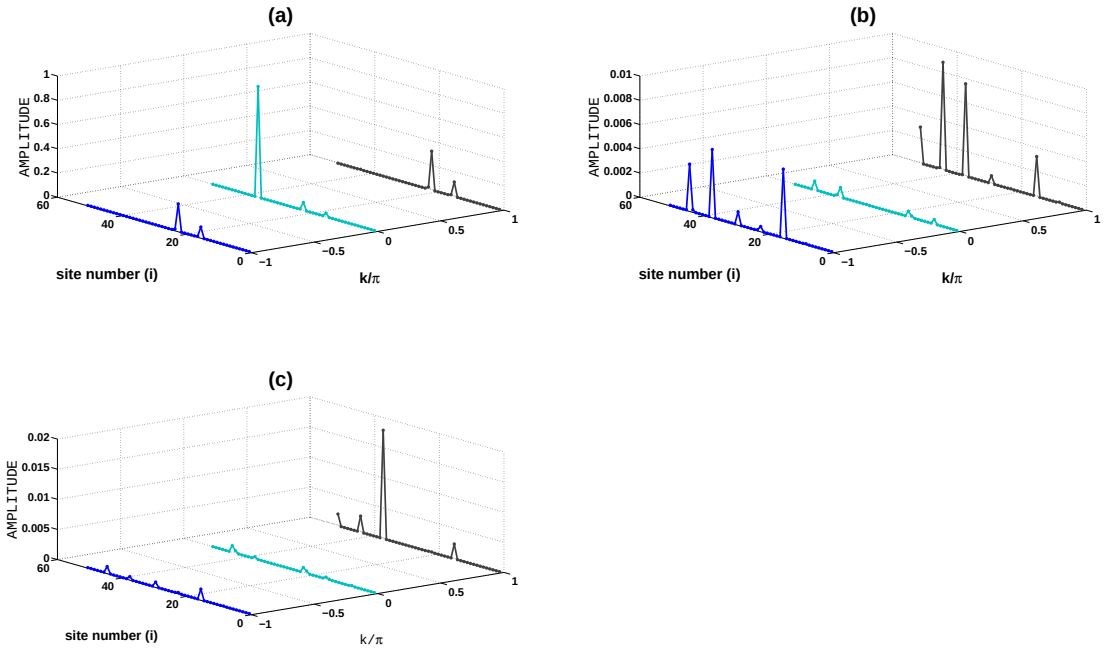

Figure 3.27: Square of the normalized Eigenfunctions of the single band (red circle symbols) located above the continuum band in Fig.3.18(b),(d) and Fig.3.19(a): (a) case of first nearest neighbors; (b) case of second nearest neighbors; (c) case of third nearest neighbors

Next, we analyze the existence and properties of the upper single band located above the continuum with red circles. We realize from Fig.3.27(a) that the value of the square amplitude is high at the centre than the value at the edges where the probability, which is around 30 per cent. This value confirms the fact that, the upper band exist and stands for a localized bound state. In Fig.3.27(b)-(c) the values of the amplitudes decrease rapidly at the edges and become nil at the centre of the Brillouin zone. This implies that the system prefers to be in the off-site bound state. This upper band stands for a delocalized state when the second and third nearest neighbors are involved in the system.

The middle single band with triangle up symbols in cyan color of Fig.3.18(d) and Fig.3.19(a), is testified by the fact that in Fig.3.28(a) the system displays a many body localization shape which rather stand for a delocalized state because its amplitude is not sizeable since it is less than 30 percent at the centre and even while second nearest neighbors are involved (see Fig.3.28(b)). This can be understood from the fact that this band is merged with the continuum in its major part. On the other hand, the same condition on

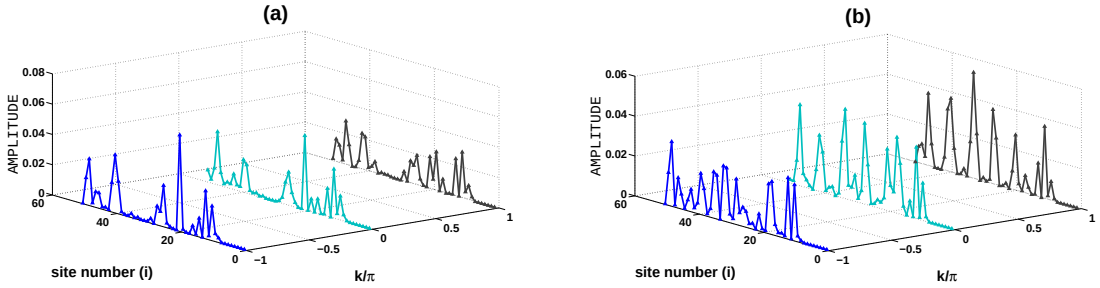

Figure 3.28: Square of the normalized Eigenfunctions of the single band (cyan triangle up symbols) located between the continuum and the upper band in Fig.3.18(d) and Fig.3.19(a): (a) case of second nearest neighbors; (b) case of third nearest neighbors

the amplitudes is reproduced at the edges of the Brillouin zone i.e. for $((k/\pi = -1)$ and for $((k/\pi = 1)$ (see Fig.3.28(a) with second nearest neighbors). Whenever the third nearest neighbors are included the unsizeable values of the amplitudes remain for $((k/\pi = -1)$ and for $((k/\pi = 1)$ (see Fig.3.28(a)).

From a physical viewpoint related to the behavior of the magnetization process; it should be noticed that the delocalized states arising here are more related to spins fluctuations and in such context the spin system would not undergo a local magnetization reversal process. A delocalized state means that the system would definitely lead to an absence of a local magnetization excitations.

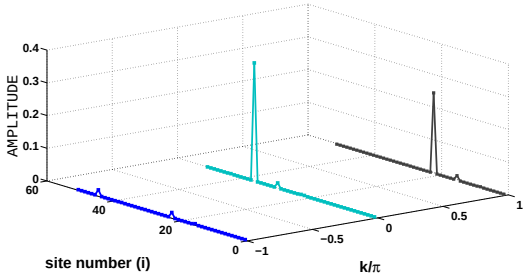

Figure 3.29: Square of the normalized Eigenfunctions of the single band (blue color with square symbols) located below the continuum band in Fig.3.20(b) and Fig.3.21(a): case of second nearest neighbors and third nearest neighbors

Now we consider four bosons in the system, with the possibility of interaction at the scale of the second neighbors in addition to the on site interactions, with the first and third neighbors interacting. Let us keep in mind that in this case Fig.3.20(b)-(c) and Fig.3.21(a)-

(b) show the signature of single bands occurring above the continuum band. Therefore with Fig.3.29, we can testify the existence and the properties of single band located below (blue color) the continuum. We realize in Fig.3.29 in the presence of second and third nearest neighbors that, the value of the amplitude at the centre is sizable since it is larger than 30 per cent and it is higher than the ones obtained at the edges of the Brillouin zone, whose values at $(k/\pi = -1)$ and at $(k/\pi = 1)$ are less the minimum sizable value of 30 per cent. This reveals that the lower single band exist and it stands for localized state. This implies that the system prefers to be in the double 2-on-site breather band $\mid 220\cdots 0 >$ plus its cyclic permutations. Here it is important to mention that, the value of the amplitudes remain unchanged when either the second or the third nearest neighbors are considered.

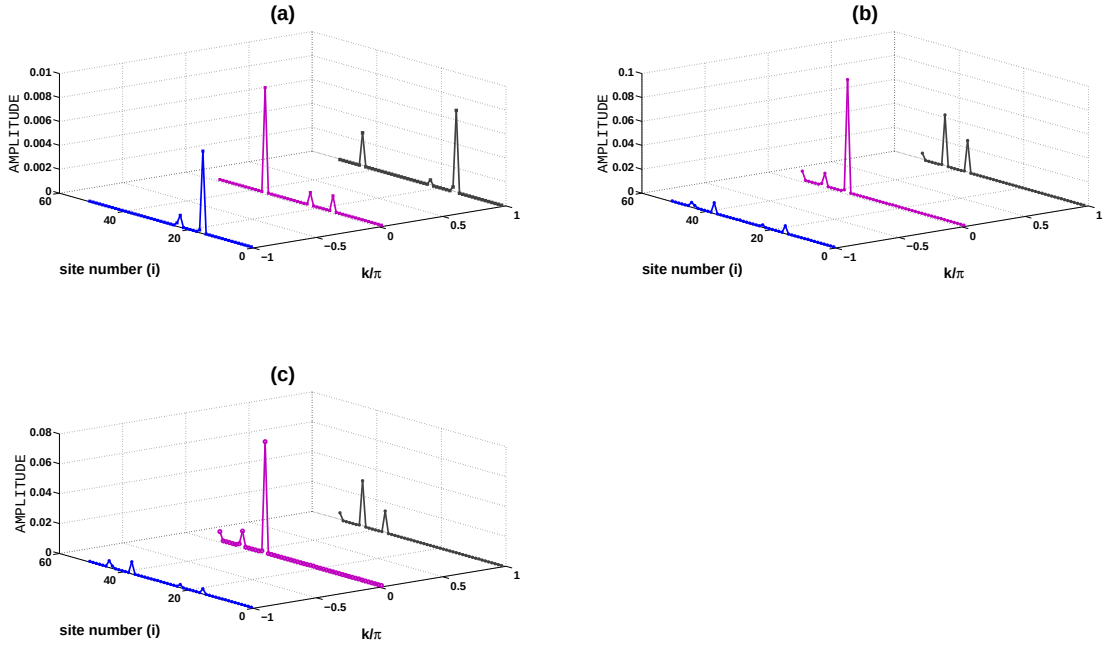

Figure 3.30: Square of the normalized Eigenfunctions of the single band (red color with circle symbols) located above the continuum band in Fig.3.20(a)-(c) and Fig.3.21(a): (a) case of first nearest neighbors; (b) case of second nearest neighbors; (c) case of third nearest neighbors

From the panel of Fig.3.30, we notice that the properties of the single band in red circle located above the continuum in Fig.3.20(a)-(c) and Fig.3.21(a)-(b) can be seen respectively in Fig.3.30(a) for the case of first neighbors, for the case of second neighbors (see Fig.3.30(b)) and for the case of third neighbor (see Fig.3.30(c)). Although this single band turn to stand for a delocalized state thanks to the size of its amplitude, we can notice here that, the value of amplitude is always more high at the centre than at the edges of the

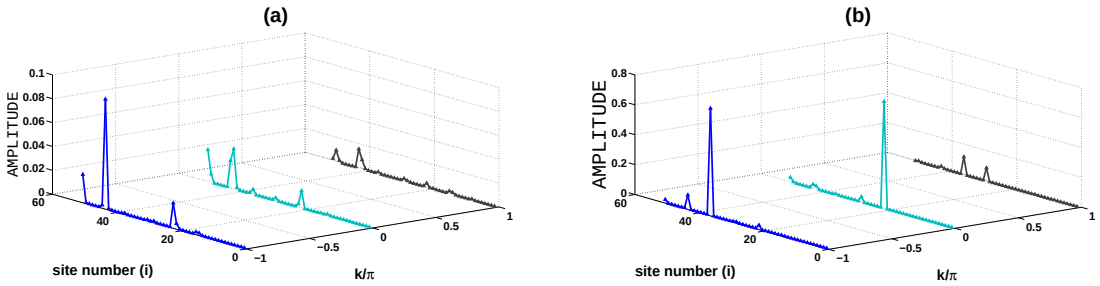

Figure 3.31: Square of the normalized Eigenfunctions of the single band (cyan color with triangle up symbols) located above the continuum band in Fig.3.20(c) and Fig.3.21(a) : (a) case of second nearest neighbors; (b) case of third nearest neighbors

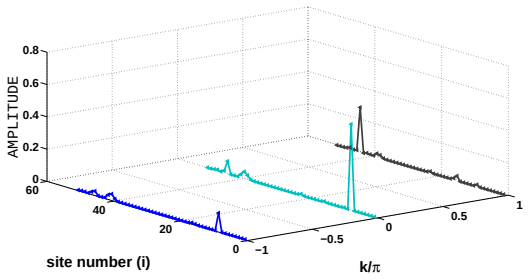

Figure 3.32: Square of the normalized Eigenfunctions of the single band (indigo color with triangle left symbols) located above the continuum band in Fig.3.21(a): case of second and third nearest neighbors

Brillouin zone. Needless to mention is that the values of amplitude of these bands decrease when the number of neighbors increases.

The band from Fig.3.20(c) realized in the presence of second neighbors, which is exhibited with triangle up (in cyan color) appears with the amplitude values as 2 per cent at the centre, 10 per cent at the edge left and 1 per cent at the edge right as depicted in Fig.3.31(a) stands for a delocalized state. However when the third neighbors are accounting in the system, we realize that this band suddenly stands for a localized state since it displays probabilities value around 70 per cent at the edge left, 75 per cent at the centre and 15 per cent at the edge right (see Fig.3.31(a))

The band that occurs above the continuum as seen in Fig.3.21(a) and (b) (in indigo triangle left) refers to a localized state since the magnitude of its eigenfunction is around 50 per cent at the centre, 12 per cent at the edge left and around 30 per cent at edge right(see in Fig.3.32. This means that its existence is confirmed and reveals a local magnetization

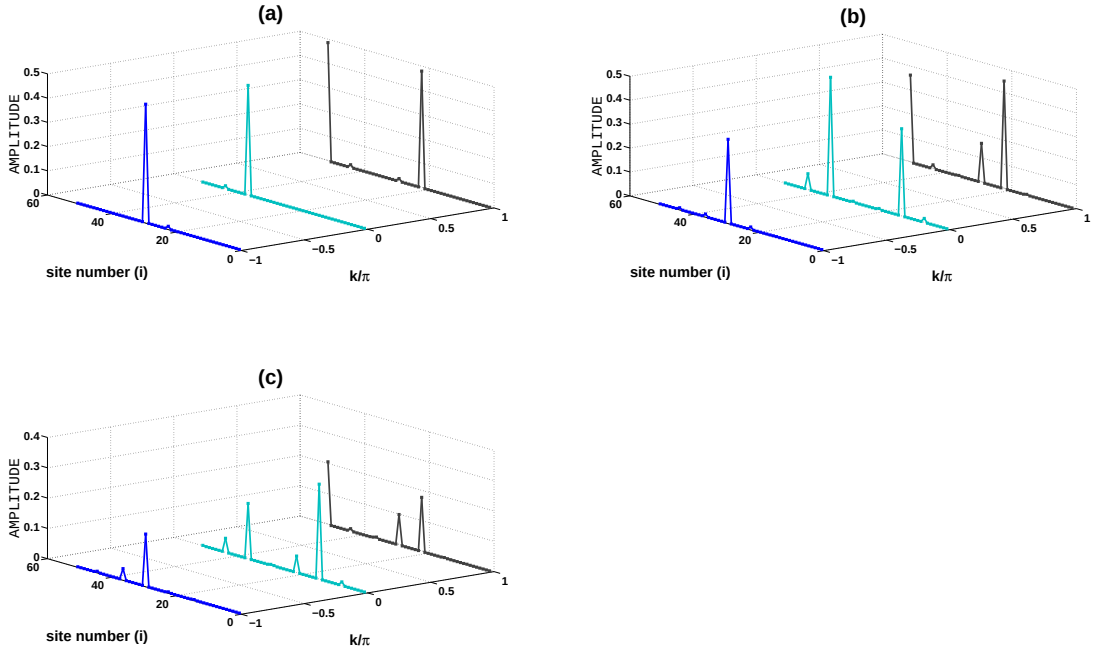

Figure 3.33: Square of the normalized Eigenfunctions of the single band (blue color with triangle left symbols) located below the continuum band in Fig.3.22(a)-(c): (a) case of first nearest neighbors; (b) case of second nearest neighbors; (c) case of third nearest neighbors

excitations that may according to some physical circumstances engage a local reversal process.

Let us now consider the case of six bosons moving in the system while interacting with the first, the second and the third neighbors. Figure 3.22(a) shows two single bands separated by a continuum where the one on top and that at the bottom correspond to localized states since they display a high probability of existence. This result was already obtained in Ref [112] and is shown here in Fig.3.33(a), which corresponds to the case of the bottom band (blue color with triangle left) where the value of the amplitude at the centre is 43 per cent and 50 per cent at the edges of Brillouin zone. This means that the ground state of the system prefers to be in the on-site bound states and corresponds to the 4-on-site and 2-on-site breather band $\mid 420\cdots 0 >$ plus the cyclic permutations. In Fig.3.33(a) while the second neighbors are taken into account, those values become 45 per cent at the centre, 35 per cent for $(k/\pi = -1)$ and 45 per cent for $(k/\pi = 1)$ (see Fig.3.33(b)). In the presence of third neighbors, we get 30 per cent at the centre, 18 per cent for $(k/\pi = -1)$ and 22 per cent for $(k/\pi = 1)$ (see Fig.3.33(c)). From these later

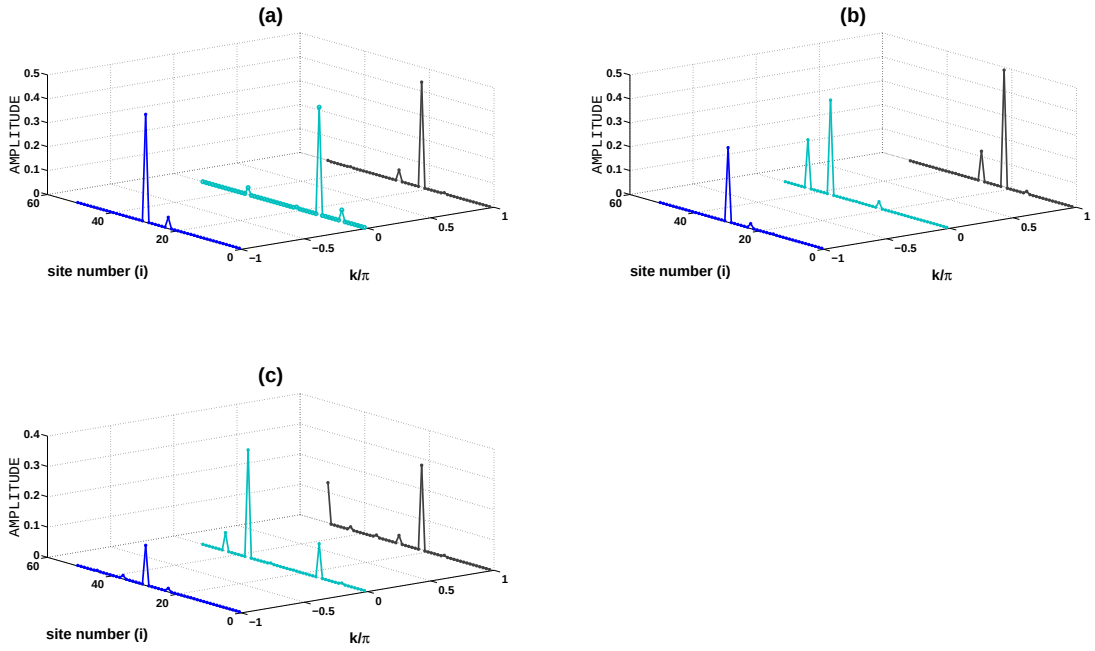

Figure 3.34: Square of the normalized Eigenfunctions of the single band (red color with triangle right symbols) located above the continuum band in Fig.3.22(a)-(c): (a) case of first nearest neighbors; (b) case of second nearest neighbors; (c) case of third nearest neighbors

figures, we notice that the values of amplitudes decrease when the number of neighbors increases. We also realize that when the number neighbors increases, the amplitude stays high enough to be sizable at the centre where the wave vector is $(k/\pi = 0)$. The band with the square symbols that is concerned with the presence of first, second and third neighbors is devoted to localized state thanks to its sizeable amplitude at the centre of the Brillouin zone. This result indicates that a local magnetization excitations process can occur in the system.

In the case of the band on top (see red color with triangle right), of Fig.3.34(a) which correspond to the first neighbors, the corresponding value of the amplitude at the centre is 40 per cent and 45 at the edges of Brillouin zone. In Fig.3.34(a), which is set up for that case of the second neighbors acouting in the system, we get 42 per cent at the centre, 32 per cent for $(k/\pi = -1)$ and 50 per cent for $(k/\pi = 1)$ (see Fig.3.34(b)). When six bosons in the system interact with third neighbors, the amplitude is around 30 per cent at the centre, 22 per cent for $(k/\pi = -1)$ and 22 per cent for $(k/\pi = 1)$ (see Fig.3.34(b)). From these figures, we notice that the difference between outcome of both bands is very weak.

The localization of the $\{3, 3\}$ band exited in from Fig.3.23 (a)-(c) can be seen in

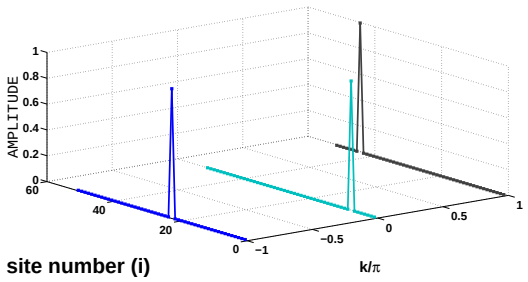

Figure 3.35: Square of the normalized Eigenfunctions of the band localized on the energy spectrum in Fig.3.23(a)-(c): case of bands (blue color with square symbols and cyan color with triangle left)

Fig.(3.35). This figure shows the plots corresponding to the wave vector k at the centre and at the edges of the Brillouin zone. From Fig.(3.35), we notice that the value of the square amplitude of the lower single band (blue color with square symbols) from Fig.3.23(a)-(c) is high enough for the wave vector k at the centre ($k/\pi = 0$) and at the edge of the Brillouin zone ($k/\pi = \pm 1$). This corresponds to the double 3-on-site breather band $\mid 330\ldots0 >$. We also realize that the value of amplitude remain high enough to be sizeable when the number of neighbors increases. This profile of amplitude testify the existence of localized bound state, which is an intrinsic localized mode in a quantum system and therefore is quantum breather. This result is already known in ref. [112]. From the physical viewpoint, this case is a good indicator of a local magnetization reversal process in the system. In Fig.3.23(a)-(c), the second and fourth bands stand for delocalized states where their amplitude is nil respectively at the centre and at the edges of Brillouin zone, whereas the third band corresponds to a localized state as exemplified by their sizable amplitude (see Fig.3.35).

3.6 Localization in the space of normal mode

While looking at the energies spectrum and the corresponding eigenfunctions in the previous section, it is realized that the existence of quantum breathers in such a spin chain is no longer doubtful. The presence of the single isolated band from the continuum definitely confirm the Fermi-Pasta Ulam (FPU) feature, as that of the localization phenomenon of nonlinear classical and quantum lattice in real space, as far as the Heisenberg spin chain

including antisymmetric interaction is considered. From the foregoing a question raised here is whether this feature of FPU remains for the underlying model whenever we move from real to normal mode space?

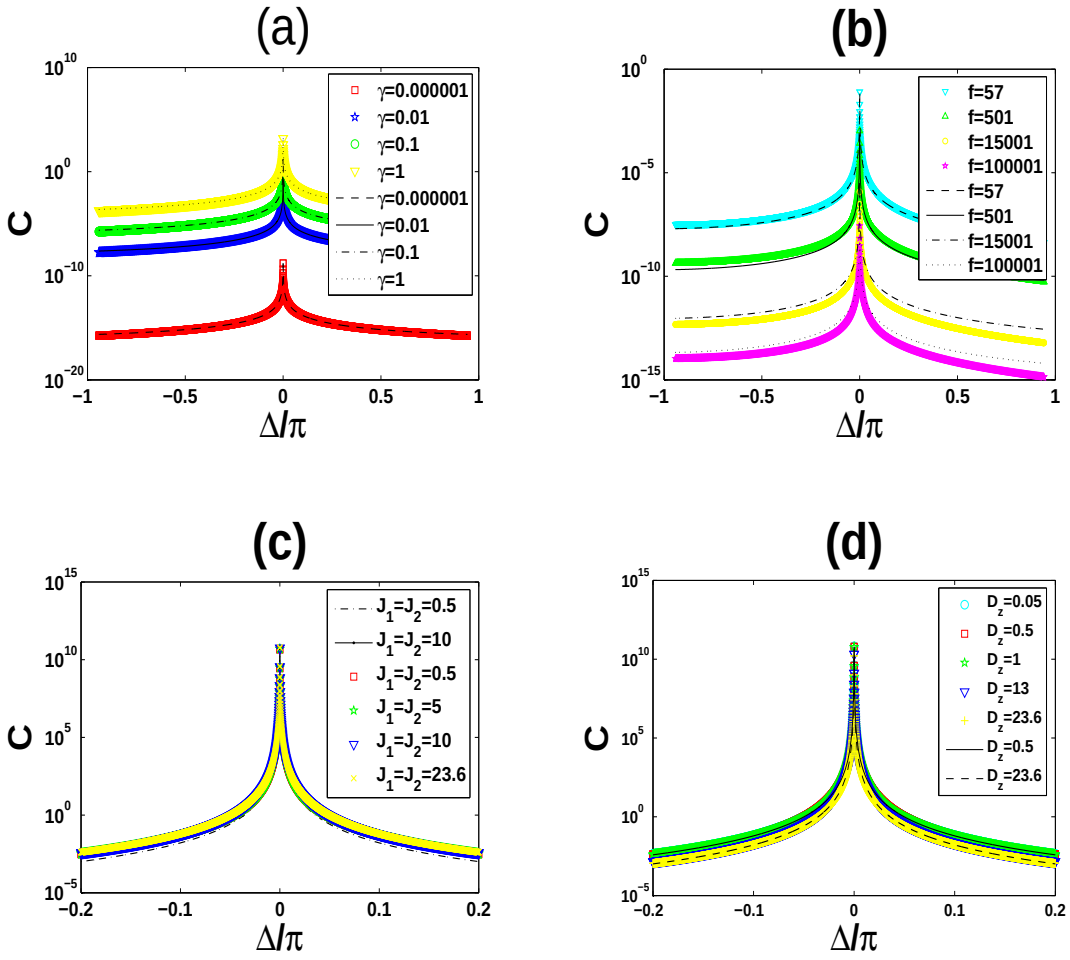

Figure 3.36: (Color online) Weight function: (a) for different values of the interaction γ where $f = 101$, $J_2 = J_1 = 1$, $D_z = 0$, $k = 0$ and $\widetilde{k}_1 = \frac{\pi}{2}$; (b) for different sizes of the system where $\gamma = 0.01$, $J_2 = J_1 = 0.5$, $D_z = 0.5$, $k = 0$ and $\widetilde{k}_1 = -\frac{2}{3}\pi$; (c) for different values of exchange interaction J_2 and J_1 where, $\gamma = 1$, $f = 101$, $D_z = 0.5$, $k = \frac{\pi}{2}$ and $\widetilde{k}_1 = -\frac{\pi}{4}$; (d) for different values of DMI D_z where, $\gamma = 1$, $J_2 = J_1 = 23.6$, $f = 101$, $D_z = 0.5$, $k = \frac{\pi}{2}$ and $\widetilde{k}_1 = -\frac{\pi}{4}$. Dashed lines are results using approximation formula Eq.(2.133), Eq.(2.134) and Eq.(2.135).

Figure3.36 exhibits the numerical results obtained by perturbation method, where we have plotted the weight function as a function of $\frac{\Delta}{\pi}$. In Fig.3.36(a), we find localization in the normal-mode space for different values of γ. This allows us to appreciate their complex character characterized by an intrinsic localized mode which in this context is interpreted as

quantum q-breathers. The weight function is more localized as γ decreases as seen with the position of weight function for the case of $\gamma = 0.000001$, which is more compactified. The dashed lines are the results obtained while using the formula of equation (2.133). These results obtained here are similar to those presented in [19]. In Fig.3.36(b), we probe the influence of the size of the nonlinear quantum lattice on the localization phenomenon and we find that the states compactifies more with increasing size. This result also provides a good agreement between the numerical diagonalization and the approximation's results given with dashed lines that are obtained from the analytical formula of equation (2.135). We also probe the influence of exchange interaction and DMI on the localization phenomenon and we find that the weight function is also localized for different values of exchange interaction and DMI, respectively. We can see a good agreement between the numerical results of the diagonalization with the approximation from the analytical formula of equation (2.135), which is clearly exemplified in Fig.3.36 (c) and (d).

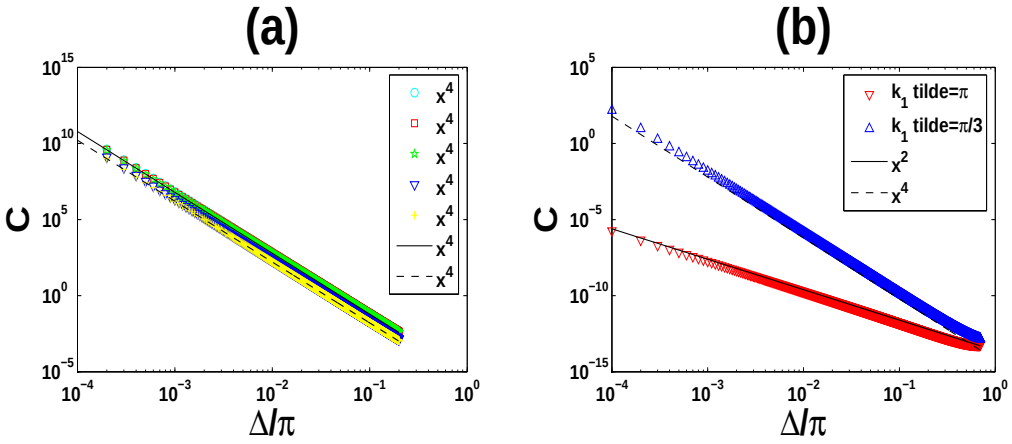

Figure 3.37: (Color online) Weight function: (a) for different values of DMI D_z in log-log scale, the same as in Fig. 3.36(d) where, $\gamma = 1$, $J_2 = J_1 = 1$, $f = 101$, $D_z = 0.5$, $k = \frac{\pi}{2}$ and $\widetilde{k}_1 = -\frac{\pi}{4}$; (b) for different values of $\widetilde{k}_1$ where $\gamma = 1$, $J_2 = J_1 = 0.5$, $D_z = 3.1$, $f = 101$ and $k = \frac{2}{3}\pi$

In Fig.3.37(a), we see the $\frac{1}{\Delta^4}$ decay for eigenstates fulfilling $2k_1 + k \neq 0 \pmod{2\pi}$ and $k = 0$, and in Fig.3.37(b), the $\frac{1}{\Delta^2}$ decay for eigenstates fulfilling $2k_1 + k \equiv 0 \pmod{2\pi}$ and $k = 0$.

3.7 Conclusion

In this chapter, we have presented the analytical/numerical results obtained in this thesis and their discussions in order to enhance the phenomenon of localization of excitation that can serve as precursor of local magnetization reversal process that can be realized in 1D ferromagnet. We have elaborated on energy spectrum in 1D Heisenberg ferromagnetic spin chain for probing the magnetization reversal process with the exchange, exchange and anisotropy, exchange and DMI and longer range interaction when two, four and six quanta are involved. Thus localization features for spin chain has been set up both in real and normal mode space.

General Conclusion

The aim of this thesis was to study the properties of quantum breathers that stand as precursors of local magnetization reversal prosses in 1D ferromagnets. To this end we proceeded mapping a classical ferromagnetic Heisenberg spin chain including DMI and longer range interactions into an extended Bose-Hubbard-like Hamiltonian. Then we study the properties of quantum breathers in the underlying one-dimensional periodic lattice containing two, four and six bosons. The resulting fine structures are studied using numerical diagonalization with non degenerate and degenerate perturbation theory. Our results confirm that in absence of DMI and longer range interactions, when the nonlinearity is significant in the ferromagnetic materials, a single band for the localized states will split from the continuum band. From a physical picture of a ferromagnetic spin chain, the continuum band here is describing a magnetic spin chain with completely delocalized excitation along the chain whereas the case of single band for two on-site bosons corresponds to the case of a local magnetization reversal process involving two switching spins. The results obtained for the case of $n = 4$ or $n = 6$ also show that we have succeeded from our mapping to describe the energy spectrum of a spin chain facing a local magnetization reversal process that reveals the presence of bound states through the appearance of single bands that are signature of quantum breathers in the system. The anisotropy energy has the same role as the exchange integral energy, that it can either enlarge the gap between the continuum and the localized state or order the position of the bands in the energy spectrum.

In the presence of DMI, which is an antisymmetric interaction revealed interesting and important features: namely, the DMI is responsible for the displacement of the degenerated point in the energy spectrum. While the degenerated point is moving, the system undergo an energy conservation process through a self compensation effect that happens with the fact that, there is a cut-off in the left zone of the energy spectrum that is automatically pasted to its right part whenever two or four quanta are involved. For the case of two quanta, this antisymmetric interaction is also responsible for the appearance of two bound states surrounding the continuum appearing symmetric with respect to the degenerated point in the energy of the system. Through our numerical computations, a critical value of the DMI parameter for which the degenerated point in the continuum spectrum stop moving was

found. Beyond this value of DMI strength, the shifting process of the degenerated point in the energy spectrum no longer occurs. The shape of the energy spectrum displays two domains walls, which is the well known elementary excitations of the Neel phase of a XXZ model of an antiferromagnet. The antisymmetric property of the DMI led the ferromagnetic spin chain to behave more like an antiferromagnetic spin chain whatever the values of the Heisenberg exchange interaction parameters J_1 and J_2. We also notice an antagonist effect between the Heisenberg exchange interaction (i.e. J_1) and DMI as far as the shifting process of the degenerated point in the energy spectrum is concerned. The Heisenberg exchange interaction J_2 in this system tends to enlarge or to order the position of the single band on the energy of the system. While the parameter J_1 is nil, the Heisenberg spin chain is reduced to the Ising ferromagnet and their energy spectrum is constituted only by the symmetric continuum band degenerated for $k = 0$. This spectrum appears once more to be similar to the energy spectrum of an antiferromagnet. This energy keep its shape and remain unchanged for non zero values of the DMI parameter. We also realized that, the impact of the DMI on the $\{4, 2\}$ and $\{2, 4\}$ bands was to influence the position of the localized bound state on the energy spectrum of the spin chain. Whereas in the $\{3, 3\}$ band, the exchange interaction and DMI produce the same effect that is the translation of the line band on the spectrum.

In presence of long range interactions, We could derive an explicit analytic expression for the Hamiltonian matrix corresponding to the case of two, four and six bosons, from which a generalized analytic expression of each matrix Hamiltonian was set up for the case of a given number of nearest neighbors. The outcome shows the existence of multi bound states. On one hand we first focus our attention on the effect of second, third and fourth nearest-neighbors on the energy spectrum of the system, and thereafter we could analyzed the properties of these states for different wave vectors used to probe the probability of localization of a given eigenstate. Thanks to the large range of interactions which are accounting in this system, new bound states could be found among which some stand for localized states as for instance, the case of two bosons interacting with the second and third neighbors, for which the energy spectrum displays in addition to a continuum band a single bound state, one new bound states located between the continuum and the upper band, only the lower and upper bands stand for a localized bound state in the case of the first neighbors interacting. In the $\{2, 2\}$ band, only the upper band stands for a delocalized state. For the case of $\{4, 2\}$ and $\{2, 4\}$ bands, we also notice that the values of amplitudes decrease when the number of neighbors increases and it is devoted to localized bound state thanks to its sizable amplitude at the centre of the Brillouin zone. Here, when the number neighbors increases, the amplitude remainds high enough to be sizable. For the case of the $\{3, 3\}$ band, the value of amplitude stays

high when the number of neighbors increases. This band corresponds to a perfect localized state. These localized states that appear thanks to the $\{2,2\}$, $\{4,2\}$, $\{2,4\}$ and $\{3,3\}$ bands are quantum breathers excitations. The intrinsic nature of these excitations led them to generated localized magnetization excitations that can be the first step towards local magnetization reversal process, which can be experienced in such a magnetic system either through a couple spins or a couple of two group of dimerized or trimerized spins. Such a process with different size of the eigenstates may have application in quantum computing. Hence further experimental studies of such phenomenon are encouraged.

In normal-mode space, we computed appropriate weight functions of the eigenstates using the perturbation theory. We observe localization of these weight functions that are interpreted as a signature of intrinsic localized mode also coined quantum q-breathers. Here, the interaction between the bosons leads to an algebraic localization. Henceforth although the Fermi Pasta-Ulam feature is clearly exhibited by the breathers excitations in real space for our model, it is once more clear that moving to normal mode space change an important aspect of the FPU feature. In any case the existence of the breather excitations here allows to know how local magnetization reversal process with few spins can be proceeded in a ferromagnetic spin chain including DMI.

Perspectives

Despite the results obtained in this thesis, other points of interests may be solved in the future.

♣ In forthcoming works, we will study the Probabilities of localization of the bound states as function of time to understand more the phenomenon of localization in a such system.

♣ In a near future, we will study the localization of energy in real and in the normal mode space by analyzing analytically their waves functions to extend our understanding of the localization phenomenon in some other magnets with more complex structures.

♣ Our study has focussed on the analytical and numerical study, experimental studies should be carried out as a complement of our knowledge in a such physical system.

♣ Based on the electronic properties of the atoms constituting, a magnetic material, bosonic excitations like quantum breather excitation can be used to activate

a localized magnetization reversal processes in ferromagnets whenever a magnetic field is not applied to storage data.

Bibliography

Bibliography

[1] **Y.Iwasaki**, J. Magn. Magn. Mater.240,305(2002).

[2] **R. W. Chantrell, M. Wongsam, J.D. Hannay and O.Chubykalo**, Comput.Mater.Sci 17,483(2002).

[3] **J. C. Eilbeck** *Localization and Energy Transfer in Nonlinear Systems*, ed L.Vazquez, R.S. Mackay, and M. P. Zorzano (Singapore: Word Scientific) p.177 (2003).

[4] **D. K. Campbell, S. Flach, and Y. S. Kivshor** *Localizing Energy Through Nonlinearity and Discreteness*, Today **57**, 43 (2004).

[5] **S. Flach and C.R. Willis**, Phys. Rep. **295**, 181, Physica D**119**, (1998). Special volume edited by S. Flach and R.S. Mackay (1999).

[6] **S.Flach, A.V. Gorbach**, Phys. Rep.**467**, 1 (2008).

[7] **E. Fermi, J. Pasta, and S. Ulam**. Los Alamos Report No.LA-1940, (Unspecified)(1955), in collected papers of Enrico Fermi, edited by E. Segre (Chicago: University of Chicago Press), Vol. II, pp 977-978 (1965); in Many Body Problems.edited by D. C. Mattis (Singapore: World Scientfic)(1993).

[8] **S. Flach, M. V. Ivanchenko, and O. I. Kamakov**, Phys. Rev. E bf 73, 036618 (2006).

[9] **M. V. Ivanchenko, O. K. Kanakov, K. G. Mishangin, and S. Flach**, Phys. Rev. Lett. **97**, 025505 (2006).

[10] **S. Flach, M. V. Ivanchenko, and O. I. Kanakov**, Phys. Rev. Lett. **95**, 064102 (2005).

[11] **J. Dorignac and J. C. Eilbeck**, Phys. Rev. Lett. **93**, 025504 (2004).

[12] **H. S. Eisenberg. Y. Silberberg, R. Morandotti, A. R. Boyd, and J. S. Aitchison**, Phys. Rev. Lett. **81**, 3383 (1998).

[13] **Ricardo A. Pinto and Sergej Flach**, Phys. Rev. B **79**, 66002(2007).

[14] **J. Elder, P. Hamm, and A. C. Scott**, Phys. Rev. Lett. **88**,067403 (2002).

[15] A. Xie, L. Van der Meer, W. Hoff,and R. H. Austin, Phys. Rev. Lett. **84**, 5435 (2000).

[16] G. L. Alfimov, V. V. Konotop. and M. Salerno, Europhys. Lett. **58**, 7 (2002): **R.Carretero-González and K.Promislow**, Physica A **66**, 033610 (2002).

[17] **R. Lai, S. A. Kiselev, and A. J. Sievers**, Phys. Rev. B**56**, 5345 (1997).

[18] **G. P. Tsironis**, Chaos **13** 657/10 (2003).

[19] **J. P. Nguenang, R. A. Pinto, and S. Flach**, Phys. Rev. B **75**, 214303 (2007); **R. A. Pinto, J. P. Nguenang, and S. Flach**, Physica D **238**, 581 (2009).

[20] **HuXin-Guang and Tang Yi**, Chin. Phys. Soc. **17** 4268-05 (2008).

[21] **P. Binder, D. Abraimov, A. V. Ustinov, S. Flach and Y. Zolotaryuk**, Phys. Rev. Lett. **84**,745(2000).

[22] **A. C. Scott, J. C. Eilbeck, and H. Gilhøj**, Physica D **78**, 194 (1994).

[23] **A. C. Scott, J. C. Eilbeck, and H. Gilhøj**, *Quantum lattice solitons*, February 7, Private Communication (2008).

[24] **A. C. Scott**, Nonlinear Science (New York: Oxford University) 2nd ed (2003).

[25] **J. C. Eilbeck and F. Palmero**, *Quantum breathers in an attractive fermionic Hubbard model, in Nonlinear Waves: Classical a Quantum Aspects*, (eds. F. Kh. Abdullaev and V.V.Konotop) Kluwer: Amsterdam, 399-412, 2004.

[26] **Laurent Proville**, *Biphonons in the klein-gordon lattice*, Phys. Rev. B **71**, 104306 (2005). **Laurent Proville** Phys. Rev. B **72**, 184301 (2005).

[27] **J. C. Eilbeck and F. Palmero**, Physics Letters A **331**, 201, (2004).

[28] **V. Pouthier and C. Falvo**, Phys. Rev. E **69**, 041906 (2004). **C. Falvo and V. Pouthier**, J. Chem. Physics **123**,184710 (2005).

[29] **C. Falvo and V. Pouthier**, Chem. Phys. **123** 184710 (2005).

[30] **J. C. Eilbeck**, *Proceedings of the third Conference: Localization and Energy transfer in Nonlinear systems*, 177-186 (2003).

[31] **L. J. Bernstein**, physica D **68**, 174 (1993).

[32] **L. Bernstein, J. C. Eilbeck, A. C. Scott**, Nonlinearity **3**, 293(1990).

[33] **S. Aubry**, Physica D **103**, 201 (1997).

[34] **J. M. Radcliffe**, J. Phys. A**4**, 313 (1971).

[35] **R. Bolakrishman and A. R Bishop**, phys. Rev. Lett. 55537 (1985).

[36] **S. Aubry, S. Flach, K. Kladko, E. Olbrich**, Phys. Rev. Lett. **76**, 1607 (1996).

[37] **I. Dzyaloshinsky**, J. Phys. Chem. Solids **4**, 241 (1958).

[38] **T. Moriya**, phys. Rev. Lett. **4**, 228 (1960).

[39] **T. Moriya**, phys. Rev. **120**, 91 (1960).

[40] **Maged Elhajal**, thesis: *Lows energies properties and anisotropies of interactions of geometricaly frustrated magnetics systems*. University Joseph Fourier- Grenoble 1 (2002).

[41] **J. Sznajd**, Phys. Rev. B **68**, 174420 (2003).

[42] **C. Ederer and N. A. Spaldin**, Phys. Rev. B **71**, 060401 (2005).

[43] **R. Ballou, B. Canals, M. Elhajal, C. Lacroix, and A. S. Wills** Phys. Stat. Sol. (b) 236, No. 2, 240 - 245 (2003).

[44] **A. Antal, B. Lazarovts, L. Udvardi, L. Szunyogh et al**, Physical Review B **77**, 174429 (2008).

[45] **E. Y. Vedmedenko, L. Udvardi, P. Weinberges and R. Wiesendager**, Physical Review B **75**, 104431 (2007).

[46] **Olivier Cepas, and Timothy Ziman** arXiv:Cond-mat. / 0207191v1 (2002).

[47] **A. L. Chenyshev**, Phys. Rev. B **72**, 174414 (2005).

[48] **I. A. Segienko and E. Dagotto**, Physical Review B **73**, 094434 (2006).

[49] **M. Oshikawa, I. Affleck**, Phys. Rev. Lett, **79**, 2883 (1997), **I. Affleck, M. Oshikawa**, Phys. Rev. B **60**, 1038 (1999).

[50] **Seije, Miyashita, Shu, Tanaka, Hans De Raedt and Bernard barbara** arXiv: Cond - mat. Stat. mech / 080815 v4 (2009).

[51] **A. Zorko, S. Nellutla, J. Van Tol, L. C. Brunel et al**, Phys. Rev. Lett. **101**, 026405 (2008).

[52] **G. A. Jorge, R. stern, M. Jaine, N. Harrison et al**, Physical Review B **71**, 092403 (2005).

[53] **Oren ofer**, thesis: *The Impact of Perturbation on frusted Magnets*, Institute of Technology (2008).

[54] **U. Schollwöck, J. Bicheter, D. J. J. Farnell and R. F. Bishop**, *Quantum Magnetism, Lecture Notes in physics*, Vol. **645** (Springer-Verlag,Berlin,2004)

[55] **F. D. M. Haldane**, Phys. Rev. B **25**, 4925 (1982).

[56] **R. D. Somma and A. A. Aligia**, Phys. Rev. B **64**, 024410 (2001).

[57] **L. Amico, R. Fazio, A Osterlch, and Venchal**, Rev. Mod. Phys. **80**, 517(2008)

[58] **C. M. Dawson and M. A. Nielsen**, Phys. Rev. A **69**, 052316 (2004).

[59] **A. Sen (De), U. Sen, J. Dziarmaga, A. Sanpera and M. Lwenstein**, Phys Rev. Lett. **101**, 187202 (2008).

[60] **Y. Chen, Z. D. Wang, and F. C. Zhang**, phys. Rev. B **73**, 224414 (2006).

[61] **X. F. Qian, T.Shi, Y. Li, Z. Song and C. P. Sun**, Phys. Rev. A **72**, 012333 (2005).

[62] **C. H. Bennett et al**, Phys. Rev. Lett. **70**, 1985 (1993).

[63] **A. Osterloh, Luigi Amico, G. Folci, and Rasario Fazio**, Nature (London) **416**, 608 (2002).

[64] **C. K. Majumdar and D. K. Ghosh**, J. Math. Phys. **10**, 1388 (1969); J. Math. Phys. **10**, 1399 (1969); C. K. Majumdar J. Phys. C **3**, 911 (1969).

[65] **Shi-Jian Gu, Haibin Li, You-Q uan Li, and Hai-Qing Lin**, Physical Review A **70**, 052302 (2004).

[66] **I.C. Kwek, Y. Takahashi and K. W. Choo**, Journal of physics: Conference series **143**, 012014 (2009).

[67] **Sunz, X. G. Wang and Y. Q. Li**, New J. Phys. **783** (2005).

[68] **P. Liu, M-L Liang and B. Yuan** , Eur. Phys. J. D **41** 571 (2007).

[69] **T. Tonegawa and I. Harada**, J. Phys. Soc. Jph. **56**, 2153 (1987).

[70] **T. Tonegawa, I. Harada and M. Kaburagi**, J. Phys. Soc. 61, 4665 (1992).

[71] **M. E. Gouvë and A. S. T. Pires**, Phys. Stat. Sol. **6** 242, No 12, 2530-2539 (2005).

[72] **W. J. Massano, J. D. Prie and J. D. Mancini**, Phys. Rev. B **46**, 11133 (1992).

[73] **J. Igarashi and T. Tonegawa**, phys. Rev. B **40**, 756 (1989).

[74] **Shu Chen, Liwang, Shi-Jian Guy, and Yupeng Wang**, Phys. Rev. E **76**, 061108 (2007).

[75] **J.P. Nguenang, M.Peyrard, A. J. Kenfack, T. C. Kofane** J.Phys.:Condens. Matter**17**, 3083 (2005).

[76] **Y. Zolotaryuk, S. Flach, and V. Fleurov**,*Discrete breathers in classical spin lattices*, Phys. Rev. B **63**, 214422 (2004).

[77] **W. Gerlach and O. Stern** *Das magnetische moment des silberatoms* Zeitschrift für, Physik A Hadrons and Nuclei, **9**, 1 pages 353:355, (1922).

[78] **E. Du Trémolet de Lacheisserie** *Magnétisme*, Tome 1: Fondements (Coll. Grenoble sciences) EDP Sciences, (2000).

[79] **Jenö Sólyom** *Fundamentals of the Physics of Solids* Volume I *Structure and Dynamics* Translated by **Attila Piróth** Springer (2002)

[80] Disk read-and-write head. All Experts, http://en.allexperts.com/e/d/di/dis*k*_read-and-writ*e*_head.htm (page consulted in September 2012).

[81] **J. Ablowitz, D. J. Kaup, A. C. Newell, H. Segur** *Method for solving the sine-Gordon equation* Physical Review Letters **30**, 25 , 1262Ű1264 (1973).

[82] **R. S. Mackay, S. Aubry**, Nonlinearity, **7**, 1623 (1994)

[83] **S. Flach, M. V. Ivanchenko and O. I. Kanakov** *q-breathers in Fermi-Pasta-Ulam chains: Existence, localization, and stability* Physical Review E **73**, 036618 (2006).

[84] **A. Bikaki, N. K. Voulgarakis, S. Aubry and G. P. Tsironis** Physic Review Letter E **59**, 1234 (1999).

[85] **S. Flach, M.V. Ivanchenko, O. I. Kanakov and K. G. Mishagin** *Periodic orbits, localization in normal mode space, and the FermiŰPastaŰUlam problem* American Journal of Physic 76, 4-5 (2008).

[86] **E. Fermi, J. Pasta, S. Ulam** *Studies of nonlinear problems* Los Alamos, Report 1955; No. LA-1940; also in Collected Papers of Enrico Fermi, edited by E. Segre (University of Chicago Press, Chicago, 1965), Vol. II, p.978; *Many-Body Problems*, edited by D. C. Mattis (World Scientific, Singapore, 1993).

[87] **N. J. Zabusky, M. D. Kruskal** , Phys. Rev. Lett. **15**, 240 (1965).

[88] **S. Flach, M.V. Ivanchenko, O. I. Kanakov** *q-Breathers and the Fermi-Pasta-Ulam Problem* Physical Review Letters 95, 064102 (2005)

[89] **M.V. Ivanchenko, O.I. Kanakov, K. G. Mishagin and S.Flach** *q-Breathers in Finite Two and Three-Dimensional Nonlinear Acoustic Lattices* Physical Review letter 97, 025505 (2006).

[90] **K. G. Mishagin, S. Flach, O. I. Kanakov; M.V. Ivanchenko** *q-breathers in Discrete Nonlinear Schrödinger lattices* American Journal of Physic 76:4-5 (2008).

[91] **W. Z. Wang, J. Tinka Gammel, A. R. Bishop and M. I. Salkola**, Phys. Rev. Lett. **76**, 3598 (1996).

[92] **S. A. Sch öefield, R. E. Wyatt and P. G. Wolynes**, J. Chem. Phys. **105**, 940 (1996).

[93] **P. D.Miller, A. C. Scott, J. Carr and J. C. Eilbeck**, Phys. Sc. **44**, 509 (1991).

[94] **J. C. Eilbeck**, *Some exact results for quantum lattice problems.* **In L. Vazquez, R. S. MacKay and M. P. Zorzano**, editors, *Localization and energy transfer in nonlinear systems* World Scientific, Singapore, pages 177Ű186 (2003).

[95] **S. Flach and V. Fleurov** *Tunneling in the nonintegrable trimer - a step towards quantum breathers*, J. Phys.: Cond. Mat. 9:7039Ű7061, (1997).

[96] **W. Z. Wang, J. Tinka Gammel, A. R. Bishop, and M. I. Salkola** *Quantum breathers in a nonlinear lattice*, Phys. Rev. Lett. 76:3598Ű3601, (1996).

[97] L. Proville, *Two-phonon pseudogap in the klein-gordon lattice* Europhys. Lett. 69:763, (2005).

[98] **B. Swanson et al.** Phys. Rev. Lett. **82**, 3288 (1999); **K. Kladko, J. Malek and A. R. Bishop** J. Phys.: Condens. Matter 11:415 (1999)

[99] **U. T. Schwarz, L. Q. English, and A. J. Sievers**, Phys. Rev. Lett. 83:223 (1999).

[100] **M. Sato, B. E. Hubbard, A. J. Sievers, B. Ilic, D. A. Czaplewski and H. G. Craighead**, Phys. Rev. Lett. 90:044102 (2003).

[101] **B. Eiermann, Th. Anker, M. Albiez, M. Taglieber, P. Treutlein, K.-P. Marzlin and M. K. Oberthaler**, Phys. Rev. Lett. 92:230401 (2004).

[102] **J. Avery** *Creation and annihilation operators* McGraw-Hill (1979).

[103] **J. P. Blaizot and G. Ripka**, *Quantum Theory of finite systems*, Cambridge Mass: MIT Press (1986).

[104] **L. Landau et E. Lifchitz**, *Mécanique quantique* Editions Mir (1967).

[105] **C. Tannoudji, B. Diu et F. Laloë**, *Mécanique quantique*- Tomes 1 et 2 Edition Heramann (1973).

[106] **Habib Bouchriha** *Introduction à la Mécanique quantique* Centre de publication Universitaire (2002).

[107] **T. Holstein and H. Primakoff**, Phys. Rev. **58**,1098 (1940).

[108] **E. VALIEJO** *Castaneda Thesis: study of spins order contribution, the charge and structurals effects in double exchange model:spins ladders and maganites* University Joseph Fourier, Grenoble I (2006).

[109] **B. Gölzer and A. Holz**, J. Phys. A: Math. Gen. **20**,3327 (1987).

[110] **Willian H. Press, A. Saul, Teukolsky, T. Willian Vetterding, B. P. Flannery**, *Numerical Recipes in Fortran 77 the Art of Scientific Computing* Cambridge University Press 1986,1992 Second Edition.

[111] **Roman Schnalle** *From Numerical Exact Diagonalization to spin wave theory tools to investigate magnetic molecules.* University of Osnabrueck, Private communication (2007).

[112] **Z. I. Djoufack, A. Kenfack-Jiotsa, J-P. Nguenang and S. Domngang**, J. Phys. Condens. Matter **22**, 205502 (2010).

[113] **M. Valiente and D. Petrosyan**, J. Phys. B: At. Mol. Opt.Phys. **41 161002 (2008).**

[114] A. Kibey, R. Sonone, Bishwajyoti Dey and J. C. Eilbeck arXiv:408.0212v1 [nlim.PS] 1 Aug (2014).

List of Publications

[1] **Z I Djoufack, A Kenfack-Jiotsa, J P Nguenang and S Domngang**, Quantum Signatures of breathers in a finite Heisenberg spin chain. *Journal of Physics Condensed Matter 2010; 22:205502.*

[2] **Z I Djoufack, A. Kenfack-Jiotsa and J P Nguenang**, Quantum breathers in a finite Heisenberg spin chain with antisymmetric interactions. *Eur. Phys. J. B (2012) 85: 96.*

[3] **Zacharie Isidore Djoufack, A. Kenfack-Jiotsa and J P Nguenang**, Quantum localized excitations in a 1D Heisenberg spin chain involving bosons interactions, submitted to *Physica D* for publication.

[4] **Zacharie Isidore Djoufack, A. Kenfack-Jiotsa and J P Nguenang**, Quantum q-breathers in a finite Bose-Hubbard with Nearest and Next-Nearest Neighbor Interactions, submitted to *Journal of Physics Condensed Matter* for publication.

Appendix

Appendix A: Elements of matrix in the $\{2,2\}$ band

In this section, we show how we have calculated with details, different matrices elements presented in chapter three. To avoid to have heavy calculations, we chose the specific odd case of $f = 7$ as an example. The different states of this class are:

$$\begin{array}{l} \mid \psi_1\rangle = \frac{1}{\sqrt{7}} \sum_{s=1}^{7} \left(\frac{\widehat{T}}{\tau}\right)^{s-1} \mid 2200000\rangle = \mid 22\rangle \\ \mid \psi_2\rangle = \frac{1}{\sqrt{7}} \sum_{s=1}^{7} \left(\frac{\widehat{T}}{\tau}\right)^{s-1} \mid 2020000\rangle = \mid 202\rangle \\ \mid \psi_3\rangle = \frac{1}{\sqrt{7}} \sum_{s=1}^{7} \left(\frac{\widehat{T}}{\tau}\right)^{s-1} \mid 2002000\rangle = \mid 2002\rangle \end{array} \qquad (A.1)$$

It is important to mention here that for $f = 7$, the periodic boundary condition becomes $\tau^7 = 1$. In this way we have taken into account others considerations such as $\mid 2001100\rangle = \tau^{-4} \mid 1100200\rangle = \tau^3 \mid 1100200\rangle$ and $\mid 2000200\rangle = \tau^{-1} \mid 0200020\rangle = \tau^{-3} \mid 2000200\rangle$. The action of each state on the operator Hamiltonian $\hat{V}$ gives

$$\begin{array}{l} \hat{V} \mid \psi_1\rangle = \hat{V} \mid 22\rangle = \alpha^* \sqrt{6}(\frac{3\gamma}{4} - 1) \mid 33\rangle + \alpha^* \tau^{-1} \sqrt{2}(\frac{\gamma}{4} - 1) \mid 112\rangle \\ +\alpha\sqrt{6}(\frac{3\gamma}{4} - 1) \mid 13\rangle + \alpha\sqrt{2}(\frac{\gamma}{4} - 1) \mid 211\rangle - 2\gamma \mid 22\rangle \\ \mid \psi_2\rangle = \hat{V} \mid 202\rangle = \alpha^* \sqrt{2}(\frac{\gamma}{4} - 1) \mid 211\rangle + \alpha^* \tau^{-1} \sqrt{2}(\frac{\gamma}{4} - 1) \mid 1102\rangle \\ +\alpha\sqrt{2}(\frac{\gamma}{4} - 1) \mid 112\rangle + \alpha\sqrt{2}(\frac{\gamma}{4} - 1) \mid 2011\rangle \\ \mid \psi_3\rangle = \hat{V} \mid 2002\rangle = \tau^{-1}\alpha^* \sqrt{2}(\frac{\gamma}{4} - 1) \mid 11002\rangle + \alpha^* \sqrt{2}(\frac{\gamma}{4} - 1) \mid 2011\rangle \\ +\alpha\sqrt{2}(\frac{\gamma}{4} - 1) \mid 1102\rangle + \tau^3\alpha\sqrt{2}(\frac{\gamma}{4} - 1) \mid 11002\rangle \end{array} \qquad (A.2)$$

The news intermediates states that appear after Hamiltonian operator acting on each base state are: $\mid 31\rangle$; $\mid 13\rangle$; $\mid 112\rangle$; $\mid 211\rangle$

Detail of the class $\mid 31\rangle$

$$\begin{array}{l} \hat{V} \mid \tilde{\psi}_1^1\rangle = \hat{V} \mid 31\rangle = \alpha^*(\frac{3\gamma}{4} - 1) \mid 4\rangle + \alpha^* \tau^{-1} \sqrt{3}(\frac{\gamma}{4} - 1) \mid 121\rangle \\ +\alpha\sqrt{6}(\frac{3\gamma}{4} - 1) \mid 22\rangle - \alpha \mid 301\rangle - \frac{3}{2}\alpha\gamma \mid 31\rangle \end{array} \qquad (A.3)$$

Detail of the class $\mid 13\rangle$

$$\begin{array}{l}\hat{V} \mid \tilde{\psi}_2^1\rangle = \hat{V} \mid 13\rangle = \alpha^*(\frac{3\gamma}{4}-1) \mid 22\rangle + \alpha^*\sqrt{3}(\frac{2\gamma}{4}-1) \mid 121\rangle \\ +\tau\alpha(\frac{3\gamma}{4}-1) \mid 4\rangle - \tau^{-1}\alpha \mid 103\rangle - \frac{3}{2}\alpha\gamma \mid 13\rangle\end{array} \tag{A.4}$$

Detail of the class $\mid 112\rangle$

$$\begin{array}{l}\hat{V} \mid \tilde{\psi}_3^1\rangle = \hat{V} \mid 112\rangle = \alpha^*\sqrt{2}(\frac{\gamma}{4}-1) \mid 202\rangle + 2\alpha^*(\frac{2\gamma}{4}-1) \mid 121\rangle \\ +\tau\alpha\sqrt{2}(\frac{\gamma}{4}-1) \mid 22\rangle + \alpha\sqrt{2}(\frac{\gamma}{4}-1) \mid 1111\rangle - \frac{3}{2}\alpha\gamma \mid 112\rangle \\ \hat{V} \mid \tilde{\psi}_3^2\rangle = \hat{V} \mid 1102\rangle = \alpha^*\sqrt{2}(\frac{\gamma}{4}-1) \mid 2002\rangle \\ +\alpha^*\sqrt{2}(\frac{\gamma}{4}-1) \mid 1111\rangle - \tau^{-1}\alpha^* \mid 10102\rangle \\ +\tau\alpha\sqrt{2}(\frac{\gamma}{4}-1) \mid 202\rangle + \alpha\sqrt{2}(\frac{\gamma}{4}-1) \mid 11011\rangle - \frac{1}{2}\alpha\gamma \mid 1102\rangle - \alpha \mid 1012\rangle \\ \hat{V} \mid \tilde{\psi}_3^3\rangle = \hat{V} \mid 11002\rangle = \alpha^*\tau^{-3}\sqrt{2}(\frac{\gamma}{4}-1) \mid 2002\rangle \\ +\alpha^*\sqrt{2}(\frac{\gamma}{4}-1) \mid 11011\rangle - \tau^{-3}\alpha^* \mid 20101\rangle \\ +\tau\alpha\sqrt{2}(\frac{\gamma}{4}-1) \mid 2002\rangle + \tau^{-3}\alpha\sqrt{2}(\frac{\gamma}{4}-1) \mid 11011\rangle - \frac{1}{2}\alpha\gamma \mid 11002\rangle - \alpha \mid 10102\rangle\end{array} \tag{A.5}$$

Detail of the class $\mid 211\rangle$

$$\begin{array}{l}\hat{V} \mid \tilde{\psi}_4^1\rangle = \hat{V} \mid 211\rangle = \alpha^*\sqrt{2}(\frac{\gamma}{4}-1) \mid 22\rangle + \alpha^*\sqrt{3}(\frac{2\gamma}{4}-1) \mid 301\rangle \\ +\tau^{-1}\alpha^*\sqrt{2}(\frac{\gamma}{4}-1) \mid 1111\rangle + \alpha\sqrt{2}(\frac{\gamma}{4}-1) \mid 202\rangle + 2\alpha(\frac{2\gamma}{4}-1) \mid 121\rangle \\ -\frac{3}{2}\alpha\gamma \mid 211\rangle - \alpha \mid 2101\rangle \\ \hat{V} \mid \tilde{\psi}_4^2\rangle = \hat{V} \mid 2011\rangle = \alpha^*\sqrt{2}(\frac{\gamma}{4}-1) \mid 202\rangle \\ +\tau^{-1}\alpha^*\sqrt{2}(\frac{\gamma}{4}-1) \mid 11011\rangle - \alpha^* \mid 2101\rangle \\ +\alpha\sqrt{2}(\frac{\gamma}{4}-1) \mid 2002\rangle + \alpha\sqrt{2}(\frac{\gamma}{4}-1) \mid 1111\rangle - \alpha \mid 20101\rangle \\ \hat{V} \mid \tilde{\psi}_4^3\rangle = \hat{V} \mid 20011\rangle = \alpha^*\sqrt{2}(\frac{\gamma}{4}-1) \mid 2002\rangle \\ +\tau^3\alpha^*\sqrt{2}(\frac{\gamma}{4}-1) \mid 11011\rangle - \alpha^* \mid 20101\rangle \\ +\tau^{-3}\alpha\sqrt{2}(\frac{\gamma}{4}-1) \mid 2002\rangle + \alpha\sqrt{2}(\frac{\gamma}{4}-1) \mid 11011\rangle - \frac{1}{2}\alpha\gamma \mid 20011\rangle\end{array} \tag{A.6}$$

Detail calculation of the elements in the Hamiltonian matrix $\mathbf{H}^{(2,2)}$

We have used the degenerate perturbation method, in this method the correction of the energy in second order is given by equation (2.65), where $\langle\psi^0_{k'i} \mid$, $\langle\psi^0_{k'i''} \mid$, H_1 and $E^0_{k'i''}$ are replaced respectively by $\langle\psi_i \mid$, $\langle\tilde{\psi}^j_i \mid$, and $\tilde{E}^{(0)}_{k'i''}$

$$E^2_{ki} = \sum_{k\neq k',i''} \frac{<\psi^0_{k'i} \mid H_1 \mid \psi^0_{k'i''}><\psi^0_{k'i''} \mid H_1 \mid \psi^0_{ki}>}{E^0_{ki} - E^0_{k'i''}}$$

$$H_{11}=\sum_{\tilde{\psi}}\frac{\left\langle\psi_i|\widehat{V}|\widetilde{\psi}\right\rangle\left\langle\widetilde{\psi}|\widehat{V}|\psi_{i'}\right\rangle}{E_{22}^{(0)}-\widetilde{E}_i^{(0)}}=\frac{\left\langle\psi_1|\widehat{V}|\widetilde{\psi}_1^1\right\rangle\left\langle\widetilde{\psi}_1^1|\widehat{V}|\psi_1\right\rangle}{E_{22}^{(0)}-\widetilde{E}_{31}^{(0)}}+\frac{\left\langle\psi_1|\widehat{V}|\widetilde{\psi}_2^1\right\rangle\left\langle\widetilde{\psi}_2^1|\widehat{V}|\psi_1\right\rangle}{E_{22}^{(0)}-\widetilde{E}_{13}^{(0)}}$$
$$+\frac{\left\langle\psi_1|\widehat{V}|\widetilde{\psi}_3^1\right\rangle\left\langle\widetilde{\psi}_3^1|\widehat{V}|\psi_1\right\rangle}{E_{22}^{(0)}-\widetilde{E}_{112}^{(0)}}+\frac{\left\langle\psi_1|\widehat{V}|\widetilde{\psi}_4^1\right\rangle\left\langle\widetilde{\psi}_4^1|\widehat{V}|\psi_1\right\rangle}{E_{22}^{(0)}-\widetilde{E}_{211}^{(0)}}=\frac{\left\langle22|\widehat{V}|31\right\rangle\left\langle31|\widehat{V}|22\right\rangle}{E_{22}^{(0)}-\widetilde{E}_{31}^{(0)}}$$
$$\frac{\left\langle22|\widehat{V}|13\right\rangle\left\langle13|\widehat{V}|22\right\rangle}{E_{22}^{(0)}-\widetilde{E}_{13}^{(0)}}+\frac{\left\langle22|\widehat{V}|112\right\rangle\left\langle112|\widehat{V}|22\right\rangle}{E_{22}^{(0)}-\widetilde{E}_{112}^{(0)}}+\frac{\left\langle22|\widehat{V}|211\right\rangle\left\langle211|\widehat{V}|22\right\rangle}{E_{22}^{(0)}-\widetilde{E}_{211}^{(0)}} \qquad (A.7)$$
$$=\frac{\alpha\sqrt{6}(\frac{3\gamma}{4}-1)\alpha^*\sqrt{6}(\frac{3\gamma}{4}-1)}{-2\gamma}+\frac{\alpha\sqrt{6}(\frac{3\gamma}{4}-1)\alpha^*\sqrt{6}(\frac{3\gamma}{4}-1)}{-2\gamma}+\frac{\alpha\sqrt{2}(\frac{\gamma}{4}-1)\alpha^*\sqrt{2}(\frac{\gamma}{4}-1)}{2\gamma}$$
$$+\frac{\alpha\sqrt{2}(\frac{\gamma}{4}-1)\alpha^*\sqrt{2}(\frac{\gamma}{4}-1)}{2\gamma}=-\frac{\alpha\alpha^*}{\gamma}[6(\frac{3\gamma}{4}-1)^2-2(\frac{\gamma}{4}-1)^2]=-\frac{m}{\gamma}[6C-2B]$$

Where $\alpha=J_1+iD_z$; $m=\alpha\alpha^*=J_1^2+D_z^2$; $C=(\frac{3\gamma}{4}-1)^2$ and $B=(\frac{\gamma}{4}-1)^2$

$$H_{12}=\frac{\left\langle\psi_1|\widehat{V}|\widetilde{\psi}_3^1\right\rangle\left\langle\widetilde{\psi}_3^1|\widehat{V}|\psi_2\right\rangle}{E_{22}^{(0)}-\widetilde{E}_{112}^{(0)}}+\frac{\left\langle\psi_1|\widehat{V}|\widetilde{\psi}_4^1\right\rangle\left\langle\widetilde{\psi}_4^1|\widehat{V}|\psi_2\right\rangle}{E_{22}^{(0)}-\widetilde{E}_{211}^{(0)}}=\frac{\left\langle22|\widehat{V}|112\right\rangle\left\langle112|\widehat{V}|202\right\rangle}{E_{22}^{(0)}-\widetilde{E}_{112}^{(0)}}+$$
$$\frac{\left\langle22|\widehat{V}|211\right\rangle\left\langle211|\widehat{V}|202\right\rangle}{E_{22}^{(0)}-\widetilde{E}_{211}^{(0)}}=\frac{2\tau\alpha^2(\frac{\gamma}{4}-1)^2}{-2\gamma}+\frac{2\alpha^{*2}(\frac{\gamma}{4}-1)^2}{-2\gamma}=-\frac{BW}{\gamma} \qquad (A.8)$$

Where $W=m'q'+2iJ_1D_zq$; $m'=J_1^2-D_z^2$; $q=\tau-1=2ie^{ik/2}\sin(k/2)$; $q'=\tau+1=2e^{ik/2}\cos(k/2)$ and $B=(\frac{\gamma}{4}-1)^2$

$$H_{13}=\frac{\left\langle\psi_1|\widehat{V}|\widetilde{\psi}_3^3\right\rangle\left\langle\widetilde{\psi}_3^3|\widehat{V}|\psi_3\right\rangle}{E_{22}^{(0)}-\widetilde{E}_{11002}^{(0)}}+\frac{\left\langle\psi_1|\widehat{V}|\widetilde{\psi}_4^2\right\rangle\left\langle\widetilde{\psi}_4^2|\widehat{V}|\psi_3\right\rangle}{E_{22}^{(0)}-\widetilde{E}_{2011}^{(0)}}=0 \qquad (A.9)$$

$$H_{21}=\frac{\left\langle\psi_2|\widehat{V}|\widetilde{\psi}_3^1\right\rangle\left\langle\widetilde{\psi}_3^1|\widehat{V}|\psi_2\right\rangle}{E_{22}^{(0)}-\widetilde{E}_{112}^{(0)}}+\frac{\left\langle\psi_2|\widehat{V}|\widetilde{\psi}_3^2\right\rangle\left\langle\widetilde{\psi}_3^2|\widehat{V}|\psi_2\right\rangle}{E_{22}^{(0)}-\widetilde{E}_{211}^{(0)}}=\frac{2\tau^{-1}\alpha^{*2}(\frac{\gamma}{4}-1)^2}{-2\gamma}$$
$$+\frac{2\alpha^2(\frac{\gamma}{4}-1)^2}{-2\gamma}=-\frac{BW^*}{\gamma} \qquad (A.10)$$

$$H_{22}=\frac{\left\langle\psi_2|\widehat{V}|\widetilde{\psi}_3^1\right\rangle\left\langle\widetilde{\psi}_3^1|\widehat{V}|\psi_2\right\rangle}{E_{202}^{(0)}-\widetilde{E}_{112}^{(0)}}+\frac{\left\langle\psi_2|\widehat{V}|\widetilde{\psi}_3^2\right\rangle\left\langle\widetilde{\psi}_3^2|\widehat{V}|\psi_2\right\rangle}{E_{202}^{(0)}-\widetilde{E}_{1102}^{(0)}}+\frac{\left\langle\psi_2|\widehat{V}|\widetilde{\psi}_4^1\right\rangle\left\langle\widetilde{\psi}_4^1|\widehat{V}|\psi_2\right\rangle}{E_{202}^{(0)}-\widetilde{E}_{211}^{(0)}}+$$
$$\frac{\left\langle\psi_2|\widehat{V}|\widetilde{\psi}_4^2\right\rangle\left\langle\widetilde{\psi}_4^2|\widehat{V}|\psi_2\right\rangle}{E_{202}^{(0)}-\widetilde{E}_{2011}^{(0)}}=\frac{2m(\frac{\gamma}{4}-1)^2}{-2\gamma}+\frac{2m(\frac{\gamma}{4}-1)^2}{-2\gamma}+\frac{2m(\frac{\gamma}{4}-1)^2}{-2\gamma}+\frac{2m(\frac{\gamma}{4}-1)^2}{-2\gamma} \qquad (A.11)$$
$$=-\frac{4mB}{\gamma}$$

$$H_{23}=\frac{\left\langle\psi_2|\widehat{V}|\widetilde{\psi}_3^2\right\rangle\left\langle\widetilde{\psi}_3^2|\widehat{V}|\psi_3\right\rangle}{E_{202}^{(0)}-\widetilde{E}_{1102}^{(0)}}+\frac{\left\langle\psi_2|\widehat{V}|\widetilde{\psi}_4^2\right\rangle\left\langle\widetilde{\psi}_4^2|\widehat{V}|\psi_3\right\rangle}{E_{202}^{(0)}-\widetilde{E}_{2011}^{(0)}}=\frac{2\tau\alpha^2(\frac{\gamma}{4}-1)^2}{-2\gamma}$$
$$+\frac{2\alpha^{*2}(\frac{\gamma}{4}-1)^2}{-2\gamma}=-\frac{BW}{\gamma} \qquad (A.12)$$

$$H_{31}=\frac{\left\langle\psi_3|\widehat{V}|\widetilde{\psi}_3^1\right\rangle\left\langle\widetilde{\psi}_3^1|\widehat{V}|\psi_1\right\rangle}{E_{22}^{(0)}-\widetilde{E}_{112}^{(0)}}+\frac{\left\langle\psi_3|\widehat{V}|\widetilde{\psi}_4^1\right\rangle\left\langle\widetilde{\psi}_4^1|\widehat{V}|\psi_1\right\rangle}{E_{22}^{(0)}-\widetilde{E}_{211}^{(0)}}=0 \qquad (A.13)$$

$$H_{32} = \frac{\left\langle \psi_3|\widehat{V}|\widetilde{\psi}_3^2\right\rangle\left\langle \widetilde{\psi}_3^2|\widehat{V}|\psi_2\right\rangle}{E_{22}^{(0)}-\widetilde{E}_{1102}^{(0)}} + \frac{\left\langle \psi_3|\widehat{V}|\widetilde{\psi}_4^2\right\rangle\left\langle \widetilde{\psi}_4^2|\widehat{V}|\psi_2\right\rangle}{E_{22}^{(0)}-\widetilde{E}_{2011}^{(0)}} = \frac{2\tau^{-1}\alpha^2(\frac{\gamma}{4}-1)^2}{-2\gamma}$$
$$+\frac{2\alpha^{*2}(\frac{\gamma}{4}-1)^2}{-2\gamma} = -\frac{BW^*}{\gamma} \tag{A.14}$$

$$H_{33} = \frac{\left\langle \psi_3|\widehat{V}|\widetilde{\psi}_3^2\right\rangle\left\langle \widetilde{\psi}_3^2|\widehat{V}|\psi_3\right\rangle}{E_{22}^{(0)}-\widetilde{E}_{1102}^{(0)}} + \frac{\left\langle \psi_3|\widehat{V}|\widetilde{\psi}_3^3\right\rangle\left\langle \widetilde{\psi}_3^3|\widehat{V}|\psi_3\right\rangle}{E_{22}^{(0)}-\widetilde{E}_{11002}^{(0)}} + \frac{\left\langle \psi_3|\widehat{V}|\widetilde{\psi}_4^2\right\rangle\left\langle \widetilde{\psi}_4^2|\widehat{V}|\psi_3\right\rangle}{E_{22}^{(0)}-\widetilde{E}_{2011}^{(0)}}$$
$$+\frac{\left\langle \psi_2|\widehat{V}|\widetilde{\psi}_4^3\right\rangle\left\langle \widetilde{\psi}_4^3|\widehat{V}|\psi_3\right\rangle}{E_{202}^{(0)}-\widetilde{E}_{2011}^{(0)}} = \frac{2m(\frac{\gamma}{4}-1)^2}{-2\gamma} + \frac{2m(\frac{\gamma}{4}-1)^2+2\tau^3\alpha^{*2}(\frac{\gamma}{4}-1)^2}{-2\gamma} + \frac{2m(\frac{\gamma}{4}-1)^2}{2\gamma} \tag{A.15}$$
$$+\frac{2m(\frac{\gamma}{4}-1)^2 2\tau^{-3}\alpha^2(\frac{\gamma}{4}-1)^2}{2\gamma} = -\frac{B[4m+m'(\tau^3+\tau_{-3})+2iJ_1D_z(\tau^3-\tau_{-3})]}{\gamma}$$
$$= -\frac{B(4m+P)}{\gamma}$$

Where $P = 2m'\cos(3k) + 4J_1D_z\sin(3k)$, increasing the number of site f, we have obtained the general form of the matrix $H^{(2,2)}$

$$H^{(2,2)} = -\tfrac{4mB}{A\gamma}I_\sigma - \tfrac{B}{A\gamma}\begin{pmatrix} \Gamma & W & & & \\ W^* & 0 & W & & \\ & \ddots & \ddots & \ddots & \\ & & W^* & 0 & W \\ & & & W^* & P \end{pmatrix} \tag{A.16}$$

Using the same technique, we could calculated the matrix elements shown in section 3.4 when the longer range interaction are involved in the Heisenberg model. To avoid overloading the thesis, we did not presented such details.